

MSc Thesis

**DESIGN AND CONSTRUCTION  
OF A  
RAILWAY ARCH BRIDGE WITH A  
NETWORK HANGER  
ARRANGEMENT**

T.J.M. Smit  
May 2013



# DESIGN AND CONSTRUCTION OF A RAILWAY ARCH BRIDGE WITH A NETWORK HANGER ARRANGEMENT

GRADUATION RESEARCH REPORT

AUTHOR

T.J.M. Smit  
Delft University of Technology

GRADUATION COMMITTEE

**Prof. Ir. F.S.K. Bijlaard**  
Delft University of Technology  
Structural Engineering,  
Steel structures

**Dr. Ir. P.C.J. Hoogenboom**  
Delft University of Technology  
Structural Mechanics

**Dr. M.H. Kolstein**  
Delft University of Technology  
Structural Engineering,  
Steel structures

**Ir. W.P.J. Langedijk**  
Daily supervisor  
Iv-Infra

**Ir. L.J.M. Houben**  
Delft University of Technology  
Road and railway engineering,  
Road engineering

DATE

May 17 2013



# PREFACE

I want to thank my graduation committee members, Prof. F.S.K. Bijlaard, Dr. M.H. Kolstein and Dr. ir. P.C.J. Hoogenboom for all the time they have devoted to reviewing my thesis and for their contribution and guidance on a regular basis.

I would like to thank my colleagues at Iv-Infra for their support, especially my supervisor W.P.J. Langedijk, who has guided and supported me throughout the process.

Finally, I would like to thank my mother for supporting my choices and funding my studies all these years. Last but not least, I want to thank my girlfriend Gina for supporting me in every possible way over the past years.

Volendam, 12.05.2013

Tom Smit



# ABSTRACT

The research question of this thesis originates from a variant study for a tender design to determine the optimal hanger arrangement for a railway arch bridge. This railway arch bridge is part of an immense project to improve the infrastructure between Almere, Amsterdam and Schiphol airport for a total value of one billion euro. The bridge will cross 10 traffic lanes of the renewed and widened A1 highway with a total span of 255m. On the November 12<sup>th</sup> 2012 it was announced that the tender was won by SAAone, a combination of contractors and engineering firms (Volker Wessels, Boskalis, Hochtief, Royal HaskoningDHV and Iv-Infra).

In the variant study for the tender design, three different hanger arrangements were investigated: vertical, diagonal and network. Finally after dimensioning the three types of bridges it was concluded that the network arrangement required the smallest amount of steel based on strength and stiffness. However, when comparing the three types at other design aspects, the diagonal hanger arrangement was preferred and chosen as final design. Why the network arch became second in the comparison is because of uncertainties about the following design aspects:

- The assembly of the hangers; how to obtain the desired force distribution
- The influence of compressive forces in hangers on the structural behaviour of the bridge
- Fatigue performance of the hangers
- Susceptibility to vibration effects, especially vortex induced vibrations

The conclusion of the variant study, which contradicts to the earlier named advantages of the network arch, raises the question whether the risks in these uncertain design aspects weren't overestimated. In order to investigate this, the following research question was posed: 'Is a railway arch bridge with a span of 255m more advantageous when the hangers are arranged as diagonals or as a network?'

To answer this research question, at first a literature study is performed. With the information gathered in this study, a competitive design for a network arch railway bridge is made. This design is based on the original tender design, except for the hanger configuration and hanger type. This results in a design for a network arch bridge which can be compared to the original tender design in order to answer the research question. The optimal hanger type and optimal hanger configuration are determined by means of a variant study. It was concluded, based on certain assumptions and the literature study, that a steel rod hanger with welded connections is the most advantageous hanger type. The geometry of the optimal hanger arrangement is also based on literature. In this competitive design, the four uncertainties are evaluated in order to solve the problem.

The first design aspect 'the assembly of the hangers' is covered in the literature study by investigating the assembly process of previously built arch bridges with a network hanger arrangement. For the hanger type that was chosen in the variant study, it is crucial to assemble the hangers under stress less conditions. This can be achieved by fully supporting the hangers during the welding of the hanger connections. When this condition is satisfied, the theoretical force distribution should be obtained. By applying this construction method a complex

tensioning procedure does not have to be performed and calculated in order to obtain the desired force distribution in the hangers.

To evaluate the remaining three design aspects, the behavior and the correct modeling of the hangers is investigated. The conclusion is that by applying geometrically nonlinear analysis, the hanger behavior can be modeled accurately.

The following design aspect which was investigated is the influence of compression in hangers on the structural behavior of the bridge. Due to the optimized hanger configuration that was determined in the variant study, no hanger compression will occur in the SLS. Hence, this will not affect the fatigue behavior of the hangers. However, when compression does occur (only in the ULS), the hangers will relax and deflect due to their self-weight, and the compressive forces will be transferred by other hangers (redistribution). The effects on the buckling behavior of this specific bridge are negligible, because hanger compression/ relaxation only occurs when a part of the span is loaded.

When considering the third design aspect ‘fatigue performance of the hangers’ also the ‘susceptibility to vibration effects’ (the fourth design aspect) has to be taken into account, because these could also cause fatigue damage. The fatigue performance is verified by using an isolated model of the longest hanger. It is assumed that the longest hanger will be affected most by the fatigue loading caused by traffic and vibration effects. To determine the fatigue performance of the longest hanger, the damage caused by traffic and vortex induced vibrations has to be combined. The conclusion is that the longest hanger has sufficient fatigue performance. This is mainly caused by the good fatigue properties of the hanger connection and the high Scruton-number which is provided by the steel rod hangers.

To fully cover the design aspect of the susceptibility to vibration effects, attention is also paid to rain- and wind induced vibrations and structural vibrations (parametric excitation). From the evaluation of rain- and wind induced vibrations it appears that these could cause severe fatigue damage. This vibration effect can be prevented by applying helical wires along the surface of the profile. The second vibration effect, structural vibrations, is also likely to occur. This vibration effect can be prevented by coupling the hangers at the crossings.

Finally after finishing the competitive design, the comparison is made between the bridge with the network and the diagonal hanger arrangement. It follows that the arch bridge with the network hanger arrangement requires 860 tons less steel for the hangers, arch and main girder. This equals 13% of the total steel weight of the arch bridge with a diagonal hanger arrangement.

Concluding: ‘Is a railway arch bridge with a span of 255m more advantageous when the hangers are arranged as diagonals or as a network?’ The comparison between both bridge designs shows that the overall performance of the arch bridge with network hanger configuration is more advantageous, because of the weight reduction and the better performance on different design aspects.

# SAMENVATTING

De hoofdvraag van dit afstudeeronderzoek is voortgekomen uit een variantenstudie voor een tenderontwerp, met als doel het bepalen van een optimale hangerconfiguratie voor een spoorboogbrug. Deze spoorboogbrug maakt deel uit van een enorm project, ter waarde van 1 miljard euro, met als doel de infrastructuur tussen Almere, Amsterdam en Schiphol te verbeteren. De spoorbrug zal tien rijstroken van de vernieuwde en verwijde A1 overbruggen, met een totale lengte van 255 meter. Op 12 november 2012 werd bekend gemaakt dat de tender gewonnen was door SAAone, een combinatie van aannemers en ingenieursbureaus (Volker Wessels, Boskalis, Hochtief, Royal HaskoningDHV en Iv-Infra).

In de variantenstudie voor het tenderontwerp zijn drie verschillende hangerconfiguraties onderzocht: verticaal, diagonaal en netwerk. Op basis van sterkte en stijfheid blijkt de netwerkvariant een aanzienlijke besparing in staalgewicht op te leveren. Wanneer er ook naar de andere ontwerpaspecten wordt gekeken, komt uiteindelijk toch de diagonaalvariant als beste optie uit de bus. De netwerkvariant is niet als winnaar uit de bus gekomen vanwege verschillende onzekerheden omtrent ontwerpaspecten:

- Het monteren van de hangers: het verkrijgen van de gewenste krachtenverdeling
- De invloed van druk in hangers op de constructieve eigenschappen
- De vermoeiingsgevoeligheid van de hangers
- De gevoeligheid voor trillingseffecten, met name vortextrillingen

In deze variantenstudie won een zwaardere brug (diagonaalvariant) het van een aanzienlijk lichtere (netwerk variant) brug. Vanwege deze vreemde uitkomst is het interessant om de bovengenoemde ontwerpaspecten in kaart te brengen. Om de onzekerheden van deze aspecten te onderzoeken, is de volgende onderzoeksvraag gesteld: ‘Heeft een boogspoorbrug, met een overspanning van 255m, meer voordelen wanneer de hangers zijn geconfigureerd als een netwerk of als diagonalen?’

Ter beantwoording van deze onderzoeksvraag is er allereerst een literatuurstudie gedaan. Vervolgens is er een competitief ontwerp van een netwerk-spoorboogbrug gemaakt. Het ontwerp hiervan is gebaseerd op het originele tenderontwerp, behalve de hangerconfiguratie en het hangertype. Uiteindelijk moeten de beide ontwerpen zuiver met elkaar kunnen worden vergeleken, om de onderzoeksvraag goed te kunnen beantwoorden. Het optimale hangertype en de optimale hangerconfiguratie zijn door middel van een variantenstudie bepaald. Op basis van bepaalde aannames en argumenten uit de literatuur, is geconcludeerd dat een massief rondstalen hanger met gelaste verbindingen de meeste voordelen oplevert. De geometrie voor de optimale hangerconfiguratie is ook gebaseerd op literatuur. In dit competitieve ontwerp zijn de vier onzekerheden die hierboven staan opgesomd uitgewerkt, met als doel de onzekerheden op te heffen.

Ten eerste: het ontwerpaspect ‘het monteren van de hangers’ wordt in de literatuurstudie behandeld door eerder gebouwde bruggen te onderzoeken. Voor het in de variantenstudie gekozen hangertype, is het belangrijk de hangers spanningsloos te monteren door ze volledig te ondersteunen tijdens de laswerkzaamheden. Hierdoor zal de krachtenverdeling binnen bepaalde grenzen gelijk zijn aan de theoretische krachtenverdeling. Door de keuze voor deze

montagemethode is het niet nodig om een complexe spanprocedure uit te voeren en door te rekenen om de juiste krachtenverdeling in de hangers te bepalen.

Om de overige drie ontwerpaspecten te kunnen verwerken, is er een subonderzoek verricht naar het gedrag van de hangers en naar hoe dit gedrag het beste gemodelleerd kan worden. Hieruit is gebleken dat door middel van geometrisch niet-lineaire analyse, het hangergedrag goed gemodelleerd kan worden.

Vervolgens is er gekeken naar de invloed op de spanningen in de constructie bij druk in de hangers. Dankzij de geoptimaliseerde hangerconfiguratie die in de variantenstudie is bepaald, treedt er geen druk op in de SLS, en daardoor zijn er geen gevolgen voor de vermoeiingsweerstand van de hangers. Verder blijkt dat wanneer er wel druk optreedt (uitsluitend in de ULS), de hangers zullen ontspannen en doorbuigen ten gevolge van hun eigen gewicht. Bovendien zullen de drukkrachten door andere hangers worden opgevangen (herverdeling). De invloed op het totale knikgedrag van deze specifieke brug is nihil, omdat gedrukte of ontspannen hangers alleen zullen voorkomen bij een deels belaste brug.

Bij onderzoek naar het derde ontwerpaspect ‘vermoeiing van hangers’, moet automatisch ‘de gevoeligheid voor trillingseffecten’ (het vierde ontwerpaspect) worden onderzocht, omdat deze ook tot vermoeiing kunnen leiden. De vermoeiingsanalyse wordt uitgevoerd op de langste hanger, die in een geïsoleerd model wordt beschouwd. Aangenomen is dat bij de langste hanger de grootste vermoeiingsschade ten gevolge van trillingseffecten en verkeer zal optreden. Om de totale vermoeiingsschade in de langste hanger te bepalen, moet de vermoeiing ten gevolge van verkeer en vortex-geïnduceerde trillingen worden gecombineerd. Hieruit blijkt dat de langste hanger over voldoende capaciteit beschikt. Dit is te danken aan de goede vermoeiingseigenschap van de hangeraansluiting en het hoge Scruton-getal dat door de massief stalen hangers wordt veroorzaakt.

Om het vierde en laatste ontwerpaspect ten aanzien van de gevoeligheid voor trillingseffecten goed te kunnen inschatten, zijn de regen- en windgeïnduceerde trillingen en trillingen vanuit de constructie (parametric excitation) bestudeerd. Uit de vermoeiingsberekening van regen- en windgeïnduceerde trillingen, is gebleken dat deze ernstige schade kunnen veroorzaken. Door het hangeroppervlak te voorzien van spiralen kan dit trillingseffect worden voorkomen. Het tweede trillingseffect, trillingen vanuit de constructie, zal waarschijnlijk ook optreden. Dit trillingseffect kan worden voorkomen door het koppelen van de hangers op de kruispunten.

Na het afronden van het competitieve ontwerp voor de netwerkboogbrug, zijn de boogbruggen met netwerk- en diagonale hangerconfiguratie met elkaar vergeleken. Uit deze vergelijking komt naar voren dat er 860 ton minder staal nodig is voor de hangers, boog, en hoofdligger van een spoorboogbrug met een netwerkhangereconfiguratie. Dit staat gelijk aan een besparing van 13% van het totale staalgewicht van de spoorboogbrug met een diagonale hangerconfiguratie.

Concluderend: ‘Heeft een boogspoorbrug, met een overspanning van 255m, meer voordelen wanneer de hangers zijn geconfigureerd als een netwerk of als diagonalen?’. Uit de vergelijking van de brugontwerpen kan worden geconcludeerd dat de boogbrug met netwerkconfiguratie meer voordelen heeft vanwege de gewichtsreductie en het gunstige gedrag ten aanzien van verschillende ontwerpaspecten.

# CONTENTS

PREFACE .....	4
ABSTRACT .....	6
SAMENVATTING.....	8
CONTENTS .....	10
1 INTRODUCTION .....	14
1.1 Strategy .....	15
2 LITERATURE STUDY .....	17
2.1 Historical overview .....	18
2.2 Preliminary design of a network arch.....	22
2.2.1 Arch and lateral bracing .....	23
2.2.2 Main girder .....	26
2.2.3 Deck.....	27
2.2.4 Hangers .....	29
2.2.5 Conclusion.....	33
2.3 Detailed design of a network arch.....	33
2.3.1 Global static analysis .....	33
2.3.2 Fatigue performance of the hangers.....	34
2.3.3 Hanger stressing procedure .....	35
2.3.4 Compression in hangers .....	35
2.3.5 Hanger vibrations.....	35
2.3.6 Conclusion.....	41
2.4 Construction of a network arch .....	42
2.4.1 Prefabrication .....	42
2.4.2 Construction of the deck and main girder .....	43
2.4.3 Construction of the arch.....	43
2.4.4 Assembly of hangers with welded connections.....	44
2.4.5 Assembly of tensioned hangers .....	45
2.4.6 Transportation to final location .....	45
2.4.7 Conclusion.....	46
3 VARIANT STUDY .....	47
3.1 Hanger arrangement .....	47
3.1.1 Number of hangers.....	47
3.1.2 Type of arrangement .....	47
3.1.3 Conclusion.....	48
3.2 Hanger type.....	48
3.2.1 General structural properties .....	49

3.2.2	Vibration effects and suppression.....	52
3.2.3	Costs.....	53
3.2.4	Constructability .....	55
3.2.5	Maintenance .....	56
3.2.6	Conclusion.....	57
4	DESIGN STAGE.....	58
4.1	Design aspects .....	58
4.1.1	Adaptations to the original tender design.....	59
4.1.2	Loads and combinations.....	59
4.2	Research: hanger behavior .....	60
4.2.1	Explanation for extreme deformations and internal forces .....	61
4.2.2	Analytical description of hanger behavior .....	61
4.2.3	Cable - or beam action .....	62
4.2.4	Hanger relaxation (compressive forces).....	62
4.2.5	Validity of linear analysis .....	63
4.2.6	Catenary effect.....	63
4.2.7	Conclusion.....	64
4.3	Modeling.....	65
4.3.1	Modeling arch cross-section.....	65
4.3.2	Modeling deck and main girder stiffness .....	67
4.3.3	Modeling hangers .....	67
4.4	Design verification .....	69
4.4.1	ULS design verification arch.....	70
4.4.2	ULS design verification main girder.....	70
4.4.3	ULS design verification hangers.....	71
4.4.4	SLS design verification.....	71
4.5	Optimizing reference design .....	72
4.5.1	Conclusion.....	72
4.6	Optimizing network arch bridge.....	73
4.6.1	Dimensioning arch and main girder.....	73
4.6.2	Optimizing hanger diameter .....	73
4.6.3	Variant study: Removal of outer hangers.....	75
4.6.4	Conclusion.....	76
5	NONLINEAR ANALYSIS .....	77
5.1	Literature review: Geometrical nonlinear analysis.....	77
5.1.1	Mesh setup.....	78
5.1.2	Solver setup .....	78
5.2	Geometrical nonlinear analysis .....	79
5.2.1	Remarks on GNL analysis.....	82

5.2.2	Conclusion.....	82
5.3	Comparison between numerical and analytical results.....	83
5.3.1	Results in-plane of the arch (self-weight loading).....	83
5.3.2	Results out of arch plane (transverse wind loading).....	84
5.3.3	Results out of arch plane (transverse wind loading + imposed rotations).....	84
5.3.4	Conclusion.....	85
5.4	Comparison between linear and geometrically nonlinear results.....	86
5.4.1	Linear analysis in global design verification.....	86
5.4.2	Evaluation of linear cable behavior on force distribution.....	88
5.4.3	Conclusion.....	90
5.5	Effect of hanger relaxation on global stability.....	90
5.5.1	Lateral buckling of compressed hanger.....	90
5.5.2	Influence of hanger relaxation on the global stability.....	93
5.5.3	Conclusion.....	94
6	VERIFICATION STAGE.....	96
6.1	Stability verification (ULS).....	97
6.1.1	Global stability: buckling resistance of the arch.....	97
6.1.2	Conclusion.....	102
6.2	Fatigue verification hanger.....	103
6.2.1	Decisive hanger for fatigue loading.....	103
6.2.2	Geometrical and fatigue properties of hanger connection.....	104
6.2.3	Isolated model of hanger number 13.....	104
6.2.4	Damage due to traffic (LM71).....	106
6.2.5	Damage due to vortex shedding.....	111
6.2.6	Damage due to rain and wind induced vibrations.....	119
6.2.7	Total fatigue damage in hanger connection.....	123
6.2.8	Conclusion.....	123
6.3	Fatigue verification arch and main girder.....	125
6.3.1	Fatigue verification arch.....	125
6.3.2	Fatigue verification main girder.....	127
6.3.3	Conclusion.....	128
6.4	Global dynamic requirements.....	129
6.4.1	Conclusion.....	130
6.5	Hanger frequencies and structural vibrations (parametric excitation).....	131
6.5.1	Conclusion.....	132
7	COMPARING NETWORK ARCH TO REFERENCE DESIGN.....	133
7.1.1	Effective steel weight.....	133
7.1.2	Conservation.....	134
7.1.3	Final comparison score system.....	135

7.1.4	Conclusion.....	138
8	CONCLUSION AND RECOMMENDATIONS.....	139
8.1	Conclusions.....	139
8.2	Recommendations for future research.....	142
	REFERENCES.....	143
	ANNEX A: Network arch model description.....	145
A.1	Geometry.....	145
A.2	Cross-sections.....	145
A.3	Loads and combinations.....	145
	ANNEX B: Optimal hanger arrangement.....	149
B.1	Summary of the research by Teich.....	149
B.2	Determining the optimal hanger arrangement.....	149
	ANNEX C: Modeling.....	154
C.1	Modeling main girder and deck stiffness.....	154
C.2	Determining class 3 arch cross-section.....	156
	ANNEX D: Original tender design.....	157
	ANNEX E: Hanger behavior.....	166
E.1	Implementing hanger arrangement in the design.....	166
E.2	Comparing linear- and cable behavior.....	168
E.3	Reduced axial stiffness (catenary effect).....	173
	ANNEX F: Analytical model of hanger number 13.....	178
	ANNEX G: Influence of mesh refinement on internal hanger forces.....	184
	ANNEX H: Variant study outer hangers.....	188
	ANNEX I: Fatigue properties.....	193
I.1	Decisive hanger for fatigue verification.....	193
I.2	Fatigue resistance of hanger connection.....	196
I.3	Hanger connection according to guidelines DIN-Fachbericht 103.....	201
	ANNEX J: Natural hanger frequencies.....	205

# 1 INTRODUCTION

In the sixties a new type of bridge was built: the network arch bridge. Comparing this new bridge to ‘old’ arch bridges, the network arch bridge has several advantages: it has higher stiffness properties, lower bending moments, and as a result of that, less steel is required. Since the sixties about a 100 network arch bridges have been built all over the world. The network arch seems to be gaining popularity since the majority of those bridges was built in the last two decades. Even the German railway authority has recently accepted the network arch as an innovative alternative for arch bridges.



**Figure 1: Artist impressions of the arch bridge with diagonal hanger arrangement that will be built to cross the widened A1 highway (10 lanes)**

The research question of this thesis originates from a variant study for the optimal hanger arrangement of an arch railway bridge for a tender design. This railway bridge is part of an immense project to improve the infrastructure between Almere, Amsterdam and Schiphol airport for a total value of one billion euro. The bridge will cross 10 traffic lanes of the to be widened A1 highway with a total span of 255m. On the November 12<sup>th</sup> 2012 it was announced that the tender was won by SAAone, a combination of contractors and engineering firms (Volker Wessels, Boskalis, Hochtief, Royal HaskoningDHV and Iv-Infra).

In this variant study, three different hanger arrangements were investigated: vertical, diagonal and network. Finally after dimensioning the three types of bridges it was concluded that the network arrangement required the smallest amount of steel based on strength and stiffness. However, when comparing the three types at other design aspects, the diagonal hanger arrangement was preferred and chosen as final design. Why the network arch became second in the comparison is because of uncertainties about the following design aspects:

- The assembly of the hangers; how to obtain the desired force distribution
- Fatigue performance of the hangers
- Susceptibility to vibration effects, especially vortex induced vibrations
- The influence of compressive forces in hangers on the structural behaviour of the bridge

The conclusion of the variant study, which contradicts to the earlier named advantages of the network arch, raises the question whether the risks in these uncertain design aspects weren't overestimated. In order to investigate this, the following research question was developed:

'Is a railway arch bridge with a span of 255m more advantageous when the hangers are arranged as diagonals or as a network?'

## **1.1 Strategy**

In order to answer the research question, a competitive design of a network arch railway bridge is needed. During the design of this network arch bridge, the uncertain design aspects will be dealt with, in order to finally determine which design will be more advantageous. For a clear comparison the overall geometry of the bridge, along with the deck structure, should both be left unchanged.

In chapter one of this thesis the introduction to the subject and the strategy to answer the research question is given. This strategy divides the thesis into the following chapters:

### ***Chapter 2: Literature study***

During the literature study the preparation for the variant study and the design stage in chapter 3 and 4 are made. Background information and solution strategies for the dynamic and fatigue behavior of the hangers are essential. Reference projects are used to develop a strategy for the construction of the bridge, especially for the assembly of the hangers.

### ***Chapter 3: Variant study***

In the variant study the information found in the literature study is used to determine the basis for an optimal design. This is done by considering the design options at a qualitative level, by using a score system. The boundary conditions will be similar as used for the reference design: this way the final comparison will be clear and fair.

During this variant study extra attention will be paid to the problems with the fatigue and dynamic behavior of the hangers and the construction of the bridge, based on the background information gathered in the literature study.

### ***Chapter 4: Design stage***

In the design stage the modelling of the arch is reconsidered and where necessary adaptations are made. However, these adaptations should also be implemented in the reference design in order to maintain a fair comparison. Therefore the reference design is also optimized in the design stage.

### ***Chapter 5: Nonlinear analysis***

In order to evaluate the uncertain design aspects more accurate results are required. By using nonlinear analysis, the behaviour of the hangers is modelled quite accurately. In this chapter the effects of compressive forces in hangers are investigated to evaluate the risks on this design aspect.

***Chapter 6: Verification stage***

To insure that the competitive network arch is also realistic, some basic structural requirements are verified. The fatigue performance of the hangers and the susceptibility to vibration effects are evaluated in order to clarify the uncertainties about these design aspects.

***Chapter 7: Comparing network arch to reference design***

To determine if the network hanger arrangement is more advantageous than the diagonal hanger arrangement, a final comparison is made. The total steel weight and conservation surface are parameters that can simply be measured. The design aspects, especially those which were mentioned in the introduction, are quantified by assigning a score to each pro or con. Finally a conclusion is drawn on which hanger arrangement is more advantageous, thereby answering the research question.

***Chapter 8: Conclusion and recommendations for future research***

In this chapter the final results of the thesis are summarized. If by lack of time some questions are not investigated thoroughly enough these are given as recommendations for future research.

## 2 LITERATURE STUDY

The main objective of this literature study is to provide enough relevant information to make a competitive design of a network arch railway bridge. The literature study is also used to find relevant information regarding the uncertain design aspects which were mentioned in the introduction:

- The assembly of the hangers; how to obtain the desired force distribution
- Fatigue performance of the hangers
- Susceptibility to vibration effects, especially vortex induced vibrations
- The influence of compressive forces in hangers on the structural behaviour of the bridge

In the first paragraph of this literature study an historical overview of the historical development of the network arch is given in order to determine if a railway network arches with a similar span have ever been built before.

The second paragraph addresses aspects which are relevant for the preliminary design of a network arch.

In paragraph 2.3 aspects are given which are important for the detailed design of a network arch bridge. Special attention is paid to the abovementioned uncertain design aspects.

In the last paragraph of the literature study, the construction of a network arch is discussed. In this paragraph the construction of the hangers, and how to obtain the desired stress distribution is clarified.

## 2.1 Historical overview

The principle of the network arch finds its origin in the year 1878. In this year the first arch bridge with crossing hangers was built, as shown in Figure 2 on an old postcard.

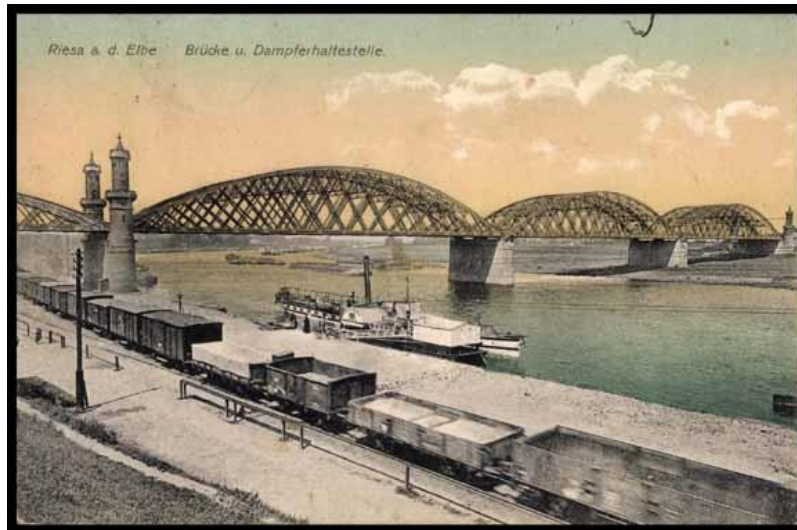


Figure 2: Postcard from Riesa a. d. Elbe (span 110m)

In 1926 the Danish engineer Octavius F. Nielsen patented the idea of a traditional arch bridge with hangers under an angle, and if necessary crossing each other, to create a net-like hanger arrangement. Around this period some 60 of these Nielsen-bridges have been built, but none of them had crossing hangers.

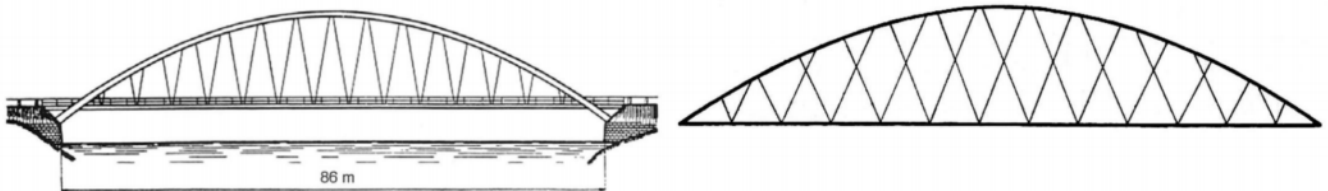
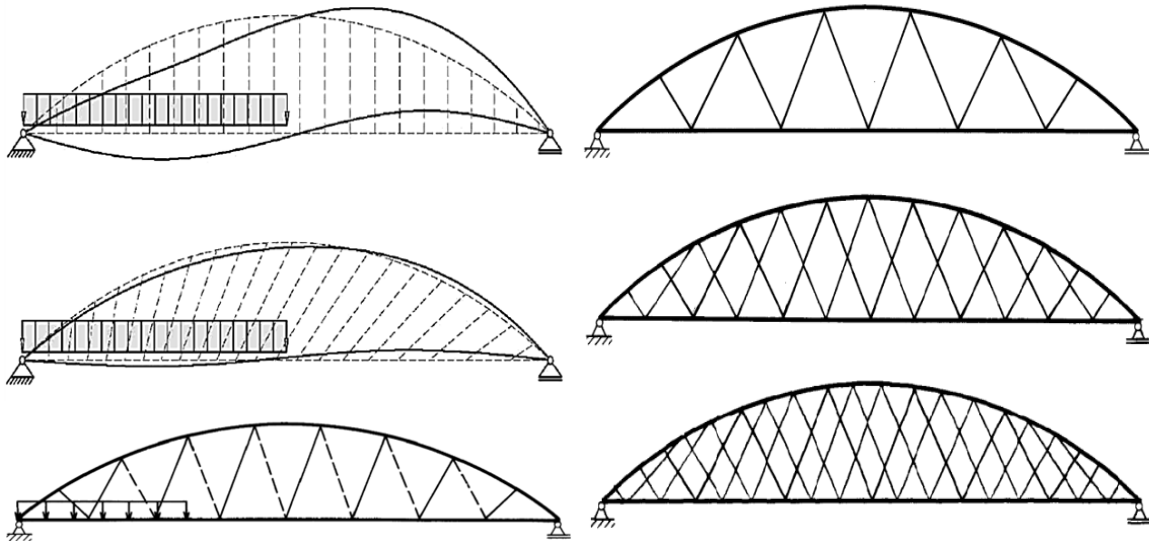


Figure 3: left: a Nielsen bridge, right: system lines from Nielsen's patent application in 1926

In the 1950's Professor Per Tveit (Norway) developed the concept of the network arch when he was investigating the bending moment distribution in Nielsen-bridges. He suggested that the bending moments could be reduced when the hangers cross each other multiple times. He described his idea in an article that was published in the June issue of "The structural engineer".

The force distribution of a (network) arch bridge can be compared to that of a simply supported beam. The arch and main girder take normal forces thereby acting as the flanges. The shear force is taken by the hangers that act as the web.

The main advantage of the network arrangement becomes clear in the load case "half load", as is shown in Figure 4. The classical arch bridge shows large horizontal deformations. As a result of that a large number of hangers in the unloaded part will become relaxed. This has disastrous consequences for the moments and buckling lengths of the arch and main girder, also the vertical deflections will be large.



**Figure 4: left: Different hanger configurations half span loaded, right: Composing a network arrangement by adding sets of diagonals**

When the hangers are gradually inclined the horizontal deflection will be significantly lower because the hangers in the unloaded part of the span remain tensioned.

The Nielsen bridge (diagonal hanger configuration) also works by the same principle, except that the opposite hangers will become relaxed (see Figure 4, the dotted lines represent the hangers susceptible for compression).

To counteract the problem of relaxation the inclination of the hangers can be increased and more self-weight can be added. With more slanting hangers the distance between the hanger nodes will also increase, resulting in larger bending moments in main girder and arch. For an optimal diagonal hanger arrangement, there are always concessions to be made. Either you accept larger bending moments without relaxing hangers or vice versa.

When an extra set of diagonals is added (see Figure 4) the distance between the nodes becomes smaller thereby reducing the bending moments in arch and main girder. When another set of hangers is added the distance becomes even smaller. This process illustrates the principle behind the network arch bridge: by adding sets of diagonal hangers to the arrangement a network arrangement is obtained, which has overcome the disadvantages of a diagonal arrangement.

The first arch bridge with multiple crossing hangers was designed by Per Tveit and was built in 1963 in Steinkjer in Norway spanning 80m, see Figure 5.



**Figure 5: Network arch at Steinkjer (left) and Bolstadstraumen (right)**

In that same year another two network arches were constructed. The Bolstadstraumen bridge spanning 84m was also designed by Per Tveit and built in Norway (Figure 5). Also the Fehmarnsund bridge in Germany spanning 248m (Figure 6). The Fehmarnsund bridge is clearly a class bigger than the two Norwegian bridges, not only in span, but also in load carrying capacity. This bridge accommodates two road lanes and a single railway track.



**Figure 6: Fehmarnsund bridge**

Until the 80's no network arches are built in Europe. However, thanks to a Japanese professor who was involved in the design of the Fehmarnsund bridge, the idea travels across the globe to become popular in Japan. In 1968 the first Japanese network arch is constructed. In Japan this bridge is called Nielsen-Lohse bridge after the original inventors. The 'Lohse' part of the name applies to the principle of the tied arch. This principle was invented by a German railway engineer Hermann Lohse who developed the 'Lohse-girder'. The Lohse-girder makes use of a tensile element in the deck to counteract the compression forces in the arch. Since 1968 over 50 Nielsen-Lohse bridges have been built in Japan, see Figure 8 for some spectacular designs.

Worldwide, over a hundred network arch bridges have been built based on an overview of the existing network arches [www.network-arch.com]. In the Netherlands two network arches have recently been constructed. In August 2012, the first Dutch network arch was transported to its final location crossing the Twentekanaal near Zutphen. In April 2013, the Oversteek bridge spanning 285m was moved into position.



**Figure 7: left: Network arch spanning Twentekanaal, right: de Oversteek, Nijmegen**



**Figure 8: Overview of Japanese Nielsen-Lohse bridges (from upper left- to lower right corner:Shinhamadera bridge (254m), Goshiki-sakura bridge (143m), Ounoura bridge (195m), Triceps bridge (131m), Mac Arthus Second bridge (210m))**

When looking at the year of construction in the overview of existing network arches it becomes clear that the network arch is gaining popularity. This shows that 30% of all the network arches are built in the last decade. Also the German Railway authorities (Deutsche Bahn) have recently adopted the network arch bridge in their ‘railway bridge design guide’ as an innovative alternative for classic arch bridges.

The rising popularity could be explained by the development of the engineering software. Because of the absence of computers in the early days of Nielsen-bridge engineering the hangers were placed under constant angle. This significantly simplified the calculation process. For this reason, the first Japanese network arches were built also with hangers under constant angles.

For an overview of the span range for which the network arch bridges are mostly applied see Figure 9. This graph is based on roughly 70% of the network arches ever built, so the numbers aren’t accurate but show clearly the most popular range, and most popular traffic type.

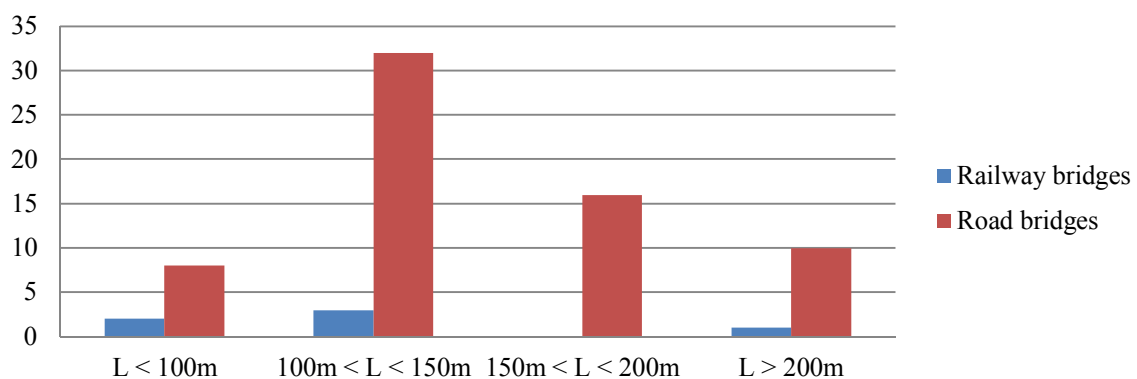


Figure 9: Global overview of span ranges based on  $\pm 70\%$  of network arches [www.network-arch.com]

## 2.2 Preliminary design of a network arch

In this chapter the design of the railway network arch bridge is discussed and guidelines or examples are given. For a systematic design process the bridge is divided into separate elements:

- Arch
- Lateral bracing
- Main girder
- Deck
- Hangers

The aspects mentioned in this paragraph can be used for an efficient determination of a preliminary design, or in a variant study.

### *Conceptual choice*

Geißler et al. [7] determined the following span range for economic application of network arches. These ranges correspond to the overview of network arches already built (Figure 9).

- Road bridges (LM1) 55m – 300m
- Railway bridges (LM71 met  $\alpha=1,0$ ; SW/2) 80m – 300m

Per Tveit [3] gives the following conditions for which network arches will also provide an economic solution:

- Bridges for which high stiffness is needed.
- Areas with bad soil conditions, network arches are beneficial because of light weight.
- Areas where labor is cheap compared to material cost. Because of low steel weight and relatively high number of connections.
- Bridges crossing water, here the bridge can be completely lifted into place.

### 2.2.1 Arch and lateral bracing

The structure of an arch bridge is generally built up by 2 arches connected with lateral bracing to provide horizontal stability. All kinds of arch variations have been developed over the years see Figure 10. The choice of the arch cross section and the type of lateral bracing mostly depends on their appearance but other factors that have a big influence are:

- Span length
- Required stiffness



Figure 10: Single arch, double arch, basket handle arch (left to right: De oversteek bridge, Bolstadstraumen bridge, Fehmarnsund bridge)

#### Span length

Per Tveit [3, 4, 5] recommends a standard H-profile to be applied for spans up to 100m. This would provide the most economical solution for double arches because of simple fabrication and relatively simple hanger connections see Figure 11. With larger spans a box-section would become more economical, because of the higher bending- and torsional stiffness. Other examples of arch sections are: hat- or tubular-section.

Other advantages of fabricated sections are that a variable cross section can be applied, leading to a more economic cross section. For instance, the required stiffness in plane of the arches could be much less than out of plane, leading to material savings.

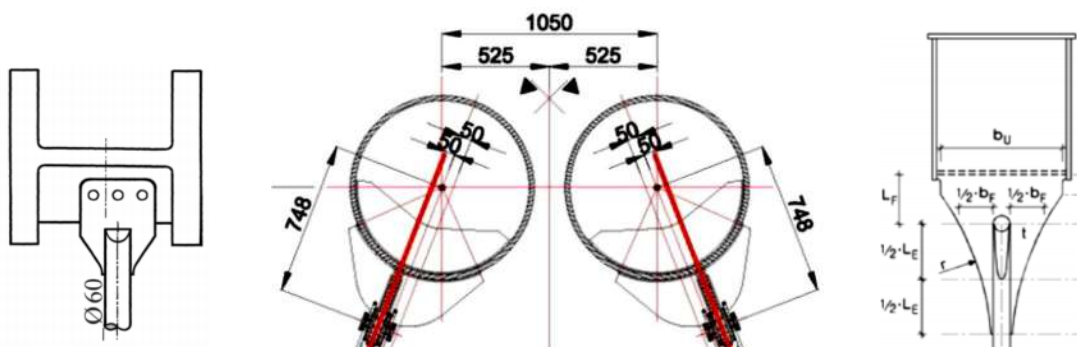


Figure 11: Examples of arch cross sections with hanger connections



Figure 12: Arches (left: arch element (Oversteek bridge), right: Palma del Rio bridge)

### ***Required stiffness***

Compared to vertical or diagonal hanger arrangements, the network arrangement provides more support in plane of the arch. This allows the arches of a network arch to be more slender. When considering the out-of-plane stiffness, no differences are found between vertical and diagonal hanger arrangements. The type and size of lateral bracing determines the out of plane stiffness. Regular solutions for lateral bracing are shown in Figure 13. Also a combination between basket handle shape and lateral bracing is possible, which leads to large horizontal stiffness.



Figure 13: lateral bracing (left: K-truss, middle: diamond truss, right: Vierendeel truss)

#### **2.2.1.1 Guidelines for design of arch and lateral bracing, according to Teich**

In the research performed by Teich, a large number of parameters is investigated to determine their influence in the force distribution in the arch. Eventually for all parameters optimal values are determined. Based on these optimal values a design guide is developed that leads to optimal arch design [1]. In this paragraph a brief evaluation of the results of the research is given for each of the following parameters:

- Hanger arrangement
- Number of hangers
- Type of lateral bracing
- Cross section of the arch
- Stiffness of the portal frame
- Arch geometry

### ***Hanger arrangement***

The hanger arrangement is of great influence on the stress distribution in the arch. Under perfect conditions the arch is fully supported in plane by the hangers. When a situation arises where some hangers become relaxed, these hangers stop supporting the arch. This could cause global instability. For more about the optimal hanger arrangement see paragraph 2.2.4.2.

### ***Number of hangers***

The amount of hangers per arch plane has a significant positive influence on the force distribution in the arches. However this influence gradually decreases. For that reason the number of hangers will not be of decisive influence for the design of the arch. In general it is concluded by Teich [1] that the maximal amount of hangers should not exceed 50 because their efficiency reduces significantly above 50.

### ***Type of lateral bracing***

When deciding on the type of lateral bracing the general conclusion can be drawn that trusses have a positive influence on the stability of the arch, along with basket handle type arches. The Vierendeel frame (frame with rigid connections) has less favorable properties, but is easier to erect.

### ***Variable cross-section***

Teich investigated the influence of the width, height and plate thickness of the arch along the length of the span. Variable dimensions often result in a complicated production and engineering process. For that reason Teich advises to use variable plate thicknesses. For guidelines and more accurate possibilities for the reduction of the arch cross-section see [1].

### ***Arch geometry***

The form of the arch mainly influences the normal force distribution in the arches. Teich concluded that two specific arch forms have significantly better properties with respect to normal force distribution. The favored forms are shown in Figure 14 and can be described as, elliptical arch and arch with double radii. For both arch forms it is concluded that the optimal ratio between both radii is 1,9.

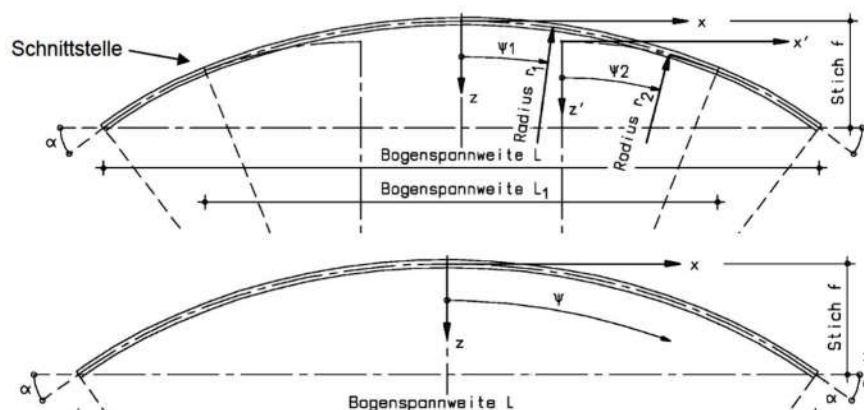


**Figure 14: Above: arch with double radii, below: elliptical arch**

The height of the arch mainly influences the magnitude of the normal force in the arch and main girder. This is no different from classical arch bridges. For that reason the height of the arch bridge is based upon the experiences with other network arch bridges: 1/5 to 1/7 of the span length. The advantage of this approach is that an aesthetical component is automatically included.

## 2.2.2 Main girder

The main girder transfers the loads from the deck to the hangers and counteracts the horizontal thrust that is created by the arches. The intermediate distance between the hangers dictates the required bending stiffness. Because the amount of hangers in network arches is a lot higher than in arch bridges with vertical and diagonal bracing, the intermediate distance is shorter. This results in a more slender main girder.

In the existing network arches, the main girder has been designed as: concrete slab, composite girder, steel I- and box-girder. All these designs have proven to be functional. But when considering execution, hanger connections and efficient material use, the best solution for a main girder would be a steel profile [7]. Depending on the type of loading, a suitable cross section can be selected. For instance, in single track railway bridges no torsional rigidity is necessary, so an I-section is sufficient.



Figure 15: Examples of concrete main girders and hanger connections (left: Trinec-Baliny Road bridge, right: Troja bridge in Prague)

The stiffness of the main girder hardly influences the overall force distribution in the bridge. Geißler et al. [7] recommend a stiffness ratio of  $EI_{\text{arch}}/EI_{\text{main girder}} = 1/8 \dots 1/10$ . Teich uses a stiffness ratio of  $1/3$  in his research. This large difference in ratio supports the statement that main girder stiffness influences the overall force distribution.

To connect the hangers to the main girder, stiffening plates or cable anchorages (see Figure 15) should be incorporated in the design. An efficient solution is to connect the hangers directly to the web of the I- or box-section as is shown in Figure 15. This of course has aesthetic consequences, but eliminates the need for extra stiffening plates (diaphragms).

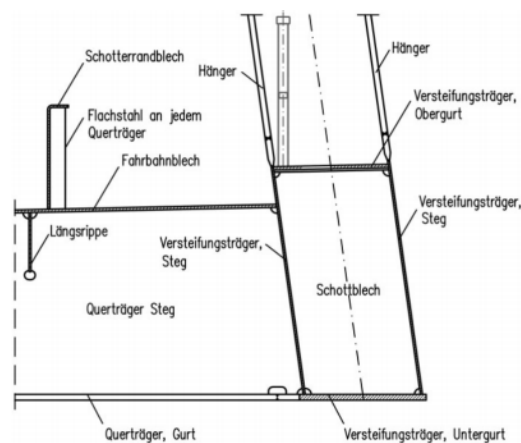


Figure 16: Design of box-shaped main girder with hanger connections directly welded to the web

### 2.2.3 Deck

The deck should accommodate pedestrian, bicycle, road or railway tracks. In some cases an additional service track is also required. The service track could also be placed on top of the main girder or outside the arch planes by means of consoles connected to the main girder. This leads to a reduction in deck width with significantly lower bending moments as a result. For examples and guidelines for the design of a bridge deck, reference is made to [4], especially for railway bridges.

In general the heavier bridge decks are preferred [4], especially for road bridges. This is because of the better sound and fatigue properties. Disadvantages are the extra weight, construction time and the specific disciplines required. Eventually all parameters should be considered to find the optimal deck structure.

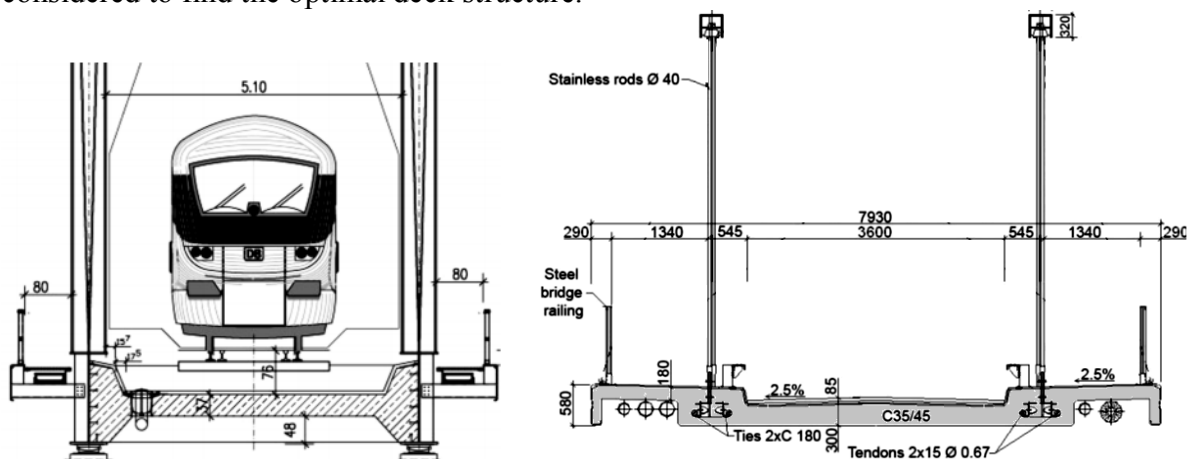


Figure 17: Concrete deck (left: Railway bridge over B6 [7],right: Bechyně roadbridge in Czech Republic)

#### *Concrete deck*

According to Per Tveit the most economic network arch is one with a longitudinally prestressed concrete slab (see Figure 17 right). In this design the deck and main girder are merged together and the tensile force is taken by the pre-stressing tendon. The main disadvantage of a full concrete deck is the need for temporary supports and scaffolding. A solution is to apply a full concrete deck in combination with a steel main girder as is shown in Figure 17 (right). A more exceptional method is used in the construction of the Troja bridge in Prague. Here precast and prestressed beams are used as cross girders in combination with a prestressed thin deck slab, see Figure 18.

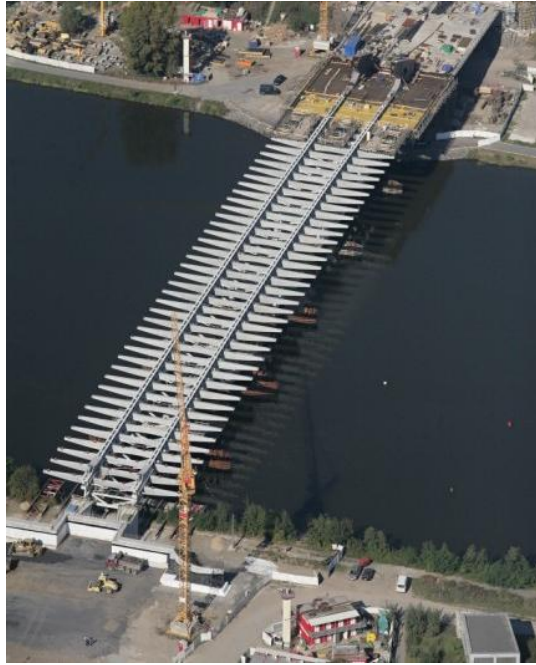


Figure 18: Special prefabricated concrete deck cross-girders of the Troja bridge in Prague [17, 18]

### Composite deck

When time, deck-height, and weight are of minor importance, a composite deck can be applied. The advantage of this deck configuration is that the additional weight causes better noise reduction properties and also could prevent the relaxation of hangers. The disadvantage is that extra time is required for the casting and hardening of the concrete.

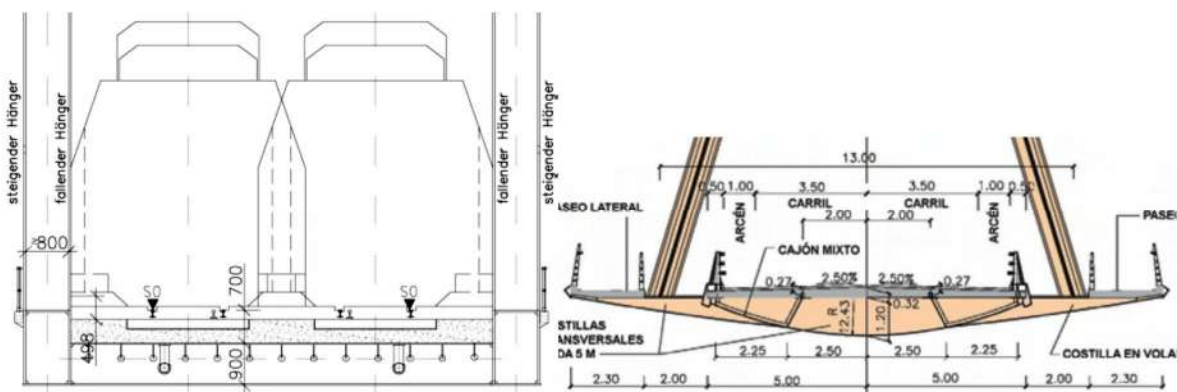


Figure 19: Composite deck (left: composite deck design [7], right: Rio Deba bridge in Spain [16])

### Steel deck

The main advantage of a steel deck is the short erection time and the possibility for prefabrication. A large weight reduction is achieved compared to concrete bridge decks. Disadvantages are: higher noise production, fatigue sensitivity of the deck and the extra maintenance when compared to concrete decks.

The deck plate is composed as an orthotropic deck with cross girders spaced every 2,5m. The tension force of the arches is taken by steel beams in longitudinal direction. When a full steel deck is applied, provisions for noise reduction have to be made.

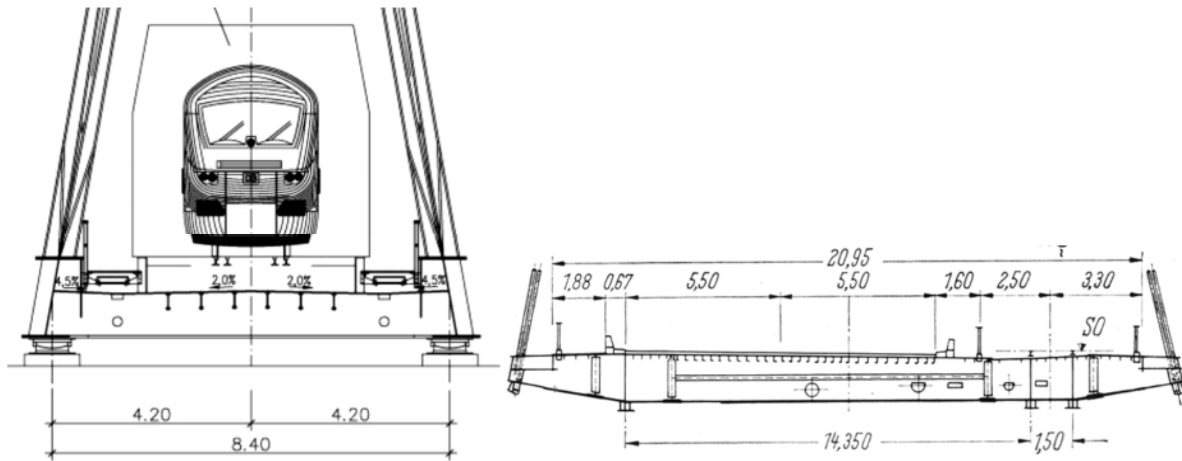


Figure 20: Steel deck (left: Flora bridge in Germany, right: Fehmarnsund bridge in Germany)

## 2.2.4 Hangers

When considering the hangers, two main design considerations must be made; hanger type and hanger arrangement. Both aspects have a large influence on the structural behavior, but also the costs and aesthetics of the bridge.

### 2.2.4.1 Hangertype

Based on the literature reviewed, three different hanger types are assessed in this paragraph. For each of the hanger types the following aspects are considered:

- Costs
- Connection type
- Aesthetics
- Vibrational effects

#### *Steel strip hangers*

This type has, up to now, only been applied in German network arches, specifically railway bridges [7]. The main advantage of this hanger type is the relatively simple hanger connection. This is done by supporting and aligning the strips before connecting them by a simple butt weld. This results in good fatigue performance. For more about the construction method see paragraph 2.4.



Figure 21: Flat steel hangers (left: unknown bridge, right: Rosenbachtal railway bridge)

Another advantage is the availability of steel strips. These are cut from steel plates and can be delivered in almost any size, length and steel grade, this results in a relatively cheap hanger type. One major aesthetical disadvantage is the rough mesh that is created by the relatively large strips. The vibrational effects that could affect these rectangular cross sections are:

- Flutter
- Galloping
- Vortex-shedding
- Structural vibrations (parametric excitation)

### ***Steel rod hangers***

The steel rod hangers can be connected in two different ways: by means of welding or with the use of special connectors, as is shown in Figure 22. For welded hanger connections, the same advantages as for strip steel hangers could be achieved. Except that the connection plate requires careful fabrication, in order to achieve the same fatigue performance.

When the steel rods are connected by bolts or connectors, a hanger stressing procedure is required. See paragraph 2.4 for more information. Steel rod hangers have good fatigue properties.

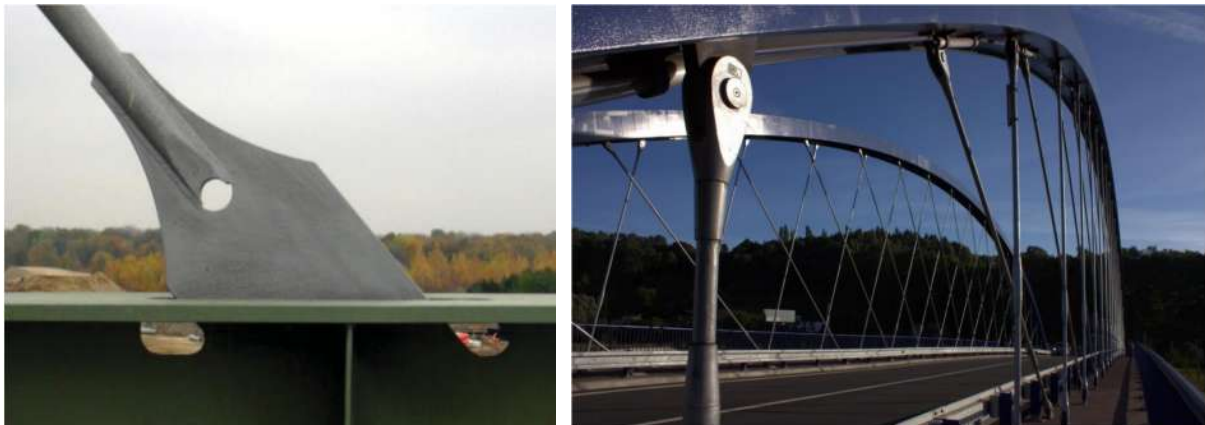


**Figure 22: Massive rod hangers (left: welded connection, right: fork connector)**

Steel rods in combination with welded connections can lead to relatively cheap hangers. Compared to strip steel they are less economic, because rods have a maximum length of 13m. This means that for longer hangers special coupling welds are necessary. When steel rods are used in combination with special connection elements, the price is assumed to be higher, because high quality products are used. The vibration effects that could affect steel rod hangers are:

- Vortex shedding
- Rain and wind induced vibrations
- Structural vibrations (parametric excitation)

### ***Cable hangers***

Cables can be connected by special anchorages which are fixed to the structure (see Figure 22), or by a set of adjustable fork connectors, as shown in Figure 23. Both cable systems require a stressing protocol for the assembly of the hangers. For cable systems, three types of cables are available: locked coil, spiral strand and parallel strand. The parallel and spiral strand types need an additional protective duct that encases the whole bundle. This bundle of wires is connected to the bridge through an anchorage device, see Figure 16 and Figure 27. The locked coil strand

is a combination of parallel wires that form the core with outer rings of interlocking Z-shaped wires, providing corrosion protection (see figure Figure 24)



**Figure 23: Fork connectors for cable systems, left: Freyssinet fork connector for parallel strand cable, middle: fork connector for spiral strand**

The vibrational effects that could affect cable hangers are the same as for steel rod hangers, because both hangers have circular cross sections. The costs for a cable system will be relatively high because of the extremely high yield strength and the specialized hanger connections.

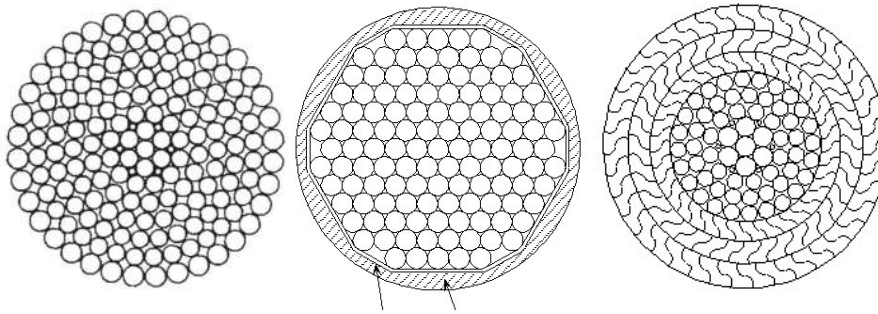


**Figure 24: Cable types (left: spiral wire, middle: parallel wire, right: locked coil)**

#### 2.2.4.2 Hanger arrangement

An optimal hanger arrangement could seriously enhance the structural performance of the bridge. S. Teich [1] developed a guideline to determine the optimal hanger arrangement. This is the most recent and extensive research on optimal hanger arrangements performed up to now.

The arrangements are optimized for the following structural parameters:

- Reducing the bending moments in arch and main beam
- Sufficient resistance against hanger relaxation (compression)
- Equal force in all hangers and optimal utilization of the cross section
- Reducing maximum forces in hangers and thereby reducing the cross section
- Reducing the force variation in the hangers to improve fatigue resistance
- Aesthetic appearance of the bridge

The results of this research are translated into a step by step design guide. Based on the number of hangers and the length of the span, three optimal arrangements are given. These combinations are all provided with a score to indicate their structural performance. The guideline does not provide any insight in the magnitude of the optimized structural behavior. It is therefore impossible to generate a hanger arrangement for which only one structural parameter is optimized.

All optimal arrangements obtained by the guideline result in no hanger relaxation in the SLS. In the ultimate limit state, hanger relaxation is almost inevitable.

For this research a double track railway load was used, represented by load model 71 (LM71). This load was applied on a full steel network arch. For a more detailed description of the network arch that was applied, see [1].

### ***Number of hangers***

To determine the amount of hangers, Teich advises not to use more than 50 hangers. In Teich's design guide, also guidance is given to determine the number of hangers. But a trade-off has to be made between costs per hanger and efficiency.

### ***Basic hanger arrangement***

Teich investigated 5 basic hanger arrangements, as shown in Figure 25. Two of these arrangements show bad structural performance. These are; constant angle Figure 25 (1) and the increasing angles (3).

The results are presented in a table and the best performing basic hanger arrangement is given the score 100. Based on the scores the differences between arrangements are showed. The final choice of basic hanger arrangement depends mostly on the score but also aesthetics should be considered. Generally hanger arrangement 4 provides the best structural performance, followed by arrangement 2. However, the differences between both types are sometimes negligible.

The optimal force distribution does not apply for the most outer hangers. These have to be configured manually. For more background information on the arrangement type, see the full research by Teich [1].

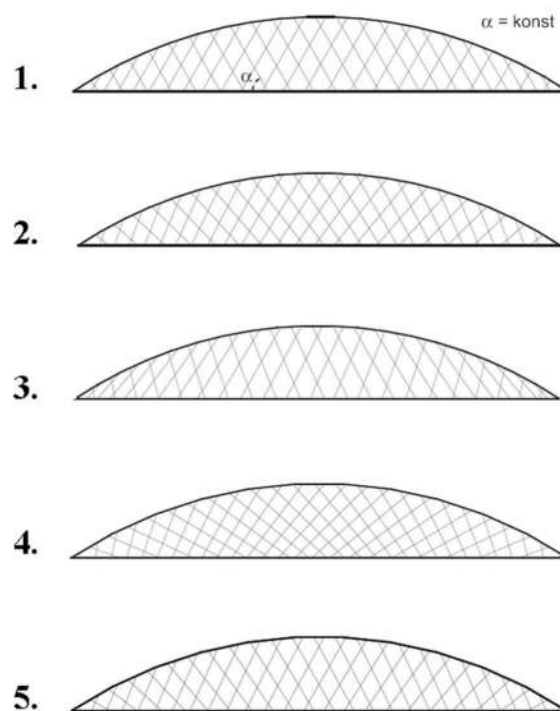


**Figure 25: Overview of basic hanger arrangements investigated by Teich. 1: constant angle, 2: decreasing angle, 3: increasing angle, 4: radial, 5: equal distance along main girder**

### 2.2.5 Conclusion

The following aspects were concluded from the literature review on the preliminary design of a network arch bridge:

- Economic range for the application of a network arch:  
Road bridges (LM1) 55m – 300m  
Railway bridges (LM71 met  $\alpha=1,0$ ; SW/2) 80m – 300m
- If the guidelines provided by Teich [1] are used to determine the hanger arrangement, no hanger compression/ relaxation will occur in the serviceability limit state (SLS). Furthermore the hanger arrangements are optimized on structural performance.
- The maximal amount of hangers should be limited to 50 per arch plane. When more than 50 hangers are applied, the efficiency of the extra hangers reduces significantly.
- An elliptical arch form and a double radii arch form result in the most efficient force distribution.
- The stiffness of the main girder has a negligible influence on the overall force distribution.
- The network hanger arrangement provides a large amount of support to the arch and main girder. This generally results in a relatively slender arch and main girder.

## 2.3 Detailed design of a network arch

In order to guarantee the structural safety of the bridge, the design has to be verified according to the Eurocodes. Some general design aspects are discussed, these are mentioned in paragraph 2.3.1. Furthermore special attention is paid to the uncertain design aspects mentioned in the introduction:

- The assembly of the hangers; how to obtain the desired force distribution
- Fatigue performance of the hangers
- Susceptibility to vibration effects, especially vortex induced vibrations
- The influence of compressive forces in hangers on the structural behaviour of the bridge

### 2.3.1 Global static analysis

The network arch is statically indeterminate to a high degree. This means that extra attention should be paid to the actual stiffness properties of the bridge because these have a large influence on the internal force distribution. Elements which must be considered carefully are:

- Hangers, the force distribution in long and slanting hangers could be affected by the catenary effect which decreases the stiffness [7].
- Arch- main girder connection, stiffness is of great influence in overall stress distribution [18].

Because non-linear analysis should be performed, the different load cases cannot simply be combined according to the principle of superposition. This means that decisive load combinations should be compiled with the use of influence lines.

Non-linear analysis should also be performed for all the construction stages and transportation steps [8].

The in-plane stability performance of network arches is generally better than classical arch bridges. This is due to the supporting effect of the hangers, provided that an optimal hanger arrangement is chosen were no hanger relaxation will occur, for more about an optimal hanger arrangement see paragraph 2.2.4.2. Special attention should be paid to the in- and out-of-plane stability when a variable arch cross-section is applied [1].

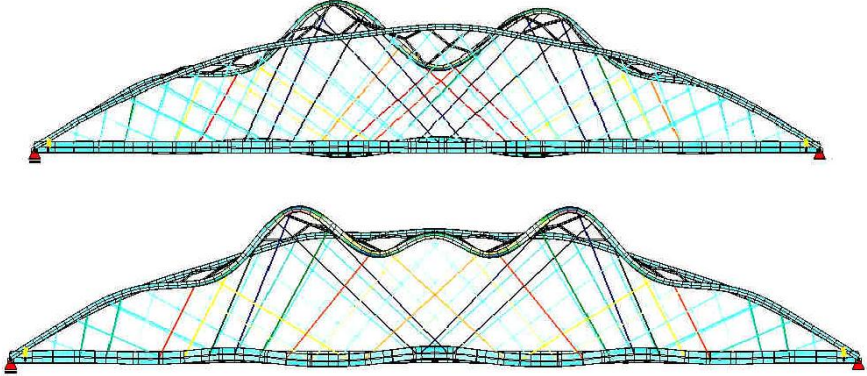


**Figure 26: Difference in buckling shape between constant (above) and variable (below) cross-section**

**2.3.2 Fatigue performance of the hangers**

Due to deflection of the main girder, small bending moments are formed at the connections. These bending moments are low, but because the bending moments are fully reversal the influence on fatigue life can be significant.

Hangers with fork connectors are not affected by this effect because the connections are fully hinged. For hangers with rigid connections, these bending moments should be evaluated by nonlinear analysis. For the anchorages of a parallel strand wire (fixed anchorage), Freyssinet has equipped the anchorages with so called “filtering guide/stuffing box” (see Figure 27) which ensures the fatigue resistance against these bending moments.

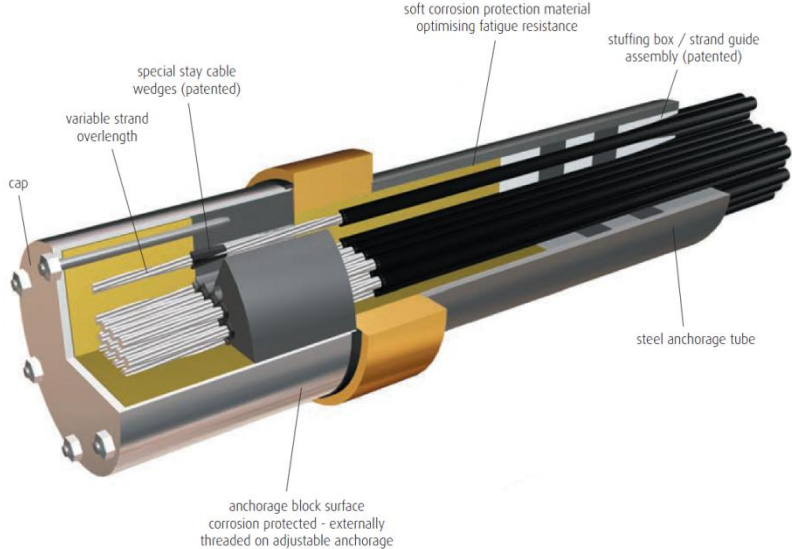


**Figure 27: Cable anchorage (Freyssinet) with bending fatigue resistant solution**

### 2.3.3 Hanger stressing procedure

When cable or tension rod systems are used, the desired stress distribution should be acquired by stressing the individual hangers. The difficulty of this procedure lies in the fact that the network arch is internally statically indeterminate. This means that the force in one hanger influences the neighboring hangers to a large extent. Another effect that complicates the stressing procedure is that the hangers are affected by the catenary effect. This nonlinear effect influences the stiffness.

In order to obtain an insight in the internal force distribution of the network arch, an influence matrix of the entire structure should be composed. [25, 26]

### 2.3.4 Compression in hangers

According to Gauthier and Krontal [8] some compression can be allowed in the hangers. If compression occurs in the shortest hanger, in the ULS, a buckling analysis should be performed. When compression or relaxation occurs in longer hangers it should be investigated how the forces are redistributed over the neighboring hangers.

When the optimal hanger arrangement is determined according to the guidelines provided by Teich, no compression will occur in the SLS. For more about this optimal arrangement see paragraph 2.2.4.2.

### 2.3.5 Hanger vibrations

A common problem with large cable structures, for instance cable stayed bridges, suspension bridges and arch bridges, is vibrations of the cables. These vibrations mostly cause fatigue damage and disturbance for the users. Network arches are even more sensitive for these phenomena, because of their length. The following vibrational effects can occur in cable-like elements according to the European norm [23].

- Galloping
- Flutter
- Vortex shedding
- Structural vibrations (parametric excitation)
- Buffeting
- Wind- rain induced vibrations
- Wake galloping

If one of the vibration effects mentioned is likely occur, a fatigue analyses has to be made. If the fatigue life is insufficient, damping provisions have to be made. Before these damping provisions are applied, in situ measurements are performed. According to [8] it's almost impossible to make a design with sufficient fatigue resistance, especially for the longer hangers. This is mainly caused by the strict value that is prescribed by the DIN for the structural damping.

In order to design for these effects, some structural properties are of large influence. Some of these properties can be influenced in the design phase, within certain limits. The structural properties with a large influence in the susceptibility for vibrations are:

- Natural frequency [ $n_i$ ]
- Scruton number [Sc]
- Logarithmic structural damping decrement [ $\delta_s$ ]

### ***Natural frequency***

The natural frequency depends on many factors but the length has the largest influence. In general: hangers with high eigenfrequencies are less susceptible for vibrational effects. According to the German codes, only hangers with an eigenfrequency below 10 Hz have to be verified for vibrational effects.

### ***Scruton number***

The susceptibility of vibrations depends on the Scruton number. This number expresses the structural damping and the ratio of structural mass and fluid mass. When the Scruton number exceeds a value of 20, no vibrations will occur [21]. A high logarithmic structural damping decrement and high density of the hanger material lead to large Scruton numbers.

### ***Logarithmic structural damping decrement***

The ability of the structure to damp oscillation, is quantified in the logarithmic structural damping decrement. The higher this value, the better damping performance. Depending on the type of structural element, a damping value can be found in the NEN-EN 1991-1-4 table F.2. In some bridges the Eurocode had overestimated the structural damping which led to vibrations. An example is the Demka bridge, the structural damping was overestimated by a factor 3. This was found out after in-situ measurements after vibrations had occurred. The former German code DIN-FB103 advises to use an absolute bottom structural damping value in the design stage [2]. By underestimating the structural damping a safe design is obtained.

#### **2.3.5.1 Galloping**

Galloping occurs when wind flows under a certain angle with the cross section. This causes an extra resulting wind force in vertical direction, as is shown in Figure 28e (component  $F_y$ ). When this force occurs at a certain interval close to the natural frequency, a vibration is produced.

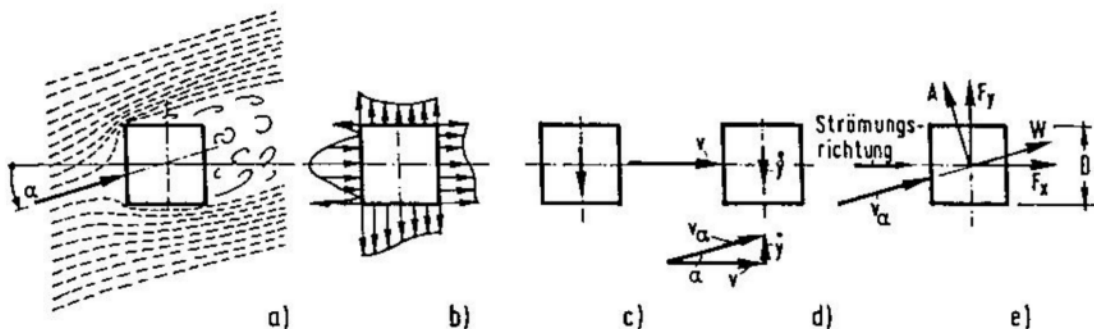


**Figure 28: Principle of galloping**

To prevent galloping from occurring, the following criteria given in E.2 of [22] must be satisfied. High Scruton numbers and high natural frequencies lead to higher galloping resistance. Rectangular cross sections are most vulnerable for galloping and in [2] a specific width over thickness ratio is given, which has proven to give good galloping resistance. From physical point of view, galloping cannot occur in circular cross sections because of the circular symmetry. When ice is formed on the cables or rods, the circular symmetry is lost and galloping could occur. According to DIN-FB103 circular cross-section do not have to be designed for galloping.

### 2.3.5.2 Flutter

Flutter is a self-induced vibration that is set off by the same principle as galloping. The difference between galloping is that besides a vertical vibration, also a torsional vibration occurs. The vertical force resultant creates a torsional bending moment along the longitudinal axis of the element, this sets off the torsional vibration. An infamous example of flutter is the Tacoma Narrows bridge.

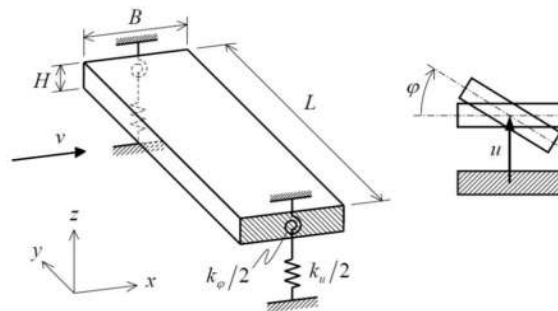


Figure 29: Mathematical model of the flutter phenomenon

The wind speed at which flutter occurs is linked to the difference between the bending and torsional frequency. The more these are apart, the higher the wind speed needs to be to cause flutter. Only rectangular cross-sections are susceptible for flutter. To avoid flutter some of the criteria's mentioned in [NEN-EN 1991-1-4 A2.3.7] have to be respected.

### 2.3.5.3 Vortex-shedding

Vortex induced vibrations occur when vortices are shed from both sides of a structural element. When this shedding occurs at the same frequency as one of the natural bending frequencies of the structural element, vibration will occur. These vortices cause a loading on the structural element perpendicular to the wind direction. Vortex shedding can occur in all structural elements independent of their cross section. The frequency at which the vortices are shed depends on the wind velocity, this is called the critical wind velocity. An additional effect arises when the vortex shedding frequency synchronizes with the natural frequency. This is called the locked-in effect and causes that the vortex shedding range expands up to 1,5 to 2 times the critical wind velocity.

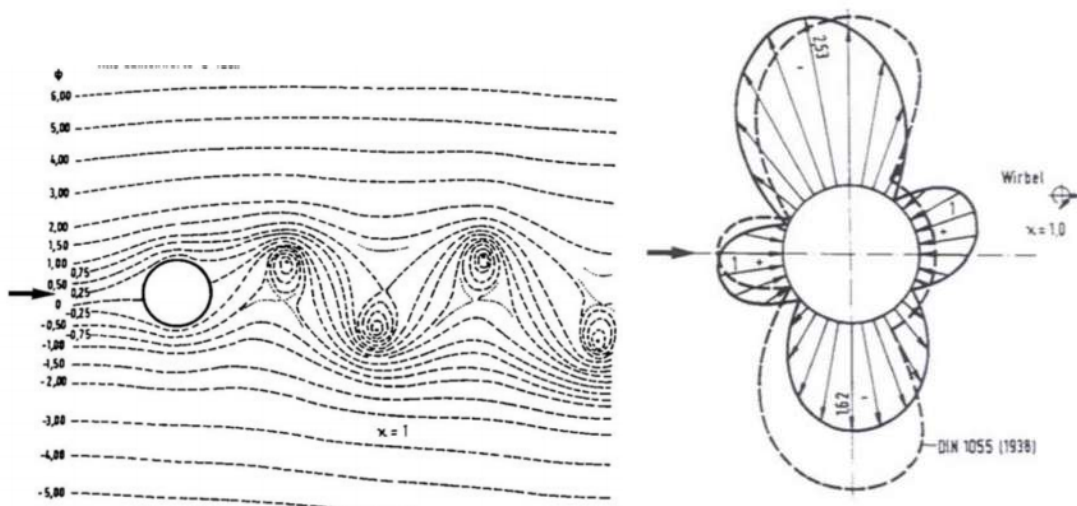


Figure 30: left: Von Karman vortices, right: external pressure on circular cross-section due to the shedding of vortices

The phenomenon vortex shedding has caused large vibrations in some of the Dutch arch bridges for which damping provisions had to be installed. See paragraph 2.3.5.8 for more about damping provisions.

To evaluate if a structural element is susceptible for vortex induced vibrations the following criterion should be met:

$$v_{crit,1} = \frac{b \cdot n_{t,y}}{St} > 1.25v_m$$

In the article by Vrouwenvelder and Hoeckman [13] another criterion is given for which vortex induced vibrations do not have to be considered:

$$Sc = \frac{2\delta_s \mu}{\rho b^2} > 20$$

This criterion depends for a large amount on the structural damping ( $\delta_s$ ) for which no accurate values can be determined at the design stage.

**2.3.5.4 Rain and wind induced vibrations**

Rain and wind induced vibrations can occur in hangers with circular cross-sections at a certain intensity of wind and rain combined. The raindrops land on the topline of a cable or rod and move down along the outer perimeter. The raindrop causes wind drag which results in a drag force. As the drops move along the outer perimeter, the direction of the drag force changes and a vibration is induced. This effect was found in the cables of the Erasmus bridge. With additional dampers these vibrations were eventually prevented. At wind velocities between 8 to 30 m/s, large vibrations can occur. Only inclined hangers are sensitive for these vibrations [2].

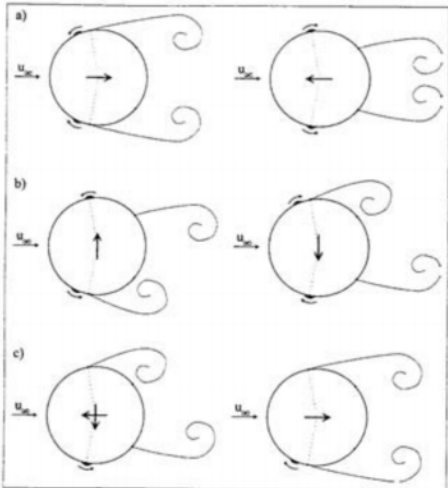


**Figure 31: Alternating force resultants in the hanger that occur due to rain- wind induced vibrations**

DIN-FB103 [2] provides a method to calculate the effects of rain and wind induced vibrations. This phenomenon is then considered as an accidental load case, for which the ULS strength and the fatigue damage can be calculated. According to DIN-FB103 rain and wind induced vibrations will only occur in circular cross-section with diameters larger than 70mm and an natural frequency lower than 6,5 Hz.

### 2.3.5.5 Structural vibrations (parametric excitation)

Structural vibrations, also known as parametric excitations, are vibrations which are caused by deformation or vibrations of the overall structure, for instance caused by the passing of a train. In order to design for structural vibrations the natural frequencies of the structure and hangers must be calculated.

NEN-EN 1993-1-11 gives criteria through which the susceptibility for structural vibrations can be assessed. The fundamental frequency of the hangers should be  $\pm 20\%$  apart from the fundamental bending frequency of the bridge. Even two times the hanger frequency should be considered. This is formulated in the following criteria:

$$0,8 \cdot n_{hanger} < n_{structure} < 1,2 \cdot n_{hanger}$$
$$0,8 \cdot n_{hanger} < 2 \cdot n_{structure} < 1,2 \cdot n_{hanger}$$

### 2.3.5.6 Buffeting

Buffeting is caused by turbulence in the oncoming wind. This is often caused by obstacles in the surroundings. In the European codes a formula is given to determine the effect of the turbulence. However, when looking at the experiences with existing network arch bridges, no vibrations caused by buffeting are mentioned.

### 2.3.5.7 Interference galloping

Interference galloping is exactly the same phenomenon as galloping, only this is caused by a turbulent oncoming wind flow created by a nearby hanger. This type of vibration can produce large excitations because it is self-induced.

NEN-EN 1991-1-4 provides safe design criteria for this phenomenon however, there have been no reports of interference galloping found in the literature reviewed.

### 2.3.5.8 Suppression of vibrations

If calculations show that vibrations are likely to occur, in-situ measurements should be performed to confirm the calculations. For instance, when the structural damping measured in-situ is higher than the value assumed, this could significantly reduce the susceptibility of the structure to vibrations. Examples of common measures for vibration control in network arches are:

- Modification of cable texture
- Intermediate hanger coupling
- Stabilizing cables
- External dampers

#### ***Modification of cable surface texture***

An effective solution to prevent rain- and wind induced vibrations in circular cross-sections, is to modify the surface texture of the cable. The most common method is the attachment of helical ribs along the outer surface of the hanger. This disturbs the wind flow and the path of the drops along the cable, hereby preventing oscillation. Parallel strand cables are provided with sheeting to which helical ribs are attached, see Figure 32.

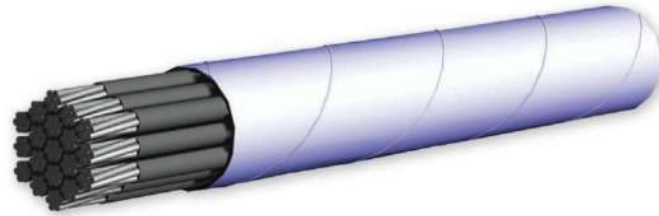


**Figure 32: Freyssinet HDPE-sheathing with helical ribs**

### ***Intermediate hanger coupling***

The intermediate coupling of hangers is most effective for vibration effects in which the natural frequency plays an important role. When the hangers are coupled, the main bending mode is altered which results in an increased natural frequency. The coupled hangers have different natural frequencies. This causes an additional damping effect [6]. See Figure 33 for some solutions for these couplers.



**Figure 33: Intermediate hanger coupling without damping**

### ***Stabilizing cables***

Stabilizing cables work by similar principles as the intermediate coupling of hangers. Additional damping is provided due to different stiffness of the stabilizing cables. This solution has large aesthetic consequences, as follows from Figure 34.



**Figure 34: Stabilizing cables**

### ***External dampers***

Dampers can be mounted on all hanger types in different configurations. Most of the dampers are mounted near the connections, to increase the damping performance of the cable. Only for parallel strand cables the dampers can be incorporated in the anchorages as shown in Figure 35 (left).



Figure 35: Dampers in anchorage of parallel wire cable (left), externally attached damper (right)

### 2.3.6 Conclusion

The following aspects were concluded from the literature reviewed on the detailed design of a network arch bridge:

- To reduce the susceptibility for vibration effects, the following parameters have a favorable influence:
  - High natural frequency
  - High structural damping
  - High Scruton number
- NEN-EN 1991-1-4 overestimates the value for structural damping, which could result in unexpected vibrations.
- DIN-FB103 recommends a conservative value for the structural damping, resulting in a safe design strategy.
- The catenary effect can influence the force distribution in the hangers.
- A frequently used method to reduce the susceptibility to vibration effects, is the coupling of hangers at the intersections.
- Circular cross-sections do not have to be verified for galloping, according to DIN-FB103.

## 2.4 Construction of a network arch

The construction process is discussed in chronological order, and the following aspects are considered:

- Prefabrication of bridge elements
- Construction of deck and main girder
- Construction of the arch
- Assembly of the hangers (hangers with welded connections and tensioned hangers)
- Transport to final location

A full steel network arch is described. For more information on network arches with concrete or composite decks see [7, 8, 3, 17, 18].

In bridge engineering, the construction method has a major influence on the final design and choice of materials. When looking at the existing network bridges the arch and of course the hangers are always made of steel. The deck and main girder are not bound to one material, for more about these elements see paragraph 2.2.3.

The costs for constructing a network arch bridge will generally be higher than for classical arch bridges. This is mainly because of the large amount of temporary supporting structures that have to be used. The extra hangers and hanger connections will also lead to higher costs. On the other hand, the on-site welding volume will be lower because the arch and main girder are lighter when compared to classical arch bridges. The transport and handling will also be more advantageous because of the lighter and more compact arch and main girder.

### 2.4.1 Prefabrication

Steel bridges are composed out of prefabricated steel segments, which are welded together on the construction site. This process has proven to be economically effective because the majority of the welding is done under optimal conditions in the fabrication shop. With the prefabrication of network arches special attention must be paid to the hanger connections, because in most cases all hanger connections are under different angles. Gauthier and Krontal [8] recommend to apply the highest available tolerance class for the prefabrication of the bridge segments. For the on-site assembly of the elements a slightly less strict tolerance class is allowed. For more information on the tolerances, see article [8].

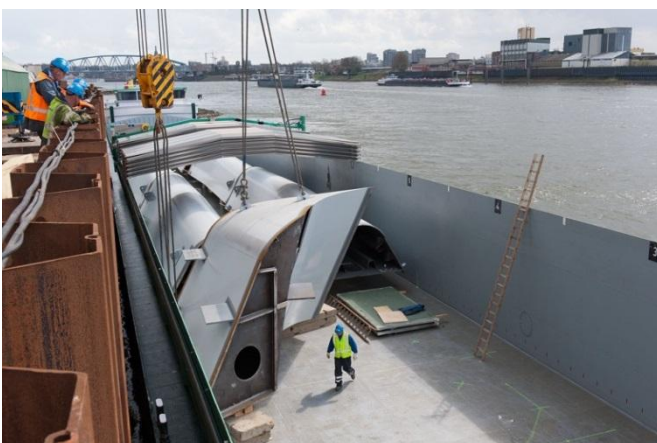


Figure 36: left: transportation of prefabricated arch segments by boat (Oversteek bridge), right: arch/ hanger connection (Rio Deba bridge)

### 2.4.2 Construction of the deck and main girder

First the deck and main girder are constructed, for which sufficient supports should be used to prevent excessive deformations. The temporary support structure should contain jacks to remove the bridge from its temporary supports. The prefabricated segments are placed on their temporary supports and should then be aligned carefully. Finally the main girder and deck structure can be fully welded.

Depending on the type of project, the bridge is assembled at the final location or at a temporary construction site.



Figure 37: left: temporary support of bridge constructed at final construction site (Palma del Rio bridge), right: temporary support of main girder (Oversteek bridge)

### 2.4.3 Construction of the arch

To construct the arch another temporary support structure must be used. This supporting structure can be placed on top of the deck positioned right above the supporting structure of the deck.

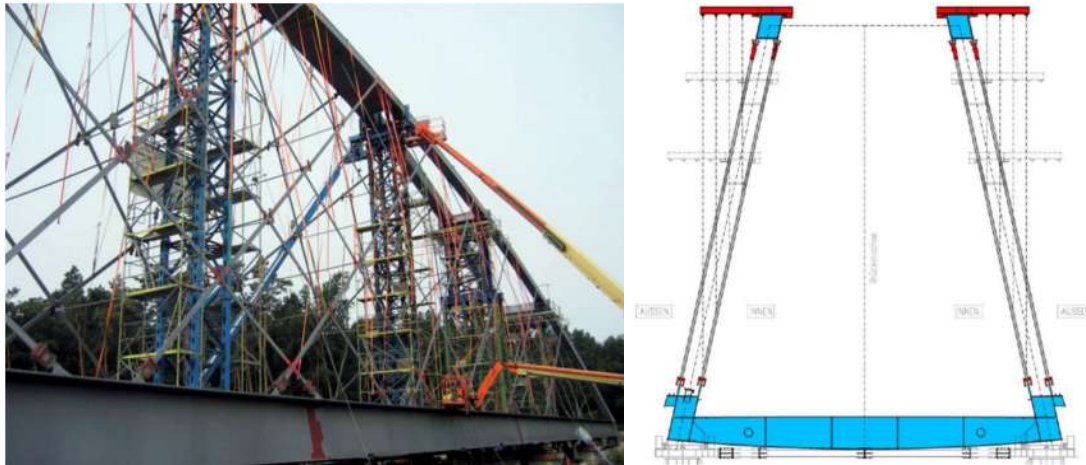
When constructing the arch, the connection between main girder and arch is initially not fully welded. Finally when all segments are in place and the temporary supports are removed, the connection is fully welded. By using this sequence imposed deformations in the arch/ main girder connection are prevented [8].



Figure 38: Final assembly of the arch, left: Oversteek bridge, right: Palma del Rio bridge

#### 2.4.4 Assembly of hangers with welded connections

When the arch is fully assembled and connected to the main girder, the hangers can be mounted. For hangers with welded connections the most important aspect is to weld the hangers under stress less conditions. In other words, the hangers must be fully straight and supported before final welding should begin. The idea behind this construction method is to obtain the theoretical force distribution when hangers are considered as straight beam elements. This temporary supporting structure can be a combination of scaffolding and straps as shown in Figure 39. Figure 39 also illustrates another method of supporting the hangers. With a temporary beam connected on top of the arch.



**Figure 39: left: hanger support as a combination of scaffolding and straps, right: hanger support as a combination of temporary beams and cables.**

When the hangers are hoisted in place the hanger connection with the arch should directly be connected by a weld. At the main girder a temporary connection should be made, see figure 40 for a temporary hanger connection. The basic idea of this procedure is to ensure that the full load is applied at the arch before welding the hangers.

The final welding of the hangers should be performed within a specified temperature range. If the final welding would be performed within a too large temperature range, the force distribution could become off. Gauthier and Krontal [8] recommend a maximum temperature interval of  $5^{\circ}$ . Depending on the season, the final welding activities should be performed at night. The final welding of the hangers should start with the hanger connection at the middle of the span.



**Figure 40: left: temporary hanger/ main girder connection, right: arch/ main girder connection**

### 2.4.5 Assembly of tensioned hangers

When a tensioned hanger system is applied, specific attention must be paid to the tensioning of the hangers. When the hangers are hoisted into position, these should also be carefully supported, in order to prevent plastic deformations.

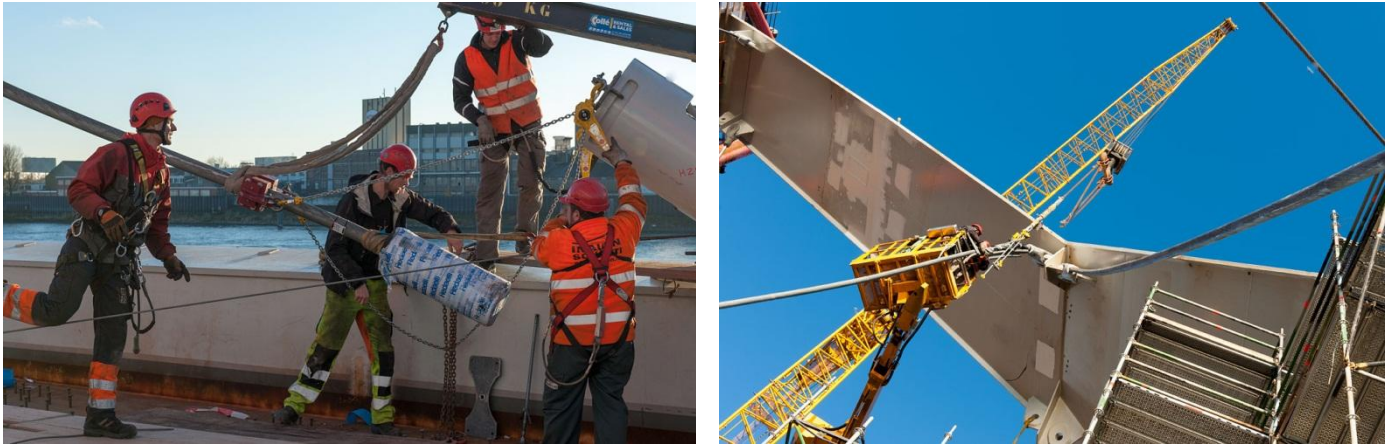


Figure 41: Pictures of the assembly of the hangers (Oversteek bridge)

To obtain the desired force distribution in the hangers a tensioning protocol should be developed. This protocol should be based on an accurate computer model in which the stiffness of all elements should be modeled with great detail. Special attention should be paid to the arch/ main girder connection. The stiffness of this connection has a large influence on the forces in the outer hangers [16]. When the bridge is constructed the stiffness of the computer model should be verified before initiating the tensioning process. It can be concluded that for network arches with tensioned hangers more complex engineering is required.

For the tensioning of the hangers of the Palma del Rio the following steps were followed in the tensioning process [16].

- Step 1: Initial tensioning to prevent excessive deformations in deck and hangers
- Step 2: Removal of the supporting structure and application of the final deck structure
- Step 3: Final tensioning according to the tensioning protocol.

The final tensioning procedure can only be performed when the full deck weight is in place.

Over time the tensile force in the hangers should be measured to ensure that the correct tensile force is present. This can be done by measuring the natural frequencies of the hangers [17]

### 2.4.6 Transportation to final location

If the network arch is built at a temporary construction site, the bridge has to be transported to the final location. Special attention should be paid to the forcedistribution that occurs during transport. This could lead to compression forces in some of the hangers with buckling as a result. This problem can be solved by temporarily supporting the compressed hangers, or by applying a prestressing force in certain hangers.

During transport the cables should be connected by straps to minimize cable vibrations.



Figure 42: left: bridge with supported hangers to prevent buckling, right: Oversteek bridge ready for transport

### 2.4.7 Conclusion

The following aspects were concluded from the literature review on the construction of a network arch bridge:

- Relatively light/ slender arch, main girder and hangers could be advantageous in transport and handling.
- The construction costs for the assembly of the hangers of a network arch bridge are generally higher than for classical arch bridges.
- Hangers with welded connections should be mounted in a stress less state in order to obtain the theoretical force distribution. The following aspects should be considered during the assembly of the hangers:
  - Support the hangers in both directions throughout construction process
  - Final welding activities within a limited temperature range
  - The arch must be unsupported during the final welding activities
- To obtain the desired force distribution in tensioned hangers a stressing protocol must be composed. For this stressing protocol a detailed three dimensional model is required where the stiffness should be modeled accurately, especially the arch/ main girder connection. The stiffness of this computer model should also be verified with the real stiffness of the structure.
- The engineering of a network arch bridge with tensioned hangers is more complex than the engineering of a network arch with welded hanger connections. For a network arch with tensioned elements the force distribution in the hangers fully depends on the accuracy of the stressing protocol. For a network arch with welded connections this force distribution depends on the accuracy of the construction process.
- The final stressing of tensioned hangers can only be carried out when the full deck weight is present.

# 3 VARIANT STUDY

Based on arguments provided by literature, the preliminary design of the network arch is made by means of a variant study. The original tender design is used as a basis for the overall structure. With this variant study the most advantageous hanger arrangement and hanger type are determined in order to finally obtain an advantageous design. For more information on the original tender design see annex D.

## 3.1 Hanger arrangement

According to Teich [1] an optimal hanger arrangement can be determined with the guidelines he has composed. The definition of ‘optimal’ is given in paragraph 2.2.4.2. Based on a certain number of hangers and type of arrangement, a geometrical description is given to compose the optimal arrangement. In this paragraph arguments are given for the number of hangers and arrangement type. For the full step-by-step design process of the hanger arrangement see, Annex B2.

### 3.1.1 Number of hangers

Based on span length, an optimal number of hangers can be determined with Table 48. For a span of 255m, the minimal amount of hangers should be 42. The maximal amount is 52. For the sake of symmetry an even number of hangers is required. If more than 52 hangers are applied the costs for the extra hangers would not be compensated by reduction of forces in the structure.

It was decided to choose the smallest amount of hangers which would still generate an optimal hanger arrangement, hence 42. It is assumed that the costs for the material and assembly of the hangers on site will be higher than the stress reduction that is obtained by the extra hangers.

### 3.1.2 Type of arrangement

To decide on the type of arrangement, Teich presents three realistic basic arrangements. These arrangements are assigned with a score to indicate their structural performance. Based on the number of hangers and length of the span, optimal arrangements can be generated, these are shown in Figure 43.

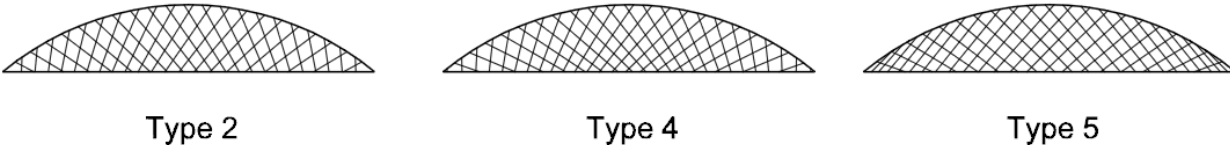


Figure 43: Three 'optimal' hanger arrangements

Finally arrangement type 2 was decided to be the best arrangement based on the following arguments:

- The structural performance of type 2 (96,1%) is just as good as that of type 4 (100%) according to Table 49.
- The steeper hangers of arrangement type 2 would lead to a more favorable constructability, according to Teich. He explains this statement by the fact that the steep angles lead to shorter hangers. Also steeper hangers can be more easily supported during construction.

### 3.1.3 Conclusion

From the variant study on the optimal hanger arrangement the following was concluded:

- The hanger arrangement is determined according to guidelines provided by Teich [1]. Figure 44 shows the final hanger arrangement which is based on 42 hangers and arrangement type 2. The outer hangers are placed at an angle of  $28^\circ$ . The following hangers have an angular increase of  $3^\circ$  for each hanger.

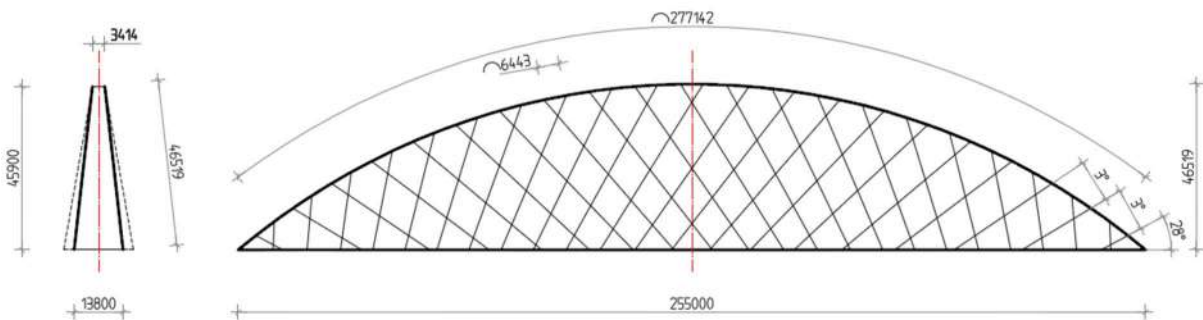


Figure 44: Final hanger network, based on arrangement type 2 and 42 hangers

- The following structural properties were optimized for this specific hanger arrangement:
  - Bending moments in arch and main girder
  - Equal force distribution in all hangers
  - Reduced maximal forces in the hangers
  - Reduced force variation ( $\Delta F$ )
  - No compression/ relaxation in SLS
- Arrangement type 2 is preferred because the relatively steep hangers can be assembled more easily and will also lead to shorter hangers.

## 3.2 Hanger type

In order to find the most advantageous hanger type for the design of the network arch bridge, the hanger types are evaluated according to the following aspects:

- General structural properties (fatigue, stiffness)
- Vibration effects and damping provisions
- Costs
- Constructability
- Maintenance

Special attention is paid to fatigue, vibration effects and construction method, because these aspects were considered as uncertainties for the design of a network arch.

The hanger types that are mentioned in the literature review will be considered except the flat steel hangers. This hanger type is not considered as realistic because of its appearance. Resulting in the following hanger types to be further investigated:

- Steel rod with welded connections (SRWC)
- Steel rod with fork connector system (SRFCS)
- Locked coil cable
- Spiral strand cable
- Parallel wire strand cable



Figure 45: from left to right: steel rods, locked coil cable, spiral strand cable, parallel strand cable

### Score system

Based on a score system which gives a favorable argument a score of 4, and an unfavorable argument 1. Finally these score will be added and the highest value gives the best hanger type based on the aspects mentioned above.

### 3.2.1 General structural properties

The structural properties can simply be found in product information sheets provided by suppliers. Table 1 gives an overview of some well-known suppliers.

Hanger type	Supplier
SRWC	- Arcelor Mittal, Histar - Tata steel
SRFCS	- Pfeifer Cable Structures - Macalloy bar & cable systems
Locked coil cable	- Bridon
Spiral strand cable	- Bridon
Parallel strand cable	- Freyssinet - BBR HiAm CONA

Table 1: Overview suppliers

#### 3.2.1.1 Stiffness

For a more complete estimation of the stiffness properties the required cross-section must be determined. This is done according to a simple formula given by Romeijn [11]. He states that an estimation of the axial hanger forces for arch bridges can be obtained by simply multiplying the distributed loads with the center to center distance of the hangers. The self-weight and ballast weights which are used for the estimation of the hanger forces are obtained from the original tender design.

Permanent loading:  $g = 235 \text{ kN/m / arch plane}$

For the traffic load the maximum load of load model 71 (LM71) is used. This maximum load is applied as a distributed load of 156 kN/m.

Traffic loading:  $q = LM71 \cdot \alpha = 156 \cdot 1,21 = 189 \text{ kN/m}$  / arch plane

The partial load factors ( $\gamma_G=1,4$  and  $\gamma_Q=1,5$ ) used for the ULS combination are obtained from the original tender design.

$$l_{center\ to\ center} = \frac{span}{number\ of\ hangers} = \frac{255}{42} = 6,1m$$

$$N_{permanent;SLS} = (6,1 \cdot 235) = 1434 \text{ kN}$$

$$N_{traffic;SLS} = (6,1 \cdot 189) = 1153 \text{ kN}$$

$$N_{SLS} = (1434 + 1153) = 2587 \text{ kN}$$

$$N_{ULS} = 1.4 \cdot N_{permanent} + 1.5 \cdot N_{traffic} = 3737 \text{ kN}$$

According to Romeijn [11] cable elements should be designed at a stress level of  $0,45f_{uk}$ . For SRWC hangers of steel grade S460 a stress level of 240 MPa should be used, according to the German design code DIN [2]. Both stress levels should result in a design with sufficient fatigue resistance

The scores given in Table 2 are based on the available stiffness in the hangers.

Hanger type	$f_{uk}$ [MPa]	$N_{min;break}$ [kN]	$D_{required}$ [mm]	Asteel [mm <sup>2</sup> ]	E-modulus [GPa]	EA [MN]	Score
SRWC S460NL	550	-	140	15394	210	3233	4
SRFCS Macalloy 520	660	-	125	12272	210	2577	3
Locked coil cable Bridon	-	8090	90	5600	165	924	1
Spiral strand cable Bridon	-	8160	95	5190	155	804	1
Parallel strand cable BBR-HiAm CONA	-	8649	160	4650	200	930	1

Table 2: Overview of required cross-sections and stiffness properties

### 3.2.1.2 Fatigue behavior

The differences in fatigue behavior between the different hanger types are evaluated in this paragraph. The SN-curve of welded hangers (SRWC) and tensile elements (all other hanger types) are fundamentally different, see Figure 46 for the SN-curves. This distinction between SRWC and the other hanger types is made in NEN-EN 1993-1-11 [23], which is the special design code for tensile elements. From both SN-curves it can be concluded that tensile elements will always have a finite fatigue life.

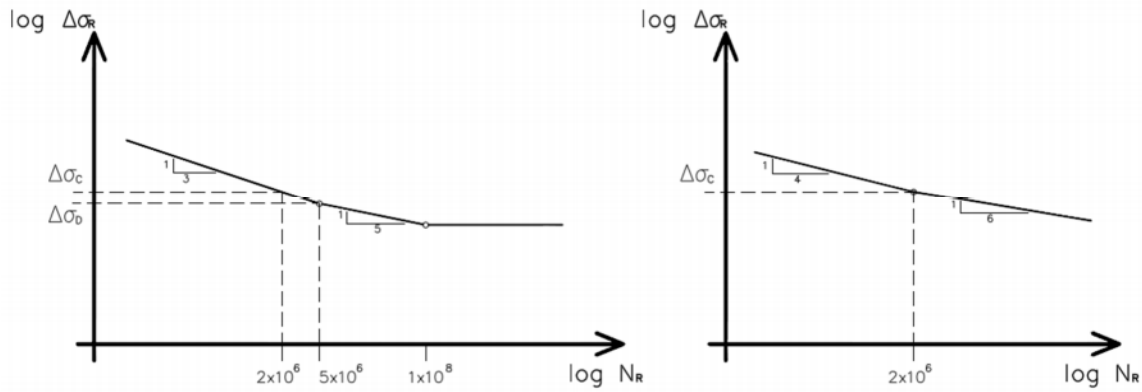


Figure 46: SN-curves, left: structural steel NEN-EN 1993-1-9, right: tensile elements NEN-EN 1993-1-11

To quantify the fatigue performance of the hangers, the number of cycles at a certain stress level is calculated. The stress amplitude at which this number of cycles is determined, is the stress amplitude caused by traffic loading. This amplitude is arbitrarily chosen, and for the actual fatigue resistance much more parameters have to be taken into account. However for the variant study this indication is sufficient. The stress amplitude for the traffic load can be determined as follows:

$$\Delta\sigma_i = \frac{N_{traffic;SLS}}{A}$$

The number of stress cycles is determined by the following formulas:

For SRWC hangers

$$N = 2 \cdot 10^6 \left( \frac{\Delta\sigma_C}{\Delta\sigma_i} \right)^3 \quad \text{if } \Delta\sigma_i \geq \Delta\sigma_D = 0,737 \cdot \Delta\sigma_C$$

$$N = 5 \cdot 10^6 \left( \frac{\Delta\sigma_D}{\Delta\sigma_i} \right)^5 \quad \text{if } \Delta\sigma_L \leq \Delta\sigma_i \leq \Delta\sigma_D$$

$$N = \infty \quad \text{if } \Delta\sigma_i \leq \Delta\sigma_L = 0,549 \cdot \Delta\sigma_D$$

For tensile elements (all hanger types except SRWC)

$$N = 2 \cdot 10^6 \left( \frac{\Delta\sigma_C}{\Delta\sigma_i} \right)^4 \quad \text{if } \Delta\sigma_i \geq \Delta\sigma_C$$

$$N = 2 \cdot 10^6 \left( \frac{\Delta\sigma_C}{\Delta\sigma_i} \right)^6 \quad \text{if } \Delta\sigma_i \leq \Delta\sigma_C$$

The detail categories for the tensile elements are determined according to NEN-EN 1993-1-11. For SRWC the detail categories are determined in annex I.2.

With the formulas mentioned above Table 3 is composed and for each hanger type a score is given based on their fatigue performance.

Hanger type	Detail category	$\Delta\sigma_i$ [MPa]	Number of stress cycles [N]	Score
SRWC S460NL (standard)	90	72	$3,9 \cdot 10^6$	4
SRFCS Macalloy 520	105	90	$5,0 \cdot 10^6$	4
<u>Locked coil cable</u> Bridon	150	198	$0,7 \cdot 10^6$	1
<u>Spiral strand cable</u> Bridon	150	214	$0,5 \cdot 10^6$	1
<u>Parallel strand cable</u> BBR-HiAm CONA	160	239	$0,4 \cdot 10^6$	1

**Table 3: Overview fatigue performance of the hanger types expressed as stress cycles (N)**

### 3.2.2 Vibration effects and suppression

#### *Vibration effects*

In this paragraph the hanger types are evaluated on their susceptibility to the relevant vibration effects. In the literature study a list of vibration effects which are relevant for hangers with circular cross-sections:

- Vortex induced vibrations
- Wind and rain induced vibrations
- Structural vibrations

In Table 4 the safe design criteria of the abovementioned vibration effects are given. From these design criteria it can be concluded that high natural frequencies ( $n_i$ ) and a high Scruton number ( $Sc$ ) have a favorable influence on the susceptibility of these vibration effects.

Vibration effect	Safe design criteria
Vortex induced vibrations	$Sc = \frac{2\delta_s\mu}{\rho b^2} > 20$
	$v_{crit,1} = \frac{b \cdot n_i}{St} > 1.25v_m$
Wind- and rain induced vibrations	$b < 70mm$
	$n_i > 6,5 Hz$
Structural vibrations	$0,8 \cdot n_i < n_{structure} < 1,2 \cdot n_i$
	$0,8 \cdot n_i < 2 \cdot n_{structure} < 1,2 \cdot n_i$

**Table 4: Overview of relevant vibration effects and their parameters**

If the hangers are considered as cables, the natural frequency can be estimated with the following formula:

$$n_{i,y} = \frac{1}{2} \sqrt{\frac{N}{\mu \cdot L^2}}$$

It can be concluded that lighter hangers (low  $\mu$ ) will have higher natural frequencies because the weight per unit length is in the denominator of the formula. In other words, hangers with

higher tensile strength will have a lower weight per unit length and therefore generally have higher natural frequencies. Therefore steel grade S460 is applied for the SRWC.

To determine the Scruton number the following values are used:

- $\rho$  is the density of the air, and should be taken as 1.25 kg/m<sup>3</sup>
- $\delta_s$  logarithmic structural damping, and is taken as 0,006 for all hanger types to provide a clear comparison. The value of 0,006 is based on the original tender design.

Hanger type	$D$ [mm]	$\mu_{hanger}$ [kg/m <sup>3</sup> ]	Scruton	Score $\mu_{hanger}$	Score Scruton	Score total
SRWC	140	120,8	59,2	1	4	5
SRFCS	125	96,3	59,2	2	4	6
Locked coil cable	90	45,0	53,3	4	4	8
Spiral strand cable	95	43,5	46,2	4	4	8
Parallel strand cable	160	43,1	16,2	4	1	5

**Table 5: Overview of scores with respect to vibration effects**

### ***Vibration suppression***

When considering the possibility to apply vibration suppression measures reference is made to the literature study. The following measures were described:

- Modifying cable texture
- Stabilizing cables
- Intermediate hanger coupling
- External damping

Only the modification of the surface texture of the hanger is different for the hanger types. The other measures can be applied to all hanger types.

### ***Modifying cable surface texture***

Parallel strand wires are standard provided with sheeting where these helical ribs are attached to its surface. Massive steel rod hangers can also be provided with these helical ribs, by attaching them to the surface. It is *assumed* that for locked coil and spiral strand cables these helical ribs cannot be attached to the cable surface.

Hanger type	Argument	Score
SRWC	Possibility to attach helical wires to the surface	3
SRFCS		
Locked coil cable	Assumption: not possible to attach helical wires directly to the outer surface of the cable	1
Spiral strand cable		
Parallel strand cable	Outer sheeting is provided with helical wires	4

**Table 6: Overview scores with respect to damping provisions**

### **3.2.3 Costs**

For the assessment of the costs only the material costs for hangers are considered. Exact values cannot be determined because suppliers are not tempted to reveal their prices. For each of the hanger types a cost indication is given with a score from 1 (unfavorable) to 4 (favorable). The costs are fully based on *assumptions*. The hanger connections are considered separately.

### ***Hanger costs***

It is assumed that standard steel rods which are used in the hanger type with welded connections provide the cheapest solution (SRWC) despite the larger diameter. Next the SRFCS type would cost slightly more, because of higher steel quality and the threads that are rolled onto the ends of the bars. These SRFCS hangers are marketed as a cheaper alternative for cable systems.

The locked coil cable is assumed to be the most expensive cable type, this is based on the fact that these cables are highly specialized elements of a high steel quality. Followed by spiral strand wires, this cable type is also manufactured from high quality wires but less advanced. A parallel strand cable is composed out of a number of standard high quality strands. This bundle of strands is then wrapped with a sheeting to ensure corrosion protection. Because of the additional sheeting, the parallel strand wire is also assumed to be relatively expensive.

<b>Hanger type</b>	<b>Argument</b>	<b>Score</b>
SRWC	Standard steel rods, no specialized supplier	4
SRFCS	Cheaper alternative for cable systems	3
Locked coil cable	High quality and complex wire pattern	1
Spiral strand cable	High quality simple wires	2
Parallel strand cable	Composed out of standard high quality wires, wrapped in sheeting	1

**Table 7: Overview scores with respect to hanger costs**

### ***Connection costs***

It is *assumed* that the welded connection is the cheapest connection, because a steel contractor is able to produce these connector plates himself, however on site welding is still required. Figure 22 shows a welded hanger connection.

The hanger types with fork connectors are *assumed* to be more expensive, because these connectors are specialized elements. The spiral, and locked coil cable is connected to the fork connector by filling the connector with liquid zinc. For the SRWCS hanger types, the fork connectors are screwed onto the rolled thread which is made at the ends of each steel rod.

The connection of the parallel strand wire which is connected by a special anchorage is assumed to be the most expensive connection type, see figure 27.

<b>Hanger type</b>	<b>Argument(s)</b>	<b>Score</b>
SRWC	Simple connection, standard steel plates, welding	4
SRFCS	Relatively simple connection, fork connectors screwed	3
Locked coil cable	Special fork connectors, connection casted with zinc	2
Spiral strand cable		
Parallel strand cable	Specialized element, consists of multiple elements, connected with patented wedges	1

**Table 8: Overview scores with respect to hanger connections**

#### **3.2.3.1 Availability**

Based on the availability of the required diameters and lengths a score is determined. When considering the SRFCS hangers, it can be concluded that Macalloy and Pfeifer (see Table 1 for the list of consulted suppliers) can only provide diameters up to 97mm. Larger diameters are available, however connectors and couplers would have to be custom made, resulting in higher costs. This is based on the suppliers that were used for this variant study.

The diameters for standard steel rods can go up to a size of 220mm, these were applied in the van Uyllander bridge (also steel grade S460 was used).

The average length of the hangers is approximately 45m (same height as the arch). For all cable hanger types these lengths are available. The steel rods (both SRWC and SRFCS) would have to be coupled by special couplers or butt welds. Both SRWC and SRFCS have a standard length of 13m, resulting in a large amount of couplers or butt-welds.

Hanger type	Argument(s)	Score
SRWC	Limited standard length, couplers or butt-welds needed	3
SRFCS	Required diameter should be custom made, large amount of couplers needed to obtain required length	1
Locked coil cable	All lengths, and sufficient diameters available	4
Spiral strand cable		
Parallel strand cable		

**Table 9: Overview scores with respect to availability**

### 3.2.4 Constructability

To differentiate the hanger types from a construction point of view the construction techniques described in paragraph 2.4 of the literature study are used as a reference. The two different methods for hanger assembly are evaluated:

- Assembly of hangers with welded connections
- Assembly of tensioned hangers

In the examples that were used in the literature study no specific details with respect to construction time are given. It is therefore assumed that the construction time is equal for both welding and stressing.

The labor intensity is evaluated by the following arguments, the score indicates the favorability of the argument. All arguments are based on the examples described in the literature study. A low score indicates bad performance on constructability, and vice versa.

Hanger type	Argument(s)	Score
SRWC	<b>Welded connections:</b> -Large amount of temporary supports for hanger assembly required -Temperature dependence - Relatively simple engineering - More on site welding	2
		2
		4
		2
	<b>Average score:</b>	
SRFCS Locked coil cable Spiral strand cable Parallel strand cable	<b>Tensioned hangers:</b> - Multiple stressing operations required - Relatively easy assembly of hangers - Relatively complex engineering	2
		4
		1
	<b>Average score:</b>	

**Table 10: Overview scores with respect to constructability**

### 3.2.5 Maintenance

With maintenance some general aspects which could be of importance during the lifetime of the bridge are considered:

- Replace-ability of hangers
- Corrosion protection

#### *Replace-ability of hangers*

When hangers become damaged by for instance a derailment or bad maintenance, hangers should be replaceable. This is prescribed in the NEN-EN 1993-1-1 and NEN-EN 1993-2. For network arches the replacement of hangers is easier than for arch bridges with a diagonal or vertical hanger arrangement. However large differences can be found between the different hanger types. Their ability to be replaced is evaluated by arguments obtained from the literature study. A score for each hanger type is given.

Hanger type	Argument	Score
SRWC	Hard to replace because of welded connections	1
SRFCS	Good replacability	3
Locked coil cable		3
Spiral strand cable		3
Parallel strand cable		4
	Best to replace. This can be done strand by strand. Traffic continuity even possible	

**Table 11: Overview of scores with respect to the replace-ability of hangers**

#### 3.2.5.1 Corrosion protection

An important aspect is the corrosion protection of the hanger types. From the technical information provided by the suppliers, information about the corrosion protection is obtained. It is assumed that the SRWC hangers are conserved in a similar way as the overall structure. These are conserved with thermally sprayed aluminum which has a maintenance free period of 40 years (mentioned in original tender design report [20]).

According to the BBR product sheet for parallel strand wires, a maintenance free period of 100 years is guaranteed.

For spiral strand and locked coil cables Bridon provides a maintenance programme where a re-coating of the strands is recommended every 10 to 15 years. It is *assumed* that the SRFCS system will require the same maintenance programme. These are also provided with Galfan® coating, similar as the individual wires of spiral strand and locked coil cables.

Hanger type	Corrosion protection	Score
SRWC	Thermally sprayed aluminum, expected maintenance-free period is 40 years.	3
SRFCS	Galfan® + metal paint, expected maintenance-free period is 10 to 15 years, based on maintenance programme Bridon	1
Locked coil cable		
Spiral strand cable		
Parallel strand cable	HDPE sheeting, expected maintenance-free period 100 years, based on product information BBR	4

**Table 12: Overview scores with respect to corrosion protection**

### 3.2.6 Conclusion

In order to determine the optimal hanger type, the scores given in Table 2 to Table 12, are used to compose a score table, shown in Table 13. The hanger type with the highest score is assumed to have the best overall performance on the aspects mentioned, based on the arguments and assumptions given in the previous paragraphs.

Hanger type	Aspects										Total
	Stiffness	Fatigue behavior	Vibration effects	Vibration suppression	Hanger costs	Connections costs	Availability	Constructability	Replace-ability	Corrosion protection	
Steel rod with welded connections (SRWC)	4	4	5	3	4	4	3	2,5	1	3	33,5
Steel rod with fork connector system (SRFCS)	3	4	6	3	3	3	1	2,3	3	1	29,3
Locked coil cable	1	1	8	1	1	2	4	2,3	3	1	24,3
Spiral strand cable	1	1	8	1	2	2	4	2,3	3	1	25,3
Parallel strand cable	1	1	5	4	1	1	4	2,3	4	4	27,3

Table 13: Score table for hanger type

From Table 13 it is concluded that steel rod hangers with welded connections provide the best hanger type for the considered structure. However, this conclusion is also largely based on assumptions, especially the following aspects:

- Diameter, based on design rule
- Vibration suppression; based on assumption that helical wires cannot be attached to locked coil and spiral strand cables
- Hanger costs and connection costs
- Availability; based on only two suppliers per hanger type.
- Corrosion protection; based on only two suppliers per hanger type. For SRFCS an assumption had to be made.

## 4 DESIGN STAGE

In this paragraph the modeling and optimization process of both the network arch and original tender design is discussed. When the original tender design was first analyzed, some simplifications and architectural restrictions in the modeling were revealed. These simplifications would make it impossible to create an optimal network arch. Therefore it is decided to adapt the modeling of the original tender design and to optimize this design according to the same restrictions as the network arch. For the final comparison it would be fair to compare this adapted and optimized original tender design to the optimized network arch. This adapted original tender design will now be referred to as “reference design”.

In paragraph 4.1 the general design parameters are discussed along with the adjustments that will be made to the original tender design to cope with the simplifications and restrictions. In paragraph 4.3 the adjusted modeling of the reference design and network arch is discussed.

In paragraph 4.2 the behavior of these massive steel rod hangers is investigated, to ensure accurate of the hangers.

Finally in paragraph 4.5 and 4.6 the network arch and reference design are optimized.

### 4.1 Design aspects

In this paragraph some aspects regarding the design and modeling of the network arch and the reference design are discussed.

#### *Linear analysis*

Linear analysis is considered crucial for an efficient design process because it allows for superposition of load cases and the use of mobile loads to determine the maximal and minimal forces in the structure. To determine if the hangers can be modeled accurately enough by linear analysis, the difference between linear and nonlinear behavior of hangers is evaluated in paragraph 4.2.

#### *Materialization*

The arch, hangers and main girder are made out of steel with steel grade S460. The arch and main girder are both box girders composed out of standard plate thicknesses. The organization Bouwen met Staal provides a list of standard plate thicknesses, which can be found on their website. The hangers are also based on standard profile sizes. It is assumed that S460 hangers with a maximal diameter of 220mm are available. This is based on the hangers that were applied for the Den Uyllander bridge, which also have a diameter of 220mm.

#### 4.1.1 Adaptations to the original tender design

As was mentioned in the introduction of this chapter, the SCIA model of the original tender design contained the following simplifications and restrictions:

- Horizontal stiffness of the deck and main girder is underestimated. This results in conservative stability performance as well as unrealistic transverse bending moments and stresses in the main girders. See paragraph 4.3.2.
- The arch is modeled as a set of segmented beam elements instead of a curved arch, see annex D. In order to implement the network hanger arrangement, a curved arch is preferred. See paragraph 4.3.3.
- The outer dimensions of the arch cross-section are based on architectural restrictions. A network requires less in plane stiffness and could with these restrictions never reach its full potential.

In order to create a fair comparison between network arch and original tender design, both designs have to be optimized according to the same restrictions and simplifications. However, the simplifications and restrictions mentioned above would make it impossible to obtain a fully optimized network arch. It is therefore decided to reject the simplifications and restrictions that apply for the original tender design, and optimize both designs according to the same modeling principles and without architectural restrictions.

#### 4.1.2 Loads and combinations

The loads and combinations from the original tender design will also be used for the modeling of the reference design and network arch. For the tender design the influence of other types of loading was evaluated, for instance: thermal loads, fire loads, aerodynamic loads and other traffic loads. They concluded that these load types had a relatively small influence and could therefore be neglected in the design stage. This led to a simple design model where only traffic (LM71  $\alpha = 1,21$ ) and wind loading are evaluated. In annex A a more detailed description of the loads and combinations is given, also the load patterns are shown.

LC1: Self-weight

LC2: Dead load (ballast and railway provisions)

LC3: Traffic full loading LM71 (a)

LC4: Traffic half span loading LM71 (b)

LC5: Traffic one sided full loading LM71 (c)

LC6: Wind load (horizontal transverse direction)

LC7: Mobile traffic load LM71

The load model which represents train loading (LM71) is specified in Figure 47. This load case is mainly used to determine the maximal hanger forces, but also the maximal and minimal deformations of the main girder.

To make the design process more efficient, two load cases were added:

LC8: Wind loading from opposite direction. When both wind directions are implemented in the design the results become symmetric and only one side of the structure has to be evaluated.

LC9: Alternating mobile loads (d), see Figure 100. With this fourth static mobile load cases all critical load patterns for arch bridges (according to Bijlaard and Kolstein [20]) are present. When designing the arch and main girder the mobile traffic load case (LC7) can be turned off, which saves a lot of time and makes the design process much more efficient.



#### 4.2.1 Explanation for extreme deformations and internal forces

When a beam undergoes a large deflection, this beam will also elongate in axial direction. This axial elongation causes an axial force. The axial elongation is a nonlinear effect, because it is caused by a deformation. This explains why linear analysis produces such extreme deformations.

When linear analysis is used for the analysis of a beam element, the transverse loads are transferred by bending moments and shear forces. In reality, some of the transverse loads are still transferred by shear forces and bending moments, but the majority is transferred by axial force. As was mentioned above, when linear analysis is applied this axial force will never develop, because of its nonlinear origin. Hence, unrealistic internal forces are formed to transfer the transverse loads.

#### 4.2.2 Analytical description of hanger behavior

To describe the behavior of a massive steel rod hanger the differential equation of an axially tensioned Euler-Bernoulli beam is used. The differential is given by Leissa and Qatu [26]:

$$EI \frac{\partial^4 w}{\partial x^4} + \rho A \frac{\partial^2 w}{\partial t^2} = T \frac{\partial^2 w}{\partial x^2}$$

When solving the differential equation for the deflection, the internal forces can be determined as follows:

Deflection:	$w(x)$
Bending moment distribution:	$M(x) = -EI \frac{d^2 w(x)}{dx^2}$
Shear forces:	$V(x) = -EI \frac{d^3 w(x)}{dx^3} + T \frac{dw(x)}{dx}$
Stresses:	$\sigma(x) = \frac{M(x)}{W} + \frac{T}{A}$

In annex J the differential equation is used to determine the natural frequencies of the longest and shortest hanger.

The hanger could also be simplified as a cable by neglecting the bending stiffness (see paragraph 4.2.3) but then the internal forces could not be determined. Also the natural frequencies in the hangers are underestimated when the bending stiffness is neglected.

In paragraph 5.3 the differential equation is used to verify the numerical results obtained by geometrically nonlinear analysis.

### 4.2.3 Cable - or beam action

If massive steel rod hangers will act more like beams or like cables is investigated in this paragraph. This is determined by evaluating the percentage of cable and beam action in the total deflection of the hanger. The formula for the deflection of an axially tensioned Euler-Bernoulli beam is given by Irvine [21].

$$\delta_{total} = \frac{mgl^2}{8T} \left( 1 - \frac{8}{\gamma^2} \left( 1 - \operatorname{sech} \frac{\gamma}{2} \right) \right) [m]$$

This can be written as:

$$\frac{\delta_{total}}{\delta_{cable}} = \left( 1 - \frac{8}{\gamma^2} \left( 1 - \operatorname{sech} \frac{\gamma}{2} \right) \right) [\%]$$

Where:

$$\gamma = \sqrt{\frac{Tl^2}{EI}}$$

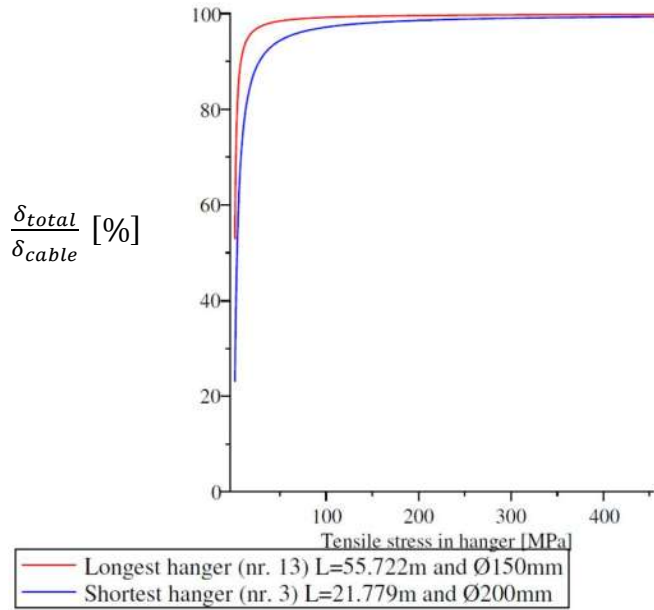


**Figure 49: Influence of cable action as a function of the stress in the hanger**

From the formula follows that for small bending stiffness ( $EI$ ) and large axial force ( $T$ ), the deflection yields to the standard formula for the deflection of a cable ( $\frac{mgl^2}{8T}$ ), or in other words full cable action. When a large amount of cable action is present, the bending moments in the hanger, and especially the connection, will be lower, because the transverse loads are mainly transferred by axial forces. By evaluating the longest (nr. 13) and shortest hanger (nr. 3) the full hanger arrangement is covered.

In Figure 49 the percentage of the cable action is plotted, as a function of the stresses in the hanger. The stresses in the permanent loading situation are approx. 65 MPa, which corresponds to 95 % cable action in the shortest hanger and nearly 100% cable action in the longest hanger. The maximum stress in ULS is limited to 240 MPa, where for both hangers 100% cable action is present. Because the percentage of cable action is nearly 100% for all loading situations, it can be concluded that all hangers act like cables for all loading situations.

### 4.2.4 Hanger relaxation (compressive forces)

For network arches, where hangers are very slender and slanting, the hangers will never be able to develop compressive forces because they will deflect due to their self weight. The self-weight will also keep the hanger tensioned in all loading situations. The short and steep hangers could develop some compressive forces, and could therefore also buckle. In paragraph 5.5 the effects of hanger compression and relaxation on the overall structure are evaluated.

For the design stage it is assumed that compressive forces are allowed in linear analysis.

#### 4.2.5 Validity of linear analysis

By isolating a single hanger and comparing the reaction forces of a linear beam to those of a cable, the interaction between the hangers and the structure is found. If the reaction forces of a linear beam deviate too much from the cable behavior, the forces in the main girder and arch are unreliable when obtained by linear analysis.

By isolating the longest hanger the largest difference between linear beam behavior and cable behavior is expected. For the research two SCIA models are made: one cable (nonlinear) and one beam (linear).

It was concluded that for low axial stresses ( $\sigma_{Nx}$ ) the difference between cable behavior and linear beam behavior is significant. When a hanger is loaded by a high axial force, which corresponds to the ULS (maximal design stress in hangers is 240 MPa), the differences become negligible. This phenomenon is found for the reaction forces in all directions (x-, y-, and z-direction), and also for the axial stresses. Based on this phenomenon it is decided that linear analysis should only be used for ULS verification. In paragraph 5.4 these conclusions are verified. When no transverse load is applied on the hangers (for instance: no wind), linear analysis should provide accurate results.

In Figure 50 the support reactions in x-direction are plotted as a function of the axial stresses. In annex E.2 the full research on these differences can be found along with plots of support reactions in the y- and z- direction.

It was also concluded that because of the large differences between linear beam and cable behavior in x- and z-direction the bending moments ( $M_y$ , in plane of the arch) in the arch and main girder are underestimated. For the permanent load situation these differences would be largest. In paragraph 5.4.2 this conclusion is verified.

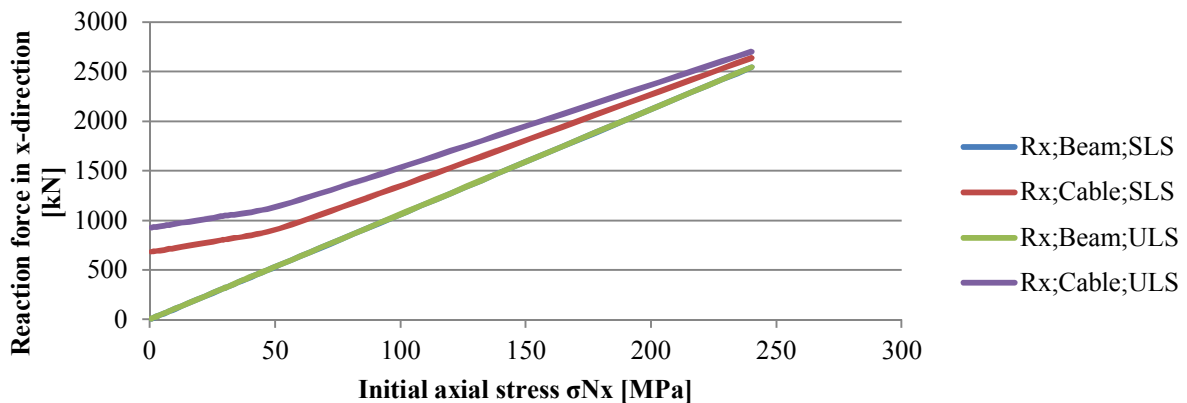


Figure 50: Support reaction in x-direction of a linear beam and a cable as a function of the axial stresses

#### 4.2.6 Catenary effect

The catenary effect arises in the cables of cable stayed bridges and other cable structures where cables span a large horizontal distance. Due to the deflection of the cable due to its own self-weight, the axial stiffness of the cable is negatively influenced. Geißler et al. [7] mention that for the design of network arch bridges, that the ‘sag’ effect will occur in the longer and more slanting hangers. Because the network arch considered in this thesis has a larger span than

usual (the majority of the network arches have spans around 150m), it is interesting to see how this effect influences the force distribution.

In annex E.3 the influence of the sag effect on the overall force distribution in the hangers is investigated. In Table 54 the results are shown. Annex E.3 also gives more background information on the catenary effect.

It was concluded that the catenary effect has a negligible influence on the axial force distribution in the hangers. When the unreduced modulus of elasticity is used, the hanger forces of the long and slanting hanger show a maximum deviation in force distribution of 5%. This corresponds to the findings of Geißler et al. [7].

When a more detailed analysis is performed, the catenary effect could become relevant. For instance when developing a tensioning protocol for tensioned hangers (see paragraph 2.4).

#### **4.2.7 Conclusion**

From the research on the behavior of the hangers in a network arch, the following was concluded:

- Large deflections are to be expected when linear analysis is performed
- For an analytical approach, a hanger should be modeled as tensioned Euler-Bernoulli beam.
- The majority of the hangers act like cables in all loading situations.
- Compression forces in the hangers are allowed in linear analysis. By nonlinear analysis the actual force distribution of the hangers should be investigated.
- Linear analysis provides good results when the ULS is considered
- Linear analysis provides good results when no transverse load is acting on the hangers (no wind).
- The bending moments in arch and main girder in plane of the arch ( $M_y$ ) are underestimated by linear analysis. In the permanent load situation with wind loading this underestimation will be larger than in the ULS.
- The axial stresses in the hangers are underestimated by linear analysis. In the permanent load situation with wind loading this underestimation will be larger than in the ULS.
- The catenary effect can be neglected in the design stage.
- When detailed analysis is performed, the catenary effect cannot be neglected, especially for long and slanting hangers.

### 4.3 Modeling

In this paragraph the modeling of the arch, deck structure and hangers is discussed. The SCIA model which is used for the design of the network arch and the reference design is based on the SCIA model of the original tender design, which is described in annex D. In this model, the position of the horizontal bracing was already adjusted. See annex D for more information on the adjustments.

#### 4.3.1 Modeling arch cross-section

In the SCIA model of the original tender design, the arch was modeled as a segmented arch, as is clearly shown in figure 114. As was mentioned in paragraph 4.1.1, this segmented arch is adjusted to curved arch. This curved arch allows the network hanger arrangement to be implemented more efficiently.

In the SCIA model, the cross-section of the arch will be simplified as a rectangular box-section, as shown in Figure 51 (right). This profile can easily be implemented in the SCIA model. When optimizing this box-section the following aspects should be considered:

- Stability of the cross-section
- Translation from box-section to final arch cross-section with stiffeners

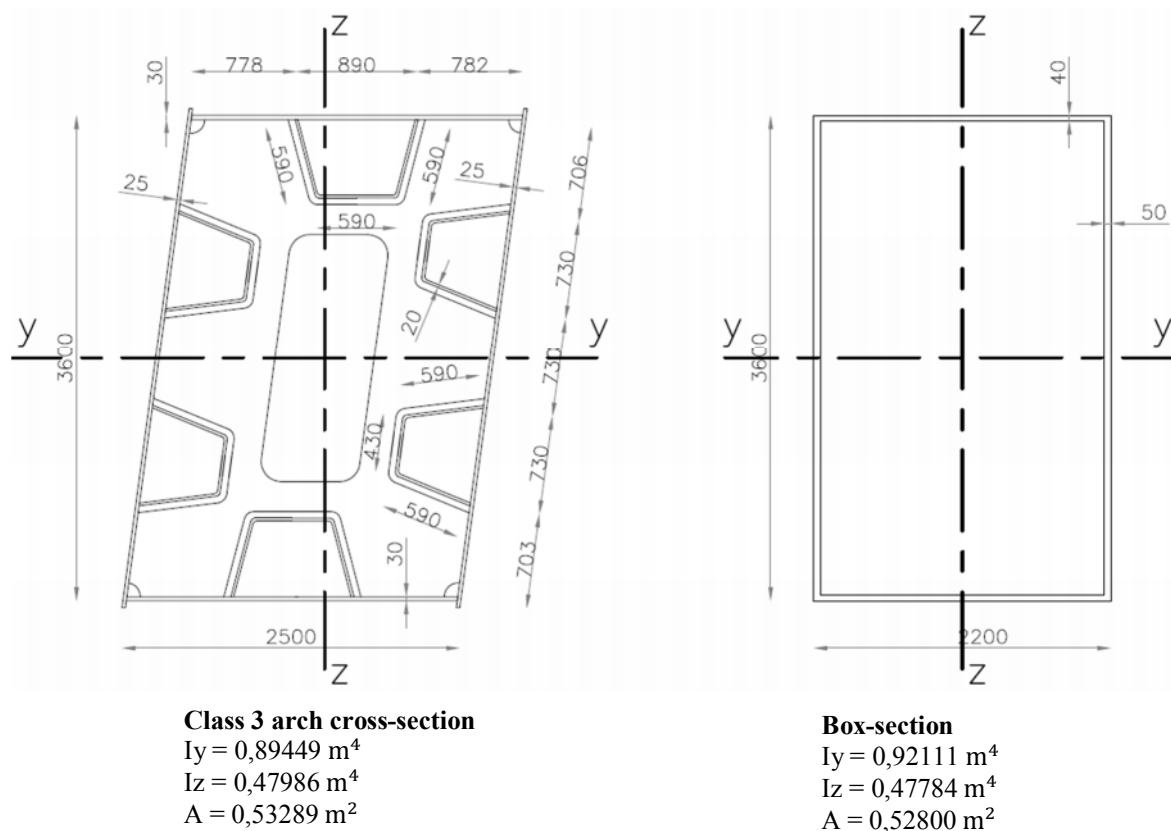


Figure 51: left: class 3 arch cross-section based on original tender design, right: simplified box-section with similar cross-sectional properties (I and A and height)

### ***Stability of the cross-section***

A compressed box-section with plate stiffeners is prone to two local instability effects:

- Plate buckling
- Stiffener buckling

The susceptibility to plate buckling is indicated by a cross-section classification class. For class 1 to 3, plate buckling will not occur. When a class 4 cross-section is applied, plate buckling should be dealt with by reducing the allowable stress, or reducing the cross-sectional area. Because simplicity is preferred in the design stage, it is decided to apply a cross-section class 3 for the arch cross-section.

To cope with the local buckling of the stiffeners, the slenderness of the stiffeners should not be too high. If very slender stiffeners were applied, the allowable stress should be reduced. This can be solved by applying diaphragms at a shorter c.t.c. distance or by applying larger stiffeners. For the class 3 section, shown in figure Figure 51, relatively large through stiffeners are applied, because the c.t.c. distance of the diaphragms is relatively large (see paragraph 4.3.3). The class 3 arch cross-section which is shown in Figure 51 (left) is based on the arch cross-section of the original tender design. In annex C.2, this cross-section is determined.

### ***Translation from box-section to final arch cross-section with stiffeners***

When the required cross-sectional properties (A, I and W) and dimensions of the box-section are determined by analyzing the SCIA model, the box-section has to be translated into a realistic cross-section with stiffeners. This translation will always lead to significantly different cross-sectional properties or dimensions. In Figure 51 a box-section and the class 3 arch cross section with similar height, cross-sectional area, stiffness is shown. The same width could not be maintained. It can be concluded that when the box-section is transformed into a stiffened box-section some properties will change.

### ***Optimizing the arch cross-section***

When optimizing the box-section, certain maximal and minimal outer dimensions should be respected. The arch and main girder should be wide enough to provide space for the hanger connection. It is assumed that 1800mm should be the minimal width. For the maximal dimensions of the arch and main girder, a plate width of 3700mm is assumed. This value corresponds to the height of the arch cross-section shown in figure 51.

In order to take the abovementioned instability effects into account when optimizing the box-section in SCIA, the plates of the box-section should not be too slender. It would be futile to determine a specific width over thickness ratio, because when the box-section is translated into an arch section with stiffeners, these ratios will be lost. When the outer dimensions and the stiffness of the box-section are respected when determining the arch cross-section with stiffeners, a significant increase in steel weight is inevitable.

For the final comparison in chapter 7, the SCIA box-section of the reference design will be compared to that of the network arch.

### **4.3.2 Modeling deck and main girder stiffness**

From the evaluation of the original tender design, it was found that the stiffness of the main girder was underestimated in the original tender design (OTD). The stiffness which is created by the composite action of the two main girders and the concrete deck plate, also known as the ‘Steiner’ component of a composed element, was neglected. This ‘Steiner’ component of the stiffness can be modeled in two ways:

- Increasing the stiffness of the concrete deck element to an equivalent stiffness.
- Applying diagonal bracing in plane of the deck with an equivalent stiffness

When diagonal bracing is applied the force distribution in the main girders is affected, and the force and stress distribution becomes unclear. To maintain a clear force distribution in the design stage it was decided to increase the stiffness of the concrete deck element. The horizontal loads are transferred by the stiff deck plate (beam) and the vertical loads are transferred by the arch, hangers and main girder. In annex C the equivalent deck stiffness is calculated and by means of an increased E-modulus implemented in the SCIA model. In this calculation the theoretical horizontal stiffness is reduced by 50% in order to take account for the following aspects:

- Creep of the concrete
- A reduced cross-section of the main girder, due to optimization

Because the relatively stiff concrete deck element will transfer all horizontal loads, the force distribution in the main girders is unrealistic. In order to obtain a more realistic stress distribution in the main girders, the stresses caused by the bending moment in the deck plate are added to the total stresses in the main girder. See paragraph 4.4.2 for how these stresses are calculated.

### **4.3.3 Modeling hangers**

In this paragraph all aspects with respect to the modeling of the hangers are discussed. The modeling is largely based on literature and on the aspects that were researched in paragraph 4.2.

#### ***Modeling the hangers with SCIA engineer***

For linear analysis the hangers can be modeled as beam elements. From paragraph 4.2.5 where the differences between linear beam and cable behavior were investigated, it was concluded that linear analysis provides sufficiently accurate results when the ULS is considered.

In order to obtain more detailed results, a geometrically nonlinear analysis is required. Through GNL analysis the cable action of a 1D beam element is taken into account.

#### ***Hanger arrangement***

From the variant study in chapter 3 the hanger arrangement shown in Figure 52 was concluded to be the most optimal arrangement. In chapter 3 also the most favorable hanger type was determined: Steel rod hanger with welded connections, estimated diameter Ø140mm.

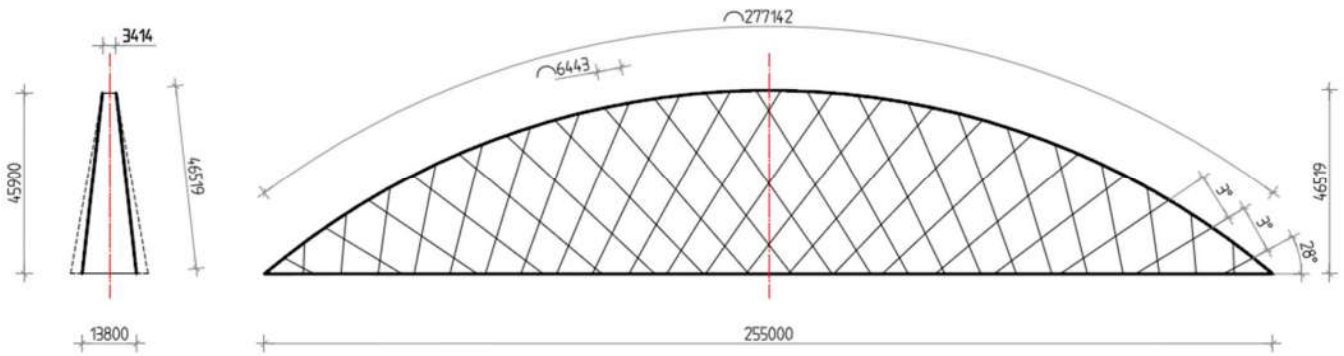


**Figure 52: Geometrical description of the preferred hanger arrangement**

The hanger arrangement is implemented in the 3D SCIA model of the reference design by following the geometrical description provided by Figure 52, and in annex B. The hangers are inserted in the plane that is formed by the apex of the arch and the main girder, as is shown Figure 52. Near the supports, where the arch and main girder are misaligned significantly, the angle of the outer hangers do not match the geometrical description. However, this should not affect the optimal force distribution in the hangers, because the outer hangers are not part of the optimal arrangement. Teich mentions specifically that the angle of the outer hangers should be manually adjusted in order to obtain a good force distribution.

To implement the optimal hanger arrangement in the 3D SCIA model, 42 nodes are placed along the arch at equal distances. Based on the coordinates of these nodes, the coordinates of the nodes along the main girder can be calculated from the angles given in Figure 52. This procedure has to be performed for only one set of hangers because by mirroring the full arrangement can be obtained. In annex B the hanger coordinates, angles and lengths are given. The hanger numbers correspond to the numbering shown in Figure 53, where the 21 individual unique hangers are shown.

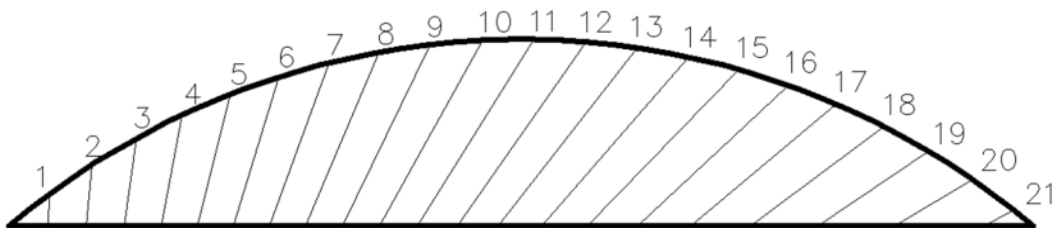


**Figure 53: Schematization of the 21 unique hangers**

### ***Connections***

The steel rod hangers are welded through a connection plate to a diaphragm in the main girder and arch. DIN-FB103 [2] provides a geometrical description of a hanger connection. This connection, shown in Figure 54 left, has been optimized for fatigue performance. In annex I.3 the hanger connection of hanger number 13 is dimensioned and modeled.

The hangers are modeled as fully fixed in the out of plane direction of the arch. In the plane of the arch, the connection plates are relatively weak in bending, therefore the hangers are modeled as hinges in the plane of the arch. For detailed analysis, a detailed isolated model of the hanger will be used. This model is provided with the realistic stiffness of the hanger connection.

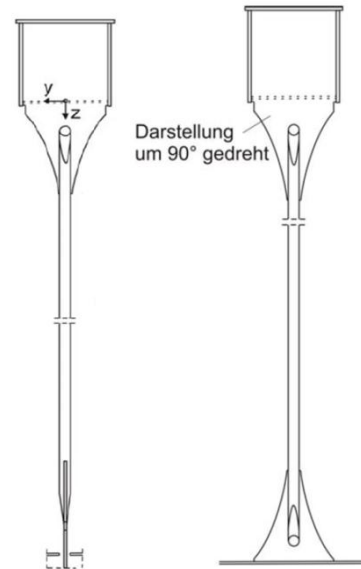


**Figure 54: Left: hanger connection directly welded to the web, right: possible orientations of hanger connections**

In Figure 54 a hanger connection is shown where the connection plate is directly welded to the web of the main girder. This results in a relatively stiff in plane hanger connection. The bending moments in the hanger connection due to the deflection of the main girder will be relatively high. Another disadvantage is the large visibility of the hanger connection. Because of the disadvantages mentioned above, the hanger connections applied in this thesis are oriented at a  $90^\circ$  angle with the main girder (see Figure 54 right).

In [25] it is recommended to apply different orientations of the hanger connections of a single hanger. ( $90^\circ$  angle between top and bottom connection) The advantage of this orientation is that the behavior in both directions is similar. Also the natural frequencies are similar for both directions.

**Remark:** This recommendation was found in the final stage of this thesis, that's why it wasn't implemented in the design of the network arch.

#### 4.4 Design verification

To verify the model for structural integrity in the design stage, a set of simplified design requirements is composed. Only the arch, main girder and hangers are verified. It is assumed that the other bridge components (deck, cross-girders, wind bracing, arch/ main girder connection) are not affected by the optimization of the arch, main girder and hangers.

For the ULS and SLS verification of the arch and main girder, the mobile load case is not considered, because the decisive load cases for these elements are already inserted as static load cases. This approach increases the efficiency of the design process because running the mobile load case is time consuming. See annex A for more information about the load cases.

From the research in paragraph 4.2 it was concluded that in order to obtain a valid design verification, the strength verifications should be performed in the ULS. The deflection could still be verified with sufficient accuracy in the SLS because no wind loading is present.

#### 4.4.1 ULS design verification arch

Large compressive forces and transverse wind loading makes the arch susceptible for buckling. The buckling resistance can be verified by evaluating the critical load factor ( $\alpha_{crit}$ ) that corresponds to a specific buckling mode. This load factor is determined as:  $\alpha_{crit} = \frac{N_{crit}}{N_{ed}}$ . By using the critical load factor from the original tender design as a reference value, the buckling resistance of the optimized reference design and network arch can be estimated. This critical load factor can be obtained by using a linear buckling analysis. A similar load combination as used in the buckling analysis of the original tender design should be used. If a different load combination was applied, the axial force in the arch ( $N_{ed}$ ) will be different and the critical load factor as well.

A maximum ULS design stress of 400 MPa is used for the arch. This stress level was also found in the original tender design in the ULS.

#### *ULS design requirements arch*

Max stress in arch ULS in the OTD: 408 MPa  $\rightarrow \sigma_{arch} \leq 400\text{MPa}$

Critical load factor ( $\alpha_{crit}$ ) OTD: 3,57  $\rightarrow \alpha_{crit} \geq 3,6$   
(Load combination:  $1,4G + 1,4G_{DL} + 1,5Q_{LM71} + 1,65Q_{wind}$ ).

#### 4.4.2 ULS design verification main girder

The main girder is mainly loaded in tension, it is assumed that buckling instability is not problematic. Due to bending, the upper and lower flange of the main girder could become compressed. Transverse wind loading also causes compression in one of the main girders due to the composite action of the deck structure and main girders. From the original tender design it was found that fatigue is not decisive for structural integrity of the main girder. For both the reference design and network arch a maximum design stress of 400 MPa is used. This stress level provides some spare capacity for eccentricities, hanger connections, drainage and other non-structural provisions.

Due to the modeling of the deck structure as a beam element, the stresses in the main girder are not fully realistic, see paragraph 4.3.2. For the ULS verification of the main girder, the stresses caused by the bending moment in the deck plate are added to the total stresses in the main girder. Because the transverse bending moment in the deck plate has a maximum at midspan, the decisive cross-section of the main girder will also be at midspan.

$$\sigma_{Mdeck} = \frac{M_{deck}}{A_{main\ girder} \cdot 13,8m}$$

Where 13,8 m is an approximated center to center distance of the main girders.

#### *ULS design requirement main girder:*

$$\sigma_{main\ girder} = \sigma_{max} + \sigma_{Mdeck} \leq 400\text{MPa}$$

#### 4.4.3 ULS design verification hangers

DIN-FB103 provides a maximum ULS design stress for hangers which should result in sufficient fatigue performance. For steel grade S460 the maximum ULS design stress is 240 MPa. To determine the maximal stress in the hangers a mobile load case is used. DIN-FB103 does not prescribe the use of a mobile load case to determine the maximum hanger stress specifically. However, for network arches a mobile load case will cause a significant stress increase. Hence, the maximum hanger forces are obtained by a mobile load case. Compression in hangers is allowed in linear analysis, see paragraph 4.2.4.

**ULS design requirement hangers:**

$$\sigma_{\text{hanger};\text{ULS}} \leq 240 \text{ MPa}$$

#### 4.4.4 SLS design verification

From the original tender design the decisive requirement in the SLS is the maximum deflection and rotation of the deck structure. In the designers guide to EN 1991-2 [10] the maximum deflection is defined as a function of the train velocity and the span length:

$$\delta_{\text{static}} < \frac{L}{15 \cdot v - 400} = \frac{L}{15 \cdot 44,44 - 400} = \frac{255}{2000} = 0,128 \text{ m}$$

Where:

$$v = \frac{160 \text{ km/h}}{3.6} = 44,44 \text{ m/s}$$

According to the designers guide [10] this strict requirement for the deflection, which is used to prevent excessive track maintenance, is stricter than the deflection requirement for the dynamic properties of the bridge. The deflection due to self-weight is counteracted by applying a pre-camber. Hence the static deflection ( $\delta_{\text{static}}$ ) due to full traffic loading should be measured. The requirements for the maximal rotation are neglected at this stage, because the stiffness of the deck is not modeled correctly. For the verification of the deflection, only full traffic loading is applied (LC3) and no wind loading, this should still provide accurate results.

**SLS design requirement:**

$$\delta_{\text{static}} < 0,128 \text{ m}$$

## 4.5 Optimizing reference design

Because some alterations were made to the modeling of the reference design, the arch and main girder should be optimized in order to obtain a fair comparison in chapter 7. In this chapter the steel weight of the reference design is compared to that of the network arch. If the reference design would not be optimized, the final comparison would give the reference design an unfair advantage.

The diagonals of the reference design were not influenced by the alterations to the modeling, for these elements no optimization is required.

### *Arch and main girder*

When optimizing the arch and main girder attention should be paid to the maximum dimensions that were specified in paragraph 4.3.1. For the arch cross-section the slenderness of the plates should not be too high.

The optimized dimensions (height x width x  $t_{web}$  x  $t_{flange}$ ) for arch and main girder are:

Arch cross-section: 3300x2900x41x40 (A = 0.49604 m<sup>2</sup>)  
 Main girder cross-section: 3700x1800x35x35 (A = 0.3801 m<sup>2</sup>)

### ULS verification

Stresses in arch: 397 MPa < 400 MPa OK  
 Critical load factor ( $\alpha_{crit}$ ): 5.15 > 3.6 OK

Stresses at midspan in main girder:

$$\sigma_{main\ girder} = 325 + \left( \frac{409175 \cdot 10^6}{0,3801 \cdot 10^6 \cdot 13,8 \cdot 10^3} = 78\ MPa \right) = 403 \approx 400\ MPa \quad OK$$

### SLS verification

Deflection main girder (LC3): 92 mm < 128 mm OK

### 4.5.1 Conclusion

The optimized reference design is modeled as shown in Figure 55. Only the arch and main girder were optimized. See annex D for more information on the original tender design.

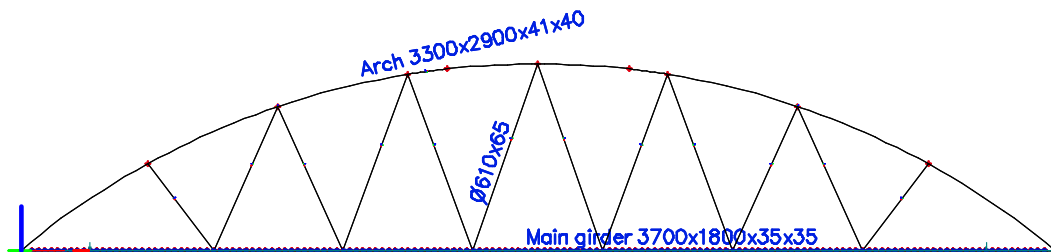


Figure 55: Relevant cross-sections optimized reference design

## 4.6 Optimizing network arch bridge

From literature it was found that for network arches the largest material reduction can be obtained by reducing the in plane stiffness of the arch. The verification of the deflection will be performed in paragraph 4.6.2. where the diameter of the hangers is optimized.

### 4.6.1 Dimensioning arch and main girder

When optimizing the arch and main girder attention should be paid to the maximum dimensions that were specified in paragraph 4.3.1. For the arch cross-section the slenderness of the plates should not be too high.

The optimized dimensions (height x width x  $t_{web}$  x  $t_{flange}$ ) for arch and main girder are:

Arch cross-section: 2300x3400x38x41 (A = 0.44737 m<sup>2</sup>)  
 Main girder cross-section: 3500x1800x35x35 (A = 0.3661 m<sup>2</sup>)

The stiffness ratio between arch and main girder is  $\frac{I_{arch}}{I_{maingirder}} = \frac{0,2483m^4}{0,6136m^4} = \frac{1}{2,5}$ . This comparable to the stiffness ratio used by Teich for his research ( $\frac{1}{3}$ ). However, from the literature study it was concluded that the stiffness of the main girder hardly influences the force distribution in the structure.

#### ULS verification

Stresses in arch: 398 MPa < 400 MPa OK  
 Load factor (stability): 5.15 > 3.6 OK

Stresses at midspan main girder:

$$\sigma_{main\ girder} = 325 + \left( \frac{409175 \cdot 10^6}{0,3801 \cdot 10^6 \cdot 13,8 \cdot 10^3} = 78\ MPa \right) = 403 \approx 400\ MPa \quad OK$$

### 4.6.2 Optimizing hanger diameter

As was explained in paragraph 4.1.2, the loads are applied in such a way that the hanger forces are symmetric. Hence, only the 21 individual hangers, shown in Figure 56, have to be evaluated. For the evaluation of the hanger forces the mobile load provides the decisive load cases. The optimized arch- and main girder cross-section are used in this evaluation.

In Table 14 the hanger forces are shown for different diameters. The stresses and deflections in the arch and main girder are also given in Table 14, to evaluate the influence of the hanger stiffness on the global force distribution.

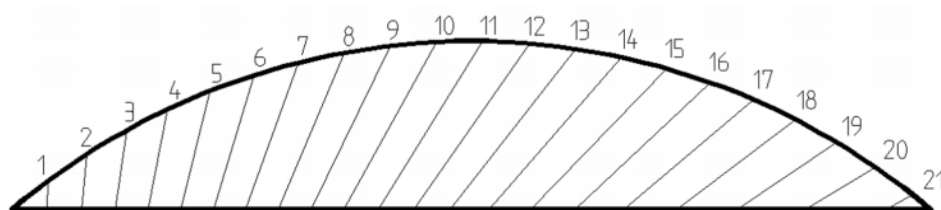


Figure 56: Schematic representation and numbering of single hanger set

Hanger diameters								
Ø140mm A = 0.0154 m <sup>2</sup> N <sub>σ240</sub> = 3695 kN		Ø150mm A = 0.0177 m <sup>2</sup> N <sub>σ240</sub> = 4241 kN		Ø160mm A = 0.0201 m <sup>2</sup> N <sub>σ240</sub> = 4825 kN		Ø200mm A = 0.0314 m <sup>2</sup> N <sub>σ240</sub> = 7540 kN		
Hanger nr.	+N <sub>ULS</sub> [kN]	-N <sub>ULS</sub> [kN]	+N <sub>ULS</sub> [kN]	-N <sub>ULS</sub> [kN]	+N <sub>ULS</sub> [kN]	-N <sub>ULS</sub> [kN]	+N <sub>ULS</sub> [kN]	-N <sub>ULS</sub> [kN]
1	1461	-1034	1323	-1228	1251	-1505	931	-2651
2	2925		2865		2858		2882	-189
3	3359		3395		3432		3561	-6
4	3627		3655	-93	3681	-112	3765	
5	3873	-70	3901	-83	3928	-112	4016	-172
6	3868	-73	3891	-4	3913	-14	3991	-178
7	3794		3815	-104	3835	-87	3905	-43
8	3815	-36	3845	-183	3872	-197	3963	-121
9	3862	-127	3904	-73	3946	-89	4106	-322
10	3826	-54	3858	-21	3888	-33	3999	-137
11	3796	-8	3825		3852	-16	3950	-61
12	3744		3779		3814		3948	-90
13	3679		3711		3744		3874	
14	3827		3885		3902		4048	-30
15	4056	-200	4107	-225	4156	-247	4342	-311
16	4241	-415	4296	-440	4348	-480	4546	-569
17	4648	-700	4713	-743	4774	-779	5000	-879
18	5107	-878	5179	-925	5243	-964	5462	-1062
19	5539	-682	5643	-730	5735	-771	6020	-858
20	6120		6371		6608		7434	
21	6613		7176		7739		9969	
$\delta_{max}$	111 mm		109 mm		108 mm		103 mm	
$\sigma_{arch}$	398 MPa		398 MPa		397 MPa		399 MPa	
$\sigma_{MG}$	326+78=404 MPa		326+78=404 MPa		327+78=405 MPa		330+78=408 MPa	

Where:  
 $N_{\sigma 240}$  = hangerforce corresponding to a maximum stress level of 240 MPa  
 $\delta_{max}$  = maximum deflection (LC3) measured at cross girder at midspan < 128 mm  
 $\sigma_{arch}$  = maximum stress (LC1 – LC6) measured along the arch  
 $\sigma_{MG}$  = maximum stress (LC1 – LC6) in main girder measured at midspan.  $\sigma_{MG} = \sigma_{max} + \sigma_{Mdeck}$ .  
For the contribution of the stress due to the transverse bending moment ( $\sigma_{Mdeck}$ ) a stress of 78 MPa is used.

**Table 14: Evaluation of axial hanger forces and maximum deflection for different diameters**

From Table 14 it is concluded that a diameter of 150mm is the most efficient diameter. However, in order to meet the maximum design stress a division in hanger diameters is needed. Therefore hangers 17 to 21 require are a diameter of at least 200mm. In the next paragraph the final diameters are determined.

The stresses in the structure are barely influenced by the hanger stiffness. The deflection of the main girder is influenced more by the stiffness of the hangers.

### 4.6.3 Variant study: Removal of outer hangers

The removal of edge hangers results in immediate savings in terms of material and labor, because the amount of hangers is reduced. Important aspects to consider when evaluating the force distribution are:

- Stress increase in arch and main girder, due to hanger removal
- Maximal- and minimal forces in hangers (ULS)
- Influence on stress amplitude ( $\Delta\sigma$ )

The maximal deflection at midspan will hardly be influenced by the removal of the outer hangers, therefore this is left out of the comparison. Also forces in the hangers at the middle of the span (hanger numbers 5 to 16) are not evaluated because these are hardly affected by the removal of outer hangers.

For the evaluation of the outer hangers a realistic range is composed. Gauthier and Krontal [8] suggest to leave the first 4 positions of the hanger arrangement blank. This vague suggestion seems very radical, nevertheless it should be investigated. It is therefore decided to make realistic combinations with the hanger numbers: 1, 2, 20, 21. In annex HANNEX the results of 9 variants evaluated.

To decide on the most favorable arrangement of the outer hangers, a table is composed where the following 3 aspects are evaluated:

- Maximal hanger force
- Force amplitude ( $\Delta N_{max;ULS}$ )
- Maximum stress in main girder ( $\sigma_{ULS;max}$ )

The other results are not relevant for the final decision, and would only make the comparison less transparent. In annex H, an overview of all the results for all variants is shown.

	Variants								
	1	2	3	4	5	6	7	8	9
Removed hangers	none	1	21	1,21	1,2	20,21	1,20, 21	1,2, 21	1,2, 20,21
$N_{max;ULS}$ [kN]	9795	9723	8430	8583	10368	8855	8954	9172	9888
$\Delta N_{max;ULS}$ [kN]	1063	1139	1139	1135	1170	1467	1464	1163	1341
$\sigma_{ULS;max}$ [MPa]	357	357	361	364	370	379	376	397	394

**Table 15: Evaluation of decisive properties for outer hanger arrangements**

From Table 15 follows that variant 3 and 4 result in the lowest maximal hanger force and also have a relatively low force amplitude. However, variant 8 is even more advantageous because of the material savings due to the removal of three of the outer hangers. This would result in a total reduction of  $3 \times 4 = 12$  hangers. This variant also leads to a more efficient material usage in the main girder.

In order to meet the requirements for maximal hanger stress, the hanger diameter of hanger number 20 needs to be increased. When a diameter of  $\varnothing 220$ mm is applied the stress level becomes 257 MPa, thereby exceeding the maximum stress level with 7%. Hanger number 3 is also provided with a diameter of 200mm. This is the most outer hanger, and has according to literature a relatively high stress amplitude due to traffic loading.

**4.6.4 Conclusion**

In the paragraphs 4.6.2 and 4.6.3 the final hanger arrangement is determined. By eliminating the 3 outer hangers (hanger numbers 1, 2, and 21) a more efficient structure is obtained. Based on literature, the hanger arrangement can be further optimized by adjusting the angles of the outer hangers.

For the hangers, three different diameters are applied. These diameters are based on a maximum ULS design stress of 240 MPa. It would be interesting to investigate if this maximum design stress is conservative or not. In paragraph 6.2 a detailed fatigue analysis of a single hanger is performed.

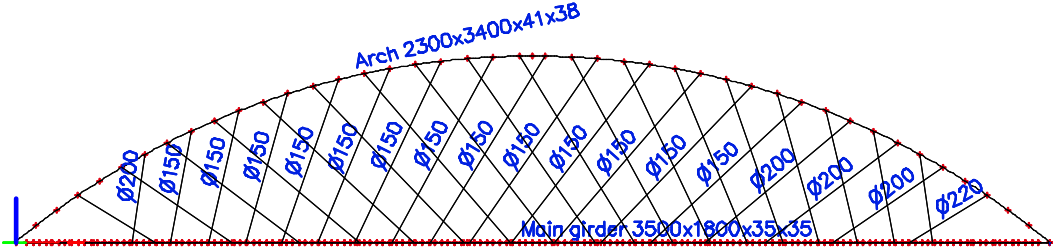


Figure 57: Relevant cross-sections optimized network arch

# 5 NONLINEAR ANALYSIS

In this chapter the geometrically nonlinear analysis (GNL analysis) is performed and the results are evaluated. In paragraph 5.1 some background information on GNL analysis is gathered. This information is used to determine a strategy in order to obtain valid results in least amount of calculation time. In paragraph 5.2 this strategy is performed and the results are validated. This validation is achieved by comparing the results obtained by GNL analysis with the force distribution in an analytical model, see paragraph 5.3.

In paragraph 5.4 the results obtained by linear- and GNL analysis are compared, and conclusions are drawn on the validity of the linear results. Specific attention is paid to the conclusions on the validity of linear analysis, that were drawn in paragraph 4.2.

In paragraph 5.5 the influence of hanger buckling and hanger relaxation on the overall structural behavior is investigated.

## 5.1 Literature review: Geometrical nonlinear analysis

In order to perform an accurate geometrical nonlinear analysis some background information is needed. The FEM program which is used for the analysis of the network arch is SCIA Engineer. The background information is obtained from SCIA manual [23] as well as from the book Finite Element Analysis of structures [22]. In this book the mathematical background of FEM analysis is explained.

In paragraph 5.2 the optimal settings for the GNL analysis are determined.

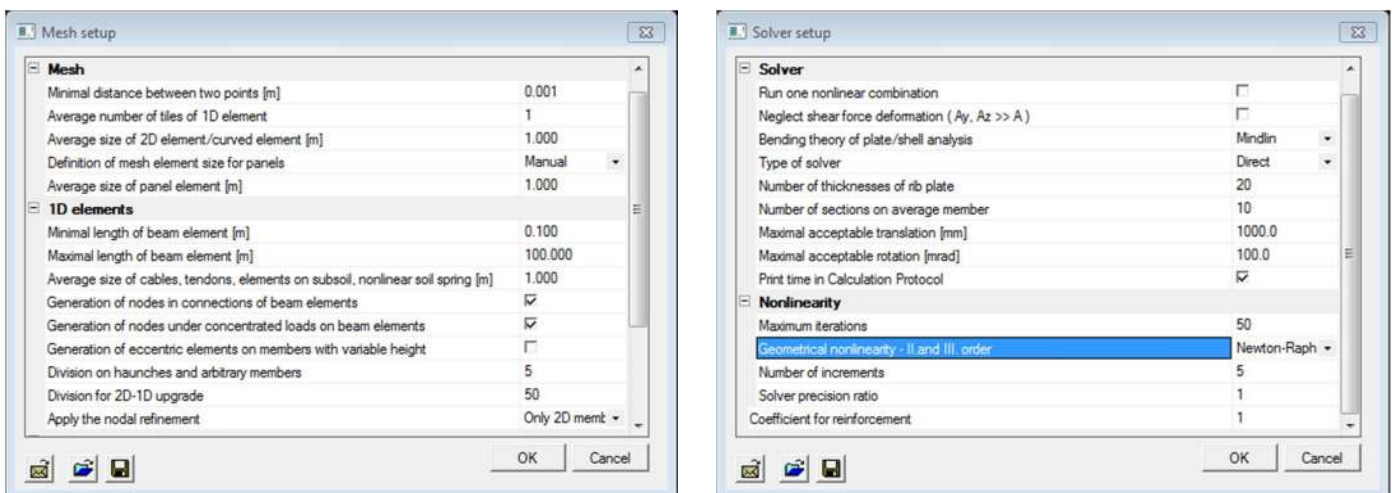


Figure 58: Default settings for solver (right), and mesh setup (left)

### 5.1.1 Mesh setup

#### ***Number of sections on member (mesh size)***

The size of the mesh has a large influence on the accuracy of the results as well as the calculation time required. A coarse mesh gives coarse results but requires the least amount of calculation time, and vice versa for a fine mesh. In [22] a number of 10 sections per element is mentioned to be sufficiently accurate at the design stage. The default mesh size of a 1D element is set by SCIA at 4 sections per element. This is also the minimal value required to perform a nonlinear calculation. In paragraph 5.2, the influence of the mesh size on the accuracy of the results is evaluated. In theory a dense mesh should result in more accurate results.

#### ***Minimal size of 1D element***

In paragraph 5.2 it was concluded that a dense mesh is required to model the behavior of the hangers correctly. By adjusting the minimal size of a 1D element the total amount of elements can be limited. The minimal element size overrules the mesh size, hence only the relatively long elements will be divided into 80 sections per element. The shorter elements are divided into elements with a minimal length as specified.

### 5.1.2 Solver setup

#### ***Maximum iterations***

The default settings give a maximum of 50 iterations. For stable structures, this maximum value is never reached, and generally around 5 iterations are required to obtain the desired accuracy.

#### ***Solution technique (geometrical nonlinearity)***

For the majority of the nonlinear problems the Newton-Raphson solution technique is the best method. Only when the solutions are near inflection points (for instance, instability) another solution method is recommended. (Modified Newton-Raphson or Picard).

#### ***Number of increments***

The number of increments is the number of steps in which the load is applied. By default, the number of increments is set to 5 increments. In paragraph 5.2, the influence of the number of increments on the accuracy of the results is evaluated.

#### ***Solver precision ratio***

This ratio is predetermined by SCIA and gives information about the accuracy that is obtained by the iteration process. Because the influence of this precision ratio on the results is unknown, the precision ratio is left unchanged (default precision ratio is 1).

## 5.2 Geometrical nonlinear analysis

From the literature review on geometrically nonlinear (GNL) analysis in paragraph 5.1 it follows that for accurate results a refined model is necessary. However, the calculation time that is required for this refined model could become quite extensive. In this paragraph the mesh and number of increments are varied to evaluate the accuracy of the results. Finally a set of optimal settings is presented for which accurate results are obtained.

The following strategy is applied:

- Step 1: Relevant results for the comparison
- Step 2: Run a GNL analysis with default SCIA settings
- Step 3: Increase the number of increments
- Step 4: Increase the density of the mesh
- Step 5: Evaluate if required accuracy is reached
- Step 6: Validation of GNL results
- Step 7: Optimizing GNL analysis

The ULS load case is used for the evaluation of the GNL analysis. This load case is specifically chosen, because other less severe load cases will not reveal all the instability effects.

### ***Step 1: Relevant results for the comparison***

For the comparison of the results, von Mises stresses are used. This is a very efficient method to evaluate the results, because von Mises stresses are built up out of all stress components working on the considered cross-section. In Table 16 the von Mises stresses are presented.

### ***Step 2: Run a GNL analysis with standard Scia settings***

As was mentioned in the previous paragraph, the following default settings are used by SCIA for a GNL analysis:

- Mesh size: 4 sections per element
- Maximal amount of iterations: 50
- Geometrical nonlinearity (method): Newton-Raphson
- Increments: 5

Total number of elements 8042

### ***Step 3/4: Increase the number of increments/ density of the mesh***

By increasing the amount of increments and the density of the mesh the model becomes more refined. In theory this should result in more accurate results. The steps that are used for the refinement of the mesh are 4, 10, 20, 40 and finally 80.

### ***Step 5: Evaluate if required accuracy is reached***

At a certain point in the procedure the results show no significant difference with the previous results. The process is monitored in Figure 59 and Table 16. It follows that the results for the stresses in the main girder, arch, deck and cross girder are not affected by the refinement of the mesh. The stresses in the hangers show a clear increase which stabilizes between a mesh size of 40 to 80 sections per element. At this point the refinement procedure can be stopped and the required accuracy is achieved.

	Default Settings						
Mesh size	4	4	10	10	20	40	80
Max. amount of iterations	50	50	50	50	50	50	50
Calculation method	N-R	N-R	N-R	N-R	N-R	N-R	N-R
Increments	5	10	5	10	5	5	5
Total elements	8042	8042	19030	19030	31358	38148	41254
Results							
$\sigma_{hanger\ nr.13;max}$	273	273	296	296	328	345	350
$\sigma_{main\ girder;max}$	363	363	363	363	364	364	364
$\sigma_{arch;max}$	426	426	425	425	425	425	425
$\sigma_{deck;max}$	45	45	45	45	45	45	45
$\sigma_{cross\ girder;max}$	162	162	162	162	162	162	162

**Table 16: Summary of von Mises stresses due to mesh refinement and increasing amount of increments**

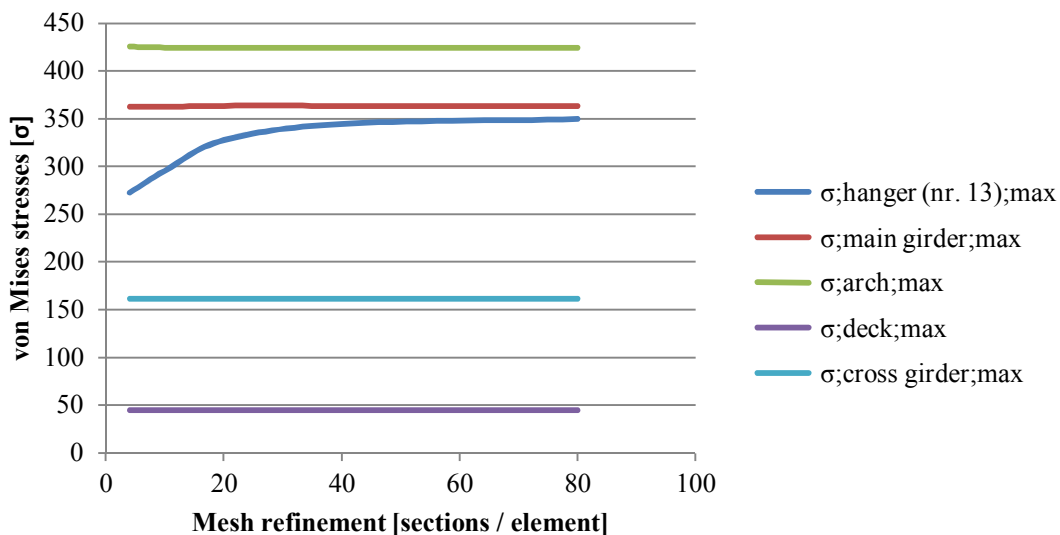


**Figure 59: Development of results as a result of mesh refinement**

### **Step 6: Validation of GNL results**

The increase in hanger stresses due to the mesh refinement can be explained by evaluating the internal forces (bending moment, shear force and axial force). It follows that the axial force is not affected by the mesh refinement (for all mesh sizes 3123 kN). The shear force and bending moment distribution are highly affected by the mesh refinement. In annex G an overview of the bending moment- and shear force distribution in hanger number 13 is given for each mesh refinement. In Figure 60 the bending moments due to wind loading are shown for a mesh size of 4, 10 and 80 sections per element.

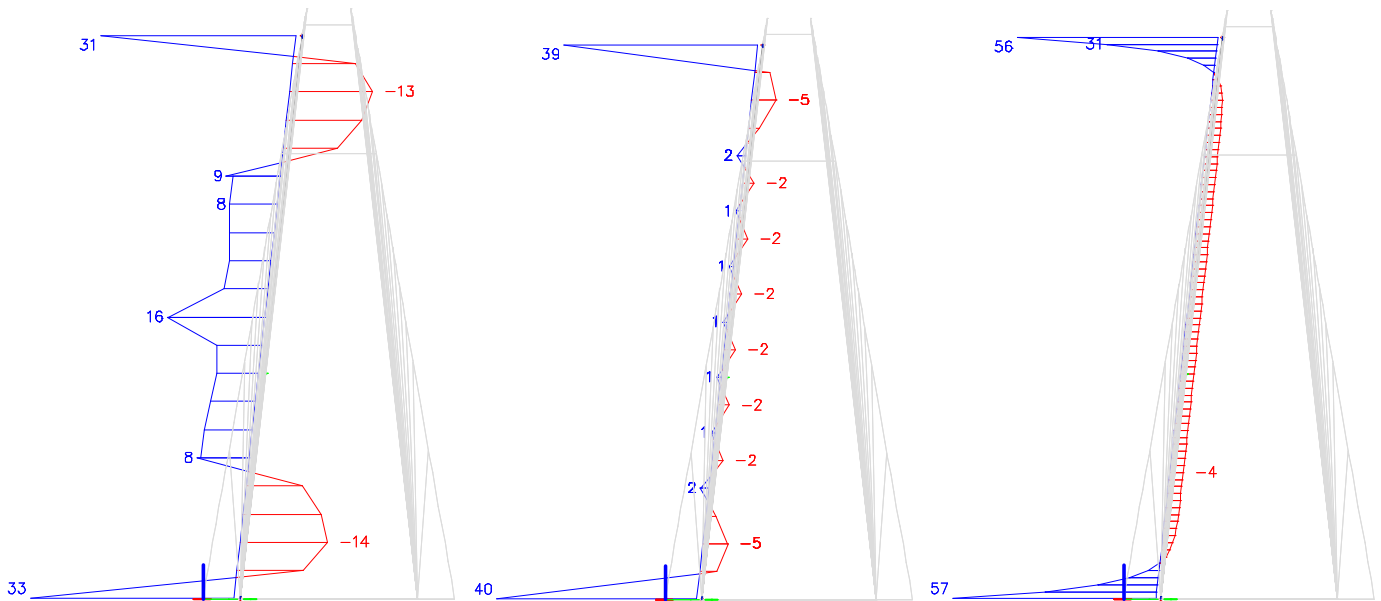


**Figure 60: Bending moment distribution  $M_z$  [kNm] due to wind loading, from left to right mesh 4, 10 and 80**

Figure 60 clearly shows that by refining the mesh, the hangers will act more as a cable. This causes the bending moment at the fixed connection to increase, thereby explaining the stress increase found in Table 16 and Figure 59. In paragraph 5.3 the bending moment and shear force diagram is compared to the analytical results, and a close fit was found.

It should be mentioned that the deformations are hardly affected by the mesh refinement. The maximum deflection ( $u_y$ ) of hanger number 13 for a mesh size of 80 sections per element is 894mm, where a mesh of 4 sections per element results in 906mm.

The accuracy of the force distribution in the arch and main girder are not affected by the mesh refinement. This is explained by the following arguments:

- A relatively high number of nodes along the arch and main girder, in order to connect the hangers and cross-girders to the main girder.
- Limited deformations

### ***Step 7: Optimizing GNL analysis***

From Table 16 becomes clear that increasing the amount of increments has no effect on the stresses in the arch, main girder and hanger. By increasing the number of sections per element (denser mesh) only the force distribution in the hanger becomes more accurate. The stresses in the arch and main girder are not affected by the mesh refinement as follows from Table 16 and Figure 59.

Because the main purpose of the GNL analysis is to evaluate real hanger behavior, a dense hanger mesh is essential. For the buckling analysis of individual hangers, a dense mesh would give the most accurate results. It is therefore decided to apply a dense mesh of 80 sections per element for the hangers. For the arch and main girder no mesh refinement is necessary because mesh refinement does not increase the accuracy of these elements.

Based on these arguments it is decided to apply local mesh refinement on the hangers. By increasing the minimal element size, the total number of elements can be reduced. The minimal element size is determined by dividing the shortest hanger into 80 sections:

$$\frac{21.779}{80} = 0,273 \approx 0,3 \text{ m}$$

If less accuracy is sufficient and calculation time is more important the minimal element size should be 1,1m (corresponding to a mesh size of 20 sections per element)

When a minimal element size of 0,3 m per section is applied the total amount of elements becomes 17390. Compared to the 41254 which would be generated for a mesh size of 80 and a minimal element size of 0,1m, an immense reduction in the amount of elements is achieved. This led to significantly lower calculation time and similar accuracy. It is decided the apply the default number of increments, because the amount of increments has no influence in the accuracy of the results.

#### ***Preferred settings for geometrically nonlinear analysis***

- Mesh size: 80 sections per element
- Average size of curved elements: 1,0 m (standard)
- Minimal length of beam element: 0,3m
- Maximal amount of iterations: 50 (standard)
- Geometrical nonlinearity (method): Newton-Raphson
- Increments: 5

#### **5.2.1 Remarks on GNL analysis**

For the GNL analysis a ULS load case should be used. If instability will occur it is most likely to occur in the ULS. During the GNL analysis instability was found in the cross girders. By changing the profile of the cross girder and increasing the stiffness, instability in the cross girder was prevented. Because the emphasis in this thesis does not lie in accurate modeling of the deck, an extremely stiff box girder was used. In order keep the self-weight of the deck structure similar, the density of the cross girder was reduced to prevent a large weight increase.

#### **5.2.2 Conclusion**

From performing and optimizing a nonlinear analysis for the network arch, the following aspects were concluded:

- The number of increments has no effect on the accuracy of the results, because the ULS shows no signs of instability.
- The amount of sections per element (mesh size) has a decisive influence in the accuracy of the results. It was concluded that at least 50 sections per element should be applied for an accurate representation of the internal forces in the hangers. For less accurate results and shorter calculation time a mesh of 20 sections per element would suffice.
- The accuracy of the force distribution in the arch and main girder is not affected by the mesh refinement.

### 5.3 Comparison between numerical and analytical results

In paragraph 4.2.2. the differential equation of an axially tensioned Euler-Bernoulli beam is given. With this differential equation the analytical force distribution can be determined. An analytical force distribution is based on a mesh size of infinite sections per element, and should therefore provide the most accurate results. In this paragraph the internal forces of an analytical (mesh =  $\infty$ ) and numerical (mesh = 80) hanger are evaluated. Hanger number 13 is used for the evaluation.

In annex F the differential equation is solved for similar boundary conditions as hanger number 13: fixed connections in-plane of the arch and hinged out of the arch plane. The force distribution in- and out of plane of the arch is assessed separately.

#### 5.3.1 Results in-plane of the arch (self-weight loading)

From Figure 61 and 62 becomes clear that the bending moment and shear force distribution obtained by the analytical- and the numerical model, in the plane of the arch, are practically similar. The difference in sign can be neglected, because this depends on the definition of the coordinate system. In the analytical model, the deformations of the overall structure are not incorporated. This could explain the slight deviation in the results.

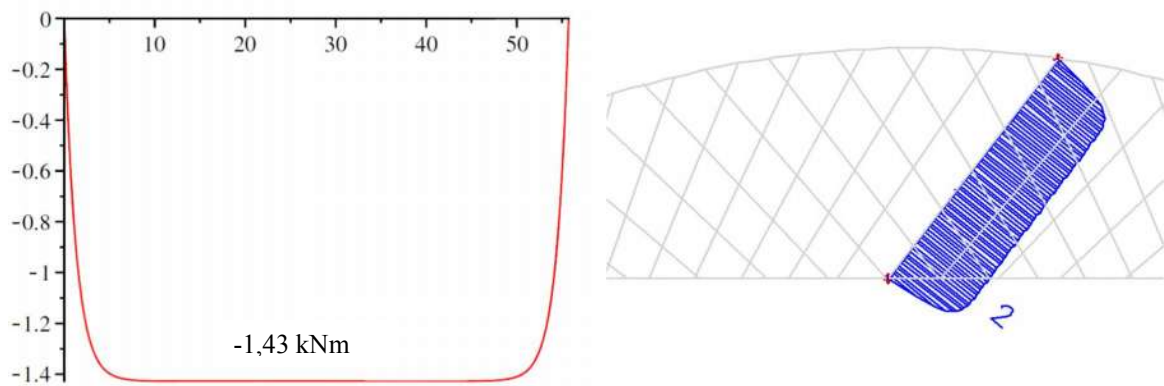


Figure 61: Bending moment distribution  $M_y$  [kNm], due to self-weight, with hinged connections. Left: analytical solution, right: numerical solution (SCIA mesh = 80)

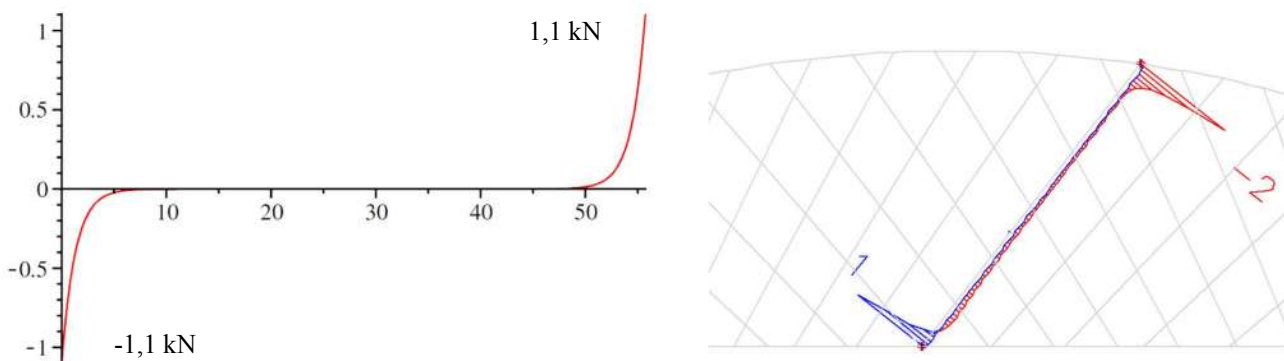


Figure 62: Shear force distribution  $V_z$  [kN], due to self-weight, with hinged connections. Left: analytical solution, right: numerical solution (SCIA mesh = 80)

### 5.3.2 Results out of arch plane (transverse wind loading)

The difference between numerical and analytical bending moments ( $M_y$ ) depicted in Figure 63, cannot be neglected. After analyzing the overall deformation of the structure it turned out that the main girder and arch undergo a serious torsional rotation. This torsional rotation causes an imposed rotation at the supports (boundaries) of the hanger. In the next paragraph, the bending moment distribution with the initial rotation is investigated.

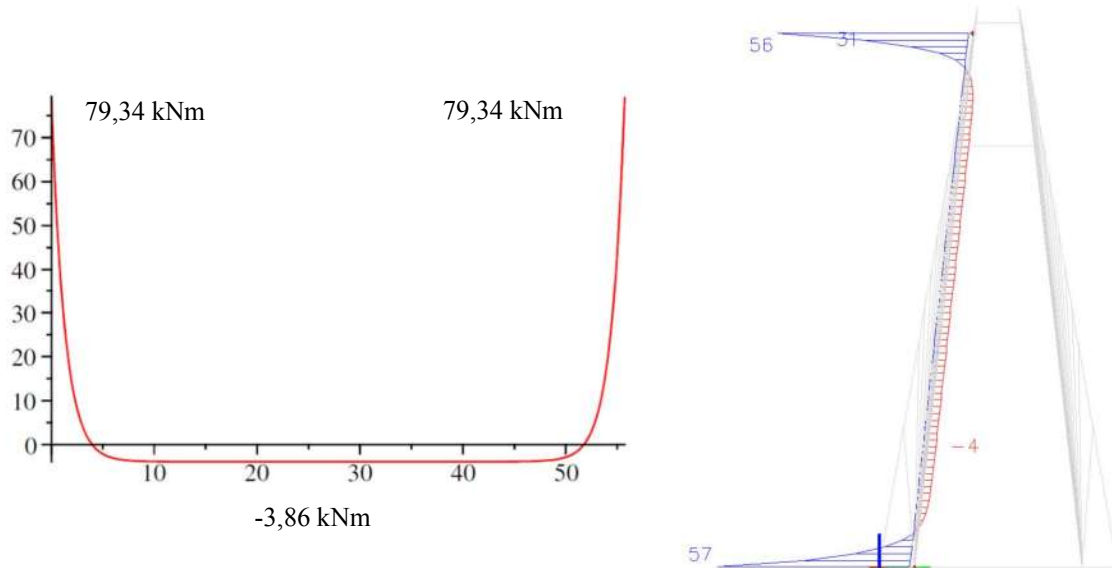


Figure 63: Bending moment distribution  $M_z$  [kNm], due to wind loading, with fixed connections. Left: analytical solution, right: numerical solution (SCIA)

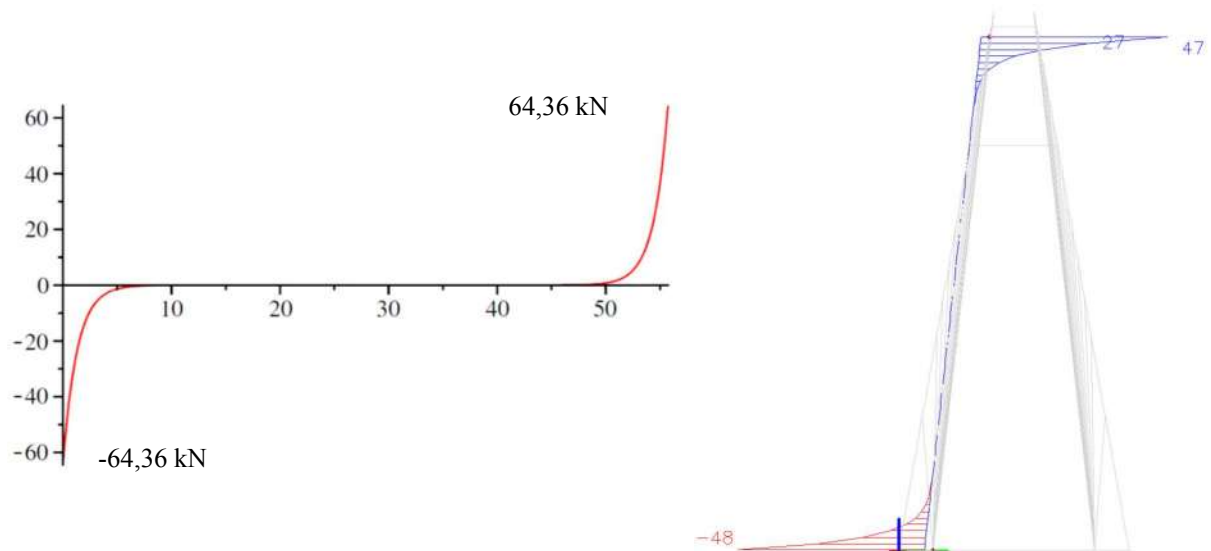


Figure 64: Shear force distribution  $V_y$  [kN], due to wind loading, with fixed connections. Left: analytical solution, right: numerical solution (SCIA)

### 5.3.3 Results out of arch plane (transverse wind loading + imposed rotations)

The initial rotations of the arch and main girder are obtained from the SCIA model:

$$\varphi_{x;main\ girder} = -12,6\ mrad$$

$$\varphi_{x;arch} = -0,4\ mrad$$

The hanger also rotates due to the deformations of the structure. It is assumed that by assigning each support with 50% of the total rotation, a good estimation is made of the initial rotation at the boundaries.

$$\varphi_{total} = -12,6 - 0,4 = -12,2 \text{ mrad}$$

The new boundary conditions for the rotation at  $x = 0$  and  $x = L$  are:

$$\varphi_{x=0} = \frac{-12,2}{2} = -6,1 \text{ mrad}$$

$$\varphi_{x=L} = 6,1 \text{ mrad}$$

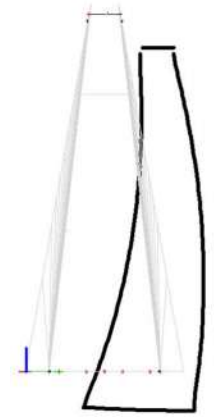


**Figure 65: Deformed structure GNL analysis (ULS)**

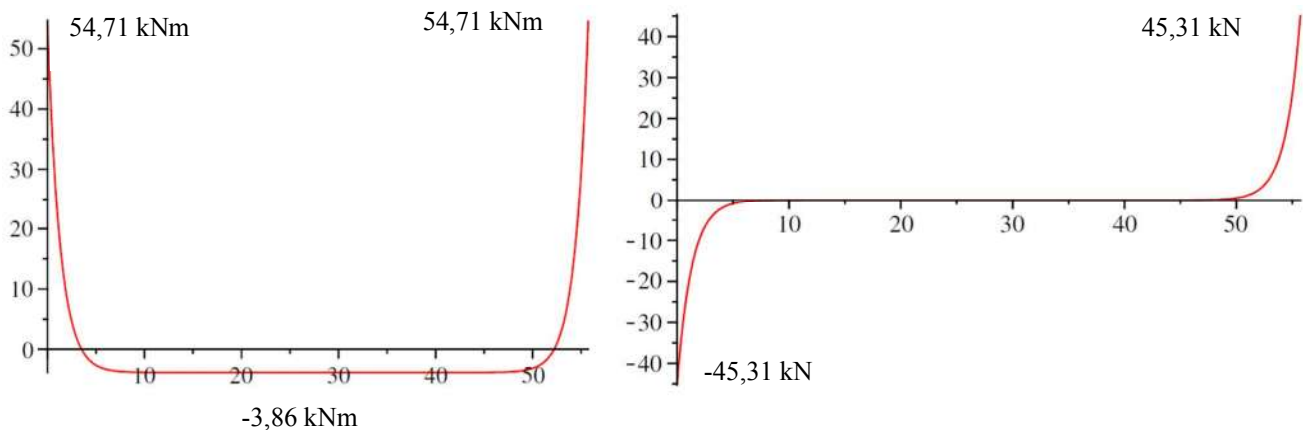


**Figure 66: Force distribution due to wind loading and initial rotations, left: bending moment distribution  $M_z$  [kNm], right: shear force distribution  $V_y$  [kN]**

### 5.3.4 Conclusion

From the comparison between the numerical (SCIA) and analytical results, the following aspects were concluded:

- When the imposed rotations are implemented as boundary conditions in the analytical model, the internal forces obtained by the analytical model correspond to the numerical results obtained from the SCIA model. Thus, the numerical results are valid.
- Bending moments: 54,71 kNm (analytical)  $\approx$  57 kNm (numerical)
- Shear forces: 45,31 kN (analytical)  $\approx$  48 kN (numerical)
- The slight deviation between numerical and analytical results can be explained by the following arguments:
  - For the analytical model, the theoretical hanger length was used. Due to deformations of the arch and main girder, this length is different.
  - Rounding differences in numerical model in forces and imposed deformations
- A mesh of 80 sections per element provides accurate results. From the graph in Figure 59 it is assumed that a mesh refinement of 50 sections per element provides sufficiently accurate results. A mesh size of 20 sections per element is advised for nonlinear analysis in the design stage, when calculation time is more important.

## 5.4 Comparison between linear and geometrically nonlinear results

In this paragraph the results of the geometrically nonlinear (GNL) analysis are compared to the results obtained by linear analysis. The conclusions of the research in paragraph 4.2, are verified in this paragraph.

In paragraph 5.4.1 the validity of linear analysis is investigated. By comparing the extreme forces and deflections a conclusion is drawn on the validity of linear analysis.

In paragraph 5.4.2 the effects of the differences between cable action and linear beam action on the global structure are investigated.

### 5.4.1 Linear analysis in global design verification

In this paragraph the extreme internal forces and deflections, obtained by linear and GNL analysis are compared.

Table 17 -Table 19 show an overview of the extreme results. In the three columns on the right the deviation is calculated as a percentage by dividing the GNL results by the linear results. If a value below 100 is found, linear analysis is conservative. When an excessive deviation between GNL and linear result is found, this is colored red.

The load cases that were considered are:

- ULS + wind
- SLS + wind
- Permanent load + wind

The ULS and SLS are investigated in order to verify if linear analysis can be used in these limit states. The permanent load situation is also investigated because the largest differences between GNL and linear force distribution are expected in this load case. This is based on the research performed in paragraph 4.2.

	Load combination: ULS + wind								
	Force distribution linear analysis (LIN)			Force distribution GNL analysis			Deviation $\frac{GNL}{LIN}$ [%]		
	Arch	Hanger Ø150mm	Main girder	Arch	Hanger Ø150mm	Main girder	Arch	Hanger Ø150mm	Main girder
$\sigma$ ;max/min [MPa]	391	2097	356	425	474	364	109	23	103
Nmax/min [kN]	-102773	3265	106240	-106227	3400	108901	103	104	102
Mx;max/min [kNm]	6653	-	13668	7131	-	10384	107	-	111
My;max/min [kNm]	28707	558	40802	30078	4	39762	105	1	98
Mz;max/min [kNm]	-67457	593	14580	-74323	104	-12696	110	18	89
Ux;max/min [mm]	260	583	271	264	589	270	102	101	99
Uy;max/min [mm]	699	11940	498	797	959	504	114	8	101
Uz;max/min [mm]	-501	-35620	-562	-502	-665	-569	100	2	101

Table 17: Comparison linear and GNL extreme results caused in ULS

	Load combination: SLS + wind								
	Force distribution linear analysis (LIN)			Force distribution GNL analysis			Deviation $\frac{GNL}{LIN}$ [%]		
	Arch	Hanger Ø150mm	Main girder	Arch	Hanger Ø150mm	Main girder	Arch	Hanger Ø150mm	Main girder
$\sigma$ ;max/min [MPa]	241	1415	220	255	314	223	106	22	101
Nmax/min [kN]	-63634	1978	65617	-65065	2028	66570	102	103	101
Mx;max/min [kNm]	4079	-	8421	4080	-	6363	100	-	76
My;max/min [kNm]	17765	390	24961	18305	4	24649	103	1	99
Mz;max/min [kNm]	-41425	359	8954	-43342	72	7377	105	20	82
Ux;max/min [mm]	161	-361	168	162	-361	168	101	100	100
Uy;max/min [mm]	424	7236	302	464	669	303	109	9	100
Uz;max/min [mm]	-312	-24723	-348	-310	-527	-347	99	2	100

Table 18: Comparison linear and GNL extreme results caused in SLS

	Load combination: Permanent load + wind								
	Force distribution linear analysis (LIN)			Force distribution GNL analysis			Deviation $\frac{GNL}{LIN}$ [%]		
	Arch	Hanger Ø150mm	Main girder	Arch	Hanger Ø150mm	Main girder	Arch	Hanger Ø150mm	Main girder
$\sigma$ ;max/min [MPa]	195	1378	167	208	312	170	107	23	102
Nmax/min [kN]	-47591	1413	51588	48797	1435	52125	103	102	101
Mx;max/min [kNm]	3577	-	7167	3631	-	5134	102	-	72
My;max/min [kNm]	13426	390	17307	13828	6	18030	103	2	104
Mz;max/min [kNm]	37000	360	7656	37722	83	6498	102	23	85
Ux;max/min [mm]	123	-267	127	125	-264	126	102	99	99
Uy;max/min [mm]	423	7258	301	466	810	302	110	11	100
Uz;max/min [mm]	-224	24652	-248	-221	583	-239	99	2	96

Table 19: Comparison linear and GNL extreme results caused by Permanent load + wind

From Table 17, Table 18 and Table 19 follows that the internal forces and deflections in arch and main girder can be modeled with sufficient accuracy by a linear model. This is valid for the three loading situations that were evaluated. The internal forces in the hangers should be fully neglected, except the axial force (N) and axial deformations (Ux).

The transverse bending moments in the arch (Mz) and the torsional bending moment (Mx) in the main girder shows a large deviation (resp. 110% and 111%) from the linear results. This can be explained by the P-delta effect (second order effect) that acts on the arch. This also explains the increased stresses and deflections in y-direction.

Because the results obtained by linear analysis are sufficiently accurate, also the linear analysis tools will still be valid, for instance:

- Linear stability, by calculating the  $\alpha_{crit}$  factor.
- Mobile load case, for which linear analysis is used.

#### 5.4.2 Evaluation of linear cable behavior on force distribution

In this paragraph the in plane bending moments ( $M_y$ ) and stresses obtained by GNL and linear analysis are compared. In paragraph 4.2 it was concluded that for relatively low axial stresses, the difference between GNL and linear force distribution increases significantly. This increase would reveal itself in the in plane bending moments in arch and main girder and the axial stresses in the hangers. The largest differences between GNL and linear results are expected in the permanent load situation.

Because the stresses in the hangers which are obtained by linear analysis are completely unrealistic (see paragraph 5.4.1) it is decided to use the stresses based on the linear axial force. The influence of the bending moments on the total stress in the hangers is neglected.

In the three columns on the right the deviation is calculated as a percentage by dividing the GNL by the linear results. If a value below 100 is found, the linear analysis is conservative. If extreme deviations are found, the result are colored red.

Load combination: ULS + wind									
Force distribution linear analysis (LIN)			Force distribution GNL analysis			Deviation $\frac{GNL}{LIN}$ [%]			
My arch node [kNm]	My main girder node [kNm]	Axial stress $\sigma$ [MPa]	My arch node [kNm]	My main girder node [kNm]	Axial stress $\sigma$ [MPa]	Arch	Main girder	Axial stress	
Hanger 10	4852	5309	182	5053	3208	195	104	60	107
Hanger 11	4980	5597	183	5300	4058	194	106	73	106
Hanger 12	5154	4662	180	4608	3986	194	89	85	108
Hanger 13	5480	5692	176	4425	5256	189	81	92	107
Hanger 14	5382	5549	173	5818	5126	175	108	92	101
Hanger 15	3911	4848	164	3328	4249	159	85	88	97
Hanger 16	3800	5940	145	875	4860	139	23	82	96

Table 20: Comparison linear and GNL force distribution in ULS

Load combination: Permanent load + wind								
Force distribution linear analysis (LIN)			Force distribution GNL analysis			Deviation $\frac{GNL}{LIN}$ [%]		
My arch node [kNm]	My main girder node [kNm]	Axial stress $\sigma$ [MPa]	My arch node [kNm]	My main girder node [kNm]	Axial stress $\sigma$ [MPa]	Arch	Main girder	Axial stress
Hanger 10	2265	2739	79	1745	848	95	77	120
Hanger 11	2264	2905	78	1548	1312	94	68	121
Hanger 12	2256	2312	74	2079	1289	92	92	124
Hanger 13	2271	1945	70	1453	1096	90	64	129
Hanger 14	2204	2000	68	1950	1101	87	88	128
Hanger 15	1694	2513	67	1208	1439	83	71	124
Hanger 16	1958	3040	59	593	1595	81	30	137

Table 21: Comparison linear and GNL force distribution by permanent load + wind

From Table 20 and Table 21 it can be concluded that the deviation between linear and GNL results are higher for the permanent loading situation with wind, hereby confirming the findings in paragraph 4.2.

In paragraph 4.2 it was concluded that the bending moments would increase due to the differences between cable and linear beam action. However, from Table 20 and Table 21 it can be concluded that the bending moments decrease instead of the increase that was expected. This shows that by linear analysis the bending moments in plane of the arch are overestimated, because the full support of the hangers in plane of the arch is not incorporated.

The extreme deviations between the bending moments in the main girder, shown in Table 21, cannot be fully explained by the increased support of the hangers. The large tensile force that acts on the main girder also counteracts some of the bending moments in the main girder.

The stresses in the hangers show a large deviation when the linear and GNL results are compared. This can be explained by the following:

- The linear hanger stresses were underestimated because these are solely based on axial forces (no bending moments)
- The additional axial force, which is generated by the cable action, causes a stress increase in the GNL results.

The extreme deviation that is measured at the arch node of hanger 16 can be explained by the horizontal bracing which is also connected to this node.

### 5.4.3 Conclusion

From the comparison between the results obtained by linear and nonlinear analysis, the following was concluded:

- By linear analysis the global extreme internal forces and deflections can be determined with sufficient accuracy for the arch and main girder.
- The *axial* force and *axial* deformation of the hangers can be determined by linear analysis with sufficient accuracy. All other internal forces and deformations of the hangers should be neglected
- When permanent load and wind are combined, the total stress cannot be estimated by simply dividing the axial force by the cross-sectional area of the hanger, due to the large deviation in the results.
- Linear analysis provides conservative results when the bending moments (My) in the arch and main girder are considered. The support of the hanger network to the arch and main girder is underestimated.
- The axial tensile force in the main girder reduces the bending moments (My). This effect is not taken into account by linear analysis.

## 5.5 Effect of hanger relaxation on global stability

From literature it follows that when certain hangers become relaxed or develop compression the structure should be examined more closely. In this paragraph two situations are investigated:

- Effect of hanger relaxation on global stability (paragraph 5.6.2)
- Effect of hanger buckling on global stability (paragraph 5.6.1)

### 5.5.1 Lateral buckling of compressed hanger

When a hanger would buckle this should not automatically mean that the structural integrity is lost. When the forces are redistributed through the hanger network to the arch and main girder, the structural integrity is still valid.

From the linear force distribution in the ULS, shown in Figure 72, it follows that the short and steep hangers will not develop compression. To investigate the effects of hanger buckling, a hypothetical load case is created which allows for sufficient compression in the shortest and steepest hanger: hanger number 3.

#### *Hypothetical load case*

To ensure that hanger number 3 will develop sufficient compressive forces, the entire ballast layer is not considered. This results in a weight reduction of:  $q_{Dead\ load} = 2 \cdot 63\text{kN/m} = 126\text{kN/m}$ . This hypothetical load case is comparable to a network arch with an orthotropic steel deck.

### Unfavorable load position hanger number 3

With the use of influence lines, a load case can be composed to generate compression in hanger number 3. By placing the loads in the negative area of the influence line, a maximal compressive force is generated. For both tracks this negative influence area lies between 53m to 255m with a maximum at 70m along the length of the span.

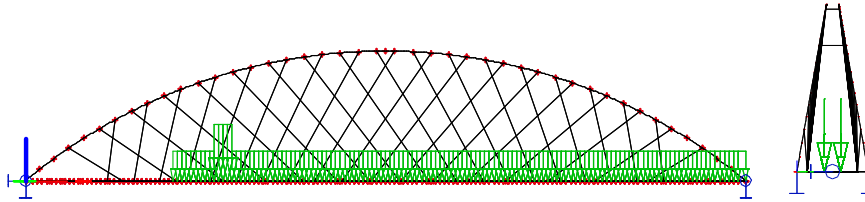


Figure 67: Load case compression hanger number 3 (LC – Comp. hanger 3)

### Imperfection

To ensure that the hanger will buckle, a local imperfection is applied in the direction transverse to the wind direction. For a conservative approach the imperfection based on buckling curve d is used. This imperfection is applied by an equivalent transverse load of 0,8 kN/m applied in the direction of the weak axis of the hanger (in-plane of the arch). SCIA engineer provides a function to insert the deformed structure from a certain load case as initial imperfection.

Imperfection:

$$e_0 = \frac{L}{150} = \frac{21.780}{150} = 0,145 \text{ m}$$

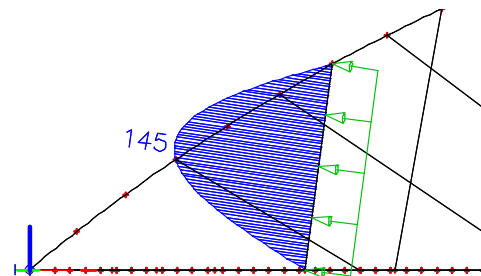


Figure 68: Imperfection obtained by transverse load of 0,8 kN/m

### Load combination

Load case	Loading	Partial safety factor
LC1	Self-weight	0,9
LC2	Dead load	0
LC6	Wind load in one direction	1,65
LC18	Compression hanger 3	1,82
Imperfection from load case shown in Figure 68		

Table 22: Load combination for evaluating influence of hanger buckling

### Results

It can be concluded that hanger number 3 has buckled as a result of the load combination shown in Table 22 (with imperfection), this conclusion is supported by the following arguments:

- Axial force obtained by linear analysis is higher than the nonlinear axial force (factor 2,1).
- Bending moments  $M_y$  obtained by nonlinear analysis are much higher than those obtained by linear analysis (factor 3,6).

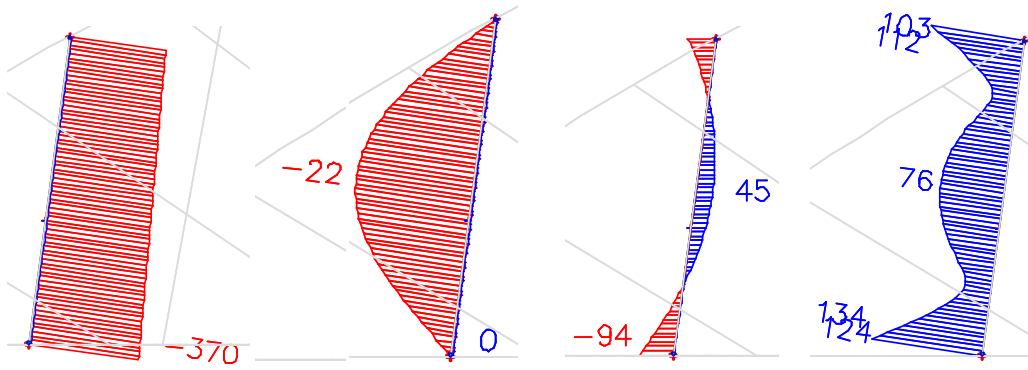


Figure 69: Internal forces in hanger nr. 3 obtained by linear analysis for the load combination shown in Table 22 without imperfection

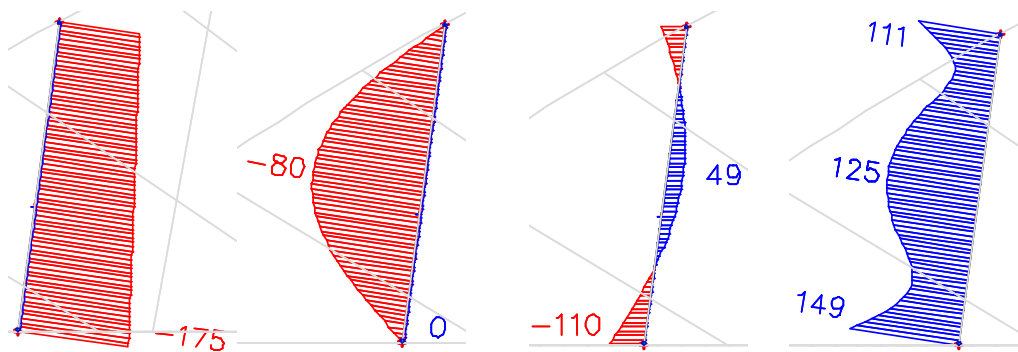


Figure 70: Internal forces in hanger nr. 3 obtained by nonlinear analysis for the load combination shown in Table 22 with imperfection

When hanger number 3 buckles, this results in a maximum von Mises stress in the arch of 303 MPa. This stress increase is nowhere near the yield strength (460 MPa). Even when an additional imperfection is applied to the arch the yield strength will not be reached.

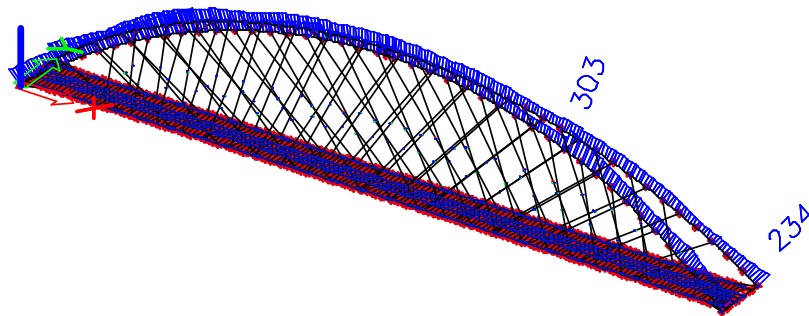


Figure 71: Von Mises stresses in arch due to buckling of hanger number 3. Obtained by nonlinear analysis for the load combination shown in Table 22 with imperfection

### 5.5.2 Influence of hanger relaxation on the global stability

When hangers become relaxed, they lose their supporting function in plane of the arch. This could cause a significant increase in bending moment ( $M_y$ ) in plane of the arch, in order to cope with the loss of support.

In this paragraph the stress increase by the relaxing hangers is determined. If this stress increase is significant, and could endanger the overall stability of the arch, a more detailed buckling analysis is performed.

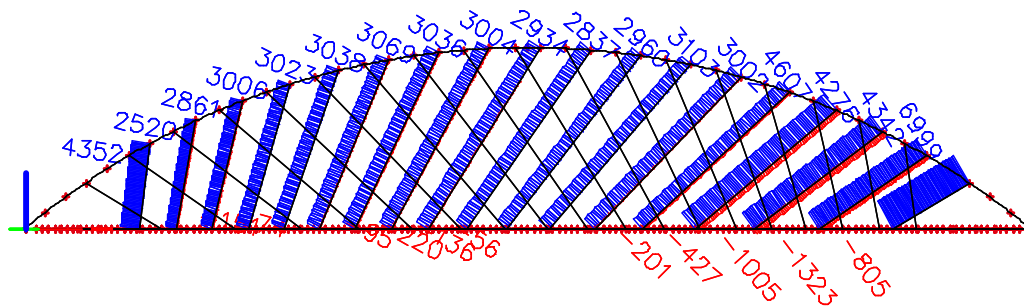


Figure 72: ULS linear force distribution, axial hanger forces [kN]

#### Unfavorable load position hangers 15 to 19

In order to find the most unfavorable loading situation which results in the largest amount of relaxed hangers combined with a high axial force in the arch, the influence lines of the compressed hangers are evaluated, see Figure 73. When the traffic load is applied in the negative influence region of hanger 15, the best combination of high axial force and most relaxed hangers is achieved. The range of the negative influence line of hanger 15 lies between 170m and 255m with a maximum at 210m along the length of the span, for both track 1 and track 2. This results in the load case shown in Figure 74.

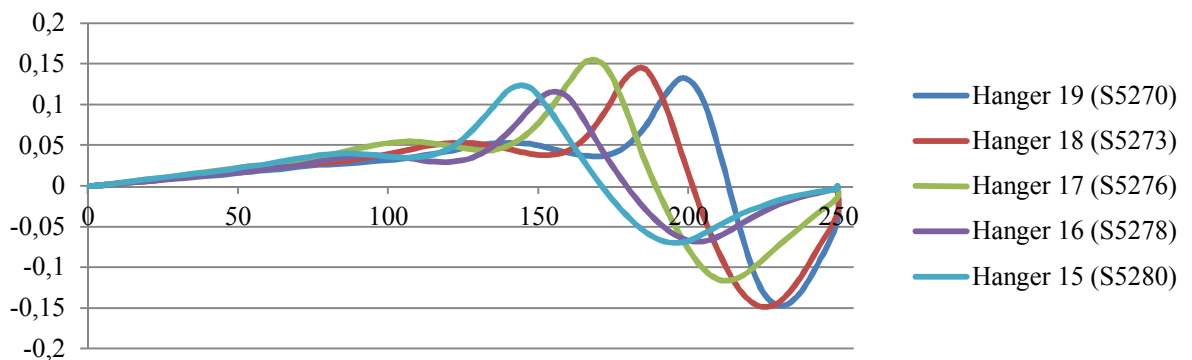


Figure 73: Influence lines of hangers 15 to 19 due to mobile load on track 1 and 2

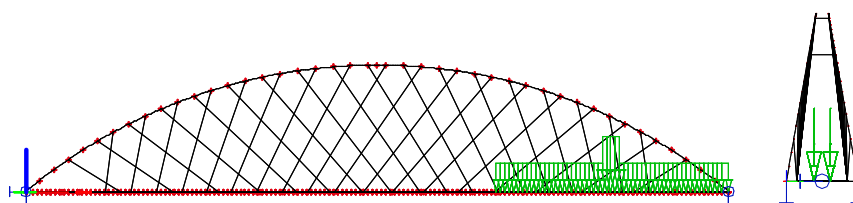


Figure 74: Load case maximal N + maximal amount of relaxed hangers (LC - Relaxation hanger 15-19)

### Load combination

Load case	Loading	Partial safety factor
LC1	Self-weight	0,9
LC2	Dead load	0,63
LC6	Wind load in one direction	1,65
LC	Relaxation hanger 15-19	1,82

Table 23: Load combination for evaluating influence of hanger relaxation

### Results

It is concluded that its very unlikely that hanger relaxation causes global instability. Because only a limited part of the span is loaded by traffic, the axial force in the arch is relatively low. The arch which is dimensioned for a fully traffic loaded bridge in the ULS has enough spare capacity to cope with the loss of in plane support caused by the relaxed hangers. Without imperfections the yield strength in the arch is 306 MPa. Even when imperfections are applied, the maximum stresses in this load case will not exceed the maximum yield strength (460 MPa).

In Figure 75 and Figure 76 the axial forces in the hangers are shown for the resp. linear and nonlinear force distribution. As was assumed in paragraph 4.2.4, no compression will occur in long and slanting hangers. The remaining axial force is a result of the self-weight of the hanger.

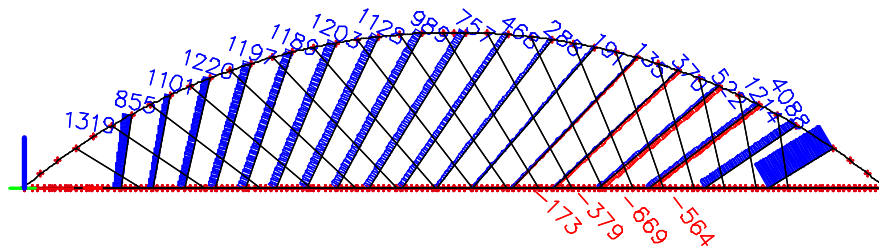


Figure 75: Linear axial force [kN] distribution of the load combination from Table 23

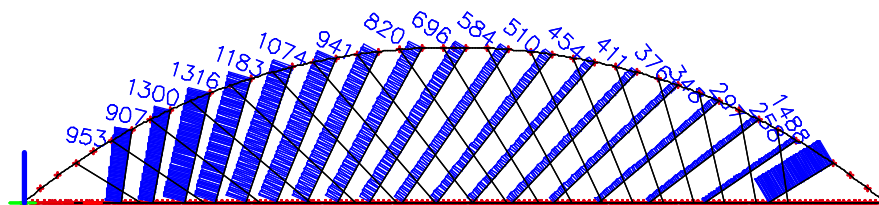


Figure 76: Geometrically nonlinear axial force [kN] distribution of the load combination from Table

23

### 5.5.3 Conclusion

From the investigation of the effects of compressed or relaxed hangers on the overall structural behavior, the following is concluded:

- No influence on fatigue behavior of the hangers because compression/ relaxation only occurs in ULS.
- Long and slanting hangers will never develop compression because these will deflect due to their self-weight.
- Only the short and steep hangers are able to buckle due to compression.

- A network arch can effectively redistribute the forces when hangers become relaxed or buckle. This is caused by the statically indeterminate network hanger arrangement.
- Global instability caused by hanger relaxation will not occur for this specific network arch bridge. The load case which causes hangers to become relaxed, results in a small axial force in the arch because only a limited part of the span is loaded by traffic. The arch which is dimensioned for a fully traffic loaded bridge in the ULS has enough spare capacity to cope with the loss of in plane support caused by the relaxed hangers.
- When a lighter deck structure is applied more hangers will become relaxed in the ULS. Therefore the effects of hanger relaxation/ compression on the global stability should be investigated for lighter deck structures.

## 6 VERIFICATION STAGE

The main objective of the verification stage is to clarify the uncertain design aspects that were mentioned in the introduction:

- Fatigue performance of the hangers
- Susceptibility to vibration effects, especially vortex induced vibrations

Along with quantifying the risks, the overall model must at least comply with the basic ultimate- and serviceability limit state criteria:

- Strength and stability
- Fatigue
- Dynamic behavior

The deflection was already verified in the design stage in paragraph 4.6.2 by linear analysis. From the evaluation of the linear and nonlinear results it was concluded that for the global deflections linear analysis provides accurate results.

In 6.1 the stability of the arch is verified by running a geometrically nonlinear analysis with an initial imperfection.

In paragraph 6.2 the fatigue performance of the hangers is investigated. For the total amount of damage caused by fatigue, the load cycles caused by vortex induced vibrations should also be taken into account. In this paragraph also the resistance of the hangers against rain and wind induced vibrations is verified. In paragraph 6.5 the susceptibility for structural vibrations is assessed.

The fatigue performance of the arch and main girder is quantified in paragraph 6.3.

In paragraph 6.4 the dynamic requirements are verified.

### ***Reference design***

For the reference design, the abovementioned ultimate- and serviceability limit state criteria should also comply. The fatigue performance and strength of the hangers was already verified by Iv-Infra for the original tender design. The arch and main girder of the reference design were also designed for a maximum stress level of 400 MPa. If the network arch meets the structural requirements with a large margin, it is safe to assume that the reference design also complies with the structural requirements.

## 6.1 Stability verification (ULS)

To verify the structure for instability effects, the following aspects must be addressed:

- Global stability: buckling resistance of the arch
- Local stability: buckling resistance of the arch cross-section

The local stability of the arch cross-section is assumed to be sufficient. In paragraph 4.3.1 where the modeling of the arch is discussed, attention is paid to these local instability effects. It was concluded that when the arch cross-section is translated into a final stiffened section the local stability verification should take place. Figure 51 shows an example of a final arch cross-section with through stiffeners of cross-section class 3. A class 4 cross-section can also provide an economic alternative, however, attention should be paid to reduction of the allowable stresses.

For the final comparison of the network arch and reference design, the exact cross-section of the arch is irrelevant because the optimized box-sections will be compared. If local buckling would be problematic and demanded an increase of steel, this would also arise in the reference design. Hence, the comparison would still be valid.

### 6.1.1 Global stability: buckling resistance of the arch

The stability verification of the arch is performed according to the following steps:

Step 1: Determining decisive buckling mode

Step 2: Calculating imperfections

Step 3: Implementing imperfections in the SCIA model

Step 4: Running a geometrically nonlinear analysis

Step 5: Verification of the results

In paragraph 5.5 the effects of hanger relaxation on global buckling behavior have been investigated. It was concluded that hanger compression/ relaxation will not lead to global instability for this specific network arch.

#### ***Step 1: Determining decisive buckling mode***

The decisive buckling mode is the buckling shape with the lowest critical load factor ( $\alpha_{crit}$ ).

This load factor is determined as:  $\alpha_{crit} = \frac{N_{crit}}{N_{ed}}$ . SCIA engineer provides a linear and nonlinear stability tool to calculate the buckling modes and their corresponding critical load factors ( $\alpha_{crit}$ ).

In paragraph 5.4 it was concluded that the linear results correspond, with sufficient accuracy, to the nonlinear results, especially to the internal forces in the overall structure. Based on this conclusion it was decided to apply the linear stability analysis with SCIA engineer.

When linear stability analysis was performed on the refined SCIA model (mesh size 80), the results showed an endless list of negative critical load factors. These negative critical load factors are a byproduct of the linear stability analysis (where the eigenvalues of the stiffness matrix of a structure are determined). SCIA is unable to filter the relevant critical buckling loads from the irrelevant negative load factors.

This problem was solved by applying linear stability analysis, with a mesh refinement of 1 section per element (mesh size 1). For the force distribution in the overall structure, this has no effect because the mesh size hardly influences the force distribution in the arch and main girder (see paragraph 5.2). For the hangers, which now consist of 1 element, this mesh size prevents the endless list of negative critical load factors.

The buckling modes and their corresponding critical load factors obtained by the linear stability analysis (mesh size 1) ( $\alpha_{crit}$ ) are shown in Figure 79. It follows that the lowest critical load factor is  $\alpha_{crit;1} = 4,8$ . However, because the critical load factor for the second buckling mode is slightly higher ( $\alpha_{crit;2} = 4,88$ ), this buckling mode should also be investigated when a detailed analysis is performed.

**Remark:** Nonlinear stability analysis was also performed. This resulted in unrealistic buckling modes e.g. unstable deck structure. A possible explanation of these strange results is the simplified modeling of the deck structure. Based on this, the recommendation is made to use a more realistic model when performing detailed calculations on a network arch. Nonlinear stability analysis is expected to result in slightly higher critical load factors, because the hangers will provide more in plane support to the arch. This is based on the comparison between linear and nonlinear analysis in paragraph 5.4. From this comparison it was concluded that with linear analysis, the in plane support of the hangers is underestimated.

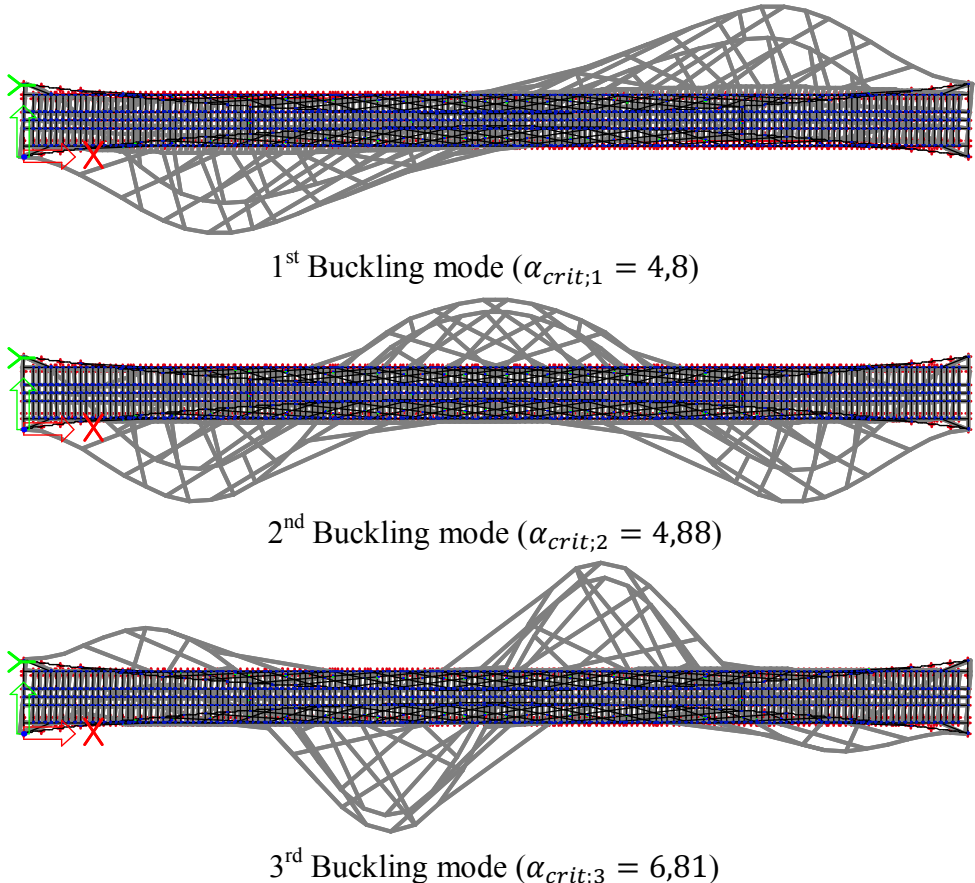


**Figure 77: Buckling modes 1 to 3 obtained by linear stability analysis and mesh size of 1 section per element**

**Step 2: Calculating imperfections**

Global imperfections can be calculated by three methods given by the NEN-EN 1993-1-1, paragraph 5.3.2. The manual for buckling analysis with SCIA engineer [27], uses method 5.3.2. (11). This method calculates an initial imperfection ( $e_0$ ) which is multiplied by the following factor:

$$\frac{N_{crit}}{EI_y \cdot \eta''_{cr,max}}$$

**Determining  $\eta''_{cr,max}$**

To determine the maximum curvature ( $\eta''_{cr,max}$ ), an intermediate step is required. The nodal displacement of the buckling shape, as shown in figure 79, is provided with a fictitious amplitude. The fictitious deflection of the buckling shape is now translated into a polynomial function by using Excel, see Figure 79. This polynomial function is then derived twice to obtain the function for the curvature. When the final imperfection is determined, the function of the buckling shape ( $\eta_{cr}$ ) is divided by a function of its curvature ( $\eta''_{cr,max}$ ). Due to this division, the fictitious amplitude is eliminated.

In Figure 79 the calculation of the term  $EI_y \cdot \eta''_{cr,max}$  is shown.

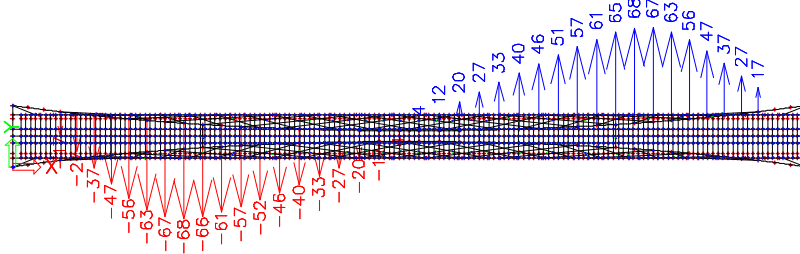
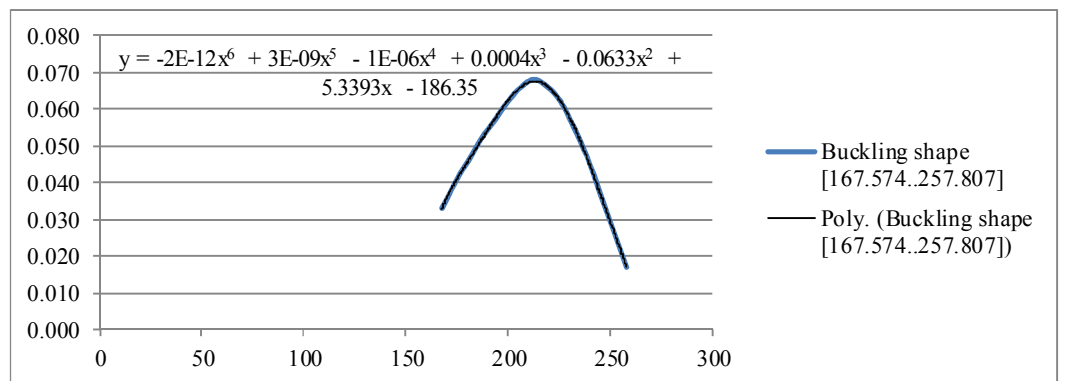


**Figure 78: Displacement of the arch in the 1<sup>st</sup> buckling mode ( $\alpha_{crit} = 4, 8$ )**

Coordinates		
Node	Dist (x)	Uy (m)
26	167.57423	0.033
27	174.0194	0.040
28	180.46456	0.046
29	186.90972	0.052
30	193.35488	0.057
31	199.80005	0.062
32	206.24521	0.066
33	212.69037	0.068
34	219.13553	0.066
35	225.5807	0.062
36	232.02586	0.055
37	238.47102	0.047
38	244.91619	0.037
39	251.36135	0.027
40	257.80651	0.017



$$\begin{aligned} \eta(x) &= -2E-12 \cdot x^6 + 3E-09 \cdot x^5 - 1E-06 \cdot x^4 + 0.0004 \cdot x^3 - 0.0633 \cdot x^2 + 5.3393 \cdot x - 186.35 \\ \eta'(x) &= -6 \cdot 2E-12 \cdot x^5 + 5 \cdot 3E-09 \cdot x^4 - 4 \cdot 1E-06 \cdot x^3 + 3 \cdot 0.0004 \cdot x^2 - 2 \cdot 0.0633 \cdot x + 5.3393 \\ \eta''(x) &= -5 \cdot 6 \cdot 2E-12 \cdot x^4 + 4 \cdot 5 \cdot 3E-09 \cdot x^3 - 3 \cdot 4 \cdot 1E-06 \cdot x^2 + 2 \cdot 3 \cdot 0.0004 \cdot x - 2 \cdot 0.0633 \\ \eta''(212.6904) &= 0.2955174 = \eta''_{max} \\ EI_y &= 147943.53 \\ E I_y \cdot \eta''_{max} &= 43720 \text{ kNm} \end{aligned}$$

**Figure 79: Conversion of numerical values to polynomial function to describe the buckling mode.**

### Imperfections

$$\eta_{init} = e_0 \cdot \frac{N_{crit}}{E I_y \cdot \eta''_{cr,max}} \cdot \eta_{cr} = 0,214 \cdot \frac{493310}{43720} \cdot 0,068 = 0,164 \text{ m}$$

$$\eta_{cr} = 68 \text{ mm}$$

$$e_0 = \alpha(\lambda_{rel} - 0.2) \cdot \frac{M_{Rk}}{N_{Rk}} = 0,49 \cdot (0,646 - 0.2) \cdot \frac{201567}{205790} = 0,214 \text{ m}$$

Where:

$$\alpha = 0,49 \quad (\text{c, welded section with thick welds})$$

$$\lambda_{rel} = \sqrt{\frac{N_{Rk}}{N_{crit}}} = \sqrt{\frac{205790}{493310}} = 0,646$$

$$M_{Rk} = W_z \cdot f_{yd} = 4,3819 \cdot 10^{-1} \cdot 460 \cdot 10^3 = 201567 \text{ kN}$$

$$W_z = 4,3819 \cdot 10^{-1} \text{ m}^3$$

$$N_{Rk} = A \cdot f_{yd} = 4,4737 \cdot 10^{-1} \cdot 460 \cdot 10^3 = 205790 \text{ kN}$$

$$A = 4,4737 \cdot 10^{-1} \text{ m}^2$$

$$N_{crit} = \alpha_{crit} \cdot N_{ULS} = 4,8 \cdot 102773 = 493310 \text{ kN}$$

$$N_{ed} = -102773 \text{ kN}$$

### **Step 3: Implementing imperfections in the SCIA model**

The calculated imperfection should be implemented in the model as the maximum deflection of the buckling shape. Normally, SCIA provides a function to assign a maximum deflection (imperfection) to the buckling shape. This function cannot be used because the buckling shapes can only be calculated with a mesh size of 1 section per element, and a geometrically nonlinear analysis can only be performed when a mesh size of 4 sections per element is used.

To overcome this problem, the imperfection is created by applying a distributed load of 10 kN in transverse direction of the arch. The deformations due to this load case can now be used as an initial imperfection. The forces created by this load case are not incorporated in the load combination for the buckling verification, only the deflections. In figure 81 the load case that generates the buckling shape is shown. In figure 82 the deflected shape due to this load case is shown, the maximum deflection of 160 mm is practically similar as the imperfection  $\eta_{init} = 164 \text{ mm}$  calculated in paragraph

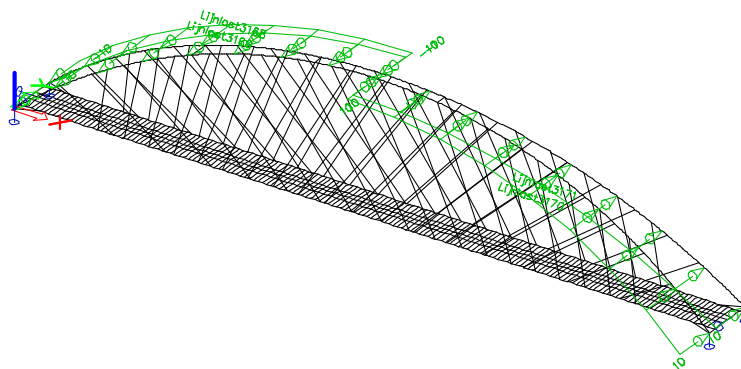


**Figure 80: LC – Buckling shape: Alternating distributed load of 22 kN to generate the first buckling shape with maximal deflections**

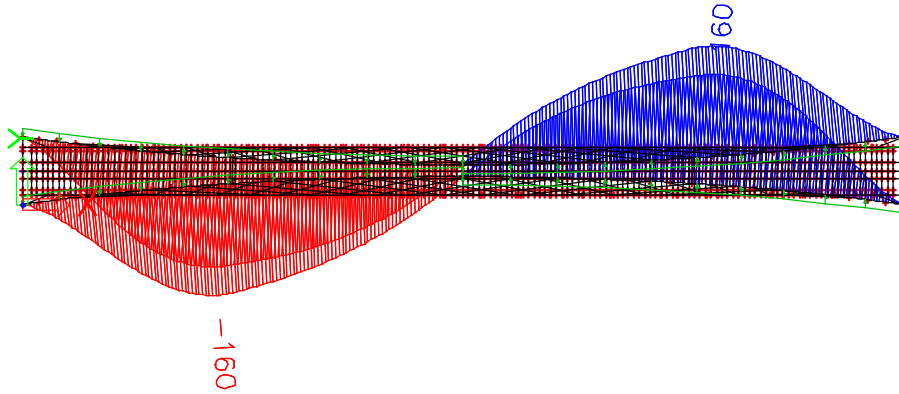


Figure 81: Deflections [mm] obtained by LC – Global buckling shape (see Figure 80). Maximum deflection at the left end of the span  $160 \approx \eta_{init} = 164$

**Step 4: Running a geometrically nonlinear analysis**

Finally the geometrically nonlinear analysis can be performed with the ULS combination, shown in table 24 combined with the imperfections that were determined by the load case shown in figure 81.

Combination	Load factor
LC1 - Self-weight	1,4
LC2 - Dead load	1,82
LC3 - Full traffic load	1,82
LC8 - Wind -Y direction	1,65
Imperfections from LC – Global buckling shape	

Table 24: ULS stability combination for the verification of the global buckling resistance

**Step 5: Verification of the results**

The maximum stresses found in ULS loading situation combined with imperfections are:

$$\sigma_{ULS} = 448 \text{ MPa} < f_{yd} = 460 \quad \rightarrow \text{OK}$$

These relatively high stresses can only be allowed when the cross-section can be loaded up to its full capacity. In paragraph 6.1 the cross-section is evaluated for cross-sectional stability and arguments are given to imply that the full yield strength can be used.

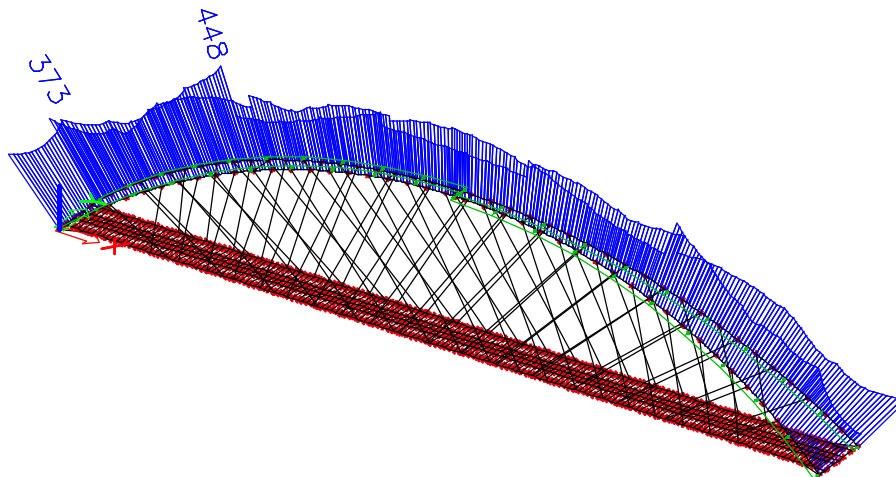


Figure 82: Stress distribution [MPa] in ULS stability combination

### 6.1.2 Conclusion

From the verification of the global stability the following was concluded:

- The maximum stress obtained by geometrically nonlinear analysis with imperfections is below the yield strength.
- The difference in critical load factors between the first and second buckling mode ( $\alpha_{crit} = 4,8$  and  $\alpha_{crit} = 4,88$  resp.) is too small to conclude that the second buckling load will never be reached. When a detailed analysis is performed on the stability of the bridge, the second buckling mode should also be verified.
- The imperfection can also be determined by a more simple method given by NEN-EN 1993-1-1 5.3.2 (3).
- When a nonlinear buckling stability analysis would be performed (instead of the linear buckling analysis performed in this paragraph) a slightly higher critical load factor ( $\alpha_{crit}$ ) is expected.

## 6.2 Fatigue verification hanger

In this paragraph the fatigue performance of one hanger is determined. To make sure that the hanger which is affected most by fatigue loading is the one that will be assessed in this paragraph, a study is performed to determine the decisive hanger. In paragraph 6.2.1 the results are summarized.

In paragraph 6.2.2 the hanger connection is dimensioned according to guidelines given by DIN-FB 103. This guideline is also used to determine the fatigue properties of the connection.

In paragraph 6.2.4 6.2.5 and 6.2.6 the damage due to traffic loading, vortex induced vibrations and rain- and wind induced vibrations is calculated.

### 6.2.1 Decisive hanger for fatigue loading

The loads which are relevant for the fatigue verification of the hangers are:

- Traffic loading (LM71)
- Wind loading
- Vibration effects
  - Vortex induced vibrations
  - Rain- and wind induced vibrations
  - Structural vibrations (parametric excitation)

*Wind loading* is not considered in the fatigue verification of a hanger, because in the literature reviewed, fatigue damage caused by wind loading has not been mentioned as problematic.

For *structural vibrations*, also known as parametric excitation, no specific fatigue verification method is given. In paragraph 6.5 the susceptibility for *structural vibrations* is evaluated.

In annex I.1 the effect of the abovementioned loads are evaluated for all hangers. An attempt is made to determine the decisive hanger without any detailed calculations. In order to achieve this, the following simplifications and assumptions had to be made:

- long hangers with a low natural frequency are damaged most by vortex induced vibrations
- The angle of the hanger has a large influence on the fatigue damage caused by rain and wind induced vibrations

From this evaluation it was concluded that hanger number 13 (longest hanger) is most susceptible for traffic loading, vortex induced vibrations and rain and wind induced vibrations.

## 6.2.2 Geometrical and fatigue properties of hanger connection

In annex I.3, the hanger connection is dimensioned according to the guidelines provided by DIN-FB 103. Along with formula for dimensions, also the fatigue performance of the hanger connection is given.

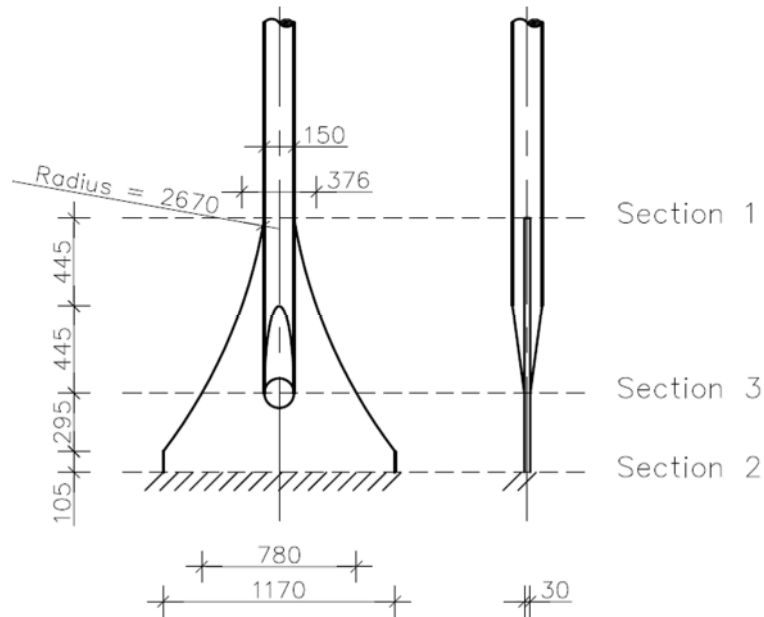


Figure 83: Dimensions hanger connection, hanger number 13

In annex I.2 the detail categories given by DIN-FB103, are linked to the detail categories used in the Eurocode (NEN-EN 1993-1-9). According to [25], section 1 is decisive for bending around the strong axis of the hanger connection, and for bending around the weak axis, section 2 will be decisive. If the hanger connection is fabricated according to the guidelines given in DIN-FB 103, especially with respect to weld treatment, section 3 will not be decisive. In Table 25 the fatigue properties of the hanger connection are summarized.

The partial material factor that is used for the fatigue verification is  $\gamma_{Mf} = 1,35$ .

	Detail category [MPa]	Size effect	$\Delta\sigma_C$ [MPa]	A [m <sup>2</sup> ]	W [m <sup>3</sup> ]
Section 1	90	No size effect	90	$1,77 \cdot 10^{-2}$	$3,33 \cdot 10^{-4}$
Section 2	80	$k_h = \left(\frac{25}{30}\right)^{0,2} = 0,964$	77,1	$3,51 \cdot 10^{-2}$	$1,76 \cdot 10^{-4}$ (weak axis)
Section 3	125	$k_h = \left(\frac{25}{30}\right)^{0,2} = 0,964$	120,5	Not relevant	Not relevant

Table 25: Fatigue properties of hanger connection

## 6.2.3 Isolated model of hanger number 13

To calculate the stresses in the hanger connections, an isolated model of hanger number 13 is used. Important aspect in this model is the way the stiffness of the hanger connection is modeled. Figure 84 shows the connection detail where the stiffness is divided into 5 segments. See annex I.3 for more about the hanger connection.



The physical length of the hanger is significantly shorter than the system length, because the hanger is connected at the top and bottom flanges of the main girder and arch. This physical length ( $L_{net}$ ) is simplified by reducing the system length with half the arch and main girder height. For the natural frequencies the reduced length ( $L_{net}$ ) of the hanger has a positive influence.

Crucial for the isolated model is that the deformations are as realistic as possible. This is achieved by applying the external axial force at the support with axial freedom (see Figure 85). By modeling the hanger in such a way, the axial force remains unchanged, and the deflection due to self-weight will be realistic.

**Relevant parameters for isolated hanger model (hanger number 13)**

$$D = 150\text{mm}$$

$$L_{system} = 55,722\text{m}$$

$$L_{net} = 52,822\text{m}$$

$$N_{PERM} = 1196\text{kN}$$

$$m(s) = \mu = \rho A = 7850 \cdot 0,25 \cdot \pi \cdot 0,15^2 = 139 \text{ kg/m}$$

**6.2.4 Damage due to traffic (LM71)**

To determine the damage due to traffic loading, a method called the ‘ $\lambda$ -coefficient’ method is applied. For this method the following condition must be satisfied:

$$\text{Fatigue assessment: } \gamma_{Ff} \cdot \Delta\sigma_{E_2} \leq \frac{\Delta\sigma_c}{\gamma_{Mf}}$$

$$\Delta\sigma_{E_2} = \lambda \cdot \phi_2 \cdot \Delta\sigma_{71}$$

Where:

$\gamma_{Ff}$  is the partial safety factor for fatigue loads. The recommended value is  $\gamma_{Ff} = 1,0$

$\gamma_{Mf}$  is the partial safety factor for the fatigue strength. When considering the safe life and high consequence of failure, the partial safety factor is taken  $\gamma_{Mf} = 1,35$

$\lambda$  is the damage equivalence factor for fatigue which takes account for the traffic on the bridge.

$\phi_2$  is the dynamic load factor.

$\Delta\sigma_{71}$  is the stress range due to the load model 71 (LM71) on both tracks being placed in the most unfavorable position for the element under consideration, without dynamic factor  $\alpha$ .

$\Delta\sigma_c$  is the reference value of the fatigue strength, based on a detail category. In the decisive sections and corresponding detail classification ( $\Delta\sigma_c$ ) for the hanger connection is determined.

### Remark

An important factor in the determination of the damage due to traffic loads is the influence length. To determine the factor  $\lambda_1$  for the hangers the NEN-EN 1993-2 advises to use an influence length  $L_\phi = 2 \cdot (\text{hanger distance})$ . To determine the dynamic load factor ( $\phi_2$ ) when considering the hangers, NEN-EN 1991-2 advises to use an influence length  $L_\phi = 4 \cdot (\text{hanger distance})$ . For a network arch, where the hanger distance is relatively short, this would lead to unfavorable factors and thereby a conservative fatigue performance.

In both cases, it is allowed to use the length of the influence line of the deflection of the considered element. For hangers the influence line is equal to the full length of the span.

Per Tveit suggested in ‘Calculation of a double track railway network arch bridge applying the European standards’ by Benjamin Brunn and Frank Schanack [28] to use  $L_\phi = \frac{1}{2} \text{span}$ . Compared to 2 or 4 times the center to center distance of the hangers, this value for the influence line seems more realistic.

For future research it would be interesting to investigate a correct estimation for the influence length to determine  $\lambda_1$  and  $\phi_2$  for the hangers.

### Determining $\lambda$

The damage equivalence factor  $\lambda$  for railway bridges with a span up to 100m should be determined as follows:

$$\lambda = \lambda_1 \cdot \lambda_2 \cdot \lambda_3 \cdot \lambda_4 \quad \text{where } \lambda \leq \lambda_{max} = 1,4$$

Where:

#### Damage equivalence factor $\lambda_1$

This factor takes into account the damage that is caused by a certain mix of traffic. NEN-EN 1991-2 specifies in annex F, the exact composition of these traffic mixes. From the boundary conditions a traffic mix with 25ton axles is specified. The value of the damage factor depends on the length of the influence line. NEN-EN 1993-2 gives in table 9.4 values for  $\lambda_1$ .

As was mentioned in the remark in, the influence length advised by Per Tveit [28] is used. To give an indication of the difference between both influence lengths see Table 26.

The center to center distance of the hangers is determined by dividing the span length by the number of hangers per arch plane:  $\frac{255m}{2 \cdot 18} = 7 m$ .

NEN-EN 1993-2	Per Tveit
$L_\phi = 2 \cdot 7 = 14 m$	$L_\phi = \frac{1}{2} \text{span} = \frac{255}{2} = 125m$
$\lambda_1 = 0,92$ (see NEN-EN 1993-2 table 9.4)	$\lambda_1 = 0,66$ (see NEN-EN 1993-2 table 9.4)

Table 26:  $\lambda_1$  factor according to NEN-EN 1993-2 and Per Tveit

When  $L_\phi = \text{span}$  would be used, the  $\lambda_1$  factor would not change, see table 9.4.

### Traffic volume factor $\lambda_2$

This factor incorporates the amount of traffic that passes the bridge. NEN-EN 1993-2 gives in table 9.6 factors that correspond to a specified traffic volume. In the boundary conditions a quantity of  $250 \times 10^6$  kN/year is specified, which corresponds with  $\lambda_2 = 1,0$ .

### Design life factor $\lambda_3$

NEN-EN 1993-2 provides in table 9.6 a set of factors ( $\lambda_3$ ) which correspond to a design life. From the boundary conditions a designlife of 100 years is specified which corresponds with a factor  $\lambda_3 = 1,0$ .

### Influence of multiple railway tracks $\lambda_4$

To account for multiple railway tracks on a single bridge, a factor ( $\lambda_4$ ) must be determined. NEN-EN 1993-2 provides in table 9.7 some basic  $\lambda_4$  factors that correspond to the following ratio:

$$\frac{\Delta F_1}{\Delta F_{1+2}} = \frac{452}{654} = 0,69 \text{ resulting in a value of } \lambda_4 = 0,77.$$

For the forces  $\Delta F_1$  and  $\Delta F_{1+2}$  the linear design model is used. LC5 (Track 1 loaded) gives  $\Delta F_1$ , and LC3 (Track 1+2 loaded)  $\Delta F_{1+2}$ .

Resulting in te following factor for  $\lambda$ :

$$\lambda_{L_\phi=14m} = \lambda_1 \cdot \lambda_2 \cdot \lambda_3 \cdot \lambda_4 = 0,92 \cdot 1,0 \cdot 1,0 \cdot 0,77 = 0,7084$$

$$\lambda_{L_\phi=125m} = \lambda_1 \cdot \lambda_2 \cdot \lambda_3 \cdot \lambda_4 = 0,66 \cdot 1,0 \cdot 1,0 \cdot 0,77 = 0,5082$$

### **Determining $\phi_2$**

The validity of the dynamic factor goes hand in hand with the validity of the verification of the dynamic behavior of the bridge. In paragraph 6.4 was verified that the eigenfrequency of the bridge is within a specified range to ensure that no further dynamic analysis is required. Hence, the dynamic factor ( $\phi_2$ ) can be used for the fatigue verification. According to Maarschalkwaard [24] for Dutch railways the dynamic factor ( $\phi_2$ ) for a carefully maintained track can be used.

$$\phi_2 = \frac{1,44}{\sqrt{L_\phi - 0,2}} + 0,82 \quad 1,00 \leq \phi_2 \leq 1,67$$

To determine the influence length  $L_\phi$  see the remark in paragraph 6.2.4. It is decided to use the influence length advised by Per Tveit, but to give an indication of the difference between both influence lengths see Table 27. When  $L_\phi = span$  would be used, the  $\phi_2$  would not change.

<b>NEN-EN 1993-2</b>	<b>Per Tveit</b>
$L_\phi = 4 \cdot 7 = 28m$	$L_\phi = \frac{255}{2} = 125m$
$\phi_2 = \frac{1,44}{\sqrt{28-0,2}} + 0,82 = 1,1$	$\phi_2 = \frac{1,44}{\sqrt{125-0,2}} + 0,82 = 0,95 < 1,0$ $\phi_2 = 1,0$

**Table 27:  $\phi_2$  factor according to NEN-EN 1993-2 and Per Tveit**

### Determining $\Delta\sigma_{71}$

#### Axial force due to double track loading

In paragraph 5.4 it was shown that for the axial force distribution the results obtained by linear analysis can be used. In annex I.1 the axial force amplitude for hanger number 13 is calculated.

$$\Delta N_{71} = 1387 \text{ kN}$$

$$\Delta\sigma_{71;section 1} = \frac{1387 \cdot 10^3}{0,25 \cdot \pi \cdot 150^2} = 78 \text{ MPa}$$

$$\Delta\sigma_{71;section 2} = \frac{1387 \cdot 10^3}{30 \cdot 1170} = 39,5 \text{ MPa}$$

#### Bending moments due to deflection of the main girder

To calculate the bending moment due to deflection of the main girder, the detailed model of the isolated hanger is used. The bottom support is subjected to an imposed rotation, which is obtained from the mobile load case. In annex I.1 the rotation of the deck is calculated for hanger number 13.

$$\Delta\varphi = 1,2 \text{ mrad}$$

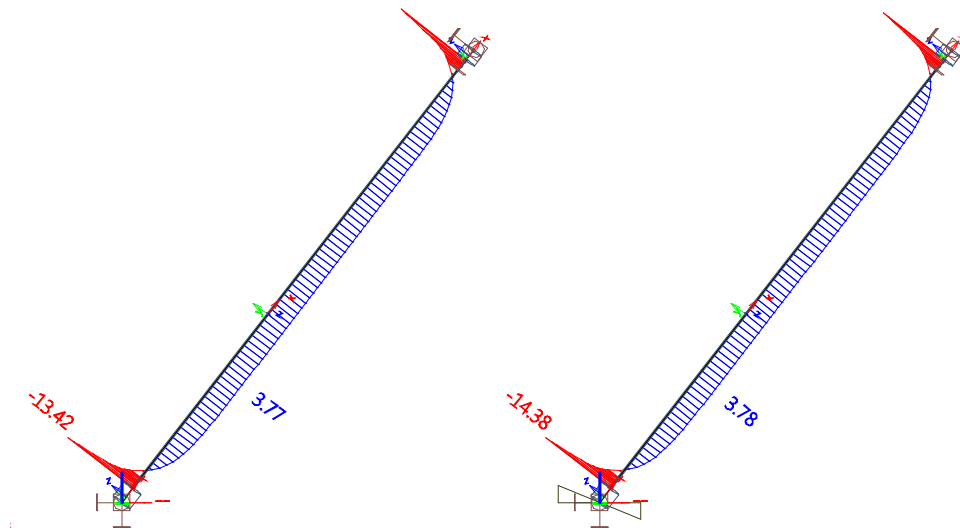


Figure 86: Bending moment [kNm] distribution in detailed hanger model, left: no transverse loading only axial force  $N_{perm}$ , right:  $N_{perm}$  + imposed rotation  $\Delta\varphi = 1,2 \text{ mrad}$

The stresses due to the imposed rotation will only affect section 2, because the rotation only acts in plane of the arch.

$$\Delta\sigma_{\Delta\varphi;section 2} = \frac{\Delta M}{W} = \frac{(-13,42+14,38) \cdot 10^6}{1,76 \cdot 10^5} = 5,4 \text{ MPa}$$

Resulting in the following total stress amplitudes in the hanger connection.

$$\Delta\sigma_{section 1} = \Delta\sigma_{71;section 1} = 78 \text{ MPa}$$

$$\Delta\sigma_{section 2} = \Delta\sigma_{71;section 2} + \Delta\sigma_{\Delta\varphi;section 2} = 39,5 + 5,4 = 44,9 \text{ MPa}$$

### ***Fatigue verification***

$$\gamma_{Ff} \cdot \lambda \cdot \phi_2 \cdot \Delta\sigma = \frac{\Delta\sigma_c}{\gamma_{Mf}}$$

$$L_\phi = \frac{1}{2} \text{span} = 125 \text{ m}$$

$$\phi_2 = 1,0$$

$$\lambda = 0,5082$$

$$U.C.Traffic = \frac{1,0 \cdot 0,5082 \cdot 1,0 \cdot 78}{\frac{90}{1,35}} = 0,59 \quad (\text{Section 1})$$

$$U.C.Traffic = \frac{1,0 \cdot 0,5082 \cdot 1,0 \cdot 44,9}{\frac{77,1}{1,35}} = 0,40 \quad (\text{Section 2})$$

#### **6.2.4.1 Conclusion**

From the verification of the fatigue damage due to traffic loading the following aspects were concluded:

- When the recommended values ( $L_\phi = 2 \cdot \text{hanger distance}$  and  $L_\phi = 4 \cdot \text{hanger distance}$ ) for the influence lines were used to determine  $\lambda$  and  $\phi_2$  the damage would be 50% higher in section 1 and 2.
- For future research it would be interesting to investigate a correct estimation of the influence length to determine  $\lambda_1$  and  $\phi_2$  for the hangers.
- Relatively good fatigue performance of the hangers because of optimized hanger connections, optimized hanger arrangement and the use of a maximum hanger stress of 240 MPa in the design stage.
- For detailed analysis of the hanger fatigue performance, all hangers should be modeled with hanger connections in the overall model. This makes the evaluation of damage due to traffic loading more efficient, because the bending moments due to deflection of the main girder are determined with more accuracy.

### 6.2.5 Damage due to vortex shedding

In this paragraph, the damage due to vortex shedding is calculated by using verification methods according to NEN-EN 1991-1-4 and DIN-FB103. The damage according to NEN-EN is calculated because this code should be applied for Dutch structures. The DIN method is used because this provides a relatively easy fatigue verification method for the higher bending modes, when compared to the NEN method. Finally a comparison between both methods is made in order to determine which method is more conservative.

#### *Aerodynamic parameters*

For the assessment of vibration effects, some specific parameters are introduced. For more information on these parameters see NEN-EN 1991-1-4, annex D.

$St = 0,18$  (for circular cross-sections)

$$\rho_{air} = 1,25 \text{ kg/m}^3$$

$$v = 1,5 \cdot 10^{-5} \text{ m}^2/\text{s}$$

$$v_{m1} = 38,91 \text{ m/s} \quad (\text{Obtained from Iv-Infra tender design})$$

$$v_{01} = 7,782 \text{ m/s} \quad (\text{Obtained from Iv-Infra tender design})$$

$$\delta_s = 0,006$$

The structural damping decrement is assumed to be  $\delta_s = 0,006$ , this value was recommended by Vrouwenvelder and Hoeckman [13].

#### *Scruton number*

$$Sc = \frac{2\delta_s\mu}{\rho b^2} = \frac{2 \cdot 0,006 \cdot 139}{1,25 \cdot 0,15^2} = 59,3$$

*Reynolds number (range) (for values of  $v_{crit}$ , see Table 32)*

$$Re_{min} = \frac{b \cdot v_{crit;z;1}}{v} = \frac{0,15 \cdot 0,69}{1,5 \cdot 10^{-5}} = 6900$$

$$Re_{min} = \frac{b \cdot v_{crit;y;5}}{v} = \frac{0,15 \cdot 4,28}{1,5 \cdot 10^{-5}} = 42800$$

*Critical wind velocity (vortex shedding)*

$$v_{crit,1} = \frac{b \cdot n_{i,y}}{St}$$

#### *Safe design criteria*

According to NEN-EN 1991-1-4 fatigue verification of a bending mode is required if the critical wind velocity is below 125% of the average wind velocity. This criteria can be rewritten to the following:

$$v_{crit,1} > 1,25v_m \rightarrow \frac{b \cdot n_{i,y}}{St} > 1,25v_m \rightarrow n_{i,y} > \frac{1,25 \cdot v_m \cdot St}{b} = \frac{1,25 \cdot 38,91 \cdot 0,18}{0,15} = 58 \text{ Hz}$$

According to DIN-FB103 all bending modes with a natural frequency below 10 Hz should be evaluated.

Because the verification of the higher bending modes is performed according to DIN-FB103, all bending modes below 10 Hz are evaluated.

### Natural bending frequencies (hanger 13)

In annex J the natural bending frequencies of the hangers are determined by using the differential equation of an axially tensioned Euler Bernoulli beam. In Table 28 the natural frequencies are presented.

Modeling	$n_1$ [Hz]	$n_2$ [Hz]	$n_3$ [Hz]	$n$ [Hz]	$n_5$ [Hz]	$n_6$ [Hz]	$n_7$ [Hz]	$n_8$ [Hz]
Hanger nr. 13 fixed connections	0,96	1,97	3,06	4,26	5,61	7,11	8,80	10,67
Hanger nr. 13 fixed connections	0,89	1,81	2,81	3,93	5,17	6,58	8,15	9,91

Table 28: Natural frequencies of hanger nr. 3 and nr. 13, corresponding to fundamental bending modes

#### 6.2.5.1 Verification according to the Eurocode (NEN-EN)

##### Static verification method

The loading caused by vortex induced vibrations can be determined with the following formula. This load should be placed at the excitation peaks of the considered bending shape.

$$F_w(s) = m(s) \cdot (2 \cdot \pi \cdot n_i)^2 \cdot \phi_{i,y}(s) \cdot y_{F,max} \quad [\text{N/m}]$$

Where:

$$y_{F,max} = b \cdot \left( \frac{1}{St^2} \cdot \frac{1}{Sc} \cdot K \cdot K_w \cdot c_{lat} \right) \quad [\text{m}]$$

Where:

$$L_e = 6D \text{ or } 12D \quad (\text{Correlation length})$$

The correlation length ( $L_e$ ) is restricted based on  $y_{F,max}$  thereby making the determination of  $L_e$  an iterative process.

Vrouwenvelder and Hoekman [13] recommend to use a correlation length of  $L_e = 0,33L$ . To see the difference, both correlation lengths are evaluated.

$$K = \frac{\sum_{j=1}^m \int_{l_j}^0 |\phi_{i,y}(s)| ds}{4 \cdot \pi \cdot \sum_{j=1}^m \int_{l_j}^0 |\phi_{i,y}^2(s)| ds} \quad (\text{Vibrational shape factor})$$

For the first bending mode the following values can be used:

$$K = 0,1 \quad (\text{hinged connections})$$

$$K = 0,11 \quad (\text{fixed connections})$$

$$K_w = \frac{\sum_{j=1}^n \int_{l_j}^0 |\phi_{i,y}(s)| ds}{\sum_{j=1}^m \int_{l_j}^0 |\phi_{i,y}(s)| ds} \leq 0,6 \quad (\text{Effective correlation length factor})$$

For the first bending mode the following formula can be used for  $K_w$ :

$$K_w = \frac{L_e}{l} + \frac{1}{\pi} \sin \left[ \pi \left( 1 - \frac{L_e}{l} \right) \right] \quad (\text{for fixed-fixed connections})$$

$$K_w = \cos \left[ \frac{\pi}{2} \left( 1 - \frac{L_e}{l} \right) \right] \quad (\text{for hinged- hinged connections})$$

$$c_{lat} = 0,7 \quad (\text{Lateral force coefficient}).$$

Based on Reynolds number  $Re < 3 \cdot 10^5$  and a critical wind velocity  $v_{crit,1} < 32,3 \text{ m/s}$ .

### Force distribution

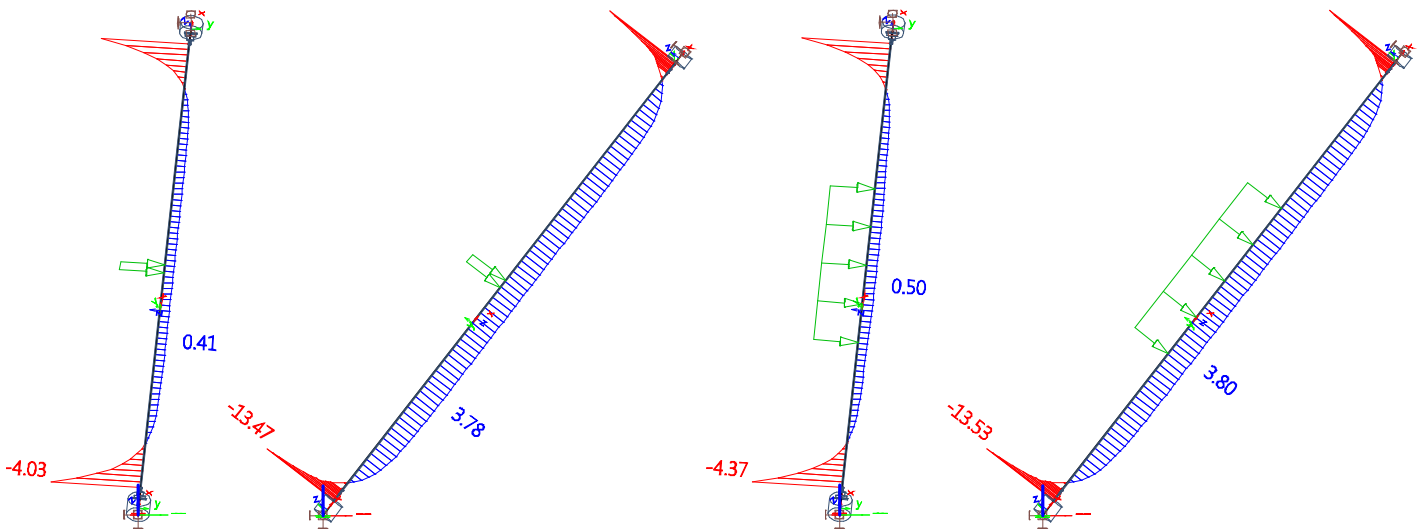


Figure 87: Bending moment [kNm] diagrams for verification according to NEN-EN 1991-1-4, left:  $L_e = 6D$ , right:  $L_e = 0, 33L$

### Fatigue verification

The fatigue verification is performed according to NEN-EN 1993-1-9. The number of cycles which must be taken into account for the fatigue verification can be determined with the following formula:

$$N = 2 \cdot T \cdot n_i \cdot \varepsilon_0 \cdot \left(\frac{v_{crit}}{v_0}\right)^2 \cdot e^{-\left(\frac{v_{crit}}{v_0}\right)^2}$$

Where:

$T$  = Design life (expressed in seconds:  $100 \cdot 3,2 \cdot 10^7 = 3,2 \cdot 10^9$  sec )

$\varepsilon_0$  = Bandwith factor which describes the range of wind velocities which could induce vibrations due to vortex shedding. This factor can be taken as  $\varepsilon_0 = 0,3$ .

$v_{01} = 7,782$  m/s

$$N_{max} = \left(\frac{\Delta\sigma_C}{\gamma_{Mf} \cdot \Delta\sigma_M}\right)^3 \cdot 2 \cdot 10^6$$

The stress interval caused by vortex induced vibrations is calculated as follows:

$$\Delta\sigma_{vortex} = \frac{\Delta M}{W} = \frac{2 \cdot (M - M_0)}{W}$$

Where:

$M_{0,Section 1} = 4,03$  kNm

$M_{0,Section 2} = 13,47$  kNm

The total damage, expressed as a unity check, is calculated as follows:

$$U. C. = \frac{N}{N_{max}}$$

NEN-EN fatigue verification (first bending mode)										
Hanger direction	$n_1$ [Hz]	$v_{crit,1}$ [m/s]	$L_e$ [m]	$F_w(s)$ [N/m]	$N$ [cycles]	$\Delta M$ [kNm]	$\Delta\sigma_M$ [Mpa]	$\Delta\sigma_C$ [Mpa]	$N_{max}$ [cycles]	U. C.
Out-of-plane (section 1)	0,97	0,81	0,9	1,1	$2,0 \cdot 10^7$	0	0	90	$\infty$	0
In-plane (section 2)	0,89	0,74	0,9	0,6	$1,53 \cdot 10^7$	0	0	77,1	$\infty$	0

Table 29: Damage in section 1 and 2, correlation length  $L_e = 6D$

NEN-EN fatigue verification (first bending mode)										
Hanger direction	$n_1$ [Hz]	$v_{crit,1}$ [m/s]	$L_e$ [m]	$F_w(s)$ [N/m]	$N$ [cycles]	$\Delta M$ [kNm]	$\Delta\sigma_M$ [Mpa]	$\Delta\sigma_C$ [Mpa]	$N_{max}$ [cycles]	U. C.
Out-of-plane (section 1)	0,97	0,81	17,431	19	$2,0 \cdot 10^7$	0,68	2,04	90	$6,98 \cdot 10^{10}$	0
In-plane (section 2)	0,89	0,74	17,431	12	$1,53 \cdot 10^7$	0,12	0,68	77,1	$1,18 \cdot 10^{12}$	0

Table 30: Damage in section 1 and 2, correlation length  $L_e = 0,33L$

### 6.2.5.2 Verification of higher bending modes according to the DIN-FB 103

With this method the fatigue damage of caused by the higher bending modes can be assessed in a relatively simple way. The damage is evaluated by means of a static method. DIN-FB103 also provides a dynamic verification method, for more about this see [2].

#### Static verification method

The static load caused by vortex induced vibrations can be determined by the following formula.

$$q_{stat} = 1,10 \cdot D \cdot v_{crit,i}^2 \cdot k_{F,i} \text{ [kN/m]}$$

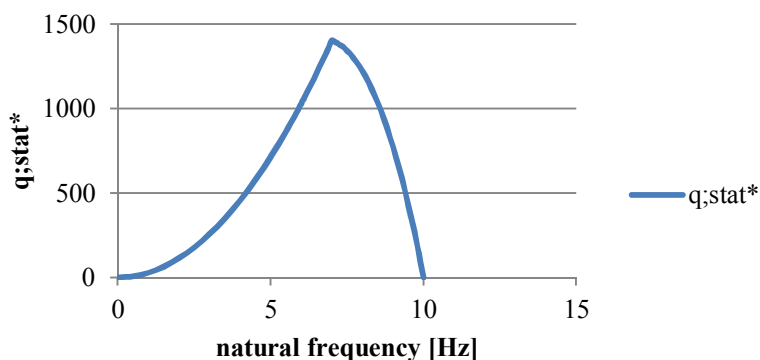
Where:

$$k_{F,i} = 1 \quad (n_i \leq 7\text{Hz})$$

$$k_{F,i} = \frac{10-n_i}{3} \quad (7\text{ Hz} < n_i \leq 10\text{Hz})$$

The value 1,10 is based on an absolute minimum value for the logarithmic structural damping decrement (0,0015). For a fair comparison between the German guideline and the European codes the logarithmic structural damping decrement must be the similar ( $\delta_s = 0,006$ ). This is done by the following formula given in the guideline:

$$q_{stat}^* = \frac{0,0015}{\delta_s} \cdot q_{stat} = \frac{0,0015}{0,006} = 0,25 \cdot q_{stat}$$



### Force distribution

The static load should be placed at the excitation peaks of the considered bending shape. The intermediate distances between these excitation peaks are given in Figure 88. For the in- and out of plane bending shapes these intermediate distances are assumed to be similar as for a hanger with hinged connections. The intermediate distances between the excitation peaks are:

$$L_i = \frac{L}{i}$$

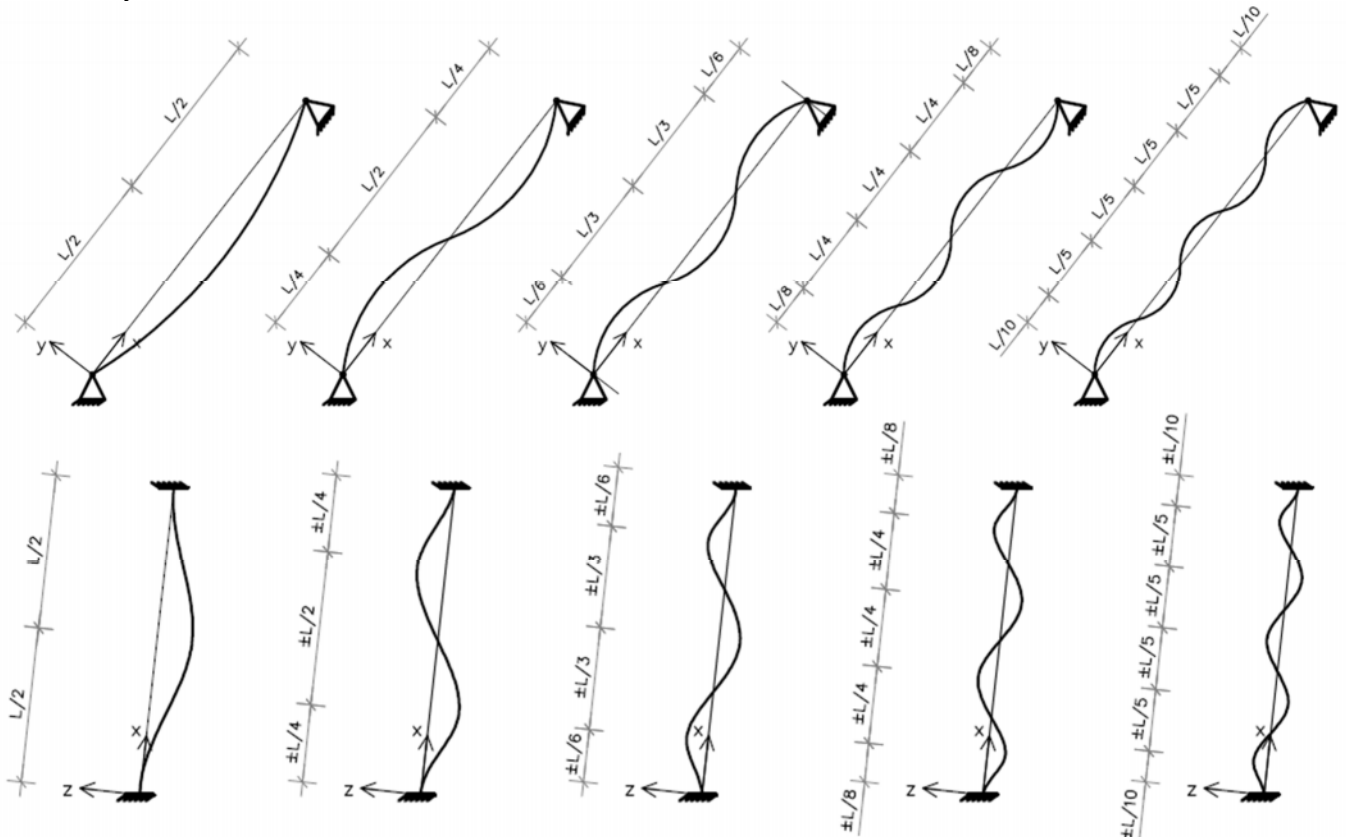


Figure 88: Natural bending shapes corresponding to the first five natural frequencies, above: hinged-hinged beam, below: fixed-fixed beam

If a short hanger with fixed connections with a larger bending stiffness is considered, these intermediate distances should be determined more precisely.

$$L_w = 24D = 24 \cdot 0,15 = 3,6 \text{ m} \quad (\text{correlation length})$$

The stress interval caused by vortex induced vibrations is calculated as follows:

$$\Delta M = 2 \cdot (M - M_0)$$

$$\Delta \sigma_{\text{vortex}} = \frac{\Delta M}{W}$$

### Fatigue verification

The number of loading cycles is incorporated in the correlation length  $L_w$ . The total damage is written as a unity check. This will be added to the damage caused by traffic. This is based on the same principle as is used in a fatigue verification according to the miner rule.

$$U. C. = \frac{\gamma_{Mf} \cdot \Delta \sigma_M}{\Delta \sigma_C}$$

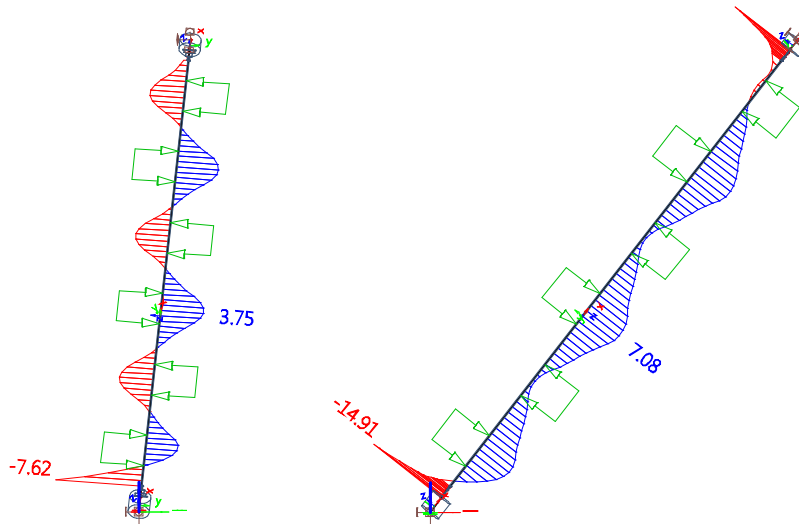


Figure 89: Decisive load cases for the bending moment [kNm] distribution in section 1 (left) and section 2 (right) caused by vortex induced vibrations (DIN-FB103)

DIN fatigue verification (all bending modes < 10Hz)									
Hanger direction: Out of plane	$n_i$ [Hz]	$v_{crit,i}$ [m/s]	$L_w$ [m]	$k_{F,i}$	$q_{stat}^*$ [N/m]	$\Delta M$ [kNm]	$\Delta \sigma_M$ [Mpa]	$\Delta \sigma_C$ [Mpa]	U. C. Section 1
1 <sup>st</sup> bending mode	0,96	0,81	3,6	1,0	27	0,2	0,6	90	0,01
2 <sup>nd</sup> bending mode	1,97	1,64	3,6	1,0	111	0,92	2,8	90	0,04
3 <sup>rd</sup> bending mode	3,06	2,55	3,6	1,0	268	1,68	5,0	90	0,08
4 <sup>th</sup> bending mode	4,26	3,55	3,6	1,0	520	3,3	9,9	90	0,15
5 <sup>th</sup> bending mode	5,61	4,83	3,6	1,0	962	3,94	11,8	90	0,18
6 <sup>th</sup> bending mode	7,11	5,93	3,6	0,96	1393	7,18	21,56	90	0,32
7 <sup>th</sup> bending mode	8,80	7,33	3,6	0,4	887	3,8	11,4	90	0,17
8 <sup>th</sup> bending mode	10,67	Not considered							

Table 31: Damage in section 1 and section 2, for higher out of plane bending modes, according to DIN-FB 103

DIN fatigue verification (all bending modes < 10Hz)									
Hanger direction: In plane	$n_i$ [Hz]	$v_{crit,i}$ [m/s]	$L_w$ [m]	$k_{F,i}$	$q_{stat}^*$ [N/m]	$\Delta M$ [kNm]	$\Delta \sigma_M$ [Mpa]	$\Delta \sigma_C$ [Mpa]	U. C. Section 2
1 <sup>st</sup> bending mode	0,89	0,74	3,6	1,0	23	0,2	0,6	77,1	0,01
2 <sup>nd</sup> bending mode	1,81	1,51	3,6	1,0	94	0,22	1,25	77,1	0,02
3 <sup>rd</sup> bending mode	2,81	2,34	3,6	1,0	226	0,5	2,84	77,1	0,05
4 <sup>th</sup> bending mode	3,93	3,28	3,6	1,0	444	0,98	5,57	77,1	0,10
5 <sup>th</sup> bending mode	5,17	4,31	3,6	1,0	766	1,6	9,09	77,1	0,16
6 <sup>th</sup> bending mode	6,58	5,48	3,6	1,0	1239	2,88	16,36	77,1	0,29
7 <sup>th</sup> bending mode	8,15	6,79	3,6	0,62	1179	2,55	14,49	77,1	0,25
8 <sup>th</sup> bending mode	9,91	8,26	3,6	0,03	84	0,21	1,19	77,1	0,02

Table 32: Damage in section 1 and 2, for most unfavorable natural frequency, according to DIN-FB 103

### 6.2.5.3 Comparison DIN and NEN-EN method

In Table 33 the fatigue verification methods of NEN-EN 1991-1-4 and DIN-FB103 are compared.

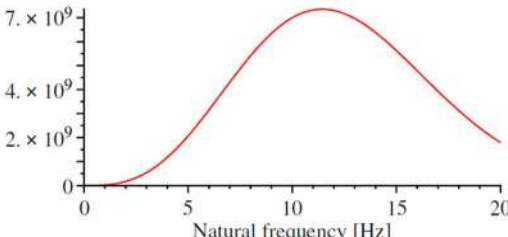
NEN-EN 1991-1-4	DIN-FB103
<b>Safe design criterion</b>	
$n_{i,y} > \frac{1,25 \cdot v_m \cdot St}{b} = 58 \text{ Hz}$	$n_{i,y} > 10 \text{ Hz}$
<b>Static load</b>	
$F_w = \mu \cdot (2 \cdot \pi \cdot n_i)^2 \cdot y_{F,max}$ $F_w = \mu \cdot (2 \cdot \pi \cdot n_i)^2 \cdot D \cdot \left( \frac{1}{St^2} \cdot \frac{1}{Sc} \cdot K \cdot K_w \cdot c_{lat} \right)$ $F_w = \mu \cdot (2 \cdot \pi \cdot n_i)^2 \cdot D \cdot \left( \frac{1}{St^2} \cdot \frac{1}{\frac{2\delta_s \mu}{\rho D^2}} \cdot K \cdot K_w \cdot c_{lat} \right)$ $F_w = \frac{D^3 \cdot n_i^2}{St^2 \cdot \delta_s} \cdot (2 \cdot \pi^2 \cdot \rho \cdot K \cdot K_w \cdot c_{lat})$ $F_w = \frac{D^3 \cdot n_i^2}{St^2 \cdot \delta_s} \cdot (17,27 \cdot K \cdot K_w)$ $K_{max} = ?$ first bending mode $K = 0,034$ $K_{w,max} = 0,6$ first bending mode $K = 0,11$ $F_w = \frac{D^3 \cdot n_i^2}{St^2 \cdot \delta_s} \cdot (0,0646) \text{ N/m}$	$q_{stat} * = \frac{0,0015}{\delta_s} \cdot 1,10 \cdot D \cdot v_{crit,i}^2 \cdot k_{F,i}$ $q_{stat} * = 10^3 \cdot \frac{0,0015}{\delta_s} \cdot 1,10 \cdot D \cdot \left( \frac{D \cdot n_i}{St} \right)^2 \cdot k_{F,i}$ $q_{stat} * = \frac{D^3 \cdot n_i^2}{St^2 \cdot \delta_s} \cdot (10^3 \cdot 0,0015 \cdot 1,10 \cdot k_{F,i})$ $q_{stat} * = \frac{D^3 \cdot n_i^2}{St^2 \cdot \delta_s} \cdot (1,65 \cdot k_{F,i})$ $k_{F,i,max} = 1,0$ $q_{stat} * = \frac{D^3 \cdot n_i^2}{St^2 \cdot \delta_s} \cdot (1,65) \text{ N/m}$
<b>Force distribution</b>	
$L_{e,min} = 6D$ $L_{e,max} = 12D$ $L_e = 0,33L$ (by Vrouwenvelder and Hoeckman [13])	$L_w = 24D$
<b>Fatigue verification</b>	
$U.C. = \frac{N}{N_{max}}$ $N_{max} = \left( \frac{\Delta\sigma_C}{\gamma_{MF} \cdot \Delta\sigma_M} \right)^3 \cdot 2 \cdot 10^6$ $N = 2 \cdot T \cdot n_i \cdot \varepsilon_0 \cdot \left( \frac{v_{crit}}{v_0} \right)^2 \cdot e^{-\left( \frac{v_{crit}}{v_0} \right)^2}$ $N = 2 \cdot T \cdot n_i \cdot \varepsilon_0 \cdot \left( \frac{D \cdot n_i}{St} \right)^2 \cdot e^{-\left( \frac{D \cdot n_i}{St} \right)^2}$  <b>Figure 90: Number of load cycles (N) as a function of the natural bending frequency</b>	$U.C. = \frac{\gamma_{MF} \cdot \Delta\sigma_M}{\Delta\sigma_C}$

Table 33: Comparison between DIN and NEN-EN fatigue verification method for vortex induced vibrations

#### 6.2.5.4 Conclusion

From the verification of the fatigue damage due to vortex induced vibrations the following aspects were concluded:

- The assumption that was made to determine the decisive hanger: long hangers with a low natural frequency are damaged most by vortex induced vibrations, seems incorrect. When the DIN method is used, hangers with a bending frequency near 7 Hz are damaged most by vortex induced vibrations. Hence, by evaluating only the first natural frequency of the hangers the susceptibility for fatigue damage caused by vortex induced vibrations cannot be estimated.
- It is hard to compare both methods because the DIN method does not give any insight in the occurrence of vortex vibrations. For the DIN method the number of load cycles is incorporated in the correlation length ( $L_w$ ). Unlike the NEN-EN method, which provides a formula to calculate the exact number of load cycles corresponding to a certain critical wind velocity.
- When comparing the DIN and NEN-EN method for the first bending mode, the DIN seems more conservative. The number of load cycles as a function of the natural bending frequency, shown in Figure 90 increases exponentially. This could indicate that for higher natural frequencies, the NEN could become more conservative. For further research it would be interesting to evaluate the differences between both verification methods.
- If the DIN method is equivalent to the NEN method, it would make the assessment of vortex induced vibrations much more efficient, especially when higher bending modes should be assessed. When higher bending modes are assessed by the NEN-EN method, for every bending mode the factors  $K$  and  $K_w$  have to be calculated which is relatively complex when compared to the DIN method.
- The safe design criteria provided by NEN-EN ( $n_{i,y} > \frac{1,25 \cdot v_m \cdot St}{b} = 58 \text{ Hz}$ ) seems unrealistic.
- The relatively good fatigue performance of the hangers for vortex induced vibrations can be explained by the high Scruton number and good fatigue performance of the optimized hanger connection.
- The maximal damage caused by vortex induced vibrations for the in- and out of plane bending modes is resp.  $U.C_{Section 2} = 0,29$  and  $U.C_{Section 1} = 0,32$ .
- Some conservatism is present in the out of plane loading situations (fixed connections), because the intermediate distances of the excitation peaks are assumed to be similar as the in plane loading situation (hinged connections).
- To reduce the amount of calculations on vortex and rain and wind induced vibrations, the hanger connections should be oriented  $90^\circ$  with respect to upper and lower hanger connection. This results in similar natural frequencies in both directions.

### 6.2.6 Damage due to rain and wind induced vibrations

To assess the damage due to rain and wind induced vibrations (RWIV), DIN-FB 103 annex II-H is used. The Eurocode emphasizes the risks of this type of vibrations but does not provide a method to verify the structural integrity. In DIN-Fachbericht 103, a static verification method for this dynamic load case is given. With this verification method RWIV are treated as an accidental loading situation.

#### Safe design criteria

If the following criteria are met, verification for RWIV is not necessary.

$$n_1 = 0,89 > 6,5 \text{ Hz} \quad \rightarrow \text{NOT OK}$$

$$D = 150 \text{ mm} < 70 \text{ mm} \quad \rightarrow \text{NOT OK}$$

#### Static verification method

The static load is determined by the following formula and should be placed at the excitation peaks of the corresponding bending shape.

$$q_{stat} = 0,0283 \cdot c \cdot v_{crit,i}^2 \cdot \frac{1}{D} \cdot k_{V,i} \text{ [kN/m]}$$

Where:

$$v_{crit,i} = 73,5 \cdot D \cdot (f_i)^{0,6} \text{ m/s}$$

$$k_{V,i} = 1 \quad (v_{crit,i} < 20 \text{ m/s})$$

$$k_{V,i} = 120 \left(\frac{D}{D_0}\right)^{-0,7} \cdot \left(\frac{v_{crit,i}}{v_0}\right)^{-2,5} \leq 1,0 \quad (20 \text{ m/s} < v_{crit,i} < 30 \text{ m/s})$$

$c$  = Excitation force coefficient (Erregerkraftbeiwert). Determined according to Figure 91. For hanger number 13, with an angle ( $\beta$ ) of  $52^\circ$ , the value for the excitation force coefficient is  $c = 0,55$ .

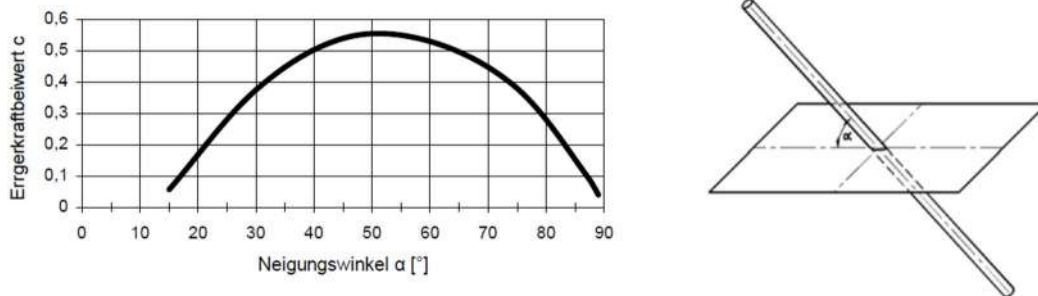


Figure 91: Excitation force coefficient as a function of the angle  $\beta$

Factor 0,0283 is based on an absolute minimum value for the logarithmic structural damping decrement (0,0015), similar as for the verification method for vortex shedding. To apply a similar structural damping decrement as for the NEN-EN verification, the following reduction factor is used to implement a logarithmic structural damping decrement of  $\delta_s = 0,006$ :

$$q_{stat}^* = \frac{0,0015}{\delta_s} \cdot q_{stat} = \frac{0,0015}{0,006} = 0,25 \cdot q_{stat}$$

$$L_w = 0,27 \cdot L_{net} = 0,27 \cdot 52,822 = 14,262 \text{ m}$$

### **Force distribution due to static loading**

To calculate the bending moment for the static verification method a clear distinction must be made between the ULS and fatigue loading situation for the axial force in the hanger. For higher axial forces the bending moment will be lower because the cable action increases, and beam action decreases (see paragraph 4.2.1).

For the ULS verification, the corresponding axial load should be used, without partial load factors because RWIV are considered as accidental load case.

$$N_{ULS;ACCIDENTAL} = N_{PERM} + N_{TRAFFIC} = 1196 + 1000 = 2196 \text{ kN}$$

The maximum stress is determined as:

$$\sigma_{M;ULS} = \frac{\Delta M}{W} = \frac{(M-M_0)}{W}$$

$$M_0 = 4,03 \quad [\text{kNm}] \quad (\text{Section 1})$$

$$M_0 = 13,47 \quad [\text{kNm}] \quad (\text{Section 2})$$

For the fatigue verification the axial force due to permanent loading should be used.

$$N_{FAT} = N_{PERM} = 1196 = 1196 \text{ kN}$$

For the stresses a cyclic loading should be considered, along with a reduction factor through which the occurrence of the RWIV is incorporated.

$$\Delta\sigma_{M;FAT} = k_{H,i} \cdot 2 \cdot \frac{\Delta M}{W}$$

$$k_{H,i} = 120 \cdot (D)^{-0.7} \cdot (v_{crit,i})^{-2.5} \leq 1,0$$

### **In plane loading (section 2)**

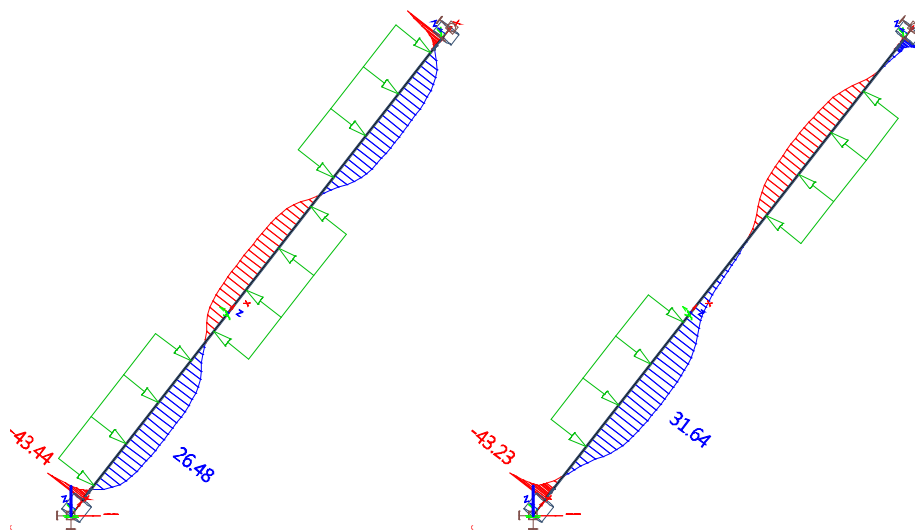


**Figure 92: Bending moment [kNm] distribution for static verification, left: decisive load case ULS, right: decisive load case fatigue**

Hanger direction: In plane	$n_i$ [Hz]	$v_{crit,i}$ [m/s]	$k_{V,i}$	$q_{stat}^*$ [kN/m]	ULS ( $N = 219$ (kN))		Fatigue ( $N = 119$ (kN))		
					$\Delta M$ [kNm]	$\Delta\sigma_{M:ULS}$ [Mpa]	$\Delta M$ [kNm]	$k_{H,i}$	$\Delta\sigma_{M:FAT}$ [Mpa]
1 <sup>st</sup> bending mode	0,89	10,28	1,0	2,74	5,53	31	12,4	1,0	140
2 <sup>nd</sup> bending mode	1,81	15,74	1,0	6,43	18,13	103	29,8	0,46	156
3 <sup>rd</sup> bending mode	2,81	20,49	0,951	10,36	29,97	170	44,13	0,24	120
4 <sup>th</sup> bending mode	3,93	22,49	0,751	9,85	20,39	116	30,98	0,19	67
5 <sup>th</sup> bending mode	5,17	29,54	0,046	1,04	-1,64	-9	2,3	0,10	3

Table 34: ULS and fatigue stress due to RWIV in section 2, for higher in plane bending modes

### Out of plane loading (section 1)

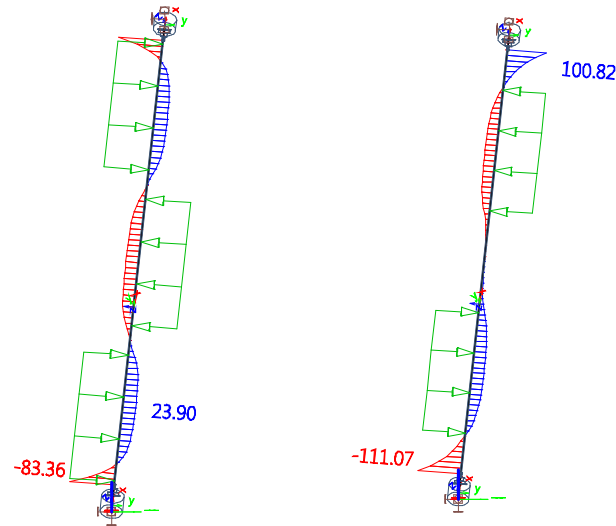


Figure 93: Static load cases to determine bending moment [kNm] in section 2 caused by rain and wind induced vibrations (DIN-FB103)

Hanger direction: In plane	$n_i$ [Hz]	$v_{crit,i}$ [m/s]	$k_{V,i}$	$q_{stat}^*$ [kN/m]	ULS ( $N = 219$ (kN))		Fatigue ( $N = 119$ (kN))		
					$\Delta M$ [kNm]	$\Delta\sigma_{M:ULS}$ [Mpa]	$\Delta M$ [kNm]	$k_{H,i}$	$\Delta\sigma_{M:FAT}$ [Mpa]
1 <sup>st</sup> bending mode	0,96	10,76	1,0	3,00	27,38	82	40,64	1,0	244
2 <sup>nd</sup> bending mode	1,97	16,56	1,0	7,11	73,43	221	111,07	0,41	273
3 <sup>rd</sup> bending mode	3,06	21,57	0,843	10,18	79,33	238	104,4	0,21	132
4 <sup>th</sup> bending mode	4,26	26,30	0,37	6,64	36,63	110	47,81	0,13	37
5 <sup>th</sup> bending mode	5,61	31,03	0						

Table 35: Damage due to rain and wind induced vibrations in section 1, for higher in plane bending modes, according to DIN-FB 103

### ***ULS verification***

For the verification of an accidental load case in the ultimate limit state no partial load factors should be used.

$$\sigma_G + \sigma_Q + \sigma_{M;ULS} \leq f_{y,k}$$

$$\sigma_G = \frac{N_{PERM}}{A} = \frac{1196 \cdot 10^3}{17674} = 67,7 \text{ MPa}$$

$$\sigma_Q = \frac{N_{LM71}}{A} = \frac{1000 \cdot 10^3}{17674} = 56,6 \text{ MPa}$$

$$f_{y,k} = 460 \text{ MPa}$$

#### Section 1

$$67,7 + 56,6 + 238 = 362,3 \text{ MPa} < 460 \text{ MPa} \quad \rightarrow \text{OK}$$

#### Section 2

$$67,7 + 56,6 + 170 = 294,3 \text{ MPa} < 460 \text{ MPa} \quad \rightarrow \text{OK}$$

### ***Fatigue verification***

The damage due to fatigue should not be combined with damage due to traffic loading because of the accidental origin of the RWIV.

$$\Delta\sigma_{M;FAT} \leq \frac{\Delta\sigma_C}{\gamma_{Mf}}$$

#### Section 1

$$273 \text{ MPa} \leq \frac{90}{1,35} = 67 \text{ MPa} \quad \rightarrow \text{NOT OK}$$

#### Section 2

$$156 \text{ MPa} \leq \frac{77,1}{1,35} = 57 \text{ MPa} \quad \rightarrow \text{NOT OK}$$

It can be questioned if a partial load factor should be used in case of an accidental load case. However in this situation little would it matter.

#### **6.2.6.1 Conclusion**

From the verification of the fatigue damage due rain and wind induced vibrations the following aspects were concluded:

- The fatigue performance of hanger number 13 is insufficient for RWIV. DIN-FB103 advises to perform in-situ measurements to determine the exact values of the natural frequencies and structural damping. If the fatigue performance can be verified with these measured natural frequencies and structural damping, no vibration suppression is required.
- The most efficient method for coping with rain and wind induced vibrations is to apply helical wires to the outer surface of the hangers.
- NEN-EN 1991-1-4 provides no guidance on the RWIV.

### 6.2.7 Total fatigue damage in hanger connection

According to DIN-FB103 the damage due to traffic loading and vortex induced vibrations must be added to determine the total fatigue damage. These loads can simply be added because they represent the damage caused by a number of load cycles in a specified cross-section, similar as the damage number (D). This principle of adding and subtracting damage is also applied in a Palmgren-Miner fatigue assessment.

According to DIN-FB103 the damage caused by rain and wind induced vibrations should not be combined with the total damage in the cross-section, because rain and wind induced vibrations are considered as an accidental load case.

#### *Total damage in section 1*

$$U.C. = U.C._{Traffic} + U.C._{vortex} \leq 1,0$$

$$U.C. = 0,59 + 0,32 = 0,91 < 1,0 \quad \rightarrow \text{OK}$$

#### *Total damage in section 2*

$$U.C. = U.C._{Traffic} + U.C._{vortex} \leq 1,0$$

$$U.C. = 0,40 + 0,29 = 0,69 < 1,0 \quad \rightarrow \text{OK}$$

### 6.2.8 Conclusion

From the verification of the fatigue performance of hanger number 13, the following aspects were concluded:

- The assumption that was made to determine the decisive hanger: long hangers with a low natural frequency are damaged most by vortex induced vibrations, seems incorrect. When the DIN method is used, hangers with a bending frequency near 7 Hz are damaged most by vortex induced vibrations. Hence, by evaluating only the first natural frequency of the hangers the susceptibility for fatigue damage caused by vortex induced vibrations cannot be estimated, therefore all hangers should be evaluated.
- Relatively good fatigue performance because of good hanger connection, and by using a maximum design stress of 240 MPa in the design stage.

#### *Conclusions on traffic loading*

- The damage due to traffic loading is based on an influence length of  $L_\phi = \text{half span}$ , recommended by Per Tveit [46]. If the influence length as recommended by NEN-EN was used, the damage due to traffic loading would be 50% higher. This recommendation by NEN-EN is probably based on arch bridges with vertical hangers.
- For a detailed analysis of a network arch, the stiffness of the hanger connections should be incorporated in the global design model. Hence, no isolated hanger models. The main advantage is that the bending moments due to traffic and vibration effects can directly be obtained from the model.

### ***Conclusions on vortex induced vibrations***

- The differences between the verification method according to NEN-EN and DIN-FB103 should be investigated. If the level safety for both methods is equal, the DIN-FB103 would provide a more efficient alternative.
- The relatively good fatigue performance of the hangers for vortex induced vibrations can be explained by the high Scruton number and good fatigue performance of the hanger connection.
- The relatively simple DIN is more efficient because fewer factors have to be calculated. This gain in efficiency results in a loss of transparency. For instance, the exact number of load cycles which is used for the fatigue verification of vortex induced vibrations cannot be traced in the formulas of the DIN method.

### ***Conclusions on rain and wind induced vibrations***

- The fatigue performance of hanger number 13 is not verified for rain and wind induced vibrations. DIN-FB103 advises to perform in-situ measurements to determine the exact values of the natural frequencies and structural damping. If the fatigue performance can be verified with these measured natural frequencies and structural damping, no vibration suppression is required.
- The most efficient method for coping with rain and wind induced vibrations is to apply helical wires to the outer surface of the hangers.

### 6.3 Fatigue verification arch and main girder

For the fatigue verification of the arch and main girder the same method as for the hangers is used. For more information about this verification method see paragraph 6.2.4.

The detail category at the hanger connection for the arch and main girder is obtained from the guidelines to DIN-FB 103 [2]. In annex I.2 this detail category is linked to the NEN-EN 1993-1-9.

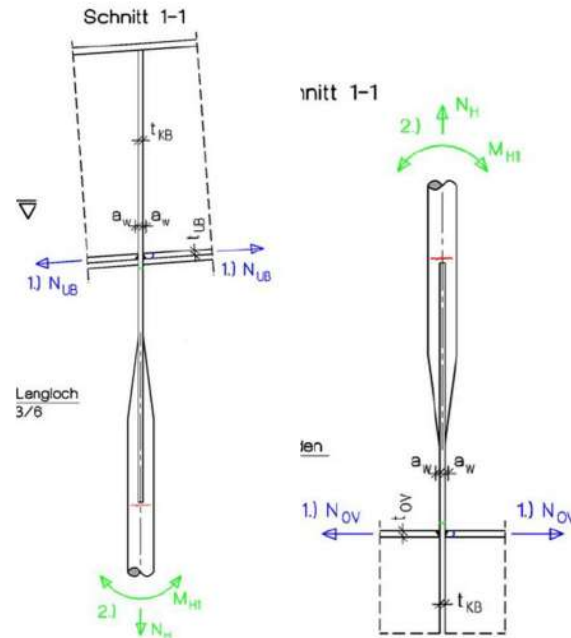


Figure 94: Connection between hanger and arch/ main girder, as recommended by DIN-FB 103 [2]

The decisive detail class of the arch and main girder is  $\Delta\sigma_c = 45 \text{ MPa}$  for both the arch and the main girder.

#### 6.3.1 Fatigue verification arch

For the main girder the influence length to determine the  $\lambda_1$ -coefficient and dynamic amplification factor ( $\phi_2$ ) is  $L_\phi = \frac{1}{2} L \text{ span}$ . All other  $\lambda$  values are similar as for the hangers.

$$\lambda_1 = 0,66$$

$$\lambda_2 = 1,0$$

$$\lambda_3 = 1,0$$

$$\lambda_4 = 0,77$$

$$\lambda = \lambda_1 \cdot \lambda_2 \cdot \lambda_3 \cdot \lambda_4 = 0,66 \cdot 1,0 \cdot 1,0 \cdot 0,77 = 0,5082 \leq \lambda_{max} = 1,4$$

$$\phi_2 = \frac{1,44}{\sqrt{L_\phi^{-0,2}}} + 0,82 = \frac{1,44}{\sqrt{\frac{1}{2} \cdot 255^{-0,2}}} + 0,82 = 0,95 \rightarrow 1,0$$

### 6.3.1.1 Determining $\Delta\sigma_{71}$

In Figure 98 the axial force and bending moment distribution caused by double track mobile loading is shown. The decisive cross-section is found at the horizontal bracing, where the bending moment is at its peak.

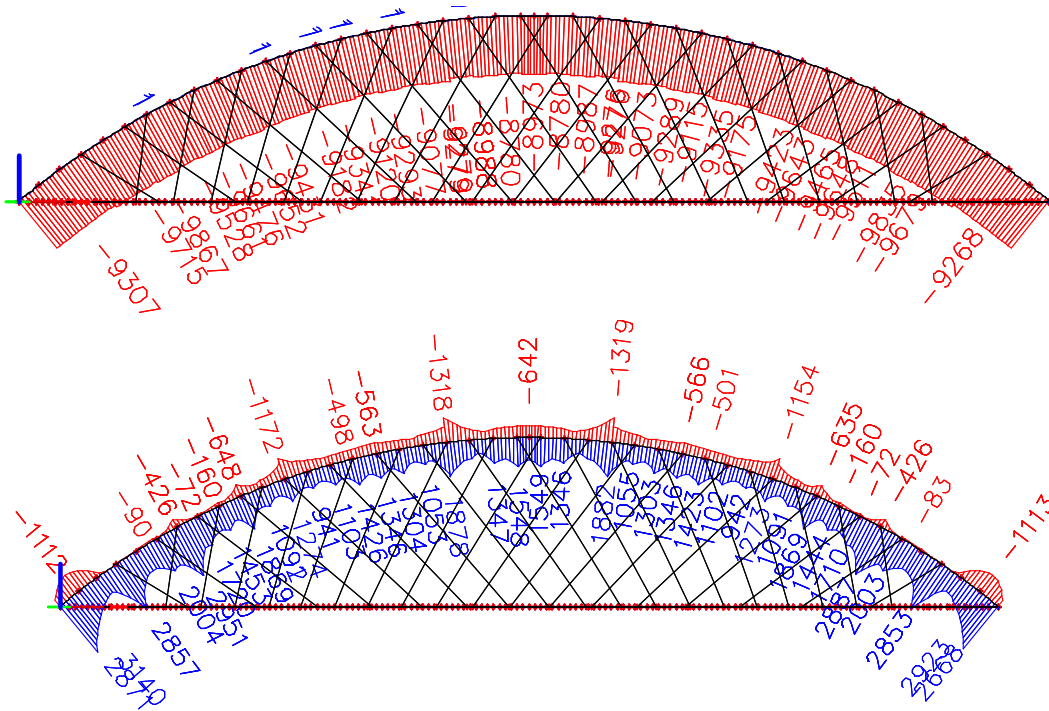


Figure 95: Force distribution in arch due to double track mobile load (LM71), above: axial force N [kN], below: bending moments My [kNm]

$$\Delta N_{midspan} = 9267 \text{ kN}$$

$$\Delta M_{midspan} = 1319 + 1882 = 3201 \text{ kNm}$$

$$\Delta\sigma_{71} = \frac{\Delta N_{midspan}}{A} + \frac{\Delta M_{midspan}}{W} = \frac{9267 \cdot 10^3}{4.4737 \cdot 10^5} + \frac{3201 \cdot 10^6}{3.6942 \cdot 10^8} = 29,4 \text{ MPa}$$

#### ***Fatigue verification***

The flanges of the arch cross-section are 25mm, therefore the size effect is not applied.

$$\gamma_{Ff} \cdot \lambda \cdot \phi_2 \cdot \Delta\sigma \leq \frac{\Delta\sigma_c}{\gamma_{Mf}} \rightarrow 1,0 \cdot 0,5082 \cdot 1,0 \cdot 29,4 < \frac{45}{1,35}$$

$$14,9 < 33,3 \quad \rightarrow \text{OK}$$

### 6.3.2 Fatigue verification main girder

For the main girder the influence length to determine the  $\lambda_1$ -coefficient and dynamic amplification factor ( $\phi_2$ ) is  $L_\phi = \text{span length}$ . All other  $\lambda$  values are similar as for the hangers.

$$\lambda_1 = 0,66$$

$$\lambda_2 = 1,0$$

$$\lambda_3 = 1,0$$

$$\lambda_4 = 0,77$$

$$\lambda = \lambda_1 \cdot \lambda_2 \cdot \lambda_3 \cdot \lambda_4 = 0,66 \cdot 1,0 \cdot 1,0 \cdot 0,77 = 0,5082 \leq \lambda_{max} = 1,4$$

$$\phi_2 = \frac{1,44}{\sqrt{L_\phi - 0,2}} + 0,82 = \frac{1,44}{\sqrt{255 - 0,2}} + 0,82 = 0,911 \rightarrow 1,0$$

#### 6.3.2.1 Determining $\Delta\sigma_{71}$

In Figure 96 the axial force and bending moment distribution caused by double track mobile loading is shown. The decisive cross-section is found at midspan where the axial force and bending moment combined are at their peak.

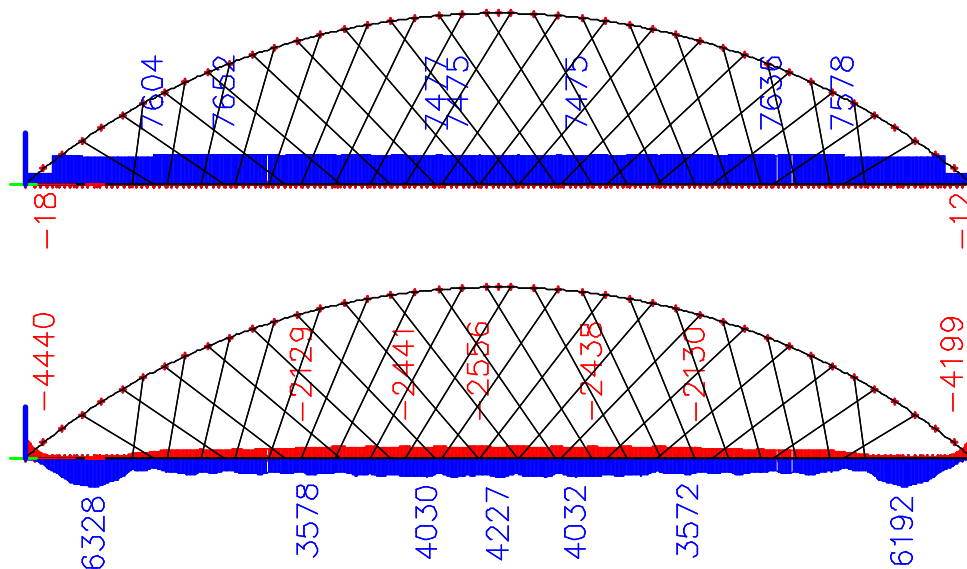


Figure 96: Force distribution in main girder due to double track mobile load (LM71), above: axial force N [kN], below: bending moments My [kNm]

$$\Delta N_{midspan} = 7475 \text{ kN}$$

$$\Delta M_{midspan} = 4227 + 2556 = 6783 \text{ kNm}$$

$$\Delta\sigma_{71} = \frac{\Delta N_{midspan}}{A} + \frac{\Delta M_{midspan}}{W} = \frac{7475 \cdot 10^3}{3.661 \cdot 10^5} + \frac{6783 \cdot 10^6}{3.5063 \cdot 10^8} = 39,8 \text{ MPa}$$

### ***Fatigue verification***

Because the top flange of the main girder has a plate thickness of 35mm, the size effect must be incorporated:

$$k_s = \left(\frac{25}{t}\right)^{0.2} = \left(\frac{25}{35}\right)^{0.2} = 0,935$$

$$\gamma_{Ff} \cdot \lambda \cdot \phi_2 \cdot \Delta\sigma \leq \frac{k_s \cdot \Delta\sigma_c}{\gamma_{Mf}} \quad \rightarrow \quad 1,0 \cdot 0,5082 \cdot 1,0 \cdot 39,8 < \frac{0,935 \cdot 45}{1,35}$$

$$20,2 < 31,2 \quad \rightarrow \text{OK}$$

### **6.3.3 Conclusion**

From the verification of the fatigue performance of the arch and main girder the following was concluded:

- The arch and main girder are less susceptible for fatigue, because a network arch provides higher in-plane support. This results in smaller bending moments in the arch and main girder caused by traffic.
- The relatively high dead load/ live load ratio has a positive influence on the fatigue behavior.

## 6.4 Global dynamic requirements

### *Vertical dynamic requirements*

In NEN-EN 1991-2 figure 6.9 a flow chart is given to determine if a dynamic analysis is required. If the following criteria are fulfilled no dynamic analysis is required.

#### General properties relevant for flow chart

- Design train velocity: 160 km/h
- Static scheme: simply supported
- Span: 255m

For a bridge with the abovementioned properties, the following criteria must be fulfilled:

$$n_{\text{Lower limit}} < n_{\text{bending}} < n_{\text{Upper limit}}$$

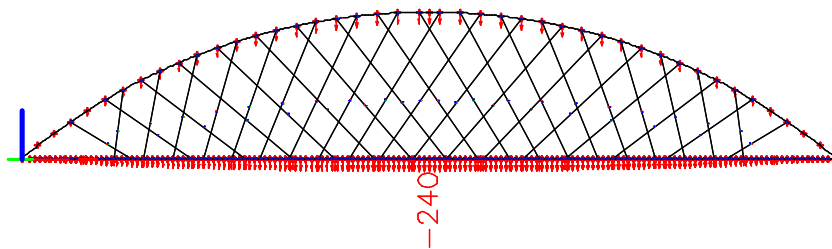


Figure 97: Deflection due to self-weight

$$n_{\text{bending}} = \frac{17.75}{\sqrt{\delta_s}} = \frac{17.75}{\sqrt{240}} = 1,15 \text{ Hz}$$

$$n_{\text{Upper limit}} = 94,76 \cdot L^{-0.748} = 94,76 \cdot 255^{-0.748} = 1,5 \text{ Hz}$$

Remark:

The lower limit of the bending frequency is not specified for spans larger than 100m, it is therefore assumed that the lower limit of the eigenfrequency is not decisive for bridges with a span larger than 100m.

$$0 < 1,15 < 1,5 \text{ Hz} \rightarrow \text{OK}$$

### *Horizontal dynamic requirements*

For a simple evaluation of the horizontal bending stiffness, some simplifications are made:

- Horizontal bending stiffness and mass of the arch is neglected.
- Half of the total mass of the hangers is assumed to be equally distributed along the main girder.

The horizontal bending frequency can be calculated with the NEN-EN 1991-1-4 annex F (5). The arch and hangers are not incorporated in the determination of the horizontal bending frequency. For the sake of simplicity, the horizontal bending frequency is based on only the horizontal bending stiffness of the deck and main girders. For more information on the horizontal bending frequency, see annex C.1.1.

$$n_{horizontal} = \frac{K^2}{2\pi L^2} \sqrt{\frac{EI}{m}}$$

$$EI = EI_{deck} + EI_{maingirder} = 3,1 \cdot 10^7 \cdot 48,1 + 48,1 \cdot 1,1 \cdot 10^8 = 678 \cdot 10^{11} Nmm^2$$

$K = \pi$  (For simply supported structures)

$$m_{deck} = d \cdot b \cdot \rho_{concrete} = 0,4 \cdot 11,3 \cdot 2500 \text{ kg/m}^3 = 11300 \text{ kg/m}$$

$$m_{dead\ load} = 2 \cdot 63 \text{ kN/m} = 12600 \text{ kg/m}$$

$$m_{main\ girder} = 2 \cdot A \cdot \rho_{steel} = 2 \cdot 0,3661 \cdot 7850 \text{ kg/m}^3 = 5748 \text{ kg/m}$$

$$m_{hangers} = \frac{\frac{1}{2} \cdot L_{hanger\ total} \cdot A_{\emptyset 150} \cdot \rho_{steel}}{L} = \rightarrow$$

$$m_{hangers} = \frac{1}{2} \cdot 3120 \cdot 0,25 \cdot \pi \cdot 0,15^2 \cdot 7850 \cdot \frac{1}{255} = 849 \text{ kg/m}$$

$$L = 255 \text{ m}$$

$$n_{horizontal} = \frac{\pi^2}{2\pi 255^2} \sqrt{\frac{678 \cdot 10^{11}}{11300 + 12600 + 5748 + 849}} = 1,14 \text{ Hz}$$

NEN-EN 1990 (national annex) prescribes a minimal horizontal bending frequency of 1,2 Hz, hence:

$$1,14 \text{ Hz} < 1,2 \text{ Hz} \quad \rightarrow \text{NOT OK}$$

Because the horizontal bending frequency is based on some very large assumptions, it is not a problem that the horizontal frequency criterion is not met. When a more detailed analysis is performed precautions could be taken if the horizontal bending frequency would still be too low.

#### 6.4.1 Conclusion

From the verification of the global dynamic requirements of the bridge, the following aspects were concluded:

- For the verification of the dynamic requirements NEN-EN only provides guidance for bridges with a maximum span of 100m. For the verification of the network arch in this thesis (span = 255m), the upper limit of the natural frequency is assumed to be valid for spans > 100m.
- The main bending frequencies of the bridge should be determined with a sufficiently accurate model. The deck should be modeled with 2D elements in order to obtain a realistic horizontal stiffness.

## 6.5 Hanger frequencies and structural vibrations (parametric excitation)

The hanger frequencies are crucial for the evaluation of vortex induced vibrations and structural vibrations. In this paragraph the susceptibility for structural vibrations is evaluated.

The natural frequencies are determined in annex J. Here the natural frequencies for all hangers with hinged connections are calculated. This corresponds to the in plane connections of the hangers. The out of plane frequency where the hangers are rigidly connected (fixed) is only determined for the longest and shortest hanger. The natural frequencies of a cable are determined to evaluate if the hanger frequencies can be estimated by the cable natural frequencies, because the natural frequency of a cable is much easier to calculate.

From Table 36 becomes clear that the frequencies of the longer hangers with hinged connections can be estimated quite accurately with the cable formula. Only when higher bending modes are considered, the influence of the beam action becomes larger, and the differences between cable and beam action increases.

For the shorter hangers, the contribution of the bending stiffness (beam action) is much larger. This is explained by the shorter length, and the higher bending stiffness. From Table 37 it can be concluded that the natural frequencies are nowhere near the cable frequency. The influence of the connection type is also larger for shorter hangers.

<b>Longest hanger (number 13), Ø150mm</b>					
<b>Modeling</b>	<b><math>n_1</math> [Hz]</b>	<b><math>n_2</math> [Hz]</b>	<b><math>n_3</math> [Hz]</b>	<b><math>n_4</math> [Hz]</b>	<b><math>n_5</math> [Hz]</b>
Cable (no bending stiffness)	0,83	1,67	2,50	3,33	4,17
Tensioned E.B. beam, fixed connections	0,96	1,97	3,06	4,26	5,61
Tensioned E.B. beam, hinged connections	0,83	1,71	2,65	3,68	4,83

**Table 36: Natural frequencies for longest hanger, modeled as cable and beam with hinged and fixed connections**

<b>Shortest hanger (number 3), Ø200mm</b>					
<b>Modeling</b>	<b><math>n_1</math> [Hz]</b>	<b><math>n_2</math> [Hz]</b>	<b><math>n_3</math> [Hz]</b>	<b><math>n_4</math> [Hz]</b>	<b><math>n_5</math> [Hz]</b>
Cable (no bending stiffness)	1,81	3,62	5,42	7,23	9,04
Tensioned E.B. beam, fixed connections	3,46	8,42	15,44	24,66	36,13
Tensioned E.B. beam, hinged connections	2,38	6,18	12,02	20,05	30,34

**Table 37: Natural frequencies for shortest hanger, modeled as cable and beam with hinged and fixed connections**

### ***Structural vibrations (parametric excitation)***

The phenomenon of structural vibrations (parametric excitation) is a forced vibration, which is fed by an external force. When the structure vibrates in its primary natural bending frequency, due to the passing of a train, the vibration will only last for a limited amount of cycles. Therefore, fatigue damage is the most likely cause of failure.

NEN-EN 1993-1-11 gives a range to determine which hangers are susceptible for structural vibrations. When the natural frequency of a hanger is within a  $\pm 20\%$  range of the fundamental bending frequency of the structure ( $n_{structure}$ )

$$0,8 \cdot n_{hanger} < n_{structure} < 1,2 \cdot n_{hanger}$$
$$0,8 \cdot n_{hanger} < 2 \cdot n_{structure} < 1,2 \cdot n_{hanger}$$

When implementing the bending frequency of the structure (determined in paragraph 6.4) in the formula, a range of susceptible hangers can be composed:

$$\frac{n_{structure}}{1,2} = \frac{1,15}{1,2} = 0,96 \text{ Hz} < n_{hanger} < \frac{n_{structure}}{0,8} = \frac{1,15}{0,8} = 1,44$$

$$\frac{2 \cdot n_{structure}}{1,2} = \frac{2 \cdot 1,15}{1,2} = 1,92 \text{ Hz} < n_{hanger} < \frac{2 \cdot n_{structure}}{0,8} = \frac{2 \cdot 1,15}{0,8} = 2,88$$

The only hanger that meets the abovementioned requirements is hanger number 5.

### **6.5.1 Conclusion**

From the evaluation of the natural frequencies of the hangers and the verification for structural vibrations, the following aspects were concluded:

- The natural frequencies of massive steel rod hangers cannot be determined by SCIA because the axial force is not considered in the analysis.
- For long hangers, the first bending frequencies can easily be estimated by considering them as cables. For short hangers the natural frequency would be underestimated significantly.
- Nearly all hangers of the network arch considered in this thesis are susceptible to structural vibrations.
- The most efficient method for coping with the structural vibrations is to apply intermediate coupling of the hangers. In the literature study more information is given on this subject.

# 7 COMPARING NETWORK ARCH TO REFERENCE DESIGN

In this paragraph the network arch is compared to the reference design in order to answer the research question: ‘Is a railway arch bridge with a span of 255m more advantageous when the hangers are arranged diagonally or as a network?’ Both designs are evaluated on steel weight and conservation surface. Finally these findings on steel weight and conservation are combined with design aspects into a trade-off matrix to determine the most advantageous design.

## 7.1.1 Effective steel weight

For the comparison of the steel weight, only the elements that were optimized for the network arch and reference design are considered:

- Arch
- Main girder
- Hangers
- Connections and diaphragms

The hanger connections and diaphragms of the network arch form a single element. For a fair comparison, also the diaphragms of the reference design should be considered. In annex I.3 the weight of the connections and diaphragms of the network arch is calculated. In annex D the weight of the connections and diaphragms of the reference design is calculated. The total steel weight of these elements will now be referred to as effective steel weight.

All steel quantities mentioned are based on the SCIA model. In reality the total amount of steel will be larger because all kinds of simplifications were made. For instance, when the optimized arch cross-section is translated into a real cross-section with through stiffeners, the total steel weight will increase in order to maintain similar cross-sectional properties.

Effective steel weight network arch						
Element	Dimensions (h x b x tw x tf)  [mm]	Amount	Total Length (net.)  [m]	Cross-section  [m <sup>2</sup> ]	Steel weight Connection+ diaphragm  [tons/hanger]	Steel weight (7850 kg/m <sup>3</sup> )  [tons]
Arch	2300x3400x38x41	2	277,1	0,44737	-	1946
Main girder	3500x1800x35x35	2	255	0,3661	-	1466
Hanger I	Ø150	4	578,0	0,0177	-	321
Hanger II	Ø200	4	131,6	0,0314	-	128
Hanger III	Ø220	4	19,6	0,038	-	23
Connection+ diaphragm I	(see annex I.3)	52	-	-	3,686	192
Connection+ diaphragm II	(see annex I.3)	16	-	-	5,073	81
Connection+ diaphragm III	(see annex I.3)	4	-	-	5,651	23
					<b>Total</b>	<b>3859 tons</b>

Table 38: Effective steel weight network arch

Effective steel weight reference design						
Element	Dimensions (h x b x tw x tf) [mm]	Amount	Length [m]	Cross-section [m <sup>2</sup> ]	Steel weight [tons/element]	Steel weight (7850 kg/m <sup>3</sup> ) [tons]
Arch	3200x2900x41x40	2	277,1	0,49604	-	2158
Main girder	3700x1800x35x35	2	255	0,3801	-	1522
Diagonals	Ø610x65	4	225,5	0,1113	-	788
Connection	(see annex D)	48	-	-	2,355	113
Diaphragm arch	2300x3400x20	70	-	-	1,502	105
Diaphragm main girder	3700x1800x20	32	-	-	1,046	33
					<b>Total</b>	4719 tons

**Table 39: Effective steel weight reference design**

In order to put the saving of the effective steel weight into perspective an indication of the total steel weight of the bridge is needed. By using the total steel weight of the original tender design also a percentage of steel reduction is calculated.

Total weight: 6400 tons  
 Total weight savings: 4719 – 3859 = 860 tons  
 Percentage: 13 %

A large amount of this difference in steel weight is caused by the diagonals. In the reference design a larger wall thickness was applied in order to increase the Scruton number.

**Remark:** When the hangers of the network arch were connected directly to the web of the main girder and/ or arch, a reduction in the amount of diaphragms could be obtained.

### 7.1.2 Conservation

The conservation method is assumed to be similar for both designs, therefore the total conservation surface becomes an interesting parameter. In Table 40 and Table 41 the total conservation surface is calculated. For the network arch, the hanger connections are also incorporated in the total conservation surface because these are placed outside the cross-section of the arch and main girder. The reference design has internal hanger connections which are sealed off from weather influences by welds, and are therefore not incorporated in the total conservation surface.

The total difference between the conservation surface of the network arch and reference design is: 14099 m<sup>2</sup> – 13476 m<sup>2</sup> = 623 m<sup>2</sup>, in favor of the network arch. However, the conservation of the network arch is assumed to be more labor intensive because of the following arguments:

- More hangers
- Hanger connection of a network arch has an irregular shape (edges, holes)

With respect to conservation it is assumed that the network arch is even less advantageous in conservation

Effective conservation surface network arch						
Element	Dimensions (h x b x tw x tf) [mm]	Amount	Length (net.) [m]	Surface/ m [m <sup>2</sup> /m]	Connection surface [m <sup>2</sup> /element]	Surface [m <sup>2</sup> ]
Arch	2300x3400x38x41	2	277,1	11,4	-	6318
Main girder	3500x1800x35x35	2	255	10,6	-	5406
Hanger I	Ø150	4	578,0	0,471	-	1089
Hanger II	Ø200	4	131,6	0,628	-	331
Hanger III	Ø220	4	19,6	0,691	-	54
Connection I	(see annex I.3)	104	-	-	1,51	157
Connection II	(see annex I.3)	32	-	-	2,68	86
Connection III	(see annex I.3)	8	-	-	3,24	26
<b>Total</b>						13467 m <sup>2</sup>

Table 40: Effective conservation surface network arch

Effective conservation surface reference design						
Element	Dimensions (h x b x tw x tf) [mm]	Amount	Length [m]	Surface/ m [m <sup>2</sup> /m]	Connection surface [m <sup>2</sup> /element]	Surface [m <sup>2</sup> ]
Arch	3200x2900x41x40	2	277,1	12,2	-	6761
Main girder	3700x1800x35x35	2	255	11	-	5610
Diagonals	Ø610x65	4	225,5	1,916	-	1728
<b>Total</b>						14099 m <sup>2</sup>

Table 41: Effective conservation surface reference design

### 7.1.3 Final comparison score system

In this paragraph the design aspects of the network arch and reference design are compared. Along with general design aspects, also specific attention is paid to the uncertain design aspects that were mentioned in the introduction.

Each design aspect is supported by a list of arguments that describe the behavior of the network arch and reference design. The behavior of the network arch is based on conclusions gathered throughout this thesis. In order to compare the properties of both designs, the behavior of the reference design should also be evaluated. Each argument of the network arch, also requires a counterargument for the reference design. This is important for a fair comparison.

Each argument is assigned with a score between 1 and 5. If some properties of the reference design are unknown, they are given a neutral score (3). Because some arguments have a larger impact than others, their scores will be doubled.

<b>General design aspects (see paragraph 2.4)</b>			
<b>Arguments network arch</b>	<b>Score</b>	<b>Arguments reference design</b>	<b>Score</b>
Complex engineering due to nonlinear hanger behavior	2(x2)	Relatively simple engineering because hanger behavior is linear	4(x2)
Conservation and maintenance is assumed to be labor intensive due to the large amount of hangers and connections	2(x2)	More advantageous in conservation and maintenance due to less hangers and internal hanger connections	5(x2)
Possible cost reduction of foundation due to weight saving	4(x2)	Relatively heavy structure	1(x2)
On-site welding volume assumed to be relatively high	1(x2)	On-site welding volume assumed to be average	3(x2)
Relatively light/ slender arch, main girder could be advantageous in transport and handling.	5	Heavier arch, main girder	2
<b>Total score:</b>	<b>24</b>	<b>Total score:</b>	<b>28</b>

**Table 42: Score table on general design aspects**

<b>Assembly of the hangers (see paragraph 2.4)</b>			
<b>Arguments network arch</b>	<b>Score</b>	<b>Arguments reference design</b>	<b>Score</b>
Large amount of temporary hanger supports required, during assembly of the hangers	1(x2)	No temporary hanger supports required because hangers have sufficient bending stiffness	5(x2)
Large weather dependence during final welding of hangers in order to obtain the desired force distribution	1(x2)	Assumed to be less susceptible for weather influences	3(x2)
Higher assembly costs because more hangers are applied	1(x2)	Low assembly costs because less hangers are applied	5(x2)
Relatively light hangers could be advantageous in transport and handling.	5	Heavy hangers	1
<b>Total score:</b>	<b>11</b>	<b>Total score:</b>	<b>27</b>

**Table 43: Score table on assembly of the hangers**

<b>Susceptibility to vibration effects (see paragraph 6.2)</b>			
<b>Arguments network arch</b>	<b>Score</b>	<b>Arguments reference design</b>	<b>Score</b>
High Scruton number ( $Sc = 59$ )	5(x2)	Scruton number barely meets requirements ( $Sc = 23 > 20$ )	2(x2)
Sufficient fatigue resistance against vortex induced vibrations	5(x2)	Insufficient fatigue resistance against vortex induced vibrations	1(x2)
Insufficient fatigue resistance against rain and wind induced vibrations, however, sufficient resistance in ULS	2	Not verified for rain and wind induced vibrations, assumed to be insufficient because of relatively low Scruton number	3
Structural vibrations are likely to occur in almost all hangers	2	Structural vibrations are likely to occur in only a couple of hangers	3
The possibility of intermediate coupling of hangers	5	Only external dampers and helical ribs can be applied to suppress vibrations	2
<b>Total score:</b>	<b>29</b>	<b>Total score:</b>	<b>14</b>

**Table 44: Score table on susceptibility to vibration effects**

<b>Fatigue performance of the hangers (see paragraph 6.2)</b>				
<b>Arguments network arch</b>	<b>Score</b>	<b>Arguments reference design</b>	<b>Score</b>	
Sufficient fatigue resistance against vortex induced vibrations	5(x2)	Insufficient fatigue resistance against vortex induced vibrations	1(x2)	
Good fatigue performance of hanger connection	5(x2)	Unknown fatigue performance	3(x2)	
Hanger arrangement optimized for fatigue performance	5(x2)	Unknown if the diagonal arrangement was optimized for fatigue	3(x2)	
<b>Total score:</b>		<b>30</b>	<b>Total score:</b>	
			<b>14</b>	

**Table 45: Score table on fatigue performance of the hangers**

<b>Influence of compressive forces in hangers on the overall behavior of the bridge (see paragraph 2.3 and 5.5)</b>				
<b>Arguments network arch</b>	<b>Score</b>	<b>Arguments reference design</b>	<b>Score</b>	
Good redistribution of forces when a hanger becomes relaxed or buckles	5	Large consequences for global stability when diagonal buckling occurs	2	
No compression in hangers in SLS	5(x2)	Additional ballast was added to prevent compressive forces in the diagonals in SLS	1(x2)	
Reduction of deck weight is possible	5(x2)	No reduction is possible	1(x2)	
<b>Total score:</b>		<b>15</b>	<b>Total score:</b>	
			<b>6</b>	

**Table 46: Score table on influence of compressive forces in hangers on the overall behavior of the bridge**

### **Results**

When adding the scores determined in Table 42 to Table 46 the following score are obtained:

Total score network arch: 109 → More favorable design aspects  
 Total score reference design: 89

When combining the outcome of the score table with the significant steel weight reduction of 860 tons, which is compared to a weight reduction of appr. 13% on the total steel weight of the reference design, it can be concluded that based on the assumptions *a network hanger arrangement is more advantageous.*

#### 7.1.4 Conclusion

In this paragraph the research question is answered. The conclusion of the comparison: ‘a network arrangement is more advantageous’, is supported by the following arguments:

- The total weight reduction by applying a network arrangement is 860 tons, which corresponds to appr. 13% of the total steel of the reference design with a diagonal hanger arrangement.
- The total steel weight reduction could also lead to savings in foundation costs and transportation.
- If the hangers are directly welded to the webs of the arch and main girder (principle is shown in Figure 22), the amount and size of the diaphragms can be reduced.
- When comparing the conservation surface, the network arch seems more advantageous because the total conservation surface is less. However, the large amount of hangers and their connections require more work and attention. Despite the lesser effective conservation surface, the network arch will probably be unfavorable to conserve and maintain.
- The engineering of a network arch bridge with tensioned hangers is more complex than the engineering of a network arch with welded hanger connections. For a network arch with tensioned elements the force distribution in the hangers fully depends on the accuracy of the stressing protocol. For a network arch with welded connections this force distribution depends on the accuracy of the construction process.
- The network arch has better performance with regard to the susceptibility to vibration effects. This is mainly caused by the high Scruton number, and the optimized fatigue performance of the hanger connection. Also the possibility of the intermediate hanger coupling has a positive influence.
- Relatively good fatigue performance of the hangers because of optimized hanger connections, optimized hanger arrangement and the use of a maximum hanger stress of 240 MPa in the design stage.
- The dead load can be reduced because no hanger compression/ relaxation will occur in the SLS. See paragraph 2.2.4 for more information on the hanger arrangement.

# 8 CONCLUSION AND RECOMMENDATIONS

## 8.1 Conclusions

In this paragraph the findings are summarized as a list of conclusions. The first conclusion answers the research question: ‘Is a railway arch bridge with a span of 255m more advantageous when the hangers are arranged as diagonals or as a network?’

- A railway bridge with a span of 255m is more advantageous when the hangers are arranged as a network. This is based on a comparison between a railway arch bridge with a network arrangement and a diagonal arrangement.
- The total weight reduction by applying a network arrangement is 860 tons, which corresponds to appr. 13% of the total steel of the reference design with a diagonal hanger arrangement.
- The engineering of a network arch bridge with tensioned hangers is more complex than the engineering of a network arch with welded hanger connections. For a network arch with tensioned elements the force distribution in the hangers fully depends on the accuracy of the stressing protocol. For a network arch with welded connections this force distribution depends on the accuracy of the construction process.
- A maximum design stress (based on mobile loads) in the hangers of 240 MPa provides a good estimation with sufficient fatigue capacity for the hanger diameter in the design stage.
- The network arch has better performance with regard to the susceptibility to vibration effects. This is mainly caused by the high Scruton number, and the optimized fatigue performance of the hanger connection. Also the possibility of the intermediate hanger coupling has a positive influence.
- Relatively good fatigue performance of the hangers because of optimized fatigue performance of hanger connections, optimized hanger arrangement and the use of a maximum hanger stress of 240 MPa in the design stage.

From the literature study the following aspects were concluded:

- Economic range for the application of a network arch:  
Road bridges (LM1) 55m – 300m  
Railway bridges (LM71 met  $\alpha=1,0$ ; SW/2) 80m – 300m
- The construction costs for the assembly of the hangers of a network arch bridge are generally higher than for classical arch bridges.
- If the guidelines provided by Teich [1] are used to determine the hanger arrangement, no hanger compression/ relaxation will occur in the serviceability limit state (SLS). Furthermore the hanger arrangements are optimized on structural performance.
- To reduce the susceptibility for vibrational effects, the following parameters have a favorable influence:
  - High natural frequency
  - High structural damping
  - High Scruton number
- Hangers with welded connections should be mounted in a stress less state in order to obtain the theoretical force distribution. The following aspects should be considered during the assembly of the hangers:
  - Support the hangers in both directions throughout construction process
  - Final welding activities within a limited temperature range
  - The arch must be unsupported during the final welding activities
- To obtain the desired force distribution in tensioned hangers a stressing protocol must be composed. For this stressing protocol a detailed three dimensional model is required where the stiffness should be modeled accurately, especially the arch/ main girder connection. The stiffness of this computer model should also be verified with the real stiffness of the structure.

Based on the experiences in the analysis and verification of a network arch with welded hanger connections, the following can be concluded:

- For a detailed analysis of a network arch, the stiffness of the hanger connections should be incorporated in the global design model. Hence, no isolated hanger models. The main advantage is that the bending moments due to traffic and vibration effects can directly be obtained from the model.
- SCIA engineer does not incorporate the effects of axial tension when determining the natural frequencies of a beam element (hangers). Other software should be used for the determination of the natural frequencies in the hangers.
- The majority of the hangers act like cables in all loading situations.
- Compression forces in the hangers are allowed in linear analysis. By nonlinear analysis the actual force distribution of the hangers should be investigated.

- Linear analysis provides good results for the forces, stresses and deformations in the arch and main girder when the ULS is considered.
- The *axial* force and *axial* deformation of the hangers can be determined by linear analysis with sufficient accuracy. All other internal forces and deformations of the hangers should be neglected
- Linear analysis provides good results when no transverse load is acting on the hangers (no wind).
- When detailed analysis is performed, the catenary effect cannot be neglected, especially for long and slanting hangers.
- In order to describe the hanger behavior with sufficient accuracy by nonlinear analysis, at least 50 sections per element (mesh size) should be applied for an accurate representation of the internal forces in the hangers. For less accurate results and shorter calculation time a mesh of 20 sections per element would suffice.
- A network arch can effectively redistribute the forces when hangers become relaxed or buckle. This is caused by the statically indeterminate network hanger arrangement.
- The hanger which is most affected by fatigue from vortex induced vibrations is not necessarily the hanger with the lowest natural frequency. When the DIN method is used, hangers with a bending frequency near 7 Hz are damaged most by vortex induced vibrations.
- When a lighter deck structure is applied more hangers will become relaxed in the ULS. Therefore the effects of hanger relaxation/ compression on the global stability should be investigated for lighter deck structures.

## 8.2 Recommendations for future research

These aspects which should be investigated in more detail were encountered during the writing of this thesis:

- A similar study on the construction and design of a network arch with tensioned elements. Specific attention should be paid to the stressing protocol and fatigue verification of the hangers. This can be used to quantify the differences between tensioned hangers and hangers with welded connections.
- A more detailed variant study to the optimal hanger type, with a minimal amount of assumptions. Closer attention should be paid to the costs of the hangers and connections, especially the on-site welding volume, which is generally an import cost driver in bridge construction.
- Investigating the influence of hanger coupling on the natural frequencies of the hangers.
- The fatigue behavior of the shortest hanger should be investigated, in order to determine if longer or shorter hangers are more susceptible for fatigue.
- Investigate if the maximum stress of 240 MPa is too conservative and, if so, determine a less conservative design stress for the hangers of a network arch.
- Investigating the most optimal deck structure, for certain construction methods, and span lengths.
- Investigate the influence length of the hangers, used to determine the dynamic load factor ( $\phi_2$ ) and damage equivalence factor ( $\lambda_1$ ) more accurately.
- The differences between the fatigue verification method for vortex induced vibrations according to NEN-EN and DIN-FB103 should be investigated. If the level safety for both methods is equal, the DIN-FB103 would provide a more efficient alternative for the fatigue verification of vortex induced vibrations.

# REFERENCES

- [1] Teich S. ( 2011): Beitrag zur Optimierung von Netzwirkbogenbrücken, Fakultät Bauingenieurwesen, Technical University Dresden
- [2] Bagayoko L. et al.(2009): Leifaden zum Anhang II-H Hänger con Stabbogenbrücken des DIN-Fachberichtes 103
- [3] Tveit P.(2012): The Network arch, bits of manuscript, Norway
- [4] Brun B. et al. (2004): Network arches for railway bridges, Arch bridges IV, Barcelona
- [5] Tveit P. et al. (2012):Systematic thesis on network arches
- [6] Geißler K. Mager M.: Die problematik der winderregten Schwingungen an Bruckenhangern
- [7] Geißler K. et al. (2008):Netzwirkbogenbrücken – Entwurf, Bemessung, Ausführung, Stahlbau 77, heft 3
- [8] Gautier P. Krontal L. (2010): Erfahrungen mit Netzwirkbogenbrücken im Eisenbahnbrückenbau, Stahlbau 79, heft 3
- [9] NEN-EN 1993-1-1+C2 2011 NB 2011 NL
- [10] Gulvanessian H. (2010) Designers guide to Eurocode 1 EN 1991-2
- [11] Romeijn A. Steel bridges Part 1
- [12] Bijlaard F. Kolstein M., Steel bridges
- [13] Vrouwenvelder A. Hoekman W. (2004) Vortex-excitatie trillingen getemd, Bouwen met Staal 176
- [14] NEN-EN 1991-1-4+A1+C2 2011 NL
- [15] NEN-EN 1993-1-10 2006-C1 2006 EN
- [16] Mato F. et al. (2010): Design and construction of two composite tubular arches with network suspension system, Hormigon y acero, volume 61, Julio-Septiembre 2010
- [17] Gregor D. et al (2012): New Troja bridge in Prague - Concept and structural analysis of steel parts, Engineering procedia 40, 131-136
- [18] Janata V. et al. (2012): New Troja bridge in Prague - Structural solution of steel parts, Engineering procedia 40, 159-164

- [19] NEN-EN 1990+A1+C2 2011 NL
- [20] Iv-Infra (2012): Rapport tenderfase ontwerp spoorbrug K050
- [21] Irvine M. (1981): Cable structure [Structural mechanics] Max Irvine
- [22] Nemeč I. et al.: Finite elements analysis of structures
- [23] Advanced calculations (manual SCIA engineer)
- [24] Maarschalkerwaard H. Vos P. (2006): Berekenen van vermoeiing van spoorbruggen volgens Eurocode 3, Bouwen met staal 191
- [25] Anpassung von DIN-Fachberichten „Brücken“ an Eurocodes
- [26] Leissa W. Qatu S. (2011): Vibrations of Continuous Systems
- [27] Advanced concept training, steel code check (manual SCIA engineer)
- [28] Brunn B. Schanack F. (2003): Calculation of a double track railway network arch bridge applying the European standards

# ANNEX A: NETWORK ARCH MODEL DESCRIPTION

## A.1 Geometry

With the coordinates given in annex E (Table 51) the geometry of the network arch can be constructed. By using symmetry, the arch plane can be mirrored along the principle axis.

## A.2 Cross-sections

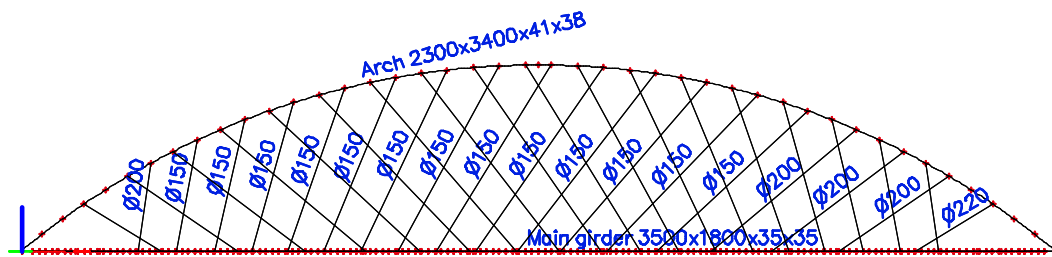


Figure 98: Relevant cross-sections optimized network arch

Element	Dimensions (h x b x tw x tf) [mm]	Amount	Length (net.) [m]	Cross-section [m <sup>2</sup> ]
Arch	2300x3400x38x41	2	277,1	0,44737
Main girder	3500x1800x35x35	2	255	0,3661
Hanger number 4 to 16	Ø150	4	578,0	0,0177
Hanger number 3 and 17 to 19	Ø200	4	131,6	0,0314
Hanger number 20	Ø220	4	19,6	0,038

## A.3 Loads and combinations

The original tender design designed by Iv-Infra was based on a set of load cases and combinations which are documented in the design report [20]. The loads and combinations used for this design are also used as a basis for this research. Some conservatism is present in these loads and combinations, but this would not be a problem for the final comparison.

### *Selfweight construction (LC1 – Self weight)*

The selfweight of the construction is determined by Scia. The volumes of the materials applied are multiplied with the following standard weights of steel and reinforced concrete.

$$\rho_{steel} = 78,5 \text{ kN/m}^3$$

$$\rho_{concrete} = 25 \text{ kN/m}^3$$

**Dead load: ballast layer + railway provisions (LC2 – Ballast)**

The ballast layer is determined by Iv-Infra, and incorporates the ballast layer as well as the railway provisions. In the codes an additional requirement should be met that the volume of the ballast can fluctuate with 30%. This increase/ decrease is incorporated through a partial load factor in the load combinations (see Table 47):

$$q_{dead\ load} = 63\text{ kN/m / track}$$

**Traffic loads (LC3-6 - LM71)**

The decisive load traffic load case was determined by Iv-Infra as the LM71 (load model 71). This load case is defined in NEN-EN 1991-2 [18], see Figure 99. The load case should be multiplied with the factor  $\alpha = 1,21$ , for this specific bridge. However this factor is incorporated in the load factors for LM71 (see Table 47). This has been done because for instance: fatigue and deflection should not be calculated with this factor.

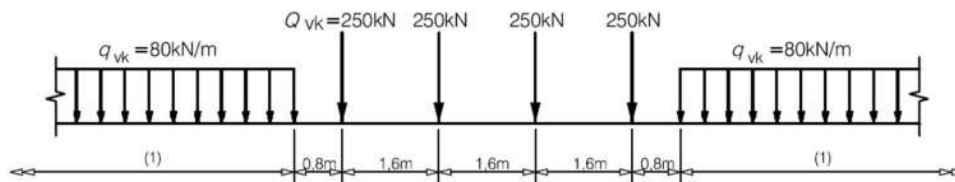


Figure 99: LM71 as defined in NEN-EN 1991-2

This load case is placed in four decisive patterns to generate the most unfavorable set of forces for the global bridge structure. These combinations are shown in Figure 100.

Because the ballast layer and concrete deck equally distribute the concentrated loads, the concentrated loads of LM71 can also be applied as an equivalent equally distributed load ( $q_{eq} = 156\text{ kN/m}$ )

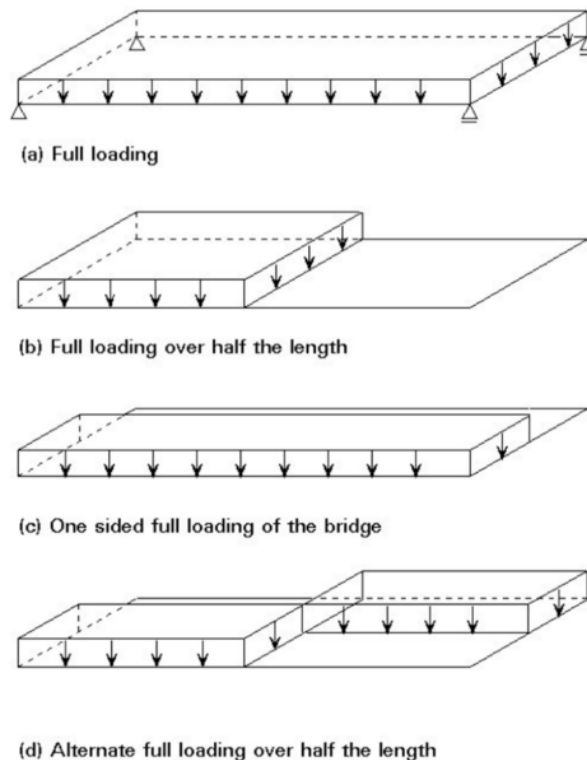


Figure 100: Critical load patterns for arch bridges [12]

- LC3 Full loading causes the highest possible axial forces in the main girder and arch. This load pattern also produces the largest deflection
- LC4 Half span loading causes a large bending moment in the arch and main girder
- LC5 One sided full loading causes a transverse loading in the main girder and deck
- LC6 Alternate full loading causes the arch planes to move horizontally in opposite directions, creating a shear force in the bracing that connects the arches.

**Wind loads (LC 7 & 8 – Wind)**

The wind loads determined by IV-Infra are based on the NEN-EN 1991-4. A load of 2,85 kN/m<sup>2</sup> was determined. Only the horizontal transverse wind load is considered. For the hangers an additional cross-section factor of 2,4 was applied to account for the possible attachment of helical spirals along the surface of the hangers. The hanger diameter to determine the wind load is 200mm. This resulted in the following loads:

Arch (3,5x2,7):  $h_{arch} \cdot p_{wind} = 3,5 \cdot 2,85 = 10 \text{ kN/m}$   
 Maingirder (3,6x2,5):  $h_{main\ girder+train} \cdot p_{wind} = 7 \cdot 2,85 = 20 \text{ kN/m}$   
 Hangers (Ø200):  $2,4 \cdot d_{hanger} \cdot p_{wind} = 2,4 \cdot 0,2 \cdot 2,85 = 1,4 \text{ kN/m}$

**Mobile loads**

To determine the maximal and minimal forces in the hangers a mobile traffic load is applied. This special module in Scia uses influence lines to determine the most unfavorable areas where the load model should be positioned. For the mobile load, load model 71 is used, see Figure 99.

**Linear combinations**

For the design and calculation of the structural elements of the railway bridge the combination formulas 6.10a and 6.10b should be used. The relevant partial load factors are given in the national annex of NEN-EN 1990 are summarized the following table. The psi ( $\psi_0$ ) factors are also obtained from the NEN-EN 1990.

Blijvende en tijdelijke ontwerp-situaties	Blijvende belastingen		Voor-spanning	Dominante verander-lijke belasting (*)	Tegelijkertijd optredende Veranderlijk belastingen (*)	
	Ongunstig	Gunstig			Belang-rijkste (indien aanwezig)	Andere
(Vgl. 6.10a)	$\gamma_{G,j,sup} G_{k,j,sup}$	$\gamma_{G,j,inf} G_{k,j,inf}$	$\gamma_P P$		$\gamma_{Q,1} \psi_{0,1} Q_{k,1}$	$\gamma_{Q,j} \psi_{0,j} Q_{k,j}$
(Vgl. 6.10b)	$\xi \gamma_{G,j,sup} G_{k,j,sup}$	$\gamma_{G,j,inf} G_{k,j,inf}$	$\gamma_P P$	$\gamma_{Q,1} Q_{k,1}$		$\gamma_{Q,j} \psi_{0,j} Q_{k,j}$

**Figure 101: Combination keys 6.10a and 6.10b**

With the combination keys from Figure 101, and the load cases mentioned above the combinations shown in Table 47 can be made.

Combination key	Permanent load $\gamma_{G,sup} = 1,4$ $\gamma_{G,inf} = 0,9$ $\xi = 0,89$	Dead load $\gamma_{G,sup} = 1,4 +30\%$ $\gamma_{G,inf} = 0,9 -30\%$	Traffic load (LM71) $\gamma_Q = 1,5$ $\psi_0 = 0,8$ $\alpha = 1,21$	Wind load $\gamma_Q = 1,65$ $\psi_0 = 1,0$
6.10a	$1,4 \cdot G$	$1,4 \cdot 1,3 \cdot G_{DL}$	$1,5 \cdot 0,8 \cdot 1,21 \cdot Q_{LM71}$	$1,65 \cdot 1,0 \cdot Q_{wind}$
6.10a	$0,9 \cdot G$	$0,9 \cdot 0,7 \cdot G_{DL}$	$1,5 \cdot 0,8 \cdot 1,21 \cdot Q_{LM71}$	$1,65 \cdot 1,0 \cdot Q_{wind}$
6.10b	$0,89 \cdot 1,4 \cdot G$	$1,4 \cdot 1,3 \cdot G_{DL}$	$1,5 \cdot 1,21 \cdot Q_{LM71}$	$1,65 \cdot 1,0 \cdot Q_{wind}$
6.10b	$0,89 \cdot 1,4 \cdot G$	$1,4 \cdot 1,3 \cdot G_{DL}$	$1,5 \cdot 0,8 \cdot 1,21 \cdot Q_{LM71}$	$1,65 \cdot Q_{wind}$
6.10b	$0,9 \cdot G$	$0,9 \cdot 0,7 \cdot G_{DL}$	$1,5 \cdot 1,21 \cdot Q_{LM71}$	$1,65 \cdot 1,0 \cdot Q_{wind}$
6.10b	$0,9 \cdot G$	$0,9 \cdot 0,7 \cdot G_{DL}$	$1,5 \cdot 0,8 \cdot 1,21 \cdot Q_{LM71}$	$1,65 \cdot Q_{wind}$
Min. coefficients	0,9	$0,9 \cdot 0,7 = 0,63$	$1,5 \cdot 0,8 \cdot 1,21 = 1,45$	1,65
Max. coefficients	1,4	$1,4 \cdot 1,3 = 1,82$	$1,5 \cdot 1,21 = 1,82$	1,65

**Table 47: Possible combinations of 6.10a and 6.10b**

From these combinations, the minimal and maximal safety coefficients can be filtered. These are used to simplify the overall design by applying only two sets of load combination factors for the ULS. One for favorable and one for unfavorable self-weight loading:

Unfavorable:  $1,4G + 1,82G_{DL} + 1,82Q_{LM71} + 1,65Q_{wind}$

Favorable:  $0,9G + 0,63G_{DL} + 1,82Q_{LM71} + 1,65Q_{wind}$

### ***Nonlinear combinations***

Because nonlinear calculation does not allow for the superposition of separate load cases, complete combinations have to be assembled for the assessment of certain effects. Therefore only the decisive load cases are evaluated. Based on the linear model, influence lines can be assembled and the decisive load cases can be determined. This method was also recommended by Gauthier and Krontal [9]. The effects that will be evaluated in this thesis are:

- Strength and stability in the ULS
- Effects of compression forces in hangers in linear calculation model
- Fatigue verification
- Deflection in SLS
- Aerodynamic effects under permanent loading conditions

# ANNEX B: OPTIMAL HANGER ARRANGEMENT

Based on the guidelines composed by Stephan Teich [1] an optimal hanger arrangement can be determined. In this annex, the optimal hanger arrangement is determined for a network arch with a span of 255m. Because the research performed by Stephan Teich is used extensively in this thesis. A short summary of his research will be provided.

## B.1 Summary of the research by Teich

The total research consists of 3 independent studies who deal with different aspects of (network) arch bridges. All studies focus on optimization with the use of special programming techniques. These studies are:

- The optimization of the fatigue performance of a hanger connection. To be more specific the geometry of the steel plate that connects a massive rod hanger to the arch and main girder. The results of this study were used in the DIN-Fachberichtes 103 [2], a specific design code for the design of hangers in arch bridges. In this design code instructions are given for the design of a connection plate with a detail category 90.
- The optimization of the hanger arrangement for network arch bridges. For this study a total of 60.172 realistic hanger arrangements are reviewed for structural performance. The results were used to create a step-by-step design manual for the optimal hanger arrangement. This manual is used in this thesis for the determination of the optimal hanger arrangement.
- The optimization of the arch and wind bracing. In this parametric study the main parameters that would influence the design of the arch are investigated. The results are also summarized into a step-by-step design manual.

## B.2 Determining the optimal hanger arrangement

### *Step 1: Number of hangers*

Based on span length, an optimal number of hangers can be determined with Table 48. For a span of 255m, the amount of hangers should be minimal 42 and maximal 52, and because of symmetry an even number. If more than 52 hangers are applied the costs for the extra hangers would not be compensated by reduction of forces in the structure.

It was decided to choose the smallest amount of hangers which would still generate an optimal hanger arrangement, namely 42. It is assumed that the costs for the material and hanger assembly on site will be higher than a small increase in cross-section of the arch and main girder.

Spannweite [m]	< 100	100	150	200	250
Hängeranzahl	34-44	36-46	38-48	40-50	42-52

**Table 48: Recommended number of hangers depending on the bridge span**

**Step 2: Arrangement type**

The 5 hanger arrangements that have been investigated by Teich are:

- Constant angle (1)
- Increasing angle (2)
- Decreasing angle (3)
- Radial arrangement (4)
- Equally spaced along main girder (only middle part) (5)

The arrangements 2 and 4 show for all span lengths the best performances. Arrangements 1 and 3 should be avoided, because of bad structural behavior. Interesting to mention is that arrangement type 1, has been applied in many arch bridges all over the world. Some examples are the Fehmarnsund bridge (Figure 6) and Shinhamadera bridge (Figure 8).

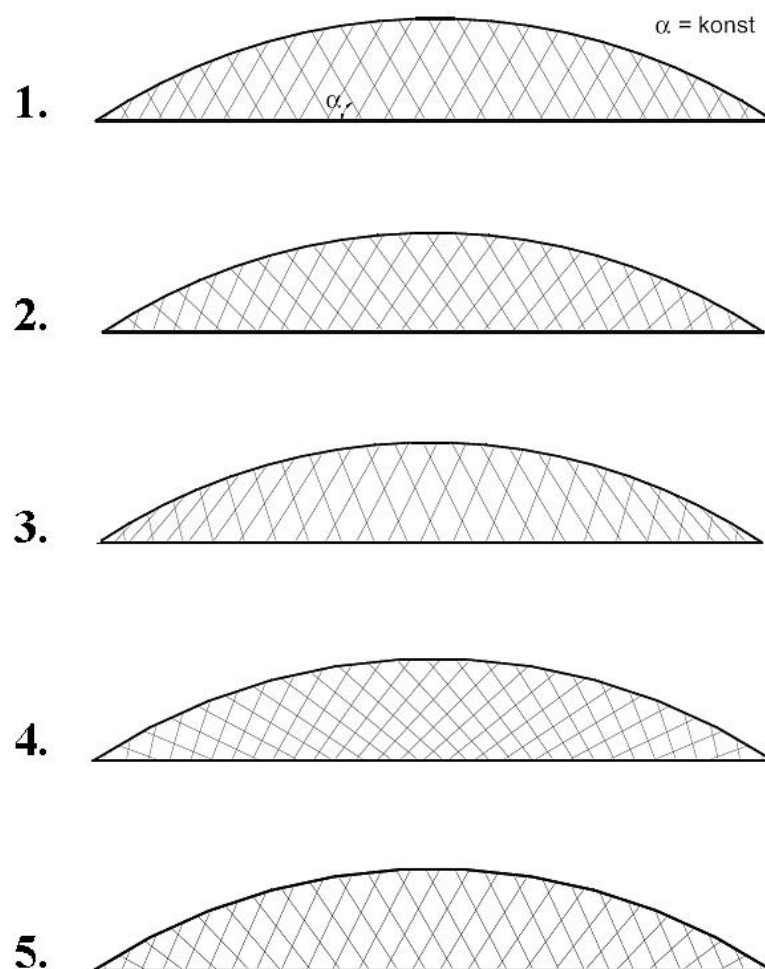


Figure 102: Hanger arrangement types that were investigated by Teich [1]

For more background information about the origin of these arrangement types, see [1]

In Table 49 the performances of these arrangements are summarized and sorted by span length. The best performance for a certain span is given a score of 100%. The performance is based on the following parameters that have been investigated:

- Fatigue performance in hangers, assessed by evaluating the stress variation ( $\Delta\sigma$ )
- Compression in hangers
- Variation in hanger forces. Less variation means an equal distribution and better efficiency.
- Maximal force in hangers

From Table 49 follows that both hanger type 2 and 4 are the preferred options for the design. To obtain a clear overview all 3 arrangements are constructed, shown in Figure 107.

Spannweite < 100 m	24 Hänger	36 Hänger	48 Hänger	60 Hänger
	Netz 2 oder Netz 4			
100 m	1. Netz 4 100	1. Netz 4 100	1. Netz 4 100	1. Netz 2 100
	2. Netz 5 88,4	2. Netz 2 94,1	2. Netz 2 98,6	2. Netz 4 99,3
	3. Netz 2 83,1	3. Netz 5 89,9	3. Netz 5 87,5	3. Netz 5 80,4
125 m	1. Netz 4 100	1. Netz 4 100	1. Netz 2 100	1. Netz 2 100
	2. Netz 5 88,2	2. Netz 2 94,3	2. Netz 4 99,9	2. Netz 4 97,9
	3. Netz 2 83,2	3. Netz 5 93,7	3. Netz 5 96,9	3. Netz 5 84,3
150 m	1. Netz 4 100	1. Netz 4 100	1. Netz 4 100	1. Netz 4 100
	2. Netz 5 85,8	2. Netz 2 94,2	2. Netz 2 99,6	2. Netz 2 99,7
	3. Netz 2 80,3	3. Netz 5 91,1	3. Netz 5 93,2	3. Netz 5 82,8
175 m	1. Netz 4 100	1. Netz 4 100	1. Netz 2 100	1. Netz 2 100
	2. Netz 5 86,1	2. Netz 2 94,7	2. Netz 4 97,6	2. Netz 4 99,6
	3. Netz 2 80,8	3. Netz 5 90,7	3. Netz 5 89,2	3. Netz 5 78,1
200 m	1. Netz 4 100	1. Netz 4 100	1. Netz 4 100	1. Netz 4 100
	2. Netz 5 84,4	2. Netz 2 93,2	2. Netz 2 99,2	2. Netz 2 97,6
	3. Netz 2 78,1	3. Netz 5 88,5	3. Netz 5 88,5	3. Netz 5 80,3
225 m	1. Netz 4 100	1. Netz 4 100	1. Netz 2 100	1. Netz 4 100
	2. Netz 5 82,4	2. Netz 2 93,2	2. Netz 4 98,9	2. Netz 2 99,3
	3. Netz 2 75,8	3. Netz 5 88,0	3. Netz 5 86,8	3. Netz 5 76,4
250 m	1. Netz 4 100	1. Netz 4 100	1. Netz 4 100	1. Netz 4 100
	2. Netz 5 75,6	2. Netz 2 93,0	2. Netz 2 99,2	2. Netz 2 98,1
	3. Netz 2 66,2	3. Netz 5 87,4	3. Netz 5 87,1	3. Netz 5 81,1

**Table 49: Structural performance of hanger arrangements depending on span and number of hangers**

When the number of hangers does not correspond with those given in the table, according to Teich linear interpolation is allowed. The following values for the structural performance can be obtained for 42 hangers.

**Structural performance**

- Type 2: 96,1%
- Type 4: 100%
- Type 5: 87,3%

### Step 3: Optimal angle

Based on the length of the span, arrangement type and number of hangers, the optimal angles can be determined. For each of the configuration types the geometrical pattern can be determined with the following graphs. Also some instructions are given on how to construct the arrangement.

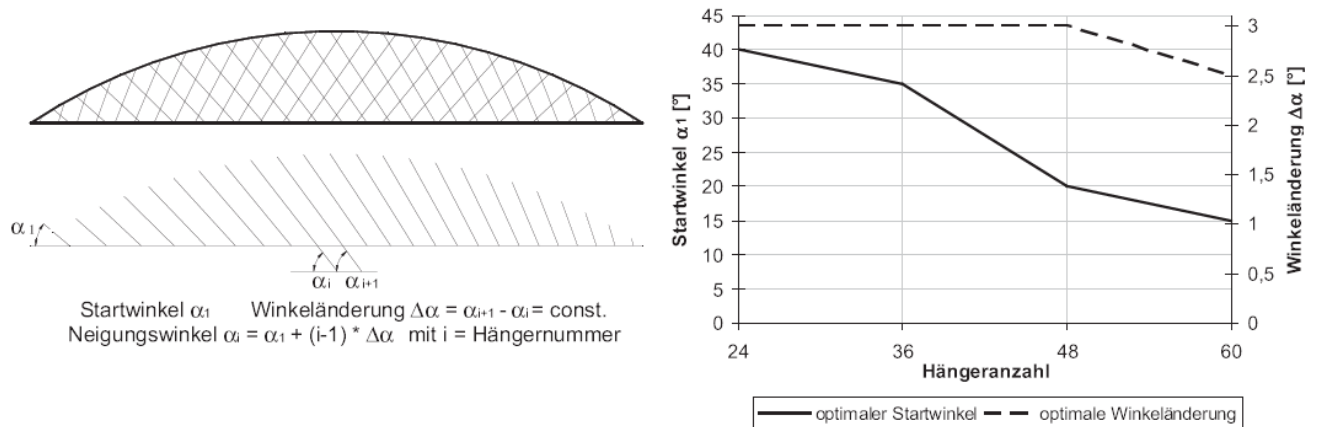


Figure 103: Optimal slope parameters for hanger arrangement type 2 ( span ≥ 150m )

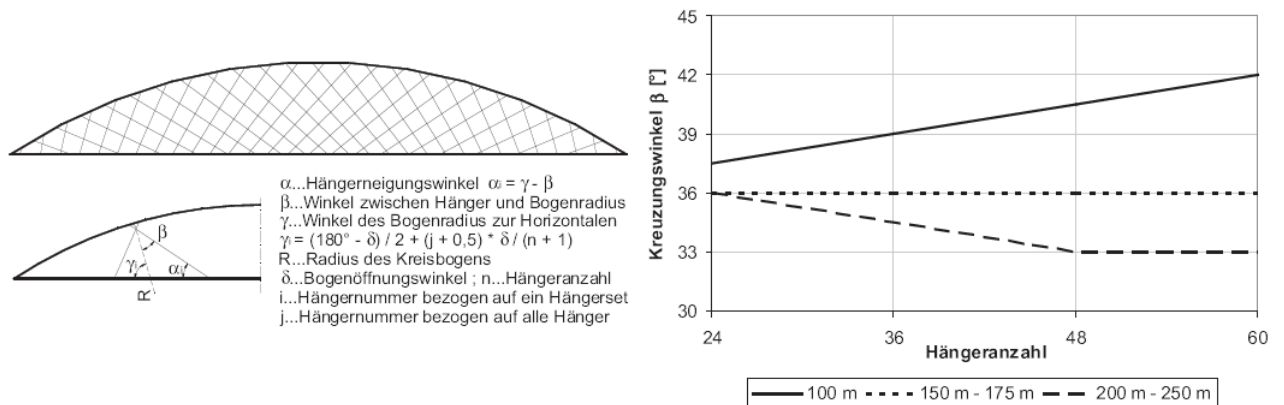


Figure 104: Optimal slope parameters for hanger arrangement type 4

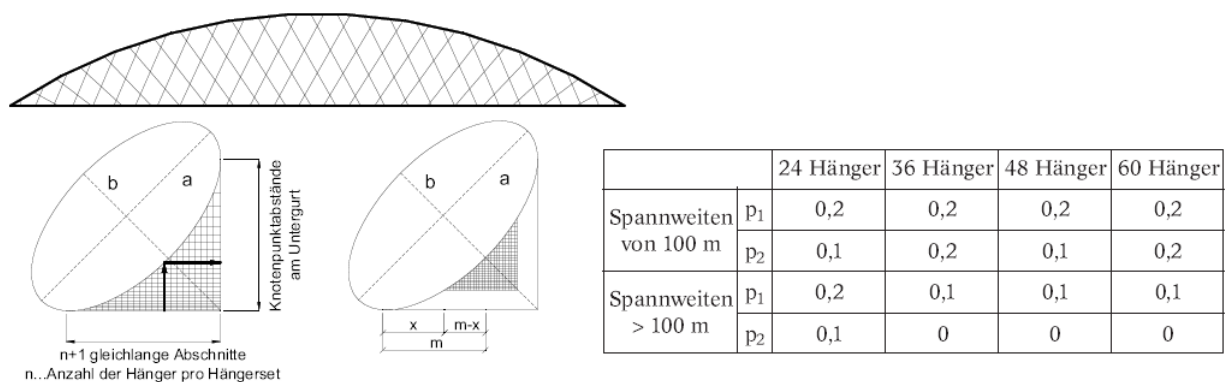


Figure 105: Optimal slope parameters for hanger arrangement type 5

### Optimal angles

Type 2:  $\alpha_1 = 28^\circ, \Delta\alpha = 3^\circ$

Type 4:  $\beta = 34^\circ$

Type 5:  $p_1 = 0,1, p_2 = 0$

**Constructing the hanger arrangement**

With the instructions given in Figure 103-Figure 105, half of the hanger arrangement can be composed. Then with the use of symmetry the full arrangement is obtained, as shown in Figure 106 for arrangement type 2. All arrangement types use the spacing along the arch as reference points. The spacing can be determined by dividing the arch length into  $(n + 1)$  segments.

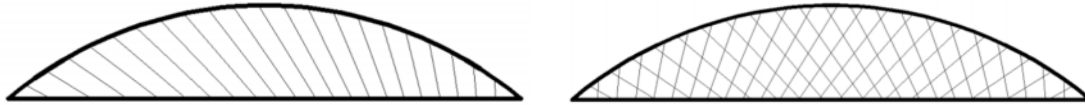


Figure 106: Half- and full network arrangement

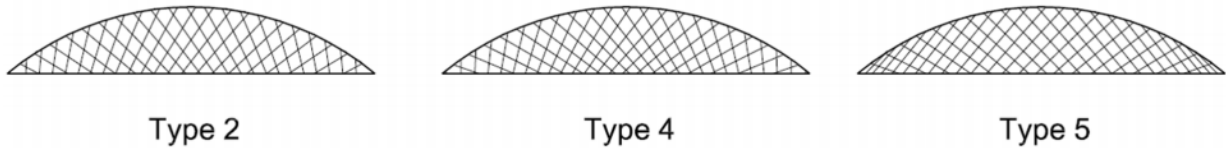


Figure 107: Three optimal hanger arrangement types

As becomes clear from Figure 107, the appearances of the three hanger types show no large differences. All types follow a certain pattern.

**Final decision**

Arrangement type 2 was decided to be the best arrangement based on the following arguments:

- The structural performance of type 2 (96,1%) is just as good as that of type 4 (100%) according to Table 49.
- The steeper hangers of arrangement type 2 would lead to a more favorable constructability, according to Teich. He explains this statement by the fact that the steep angles lead to shorter hangers. Also steeper hangers can be more easily supported during construction.

The final hanger network implemented in the arch geometry is given in Figure 108. With a starting angle of  $28^\circ$  and an angular change of  $3^\circ$  per hanger. The plane in which the arrangement is generated is not the plane of the arch. The plane that is formed by the apex of the arch and the main girder is used as plane for the hanger arrangement.

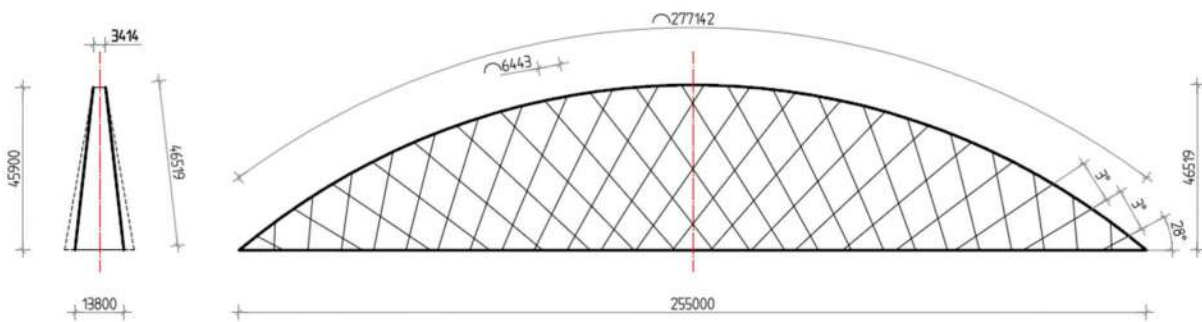


Figure 108: Final hanger network, based on arrangement type 2 and 42 hangers



From the original tender design the cross-section of the main girder is determined as:

$$A_{maingirder} = 0.4552m^2$$

$$E_{steel} = 2,1 \cdot 10^8 \text{ GPa}$$

$$E_{concrete} = 3,1 \cdot 10^7 \text{ GPa}$$

The ‘Steiner’ component of the moment of inertia is calculated:

$$I_{maingirder} = 2 \cdot 6,9^2 \cdot A_{maingirder} = 2 \cdot 6,9^2 \cdot 0,4552 = 43,34 \text{ m}^4$$

The moment of inertia of the concrete slab

$$I_{deck} = \frac{1}{12} db^3 = \frac{1}{12} \cdot 0,4 \cdot 11,3^3 = 48,1 \text{ m}^4$$

Finally the stiffness (EI) of the main girder and the concrete slab are added and divided by  $I_{deck}$ . This results in a modulus of elasticity where the stiffness of the ‘Steiner’ component of the main girders is incorporated

$$E_{eq} = \frac{EI_{deck} + EI_{maingirder}}{I_{deck}} = \frac{3,1 \cdot 10^7 \cdot 48,1 + 43,34 \cdot 2,1 \cdot 10^8}{48,1} = 2,2 \cdot 10^8 \text{ GPa}$$

As was mentioned above, the final stiffness will be reduced with 50% to account creep of the concrete and a reduced cross-section of the main girders.

$$\text{Reduced stiffness: } 50\% (2,2 \cdot 10^8) = 1,1 \cdot 10^8 \text{ GPa}$$

The total increase in horizontal stiffness between the original tender design (3 separate beams) and the reference design (composed beam) is, even with a reduction of 50%, a factor 3,5 higher.

$$\frac{E_{equivalent}}{E_{original}} = \frac{1,1 \cdot 10^8}{3,1 \cdot 10^7} = 3,5$$

In the SCIA model the concrete slab will be given a stiffness of  $1,1 \cdot 10^8 \text{ MPa}$  to incorporate the composed beam effect.

### C.2 Determining class 3 arch cross-section

The class of the cross section can simply be determined by evaluating the plate width over the thickness (b/t ratio). The b/t ratio is limited by an upper boundary which depends on the steel grade and loading conditions. The arch can be considered as a fully compressed section, therefore the limits for the plate width according to NEN-EN 1993-1 are given in Table 50. The plate thicknesses are based on standard plate thicknesses obtained from Arcelor Mittal ([www.arcelormittal.com](http://www.arcelormittal.com)).

$$\frac{b}{t} \leq 42 \cdot \varepsilon_{S460}$$

Where:

$$\varepsilon_{S460} = 0.71$$

Plate thickness [mm]	10	12	15	20	25	30	35	40
Max. width [mm]	298	358	447	596	746	895	1044	1193

Table 50: Maximum plate width for class 3 classification

It is decided to choose a through stiffener with a plate thickness of 20mm. This results in through stiffeners with a relatively high buckling resistance, which increases the resistance for stiffener buckling. The trough-shaped stiffeners can be spaced at the maximum widths (given in Table 50).

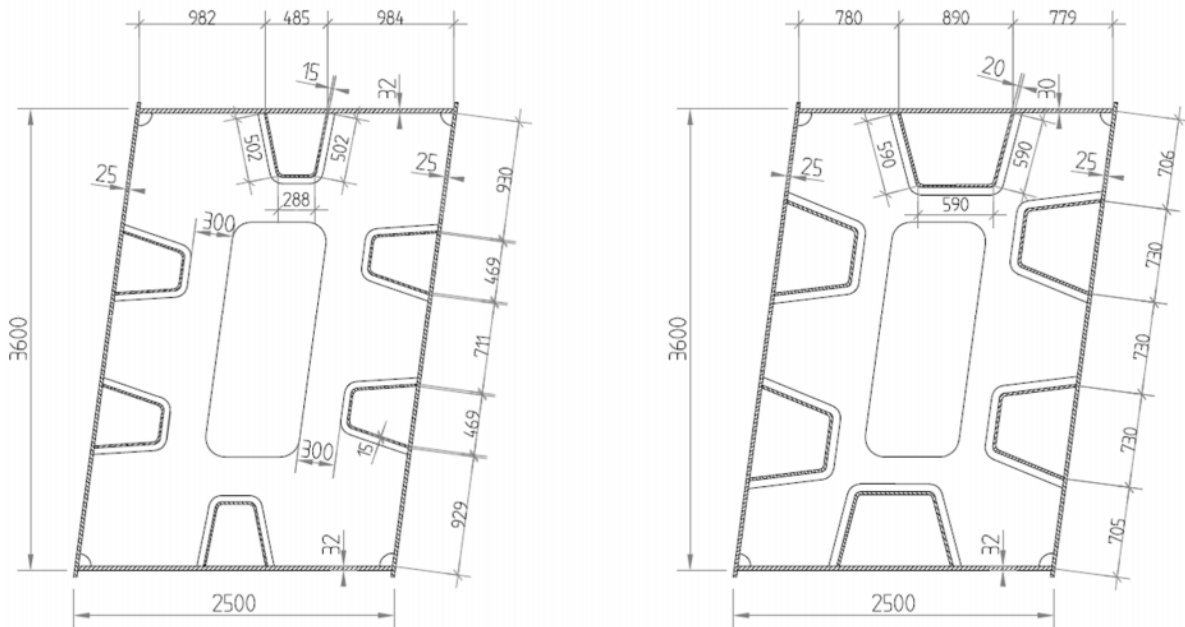


Figure 111: left: cross-section original tender design based on S355, right: adjusted cross-section based on S460

# ANNEX D: ORIGINAL TENDER DESIGN

The research question of this thesis originates from a variant study for the optimal hanger arrangement of an arch railway bridge for a tender design. This railway bridge is part of an immense project to improve the infrastructure between Almere, Amsterdam and Schiphol airport for a total value of one billion euro. The bridge will cross 10 traffic lanes of the to be widened A1 highway with a total span of 255m. On the November 12<sup>th</sup> 2012 it was announced that the tender was won by SAAone, a combination of contractors and engineering firms (Volker Wessels, Boskalis, Hochtief, Royal HaskoningDHV and Iv-Infra).

From the overall project which contains multiple bridges and viaducts and roads, specific guidelines for this railway bridge were formulated. Also architectural restrictions were given. The bridge had to be an arch bridge, with touching arches.

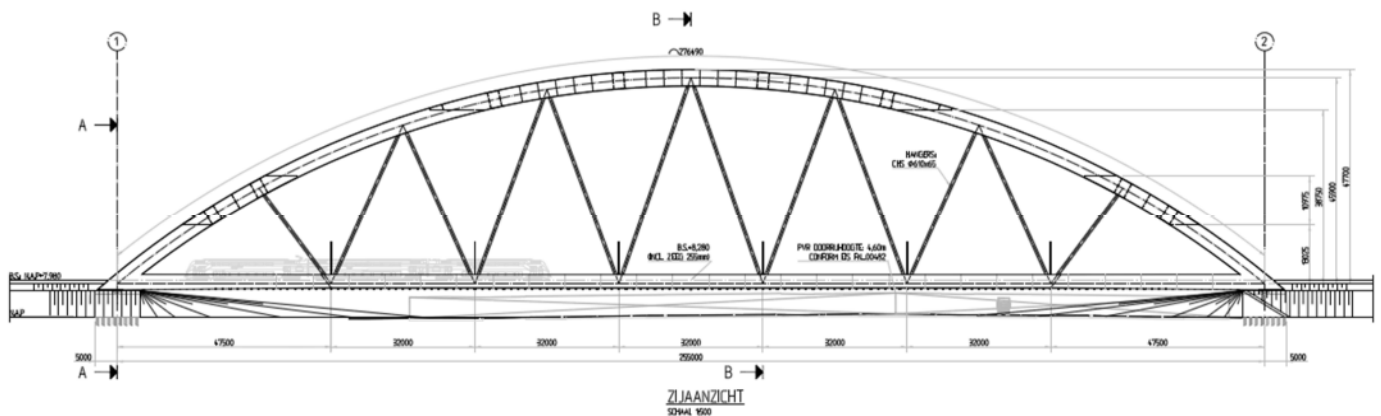
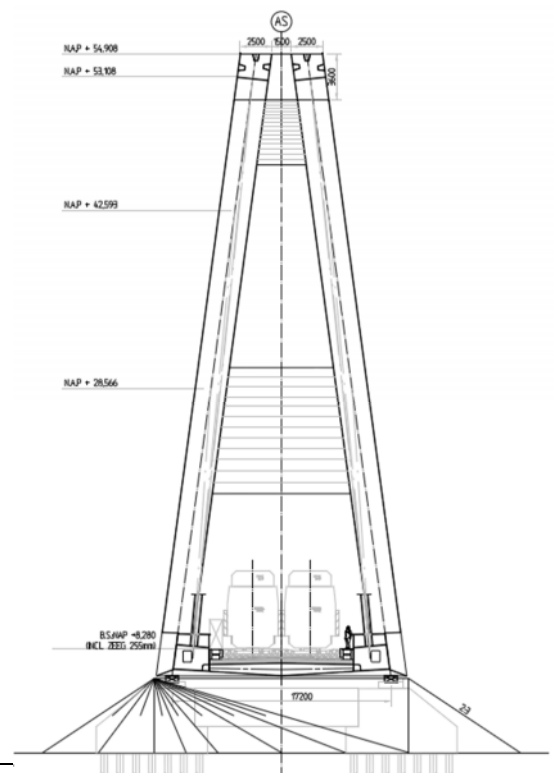


Figure 112: Side elevation of the original tender design

## Main design considerations

The design considerations that played an important role in the design were the following:

- Preventing vibration effects caused by vortex shedding. Vortex induced vibrations caused a lot of problems with the hangers of arch bridges in the last decades. Expensive damping provisions had to be installed to prevent the vibrations. To meet this demand the hangers are dimensioned with a Scruton number above 20. This was achieved by applying a large wall thickness. Also a logarithmic structural damping of  $\delta_s = 0,006$  was prescribed in the boundary conditions.



- Providing structural provisions for the installation of dampers. If unforeseen vibration effects would occur, the damping provisions must be easily installed.
- Strict time schedule for the final placing of the bridge: The bridge will replace an existing railway bridge. The continuity of the rail traffic is of high importance and a construction time of only 72 hours is allowed.
- The span and construction method were mainly determined by the requirement of minimal hindrance to the surroundings. Especially the highway A1, which it crosses.
- The overall shape of the bridge was advised by an architect.
- Strict limitations with regard to noise emission. This led to a composite deck structure.
- Limits to the weight and size of the prefabricated steel sections and of the overall bridge structure. The weight is dictated by the capacity of the transportation system that slides the bridge into its final location. This led to the application of S460 for the main girder itself.
- No compression in SLS in hangers allowed. This condition was not satisfied. The deck weight was increased to reduce the compression forces. To cope with the compressive forces tubular sections were applied.

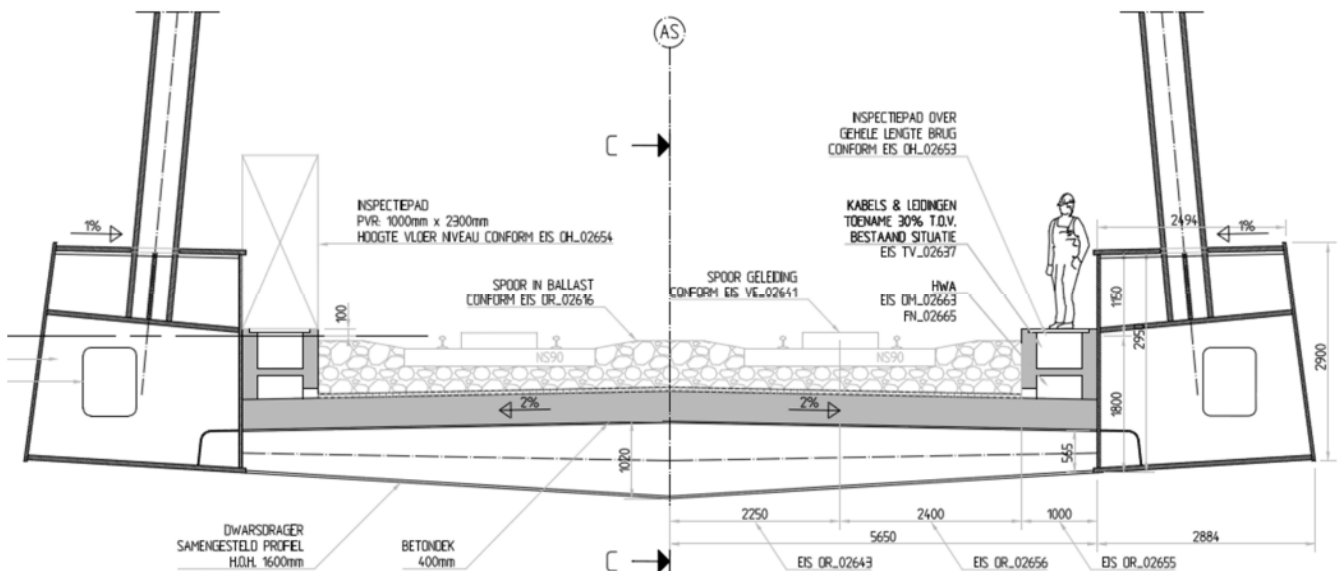


Figure 113: Deck structure of the original tender design

### **SCIA model**

To evaluate the force distribution and global stability in the bridge, FEM analysis program ‘SCIA engineer’ is used to calculate the force distribution. The preliminary design was made by using a 2D model. This model was also used to evaluate alternative hanger arrangements. When finally the diagonal hanger configuration was chosen, a three dimensional (see Figure 114) was constructed to perform a more detailed analysis. The main purpose of the 3D model was to verify the global stability of the arch.

The 3D model solely consists of 1D beam elements, to keep the force distribution as clear as possible and to minimize the calculation time. Even the concrete deck plate is modeled as a 1D beam. This simplification makes the model less accurate, but more flexible to work with during a design process.

In this paragraph the following aspects of the SCIA model are considered:

- Arch
- Main girder
- Deck
- Diagonals/ Hangers
- Bracing
- Arch- main girder connection
- Hanger connection

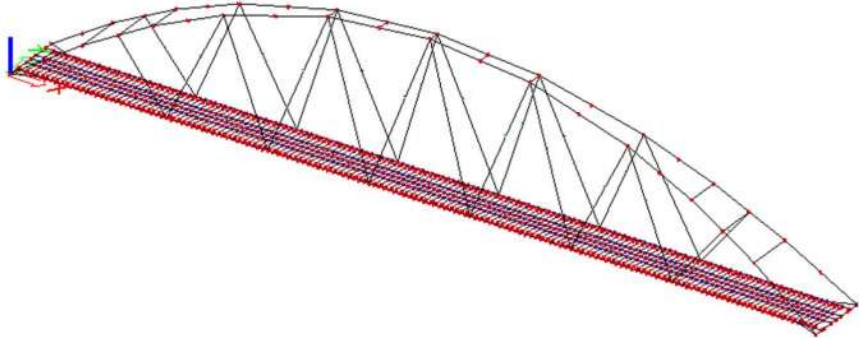


Figure 114: 3D SCIA model with old positions of the wind bracing

**Arch**

The geometry of the arch is built up out of straight arch elements. This segmented arch is easier to model (for a diagonal hanger arrangement), but underestimates the bending moments in the plane of the arch. In a fully curved arch, an additional bending moment is formed, due to the curvature of the arch.

The cross-section of the arch is modeled in SCIA as a rectangular box-section (as shown in figure 115). In reality the cross-section of the arch is provided with stiffeners and diaphragms to ensure sufficient local stability of the element. The contribution of the stiffeners is taken into account by adding their cross-sectional area to the total thickness of the box-section. To model this correctly the cross-sectional properties (A, I<sub>y</sub>, I<sub>z</sub>) of the real arch section should be similar as the box-section. In the original tender design, these properties are overestimated.

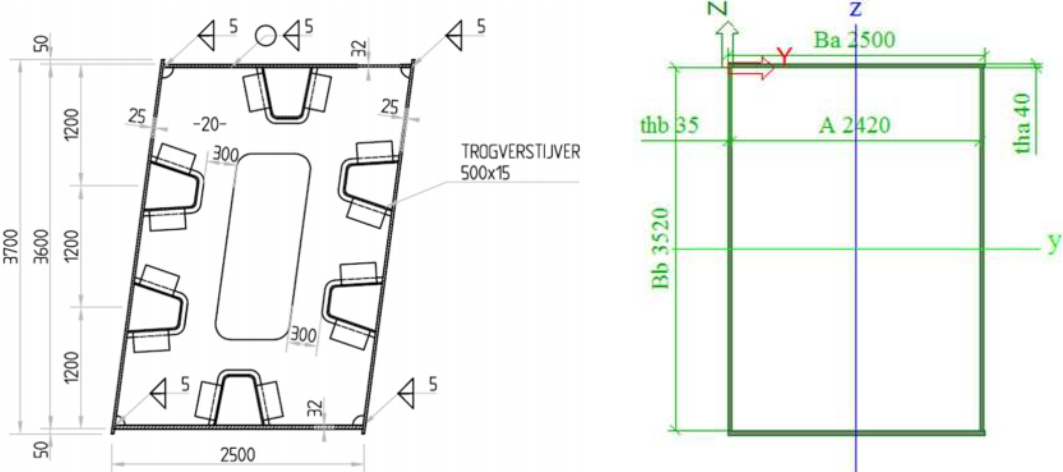


Figure 115: Arch cross-section from drawing (left) and Scia model (right)

### Main girder

The main girder is mainly subjected to a large tensile force, therefore no stiffeners are required. The modeling of the main girder is based on the average outer dimensions and the applied plate thicknesses. In reality the cross girders are eccentrically connected to the main girder, which produces a torsional bending moment in the main girder. This effect is not incorporated in this simplified model.

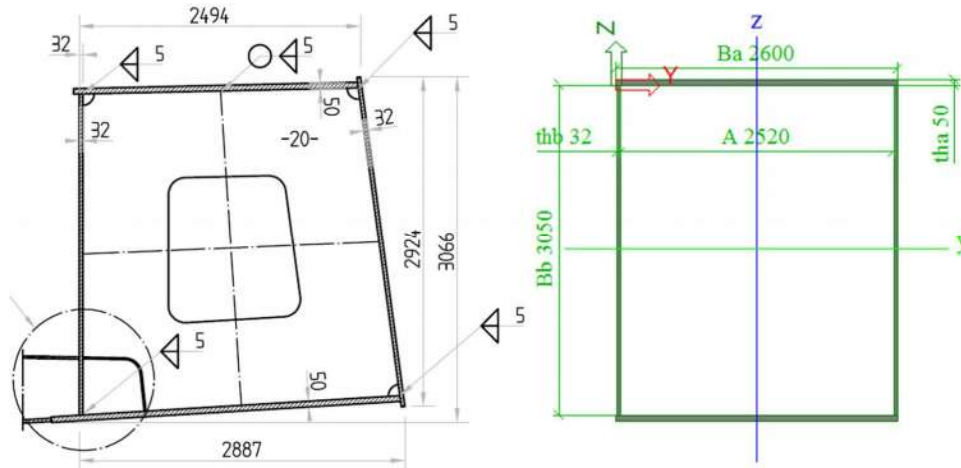


Figure 116: Main girder cross-section from drawing (left) and Scia model (right)

### Deck

The deck is composed out of cross girders and a concrete slab which supports the ballast layer and all other railway components. On the deck two IPE600 girders are placed along the length of the bridge to represent the railway tracks. All loads are placed on these tracks. The cross girders are spaced 1,6m and connected to the concrete slab by shear connectors. This ensures composite beam action, which increases the strength and bending stiffness significantly. In the mathematical model the cross girder is simplified as a HEB900 beam, which is insufficient to model the stiffness of the composite beam.

The 'tracks' (IPE600 beams) and concrete deck are not able to develop axial forces, because they are freely supported in axial direction. This has been done to keep the force distribution in the main girder as clear as possible, because all axial force will then be transferred by the main girder.

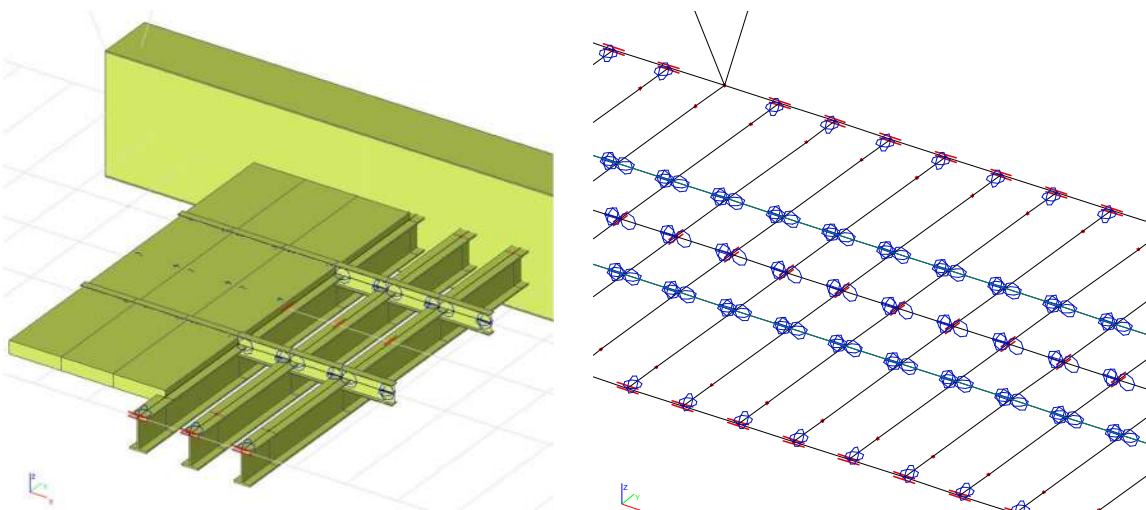


Figure 117: Deck structure as modeled in SCIA engineer

In the modeling of the deck large simplifications are made to keep the model as simple as possible. For instance: no 2D plate elements were applied, the deck is modeled as a beam with similar dimensions as the concrete deck. In reality, the main girder is connected to the concrete deck by means of shear connectors. This connection allows the main girders and concrete deck to act as a composite beam in bending, creating a high transverse stiffness (see Figure 118 right). In the SCIA model, this shear connection is not incorporated; hence the Steiner component of the bending stiffness is not incorporated. This has significant influence on the horizontal stiffness, and also affects the global stability of the structure in a negative way.



Figure 118: Deck structure as modeled in original tender design (left), Real behavior of deck structure (right)

**Diagonals**

The diagonal hangers that were applied in the original tender design are circular hollow sections with a diameter of 610mm and a wall thickness of 65mm. The hangers are fully welded to the arch and main girder. The dimensions of the diagonals are chosen to obtain a Scruton number above 20.

The length of the hangers, which is relevant for determining the steel weight of the bridge, is given by figure 119. In Figure 119 the system- and net. Lengths of 6 unique hangers is shown. Because the model is double symmetric, these 6 hanger can be mirrored to obtain the full diagonal hanger arrangement.

Hanger nr.	Lsystem [m]	Lnet [m]
1	26.785	23.285
2	38.94	35.440
3	39.015	35.515
4	46.42	42.920
5	46.44	42.940
6	48.885	45.385
<b>Total</b>		225.485

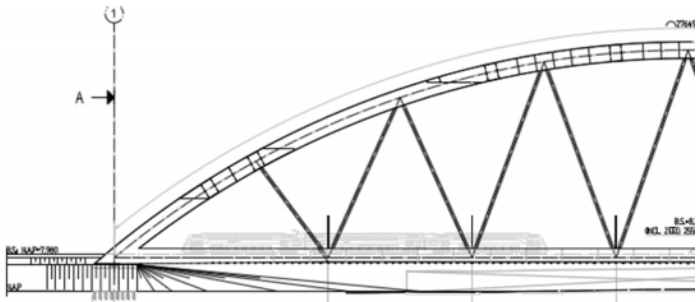


Figure 119: System length and net. length of a single set of diagonal hangers, the hangers are numbered 1 to 6 from left to right

**Horizontal bracing**

The bracing of the original tender design was designed from a more structural point of view. Large bracings were used as shown in Figure 120, which would provide sufficient out of plane stability. To simplify the design, the bracing as shown in Figure 120, was modeled as a set of three box-sections. For the box-sections, the same cross-section as for the arch was used. The stiffness of these bracing elements is roughly estimated. For this thesis, the horizontal bracing is of minor importance.

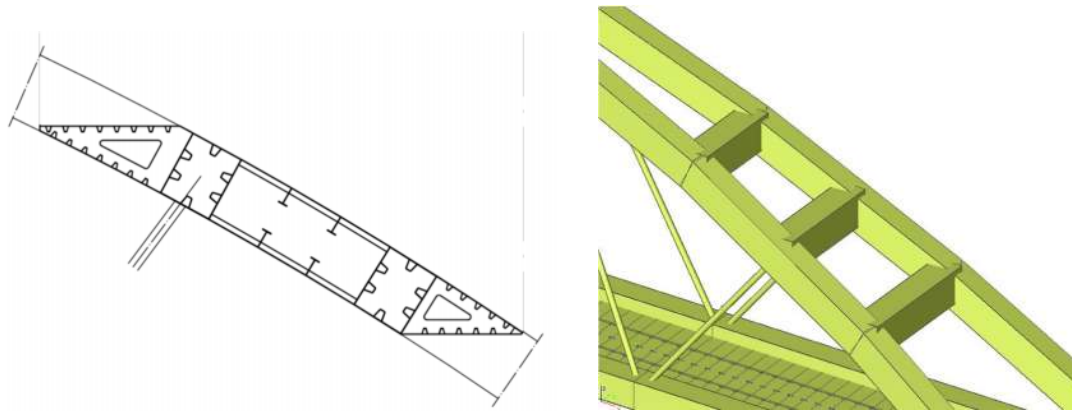


Figure 120: Bracing original tender design, drawing (left) and model (right)

### *Arch-main girder connection*

To create sufficient spacing between the trains and the arches, the arches were spaced slightly outside the alignment of the main girder, as shown in Figure 121. In reality, the main girder is widened and strengthened locally to transfer the gigantic forces that act on this specific part of the structure. In the mathematical model, the stiff connection is modeled by applying a truss which consists of heavy profiles, as is highlighted in Figure 121. The cross-sections used for the arch-main girder connections were roughly estimated.

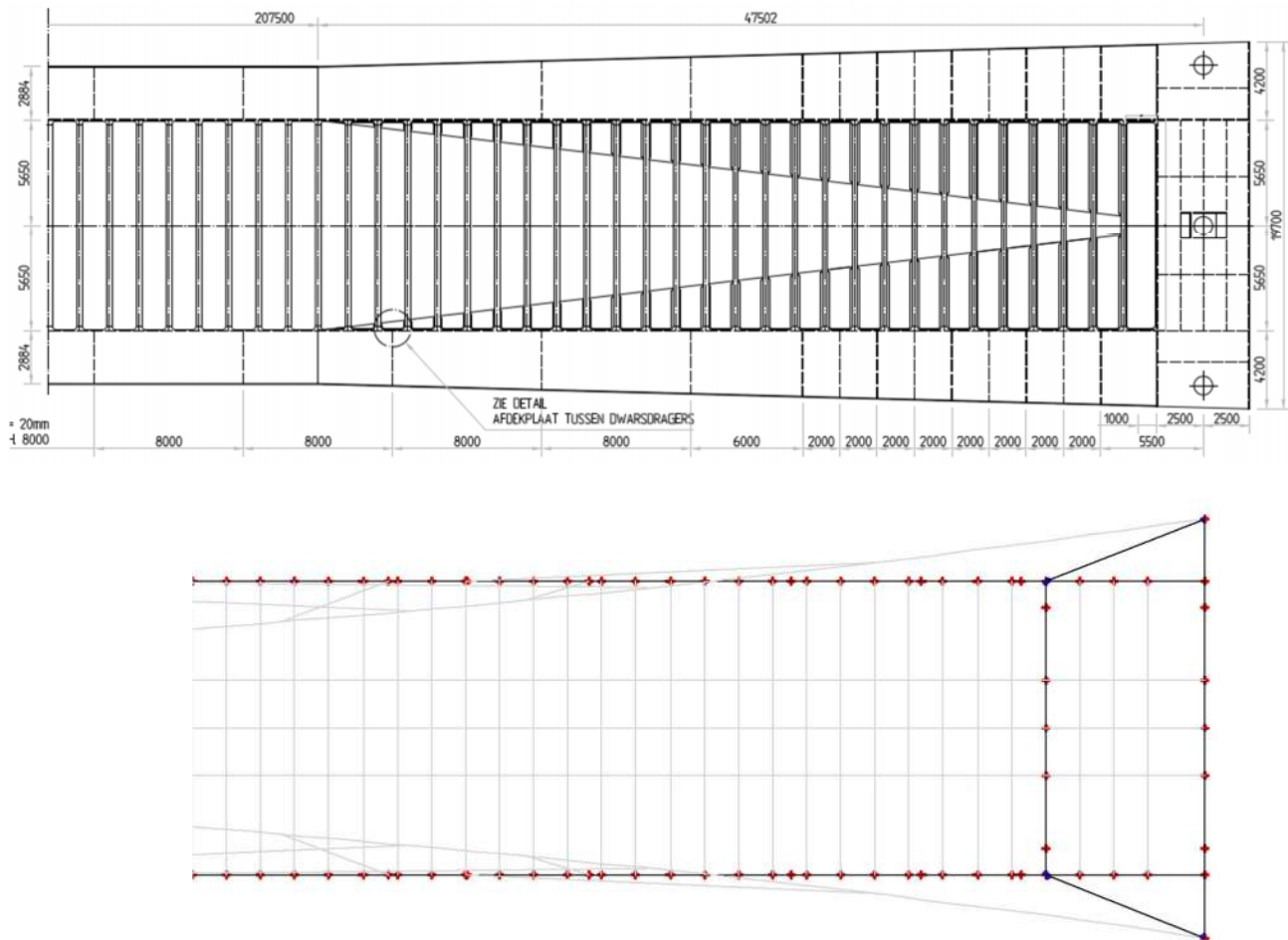


Figure 121: Arch and main girder connection, drawing (top), model (bottom)

### Hanger connections and diaphragms

To compare the steel weight of both designs the amount of steel for the hanger connection of the reference design is estimated. This steel weight is determined according to the hanger connection shown in Figure 122.

$$\text{Bottom plate} = 1200 \cdot \frac{2}{3} \cdot 2600 \cdot 60 = 0,1248 \text{ m}^3$$

$$\text{Vertical plate 1} = 1000 \cdot 2600 \cdot 60 = 0,156 \text{ m}^3$$

$$\text{Vertical plate 2} = \pm 1000 \cdot 1200 \cdot 15 = 0,018 \text{ m}^3$$

$$\text{Total volume of hanger connection: } 0,2988 \text{ m}^3 \approx 0,3 \text{ m}^3$$

$$\text{Steel weight per diagonal connection: } 0,3 \text{ m}^3 \cdot 7850 \frac{\text{kg}}{\text{m}^3} = 2355 \text{ kg}$$

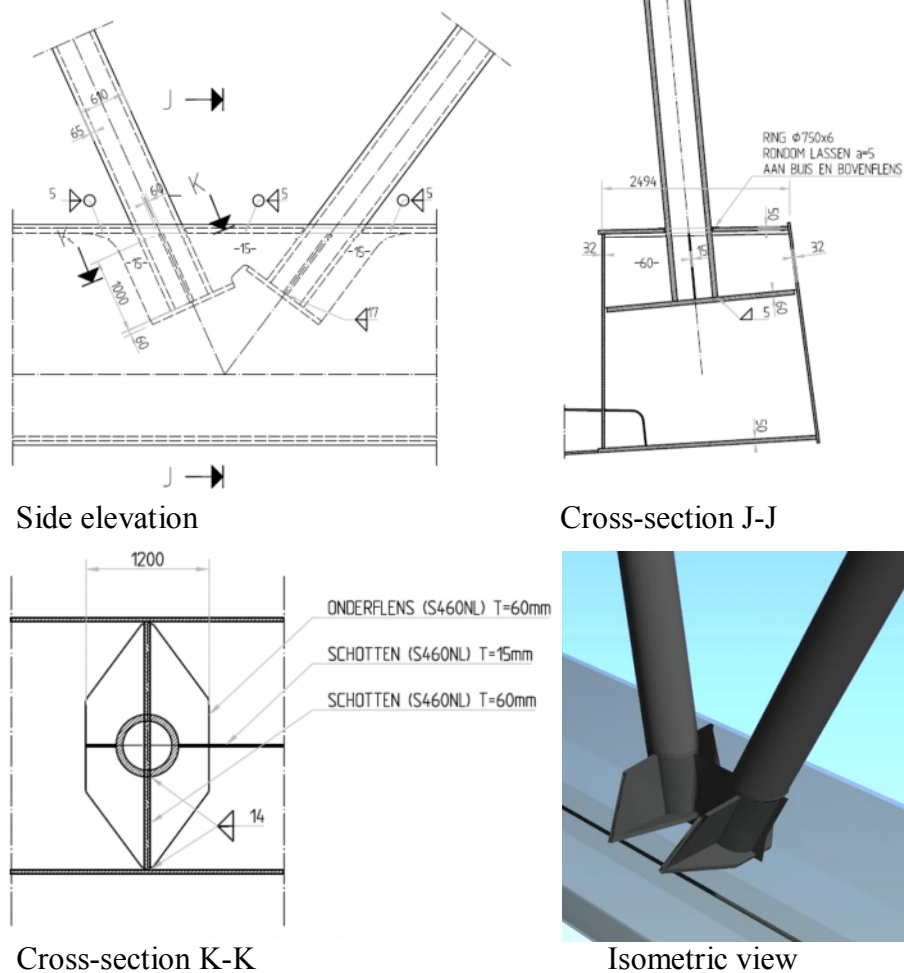


Figure 122: Hanger connection of the reference design

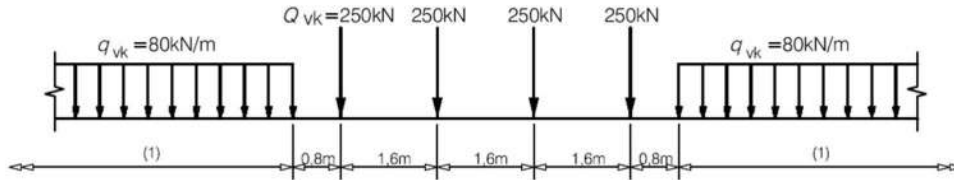
### Connections and diaphragms reference design

For the reference design, the diaphragm is placed at a c.t.c. distance of 4m in the arch and at 8m in the main girder. This results in  $\frac{255}{8} = 32$  diaphragms for the main girder, and  $\frac{277,142}{4} = 70$  for the arch. For all diaphragms a thickness of 20mm is applied.

### Loads and combinations

For sake of simplicity, the tender design makes use of the following basic load cases:

- Self-weight
- Ballast layer + track and other railway provisions
- Traffic load (Load model 71 applied as static- and mobile load case)
- Wind



Other load cases, for instance: thermal-, fire-, aerodynamic load and other traffic load types where investigated and concluded insignificant for the design stage. Some conservatism is present in the combinations and determination of some of the load cases. This conservatism provides an extra layer of safety for the determination of maximal forces.

### Adjusted tender design

When the tender design was submitted, some architectural changes had to be applied to the design. The size and position of the wind bracing had to be changed to obtain a more transparent design. Also the shape of the cross-section of the main girder was adjusted, as shown in Figure 124.

The adjustment of the wind bracing had a large negative effect on the stability of the arch. To cope with the increase of stresses due to 2<sup>nd</sup> order effects, the steel grade was upgraded from S355 to S460. This was done to prevent a large increase in steel weight and to provide a quick fix for the stability problem. However, this upgrade in steel grade also changed the cross-section class of the arch from class 3 to 4.

In Figure 123 the final tender design is shown:

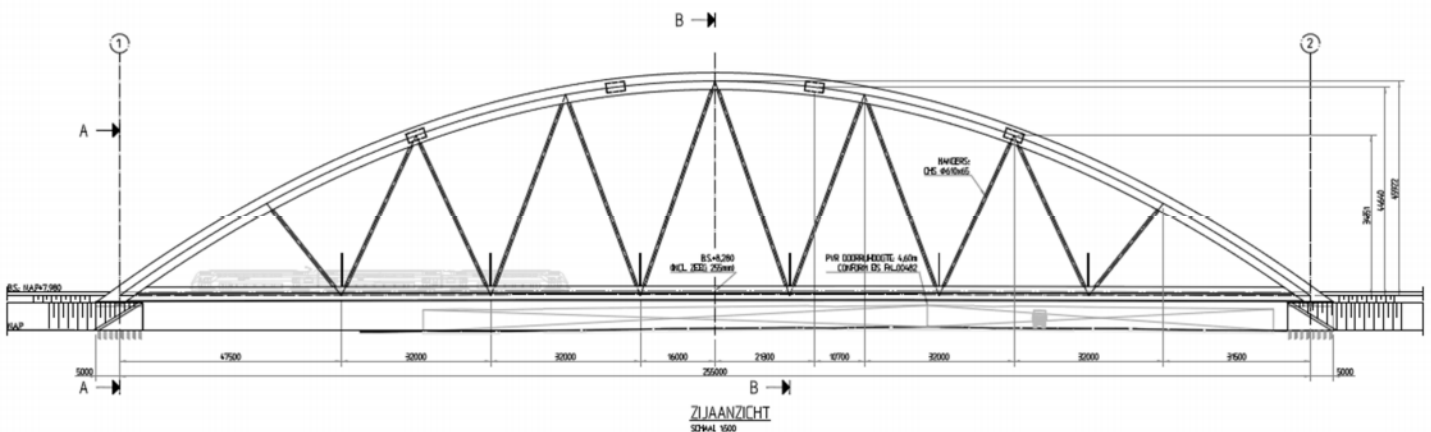
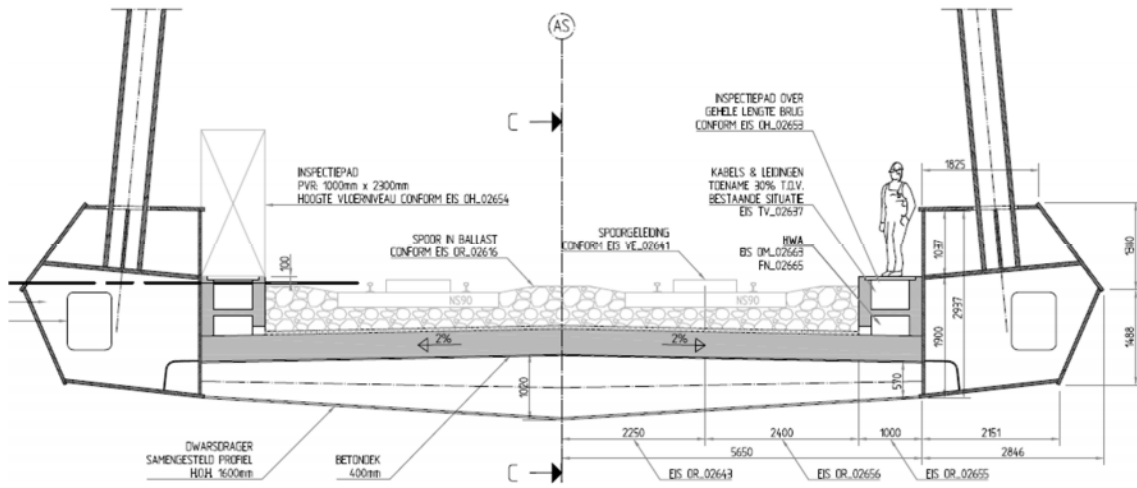


Figure 123: Final tender design



**Figure 124: Cross-section of the final tender design**

# ANNEX E: HANGER BEHAVIOR

## E.1 Implementing hanger arrangement in the design

The hanger arrangements that were generated by Teich [1] are based on a network arch bridge with two separate vertical arches, see left Figure 125. The hanger arrangement is implemented in the 3D SCIA model of the reference design by following the geometrical description provided in figure 127. The hangers are inserted in the plane that is formed by the apex of the arch and the main girder, as is shown Figure 127. Near the supports, where the arch and main girder are misaligned significantly, the angle of the outer hangers do not match the geometrical description. However, this should not affect the optimal force distribution in the hangers, because the outer hangers are not part of the optimal arrangement. Teich mentions specifically that the angle of the outer hangers should be manually adjusted in order to obtain a good force distribution.

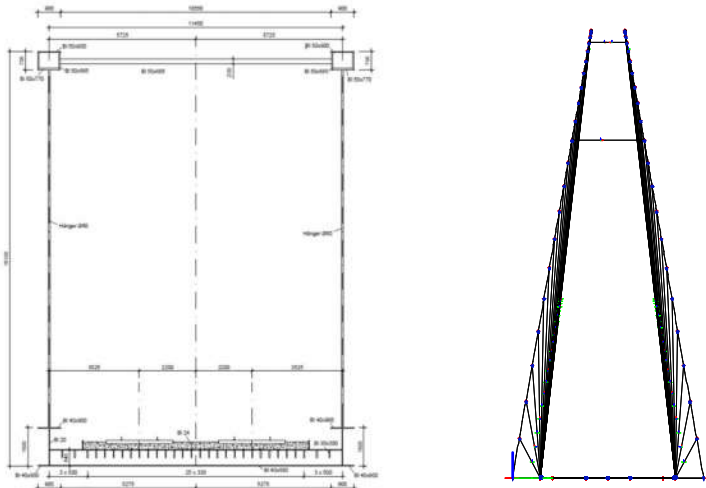


Figure 125: Left: side elevation of structure used by Teich [1], right: side elevation of the network arch

In chapter 3 the hanger arrangement and hanger type were determined. The following conclusions were drawn, and will be used to design the network arch:

- Hanger arrangement: Type 2 with 42 hangers per arch plane (Figure 108: Final hanger network, based on arrangement type 2 and 42 hangers)
- Hanger type: Steel rod hanger with welded connections, estimated diameter  $\varnothing 140\text{mm}$

This results in the following geometrical description of the hanger arrangement.

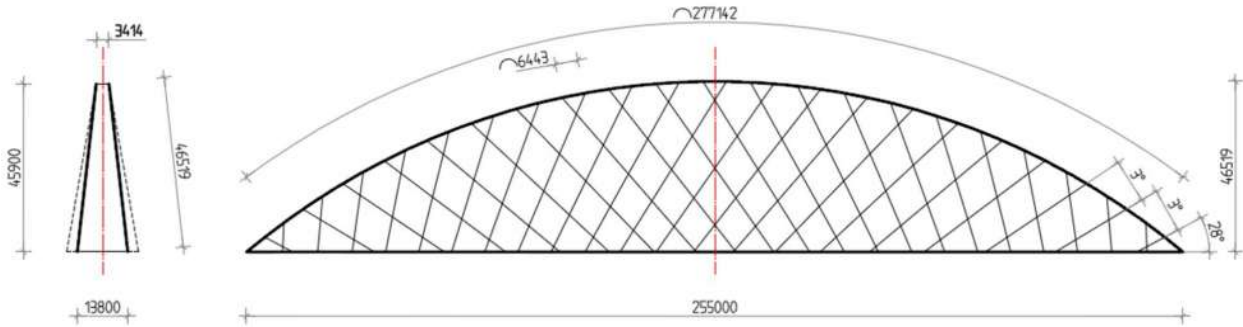


Figure 126: Geometrical description of the preferred hanger arrangement

### Creating the hanger arrangement

To implement the optimal hanger arrangement in the 3D SCIA model, 42 nodes are placed along the arch at equal distances. Based on the coordinates of these nodes, the coordinates of the nodes along the main girder can be calculated from the angles given in Figure 52. This procedure has to be performed for only one set of hangers because by mirroring the full arrangement can be obtained. In annex B the hanger coordinates, angles and lengths are given. The hanger numbers correspond to the numbering shown in Figure 53, where the 21 individual unique hangers are shown.

In Table 51 the hanger coordinates, angles and lengths are given. The numbers correspond with the numbering shown in Figure 53, where the 21 individual unique hangers are shown. The shortest (nr. 1), longest (nr. 13) and average (nr. 7) hangers are highlighted.

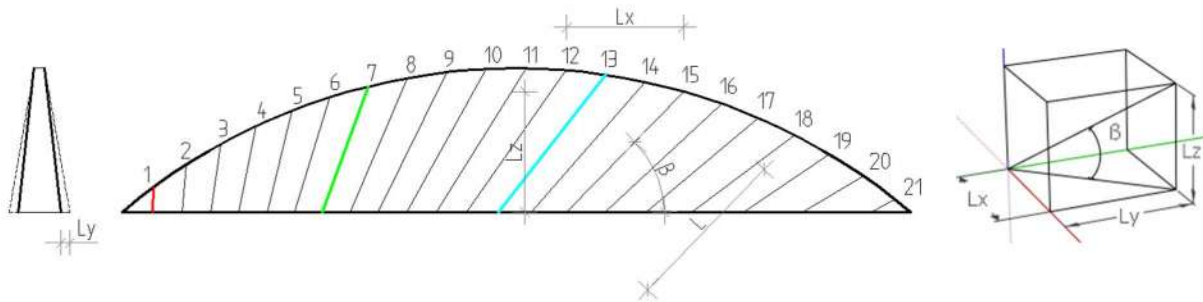


Figure 127: Schematization of the 21 unique hangers

Hanger nr.	Arch node			Angle $\beta$ [°]	Main girder node			Hanger length			
	x [m]	y [m]	z [m]		x [m]	y [m]	z [m]	L [m]	Lx [m]	Ly [m]	Lz [m]
1	10.115	1.387	7.865	88	8.628	2.900	0.000	8.146	1.487	-1.513	7.865
2	20.730	2.656	15.064	85	19.435	2.900	0.000	15.122	1.295	-0.244	15.064
3	31.797	3.803	21.567	82	28.901	2.900	0.000	21.779	2.896	0.903	21.567
4	43.272	4.822	27.346	79	38.302	2.900	0.000	27.860	4.970	1.922	27.346
5	55.105	5.709	32.377	76	47.505	2.900	0.000	33.376	7.600	2.809	32.377
6	67.425	6.460	36.637	73	56.749	2.900	0.000	38.326	10.676	3.560	36.637
7	79.641	7.072	40.109	70	65.569	2.900	0.000	42.710	14.072	4.172	40.109
8	92.242	7.543	42.779	67	74.577	2.900	0.000	46.515	17.665	4.643	42.779
9	104.991	7.870	44.634	64	83.658	2.900	0.000	49.719	21.333	4.970	44.634
10	117.836	8.052	45.667	61	92.888	2.900	0.000	52.292	24.948	5.152	45.667
11	130.723	8.088	45.874	58	102.345	2.900	0.000	54.191	28.378	5.188	45.874
12	143.595	7.979	45.254	55	112.116	2.900	0.000	55.359	31.479	5.079	45.254
13	156.399	7.724	43.809	52	122.304	2.900	0.000	55.722	34.095	4.824	43.809
14	169.081	7.325	41.545	49	133.033	2.900	0.000	55.182	36.048	4.425	41.545
15	181.586	6.783	38.472	46	144.448	2.900	0.000	53.614	37.138	3.883	38.472
16	193.860	6.101	34.604	43	156.731	2.900	0.000	50.855	37.129	3.201	34.604
17	205.854	5.282	29.956	40	170.120	2.900	0.000	46.690	35.734	2.382	29.956
18	217.513	4.328	24.549	37	184.912	2.900	0.000	40.836	32.601	1.428	24.549
19	228.790	3.245	18.405	34	201.501	2.900	0.000	32.917	27.289	0.345	18.405
20	239.638	2.036	11.550	31	220.381	2.900	0.000	22.472	19.257	-0.864	11.550
21	250.008	0.708	4.014	28	241.690	2.900	0.000	9.492	8.318	-2.192	4.014

Table 51: Hanger coordinates and lengths

## E.2 Comparing linear- and cable behavior

The comparison between linear beam behavior and cable behavior is vital for a reliable linear analysis. If the linear results would deviate too much from the real hanger behavior, the whole linear analysis would be invalid. In Figure 128 the fundamental difference becomes clear. When linear analysis is performed loads are transferred through bending moments and shear forces. Where a cable uses axial forces to transfer transverse loads.

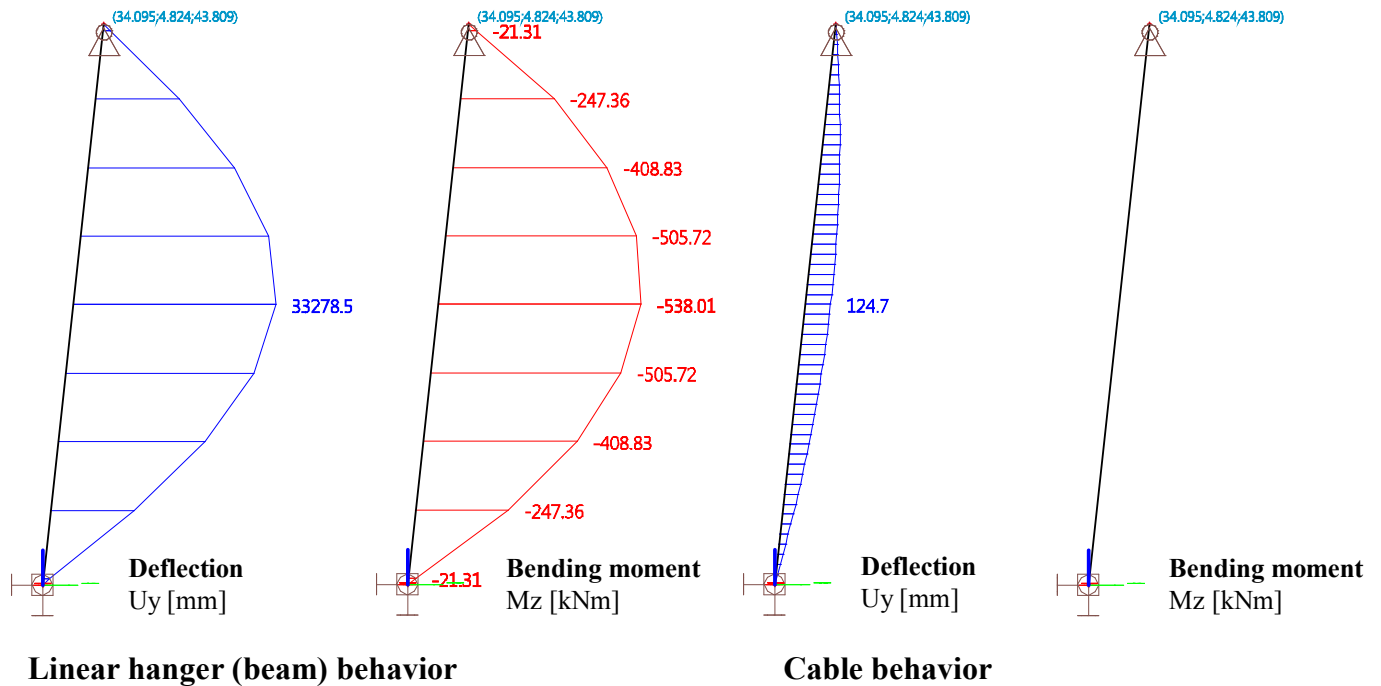


**Figure 128: Results of a beam (left) and a cable (right) loaded with a transverse wind load (SLS). The linear hanger (beam) transfers the load by bending moment where the cable develops axial force**

An important aspect that needs to be investigated is the difference in reaction forces between a linear hanger and a cable. These forces show the interaction between structure and hangers. If these reaction forces would differ too much, the overall linear force distribution would be invalid.

Also of interest is the stress increase due to the transverse load. If the stress increase is much higher than the linear stress, precautions should be taken in the design stage. For instance by lowering the maximal design stress.

By evaluating the longest hanger, the largest differences between linear beam behavior and cable behavior are expected. This is based on the following arguments:

- For the longest hanger, the cable action is dominant.
- The longest hanger transfers the largest amount of wind loading, simply because of its length.

### Modeling linear- and cable hanger behavior

For the comparison between linear beam and cable behavior, two separate models are used. The linear beam behavior is evaluated by the model depicted in Figure 129. This model is used to determine the reaction forces. These are obtained by applying a concentrated load ( $N_x$ ) near the supports. The full load is directly transferred to the supports. The stresses that develop in the linear hangers are completely irrelevant because these are based on load transfer by bending moments and shear forces (see Figure 128).

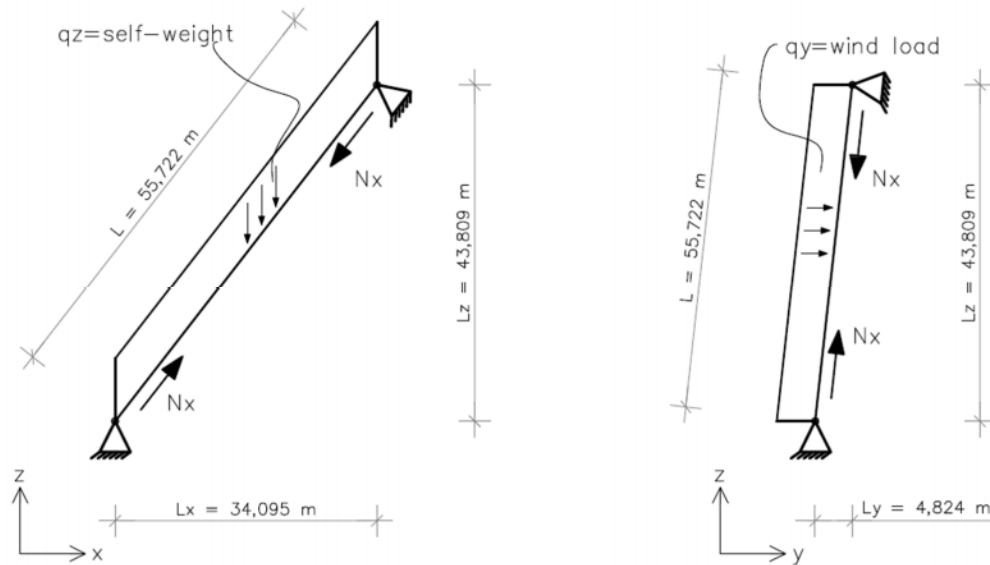


Figure 129: Hanger nr. 13 for the evaluation of linear hanger behavior, near the supports the initial force [ $N_x$ ] is applied to evaluate the reaction forces

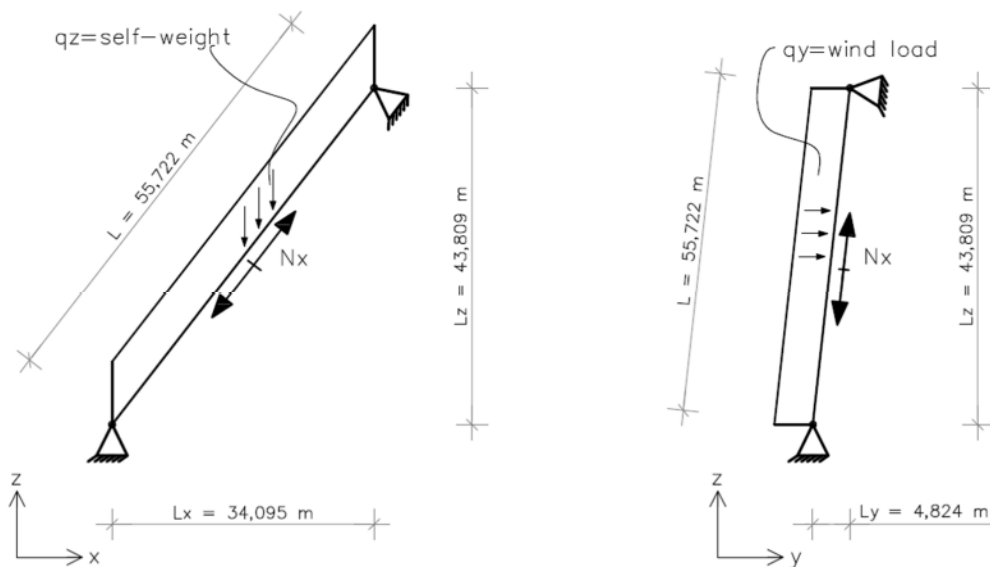


Figure 130: Hanger nr. 13 for the evaluation of cable behavior, an initial prestressing force [ $N_x$ ] is applied.

For the modeling of the cable, a specific module is SCIA engineer is used. With this module an initial prestressing force can be applied in the cable ( $N_x$ ), and by nonlinear analysis results are obtained.

### Evaluation of hanger behavior

For the evaluation of the stresses and reaction forces in the hangers, 5 prestressing forces (Nx) with a magnitude of 10, 100, 500, 1000 and 4241kN are applied. The last force is based on the maximum stress level of 240 MPa in the hangers.

#### Loads:

$$q_{y;wind\ load;SLS} = 1,4\ kN/m$$

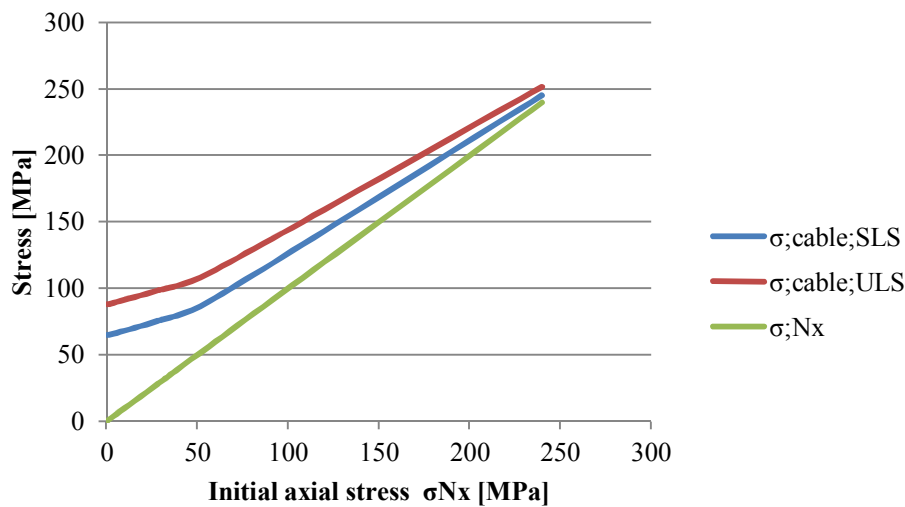
$$q_{y;wind\ load;ULS} = 1.65 \cdot 1,4 = 2,31\ kN/m$$

#### Settings:

The settings applied for cable analysis, are obtained from SCIA manual [23].

Remark: no specific mesh refinement is required for this type of calculation. A standard mesh size refinement of 4 sections per element is applied.

### Stress increase due to transverse wind loading



Nx	$\sigma;Nx$	$\sigma;cable;SLS$	$\sigma;cable;ULS$
10	0.57	65	88.1
100	5.66	66.7	89.9
500	28.29	75.7	98.5
1000	56.59	90.2	111.5
4241	239.99	245.4	251.8

Figure 131: Difference in axial stresses between cable and linear beam

## Reaction forces

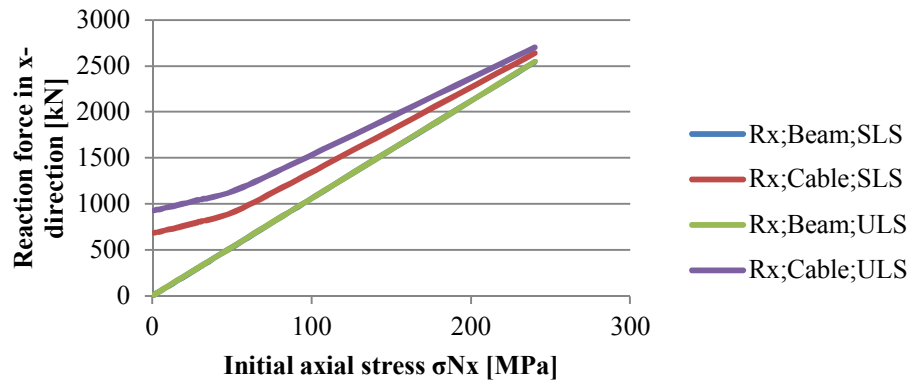


Figure 132: Difference in reaction force in x-direction between cable and linear beam

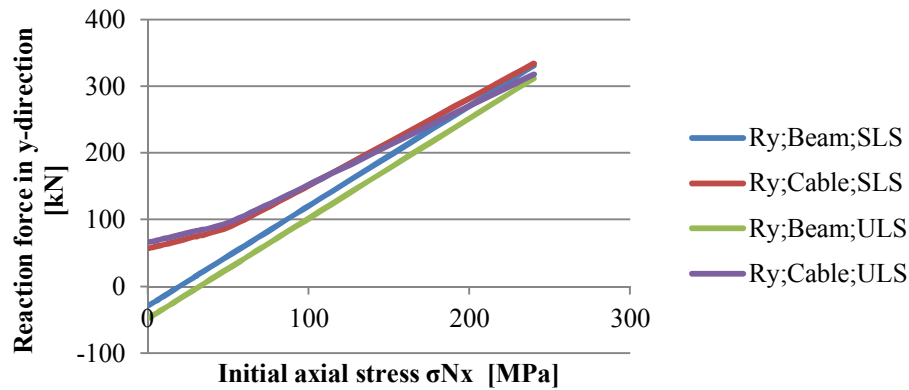


Figure 133: Difference in reaction force in y-direction between cable and linear beam

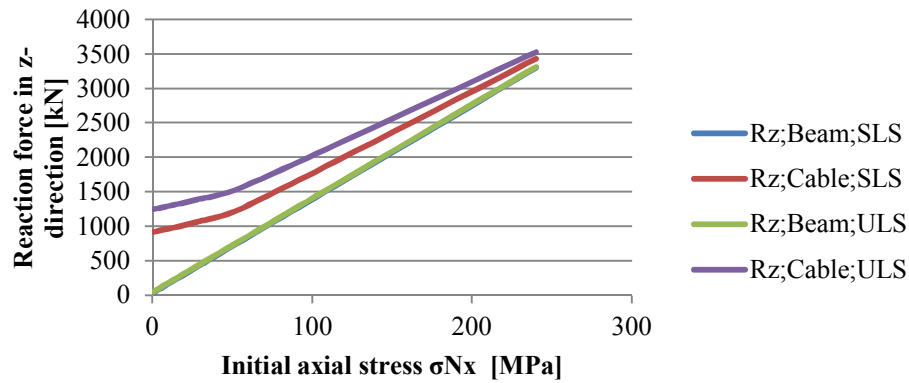


Figure 134: Difference in reaction force in z-direction between cable and linear beam

		Reaction forces at arch connection in SLS					
$N_x$	$\sigma_x;N_x$	Rx;Beam;SLS	Ry;Beam;SLS	Rz;Beam;SLS	Rx;Cable;SLS	Ry;Cable;SLS	Rz;Cable;SLS
10	0.57	10.05	-27.84	41.39	686.65	57.83	920.57
100	5.66	64.01	-20.2	110.74	705.62	60.52	944.93
500	28.29	303.87	13.74	418.93	803.22	74.37	1070.31
1000	56.59	603.69	56.16	804.17	959.97	96.59	1271.67
4241	239.99	2547.11	331.13	3301.29	2640.95	334.57	3431.44

Table 52: Reaction forces in SLS as a result of different axial forces ( $N_x$ )

		Reaction forces at arch connection in ULS					
Nx	$\sigma;Nx$	Rx;Beam;ULS	Ry;Beam;ULS	Rz;Beam;ULS	Rx;Cable;ULS	Ry;Cable;ULS	Rz;Cable;ULS
10	0.57	11.54	-46.64	54.7	931.17	66.85	1250.08
100	5.66	65.5	-39.01	124.05	949.97	69.52	1274.23
500	28.29	305.36	-5.07	432.24	1043.08	82.75	1393.83
1000	56.59	605.18	37.35	817.48	1183.96	102.74	1574.8
4241	239.99	2548.6	312.32	3314.6	2704.54	318.12	3528.41

**Table 53: Reaction forces in ULS as a result of different axial forces (Nx)**

### Conclusion

From E.5.2.1 and E.5.2.2 a clear pattern can be found. When high stress levels are reached (approx. between 200 and 240 MPa) which corresponds to the ULS design stress of the hangers, the differences between linear hanger behavior and cable behavior become small. Based on this conclusion it is decided to verify the linear design model only in the ULS.

The differences between linear beam action and cable action are significant for the reaction forces in x- and z-direction. These forces act perpendicular to the main axis of the arch and main girder (see Figure 135), resulting in bending moments (My). In y-direction the influence of the differences between linear beam action and cable action are negligible.

When comparing the linear and geometrically nonlinear force distribution (see paragraph 5.4) in the network arch, the following phenomenon is expected: The deviation between the bending moments (My) is expected to be higher in the permanent load + wind situation than for the ULS.

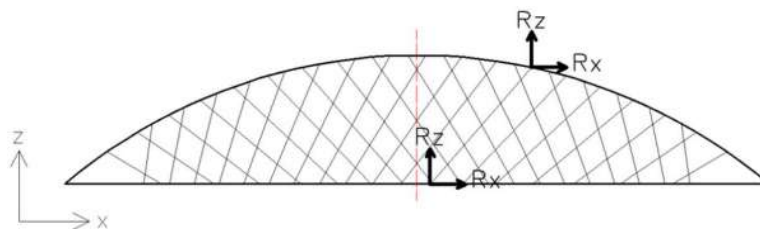


**Figure 135: Reaction forces (Rx and Rz) positioned in global coordinate system**

When comparing the linear and nonlinear axial stresses in the hangers a larger difference is expected in the permanent + wind loading situation. This is based on the comparison between linear beam behavior and cable behavior, shown in Figure 131.

In paragraph 5.4 the differences between linear and geometrically nonlinear analysis are evaluated.

### E.3 Reduced axial stiffness (catenary effect)

The catenary effect occurs in cable elements with large horizontal spans. These cable elements have a very low bending stiffness compared to their length, and due to its own self-weight the cable deflects significantly. Depending on force in the cable, the deflection can be relatively large. When the cable is tensioned again, the deflection reduces and the cable is strained elastically according to its standard modulus of elasticity. In order to model cable structures, iteration steps are necessary, this means nonlinear analysis. To incorporate the catenary effect in linear analysis, the variation in stiffness can be estimated by means of an equivalent modulus of elasticity.



Figure 136: Hangers of a cable stayed bridge, the catenary effect becomes visible

#### Determining fictitious E-modulus

This fictitious modulus can be determined in two ways, the tangent, and the secant modulus. The tangent modulus is based on the stiffness at a certain stress level, see Figure 137. The secant modulus is based on two stress levels, from where the stiffness is linearized and interpolated, see Figure 137. The secant modulus is the more exact method, however, to determine the secant modulus, the stress level in the live loading situation must be estimated in advance. For this estimation the tangent modulus can be used.

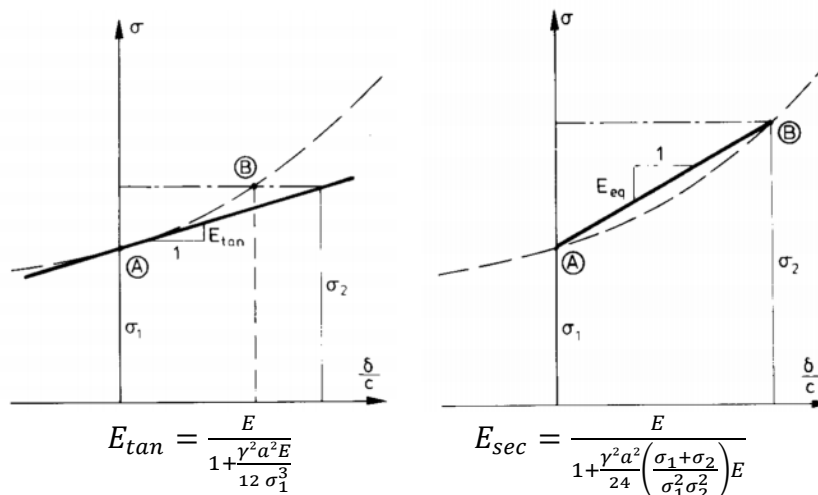


Figure 137: left: tangent modulus, right: secant modulus

Where:

- $\gamma$  = Density of hanger material
- $a$  = Horizontal distance of the hanger
- $\sigma_1$  = Initial stress due to dead load
- $\sigma_2$  = Final stress SLS

From the formulas above it becomes clear that the stress level has the largest influence on the stiffness reduction ( $\sigma^3$  and  $\sigma_1^2 \cdot \sigma_2^2$ ). Low stresses lead to larger reductions. The horizontal span ( $a$ ) also has a large influence.

Based on the formula for the secant modulus of elasticity the following graph can be plotted. Here the secant modulus of elasticity is plotted as a function of the stress ( $\sigma_2$ ). The initial stress due to dead load is obtained from Table 53, where the average stress in the hangers due to permanent loading is 65 MPa. The properties of the hangers are also obtained from Table 53.

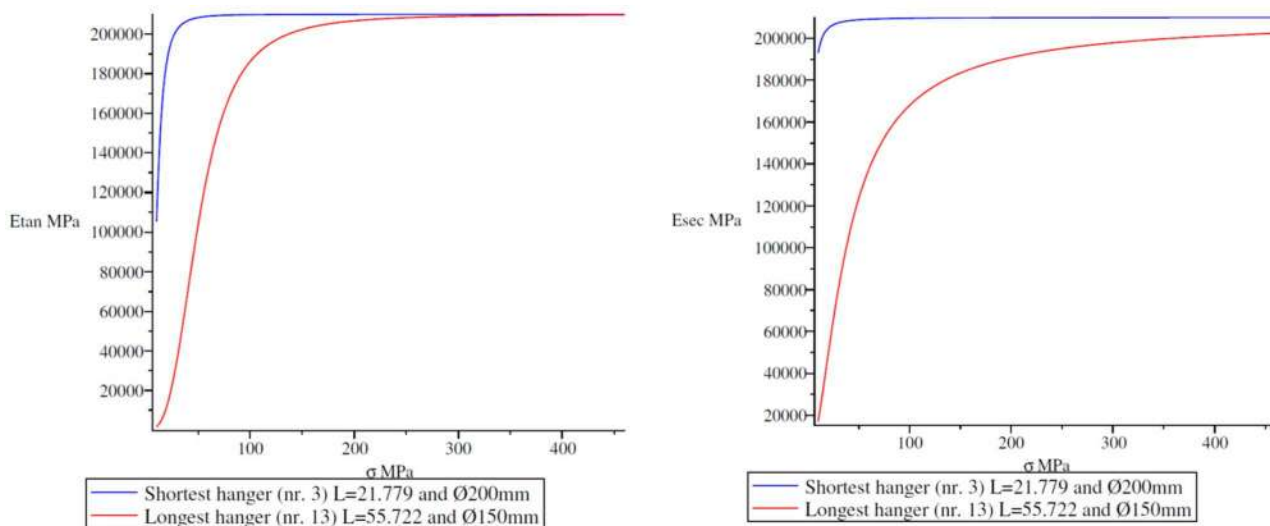


**Figure 139: Fictitious E-modulus as a function of the hanger stress, left: tangential modulus, right: secant modulus**

From figure 139 follows that the short and steep hangers are hardly affected by the catenary effect. The longer and more slanting hangers on the other hand, are seriously affected. For large stresses the fictitious modulus of elasticity yields to the unreduced value of 210 GPa.

### ***Investigating influence of catenary effect***

To evaluate the influence of the catenary effect, the fictitious secant modulus should be used to obtain accurate results. To determine this secant modulus, two stress levels have to be known in advance ( $\sigma_1$  and  $\sigma_2$ ). Finally the hanger forces obtained by the unreduced stiffness are compared to the reduced hanger forces of the secant modulus of elasticity. Through the following steps this reduced force distribution can be determined:

#### ***Step 1: Determine $\sigma_1$***

From the permanent loading situation  $\sigma_1$  can be obtained. Because all hangers are supported during the assembly of the hangers, the catenary effect does not influence the hanger forces in the permanent loading situation.

#### ***Step 2: Determine $\sigma_2$ by using tangent modulus of elasticity***

To determine  $\sigma_2$  some intermediate steps are required. First the ULS hanger forces with an unreduced stiffness are determined. Based on these hanger stresses, the tangent modulus of elasticity is calculated. The tangential stiffness is now implemented in the SCIA model, and the ULS hanger forces are calculated again. In these ULS hanger forces the catenary effect is included. This force distribution is now used to determine  $\sigma_2$ , and thereby the secant modulus of elasticity. By implementing the secant modulus of elasticity into the SCIA model, the hanger forces based on the secant modulus of elasticity can now be calculated. This force distribution is assumed to be the force distribution in which the catenary effect is incorporated.

#### ***Step 3: Comparing the unreduced hanger forces to the catenary hanger forces***

In Table 54, the deviation between the unreduced and catenary hanger forces in the ULS and SLS are calculated. By dividing the reduced force by the catenary force, a percentage is determined to indicate the deviation.

In table 53, the steps 1 and 2 are performed. In table 54, step 3 is performed.

**General parameters**

Hangertype	Steel rod hanger	
Self-weight steel [ $\rho$ ]	78.5	kN/m <sup>3</sup>
E-modulus;initial [E]	210	GPa

Hanger nr.	Hanger length		Properties			Force distribution		Force distribution		Tangential stiffness		Force distribution		Secant stiffness		Force distribution	
	L [m]	Lx [m]	$\emptyset$ [mm]	A [mm <sup>2</sup> ]	$\rho$ [kN/m]	Dead load		ULS (no wind)		Etan/E		ULS (no wind)		Esec/E		(no wind)	
						N;E=210	$\sigma$ ;E=210	N;E=210	$\sigma$ ;E=210	E;tan	%;tan	N;E=Etan	$\sigma$ ;E=Etan	E;sec	%;sec	N;E;sec;ULS	N;E;sec;SLS
1	Removed	-	-	-	-	-	-	-	-	-	-	-	-	-	-	-	-
2	Removed	-	-	-	-	-	-	-	-	-	-	-	-	-	-	-	-
3	21.779	3.034	200	31416	2.466	1580	50	4112	131	210	100	4157	132	209.6	100	4144	2484
4	27.860	5.329	150	17671	1.387	877	50	2211	125	210	100	2254	128	208.6	99	2267	1368
5	33.376	8.103	150	17671	1.387	1052	60	2632	149	210	100	2635	149	208.0	99	2641	1596
6	38.326	11.254	150	17671	1.387	1164	66	2869	162	209	100	2869	162	207.2	99	2862	1734
7	42.710	14.677	150	17671	1.387	1185	67	2866	162	209	99	2870	162	205.4	98	2898	1762
8	46.515	18.265	150	17671	1.387	1157	65	2782	157	208	99	2786	158	202.4	96	2745	1670
9	49.719	21.904	150	17671	1.387	1126	64	2727	154	207	99	2732	155	198.4	94	2749	1671
10	52.292	25.474	150	17671	1.387	1151	65	2818	159	206	98	2820	160	195.8	93	2879	1750
11	54.191	28.848	150	17671	1.387	1177	67	2911	165	206	98	2908	165	193.3	92	2857	1735
12	55.359	31.886	150	17671	1.387	1181	67	2972	168	205	98	2976	168	190.6	91	2942	1785
13	55.722	34.434	150	17671	1.387	1194	68	3048	172	205	98	3091	175	189.0	90	3042	1844
14	55.182	36.319	150	17671	1.387	1209	68	3056	173	204	97	3002	170	186.6	89	3096	1880
15	53.614	37.341	150	17671	1.387	1177	67	2906	164	203	97	2897	164	183.3	87	2877	1753
16	50.855	37.267	150	17671	1.387	1043	59	2555	145	200	95	2591	147	174.2	83	2681	1636
17	46.690	35.813	200	31416	2.466	1500	48	3577	114	192	91	3538	113	151.8	72	3449	2115
18	40.836	32.633	200	31416	2.466	1265	40	2947	94	184	88	2932	93	136.1	65	2799	1726
19	32.917	27.291	200	31416	2.466	1509	48	3496	111	198	94	3490	111	171.5	82	3488	2153
20	22.472	19.276	220	38013	2.984	3443	91	8010	211	209	100	8040	212	206.6	98	8155	5022
21	Removed	-	-	-	-	-	-	-	-	-	-	-	-	-	-	-	-

Median values																	
46.602	26.383					1179	65	2909	158					195	93	2878	1752

**Table 53: Calculation of force distribution with catenary effect included (step 1 and 2)**

Hanger nr.	Force distribution		Force distribution		Deviation	
	Fictitious E-modulus		E-modulus = 210 Gpa		N;E;sec / N	
	N;E;sec;ULS	N;E;sec;SLS	N;ULS	N;SLS	%	%
1	Removed	-	-	-	-	-
2	Removed	-	-	-	-	-
3	4144	2484	4112	2464	100.8	100.8
4	2267	1368	2211	1333	102.5	102.6
5	2641	1596	2632	1590	100.3	100.4
6	2862	1734	2869	1738	99.8	99.8
7	2898	1762	2866	1742	101.1	101.1
8	2745	1670	2782	1693	98.7	98.6
9	2749	1671	2727	1658	100.8	100.8
10	2879	1750	2818	1713	102.2	102.2
11	2857	1735	2911	1768	98.1	98.1
12	2942	1785	2972	1803	99.0	99.0
13	3042	1844	3048	1847	99.8	99.8
14	3096	1880	3056	1856	101.3	101.3
15	2877	1753	2906	1770	99.0	99.0
16	2681	1636	2555	1558	104.9	105.0
17	3449	2115	3577	2193	96.4	96.4
18	2799	1726	2947	1818	95.0	94.9
19	3488	2153	3496	2158	99.8	99.8
20	8155	5022	8010	4933	101.8	101.8
21	Removed	-	-	-	-	-

Median values					
2878	1752	2909	1769	100	100

**Table 54: Comparison of the results to evaluate the differences between an equivalent E-modulus and a standard E-modulus for steel**

### **Conclusion**

From Table 54 follows that the majority of the hangers is hardly affected by the sag effect. Only the long and more slanting hangers 16-18 show a deviation in axial force around 5%. This corresponds to the notion about the catenary effect made by Geißler et al. [7]: the force distribution in long and slanting hangers could be affected by the catenary effect.

In the Eurocode for tensile elements NEN-EN 1993-1-11 [23], it is recommended for massive rod hangers to use the standard stiffness and recommends for other hanger types (e.g. locked coil, spiral strand) to use the secant modulus of elasticity.

When a more detailed analysis is performed the ‘catenary’ effect could become relevant. For instance when a cable system was applied as hangers and a protocol for the tensioning of the hangers must be developed.

# ANNEX F: ANALYTICAL MODEL OF HANGER NUMBER 13

*Force distribution hanger nr. 13 in plane of the arch (self-weight loading)*

*Differential equation for the shear force equilibrium of an axially tensioned Euler-Bernoulli beam*

$$DE1 := -EI \cdot (\text{diff}(w(x), x, x, x, x)) + H \cdot (\text{diff}(w(x), x, x)) = -q;$$

$$-EI \left( \frac{d^4}{dx^4} w(x) \right) + H \left( \frac{d^2}{dx^2} w(x) \right) = -q \quad (1)$$

SOL := dsolve(DE1, w(x)); assign(SOL) :

$$w(x) = \frac{C2 \cdot EI \cdot e^{\frac{\sqrt{H} \cdot x}{\sqrt{EI}}}}{H} + \frac{C1 \cdot EI \cdot e^{-\frac{\sqrt{H} \cdot x}{\sqrt{EI}}}}{H} - \frac{1}{2} \cdot \frac{q \cdot x^2}{H} + C3 \cdot x + C4 \quad (2)$$

$$W := \frac{C1 \cdot EI}{H} \cdot \exp\left(\frac{\sqrt{H} \cdot x}{\sqrt{EI}}\right) + C2 \cdot \frac{C1 \cdot EI}{H} \cdot \exp\left(\frac{-\sqrt{H} \cdot x}{\sqrt{EI}}\right) - \frac{1}{2} \cdot \frac{q \cdot x^2}{H} + C3 \cdot x + C4 :$$

*Boundary conditions for hinged-hinged beam*

$$BC1 := \text{simplify}(\text{subs}(x=0, W)) = 0 ;$$

$$BC2 := \text{simplify}(\text{subs}(x=l, W)) = 0 ;$$

$$BC3 := \text{simplify}(\text{subs}(x=0, \text{diff}(W, x, x))) = 0 ;$$

$$BC4 := \text{simplify}(\text{subs}(x=l, \text{diff}(W, x, x))) = 0 ;$$

$$SOL1 := \text{solve}(\{BC1, BC2, BC3, BC4\}, \{C1, C2, C3, C4\}) : \text{assign}(SOL1) ;$$

*Structural properties of hanger number 13*

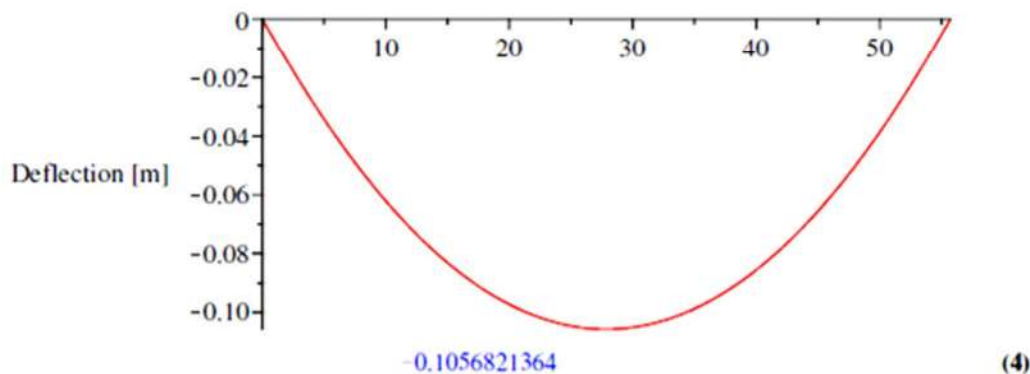
$$d := 0.15 : A := 0.25 \cdot \pi \cdot d^2 : EI := 2.1 \cdot 10^8 \cdot \frac{\pi \cdot d^4}{64} : q := -A \cdot 78.5 \cdot \cos\left(\frac{52 \cdot \pi}{180}\right) : l := 55.722 : H := 3123 ;$$

*Internal force and stress distribution*

$$M := -EI \cdot (\text{diff}(W, x, x)) : V := -EI \cdot (\text{diff}(W, x, x, x)) : \sigma := \text{abs}\left(\frac{M \cdot 10^6}{\frac{\pi \cdot d^3}{32} \cdot 10^9}\right) + \frac{H \cdot 10^3}{A \cdot 10^6} ; \quad (3)$$

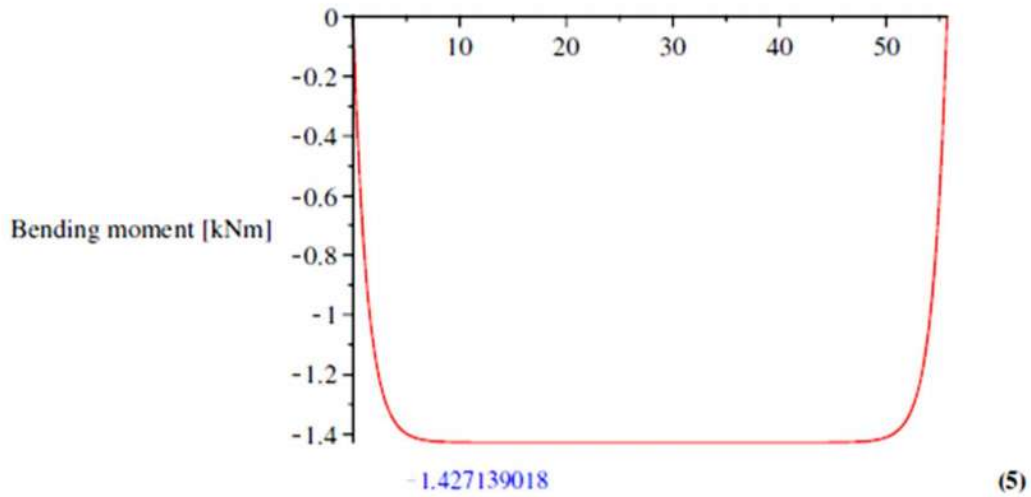
*Deflection*

plot(W, x=0..l, labels=["", "Deflection [m]"]); evalf(subs(x=0.5 \cdot l, W))



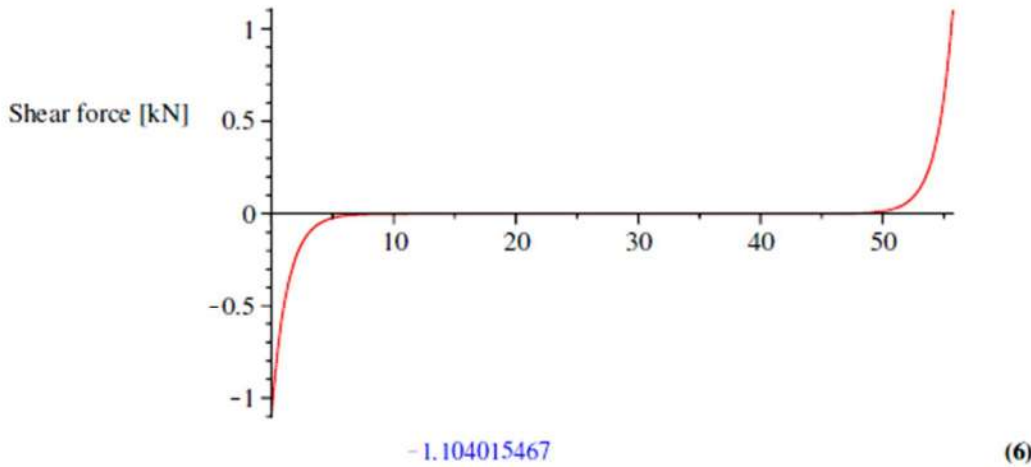
**Bending moment distribution**

`plot(M, x = 0..l, labels = ["", "Bending moment [kNm]"]); evalf(subs(x = 0.5 * l, M));`



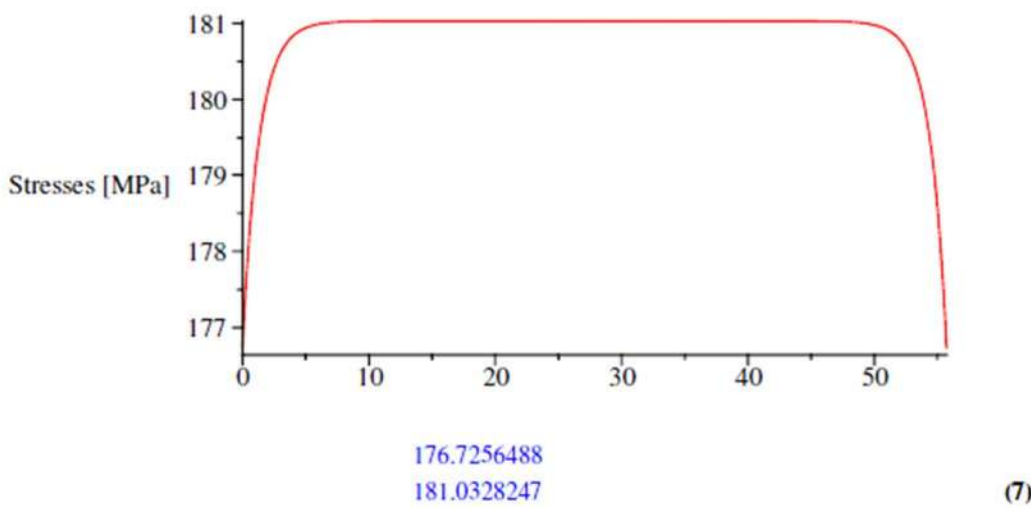
**Shear force distribution**

`plot(V, x = 0..l, labels = ["", "Shear force [kN]"]); evalf(subs(x = 0, V));`



**Stress distribution (axial force and bending moment)**

`plot(σ, x = 0..l, labels = ["", "Stresses [MPa]"]); evalf(subs(x = 0, σ)); evalf(subs(x = 0.5 * l, σ));`



**Force distribution hanger nr. 13 out of arch plane (wind loading)**

**Differential equation for the shear force equilibrium of an axially tensioned Euler-Bernoulli beam**

$$DE1 := -EI \cdot (\text{diff}(w(x), x, x, x, x)) + H \cdot (\text{diff}(w(x), x, x)) = -q;$$

$$-EI \left( \frac{d^4}{dx^4} w(x) \right) + H \left( \frac{d^2}{dx^2} w(x) \right) = -q \quad (1)$$

SOL := dsolve(DE1, w(x)); assign(SOL) :

$$w(x) = \frac{C2 \cdot EI \cdot e^{\frac{\sqrt{H} \cdot x}{\sqrt{EI}}}}{H} + \frac{C1 \cdot EI \cdot e^{-\frac{\sqrt{H} \cdot x}{\sqrt{EI}}}}{H} - \frac{1}{2} \cdot \frac{q \cdot x^2}{H} + C3 \cdot x + C4$$

$$W := \frac{C1 \cdot EI}{H} \cdot \exp\left(\frac{\sqrt{H} \cdot x}{\sqrt{EI}}\right) + C2 \cdot \frac{C1 \cdot EI}{H} \cdot \exp\left(-\frac{\sqrt{H} \cdot x}{\sqrt{EI}}\right) - \frac{1}{2} \cdot \frac{q \cdot x^2}{H} + C3 \cdot x + C4;$$

**Boundary conditions for fixed-fixed beam**

BC1 := simplify(subs(x=0, W)) = 0 ;  
 BC2 := simplify(subs(x=l, W)) = 0 ;  
 BC3 := simplify(subs(x=0, diff(W, x))) = 0 ;  
 BC4 := simplify(subs(x=l, diff(W, x))) = 0 ;  
 SOL1 := solve({BC1, BC2, BC3, BC4}, {C1, C2, C3, C4}) : assign(SOL1) ;

**Structural properties of hanger number 13**

d := 0.15 ; A := 0.25 \cdot \pi \cdot d^2 ; EI := 2.1 \cdot 10^8 \cdot \frac{\pi \cdot d^4}{64} ; q := -2.31 ; l := 55.722 ; H := 3123 ;

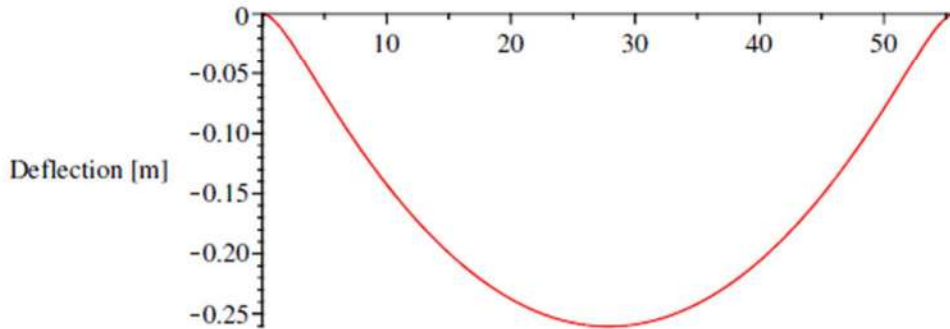
**Internal force and stress distribution**

$$M := -EI \cdot (\text{diff}(W, x, x)) ; V := -EI \cdot (\text{diff}(W, x, x, x)) ; \sigma := \text{abs}\left(\frac{M \cdot 10^6}{\frac{\pi \cdot d^3}{32} \cdot 10^9}\right) + \frac{H \cdot 10^3}{A \cdot 10^6} ;$$

(3)

**Deflection**

plot(W, x=0..l, labels=["", "Deflection [m]"]); evalf(subs(x=0.5 \cdot l, W))

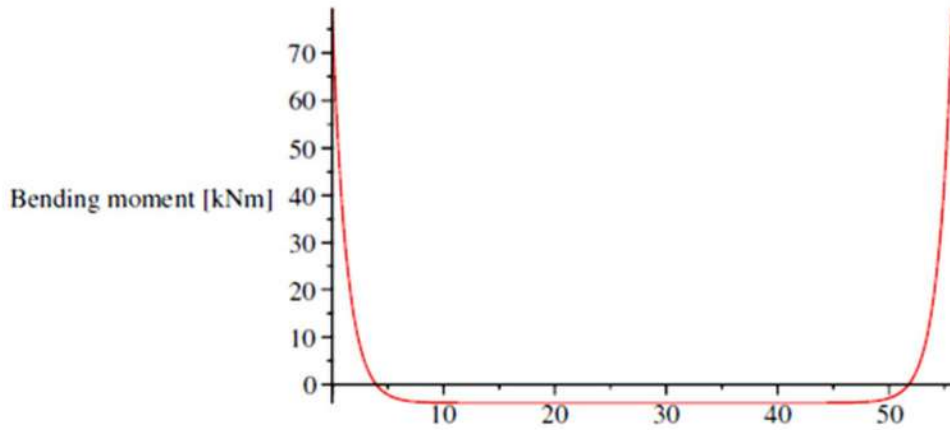


-0.2604406982

(4)

**Bending moment distribution**

`plot(M, x = 0..l, labels=["", "Bending moment [kNm]"]); evalf(subs(x = 0, M)); evalf(subs(x = 0.5 * l, M));`

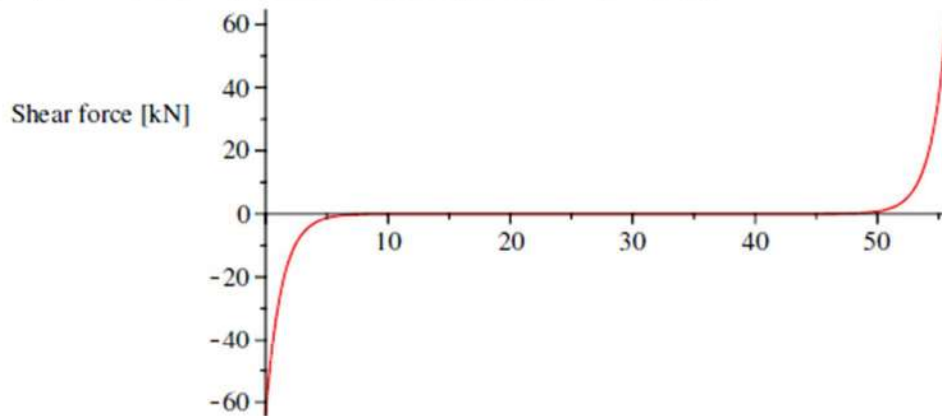


79.33543204  
-3.860061438

(5)

**Shear force distribution**

`plot(V, x = 0..l, labels=["", "Shear force [kN]"]); evalf(subs(x = 0, V));`

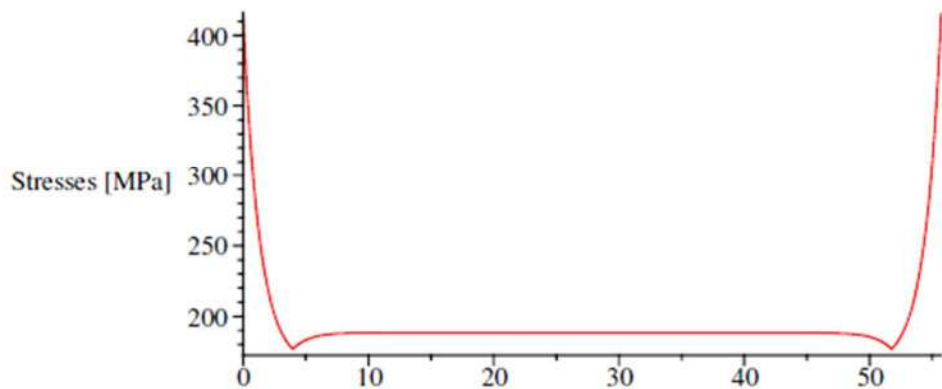


-64.35890995

(6)

**Stress distribution (axial force and bending moment)**

`plot( $\sigma$ , x = 0..l, labels=["", "Stresses [MPa]"]); evalf(subs(x = 0,  $\sigma$ )); evalf(subs(x = 0.5 * l,  $\sigma$ ));`



416.1638932  
188.3755045

(7)

### Force distribution hanger nr. 13 (wind loading + imposed rotation)

Differential equation for the shear force equilibrium of an axially tensioned Euler-Bernoulli beam

$$DE1 := -EI \cdot (\text{diff}(w(x), x, x, x, x)) + H \cdot (\text{diff}(w(x), x, x)) = -q;$$

$$-EI \left( \frac{d^4}{dx^4} w(x) \right) + H \left( \frac{d^2}{dx^2} w(x) \right) = -q \quad (1)$$

SOL := dsolve(DE1, w(x)); assign(SOL) :

$$w(x) = \frac{C2 \cdot EI \cdot e^{\frac{\sqrt{H} \cdot x}{\sqrt{EI}}}}{H} + \frac{C1 \cdot EI \cdot e^{-\frac{\sqrt{H} \cdot x}{\sqrt{EI}}}}{H} - \frac{1}{2} \frac{q \cdot x^2}{H} + C3 \cdot x + C4 \quad (2)$$

$$W := \frac{C1 \cdot EI}{H} \cdot \exp\left(\frac{\sqrt{H} \cdot x}{\sqrt{EI}}\right) + C2 \cdot \frac{C1 \cdot EI}{H} \cdot \exp\left(-\frac{\sqrt{H} \cdot x}{\sqrt{EI}}\right) - \frac{1}{2} \frac{q \cdot x^2}{H} + C3 \cdot x + C4 :$$

Boundary conditions for fixed beam with initial rotation [mrad]

BC1 := simplify(subs(x=0, W)) = 0 :

BC2 := simplify(subs(x=l, W)) = 0 :

BC3 := simplify(subs(x=0, diff(W, x))) = -0.0061 :

BC4 := simplify(subs(x=l, diff(W, x))) = 0.0061 :

SOL1 := solve({BC1, BC2, BC3, BC4}, {C1, C2, C3, C4}) : assign(SOL1) :

Structural properties of hanger number 13

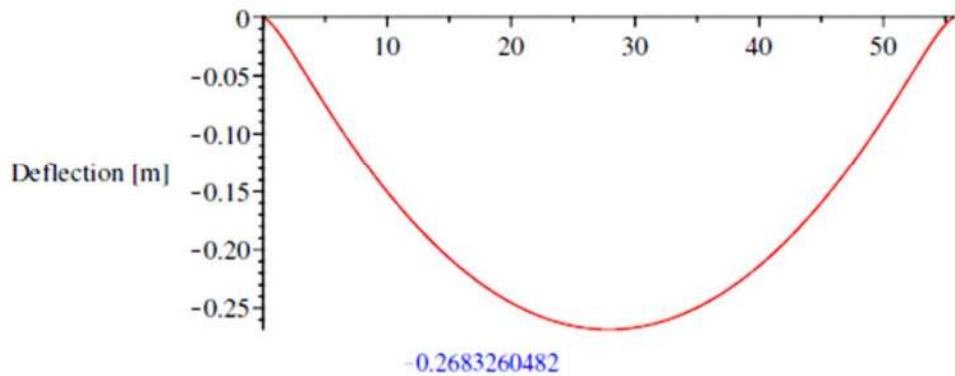
$$d := 0.15 : A := 0.25 \cdot \pi \cdot d^2 : EI := 2.1 \cdot 10^8 \cdot \frac{\pi \cdot d^4}{64} : q := -2.31 : l := 55.722 : H := 3123 :$$

Internal force and stress distribution

$$M := -EI \cdot (\text{diff}(W, x, x)) : V := -EI \cdot (\text{diff}(W, x, x, x)) : \sigma := \text{abs}\left(\frac{M \cdot 10^6}{\frac{\pi \cdot d^3}{32} \cdot 10^9}\right) + \frac{H \cdot 10^3}{A \cdot 10^6} : \quad (3)$$

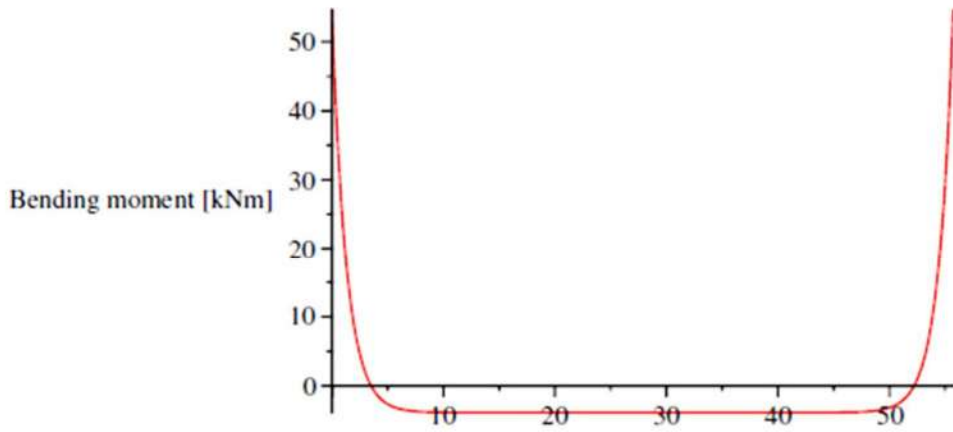
Deflection

plot(W, x=0..l, labels=["", "Deflection [m]"]); evalf(subs(x=0.5 \cdot l, W))



**Bending moment distribution**

`plot(M, x = 0..l, labels = ["", "Bending moment [kNm]"]); evalf(subs(x = 0, M)); evalf(subs(x = 0.5 * l, M));`

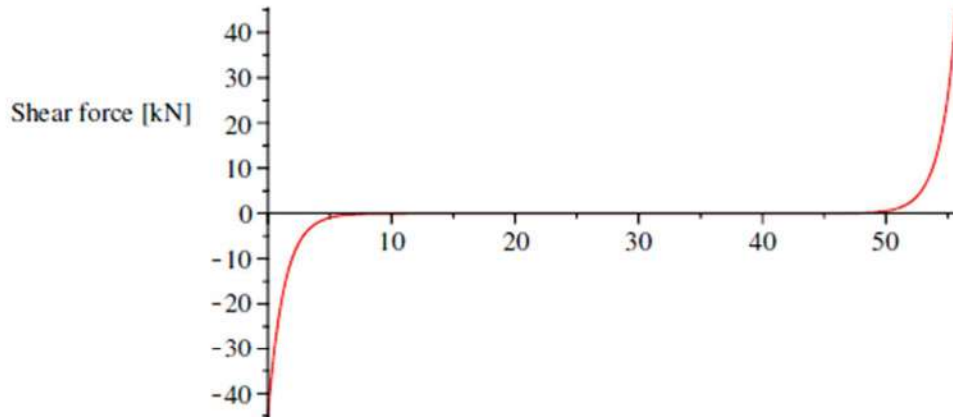


54.70948504  
-3.860061460

(5)

**Shear force distribution**

`plot(V, x = 0..l, labels = ["", "Shear force [kN]"]); evalf(subs(x = 0, V));`

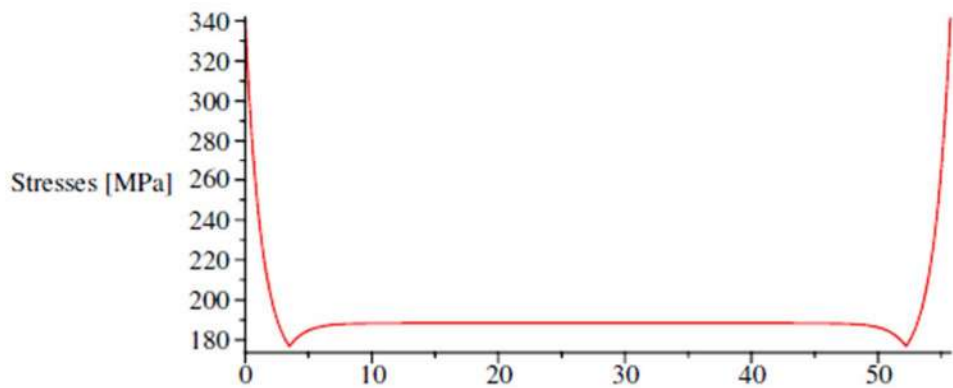


-45.30861002

(6)

**Stress distribution (axial force and bending moment)**

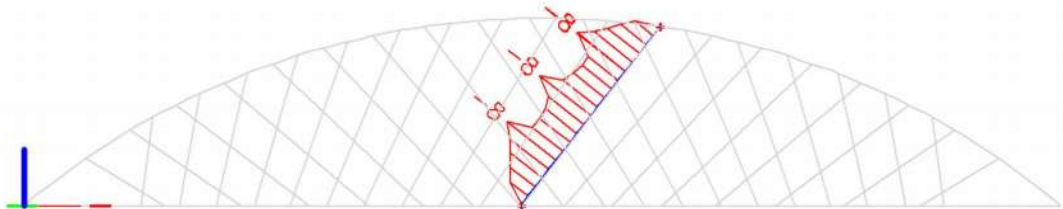
`plot(σ, x = 0..l, labels = ["", "Stresses [MPa]"]); evalf(subs(x = 0, σ)); evalf(subs(x = 0.5 * l, σ));`



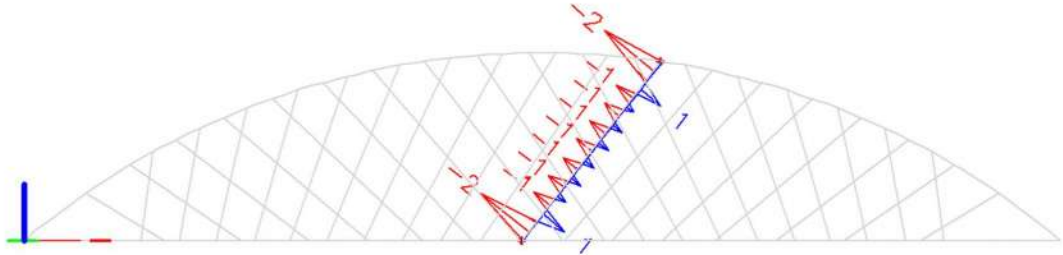
341.8415712  
188.3755046

(7)

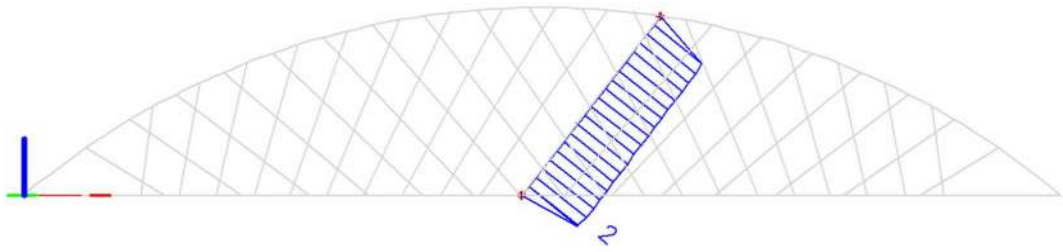
# ANNEX G: INFLUENCE OF MESH REFINEMENT ON INTERNAL HANGER FORCES



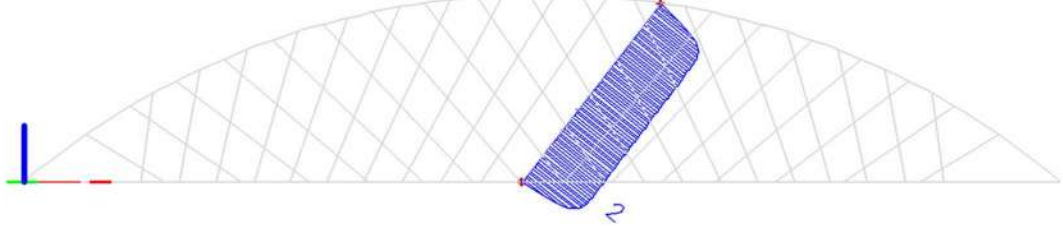
Mesh 4



Mesh 10

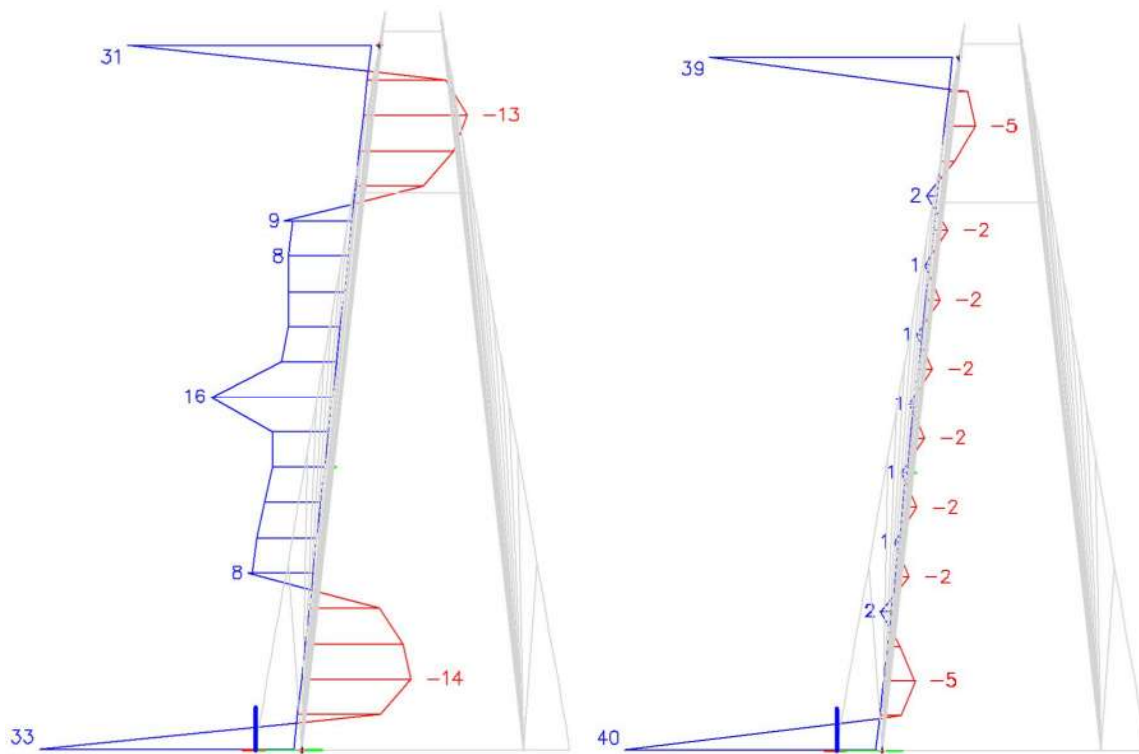


Mesh 20



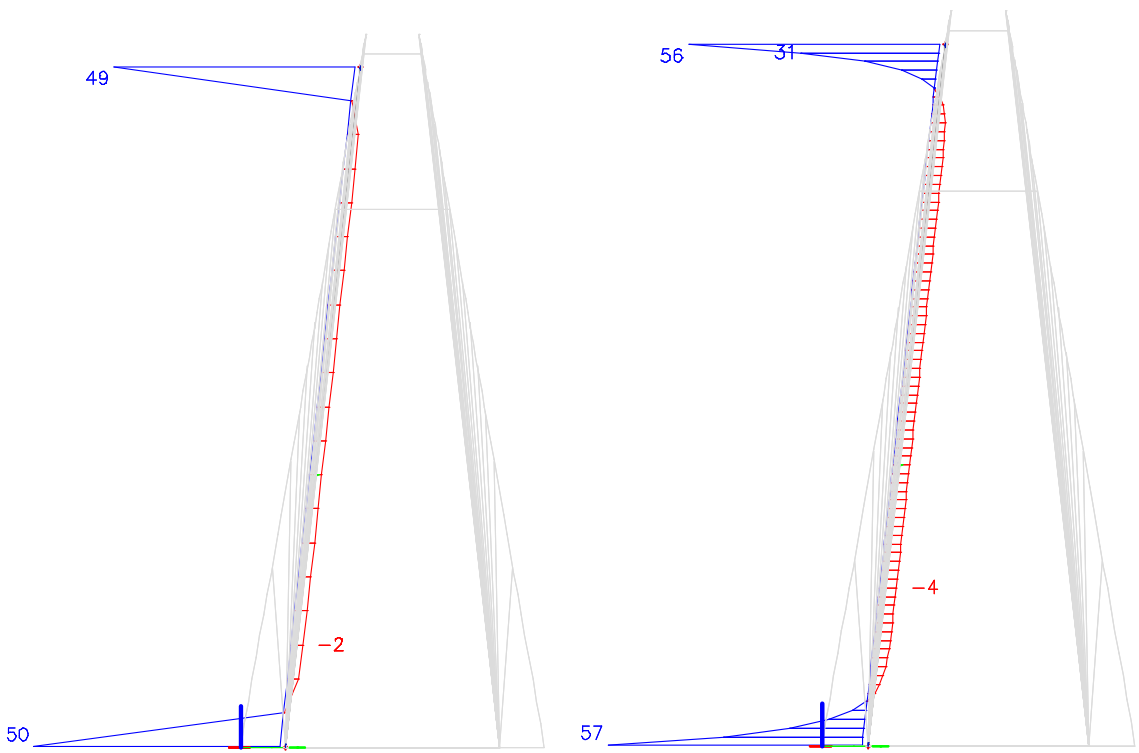
Mesh 80

Figure 138: Moment distribution  $M_y$  [kNm] due to self-weight, in longest hanger (number 13) for mesh sizes 4, 10, 20 and 80.



Mesh 4

Mesh 10



Mesh 20

Mesh 80

**Figure 139: Moment distribution  $M_z$  [kNm] due to wind loading, in longest hanger (number 13) for mesh sizes 4, 10, 20 and 80.**

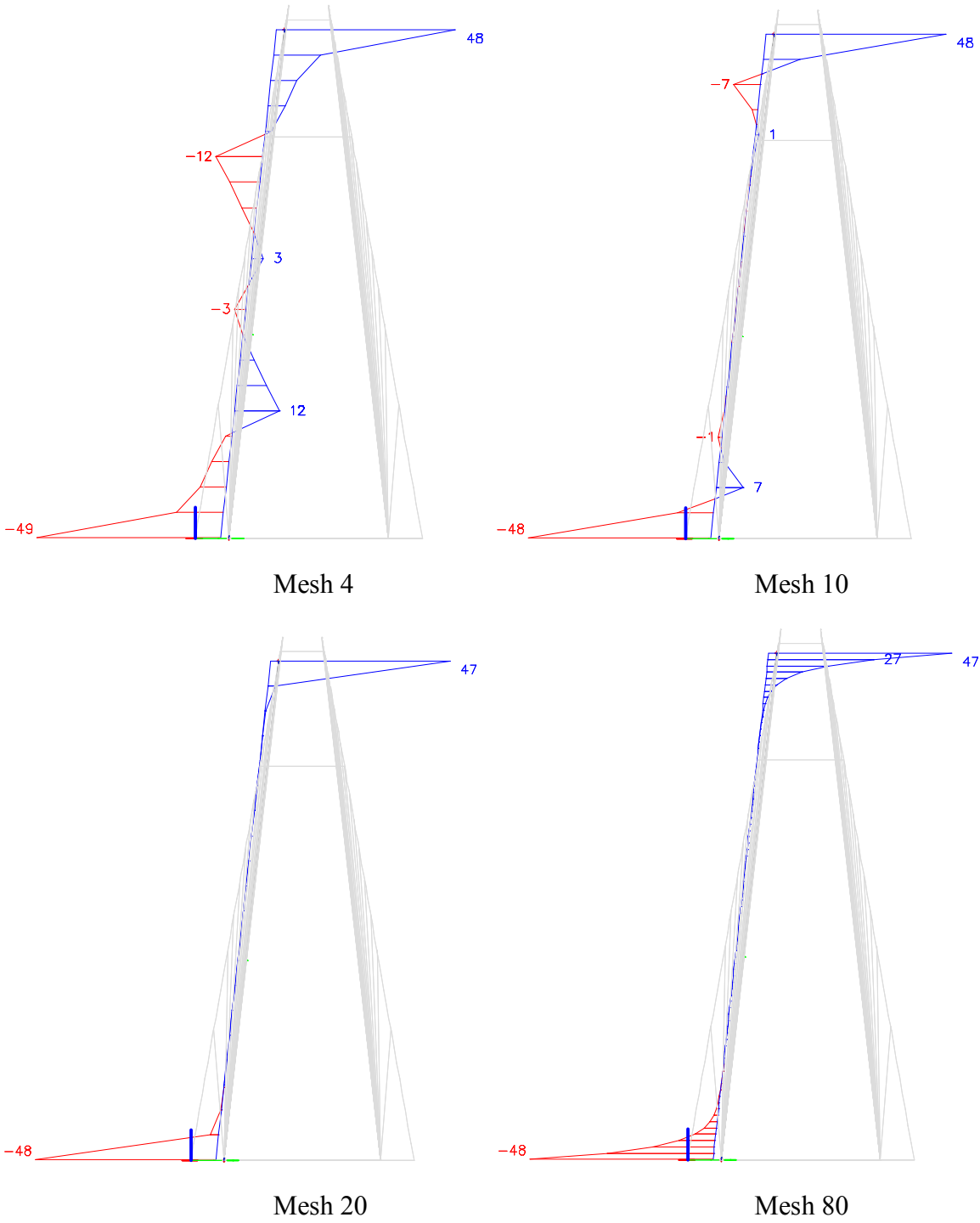
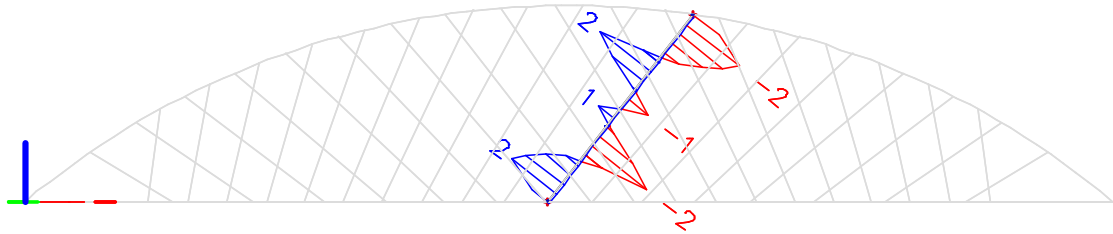
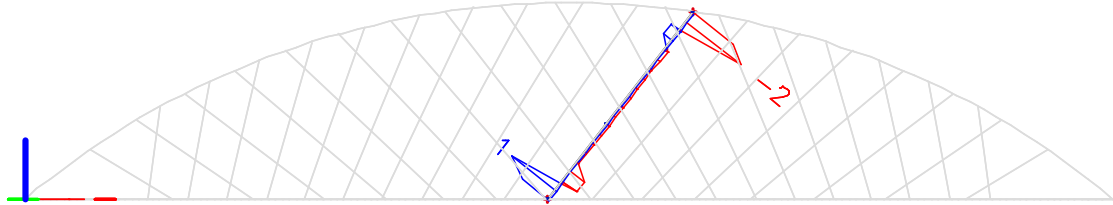


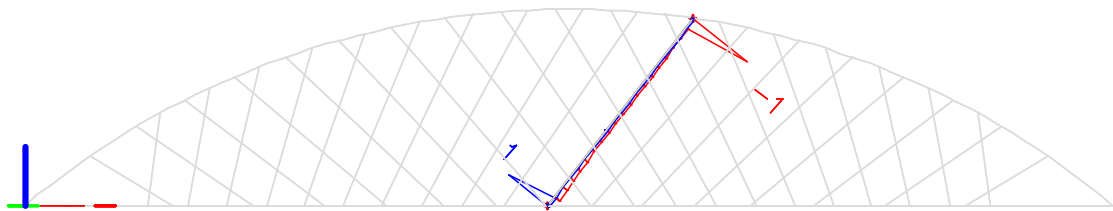
**Figure 140: Shear force distribution  $V_y$  [kN] due to wind loading, in longest hanger (number 13) for mesh sizes 4, 10, 20 and 80.**



Mesh 4



Mesh 10



Mesh 20

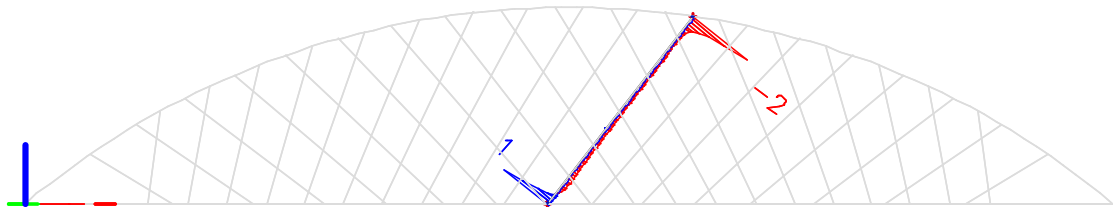


Figure 141: Shear force distribution  $V_z$  [kN] due to wind loading, in longest hanger (number 13) for mesh sizes 4, 10, 20 and 80.

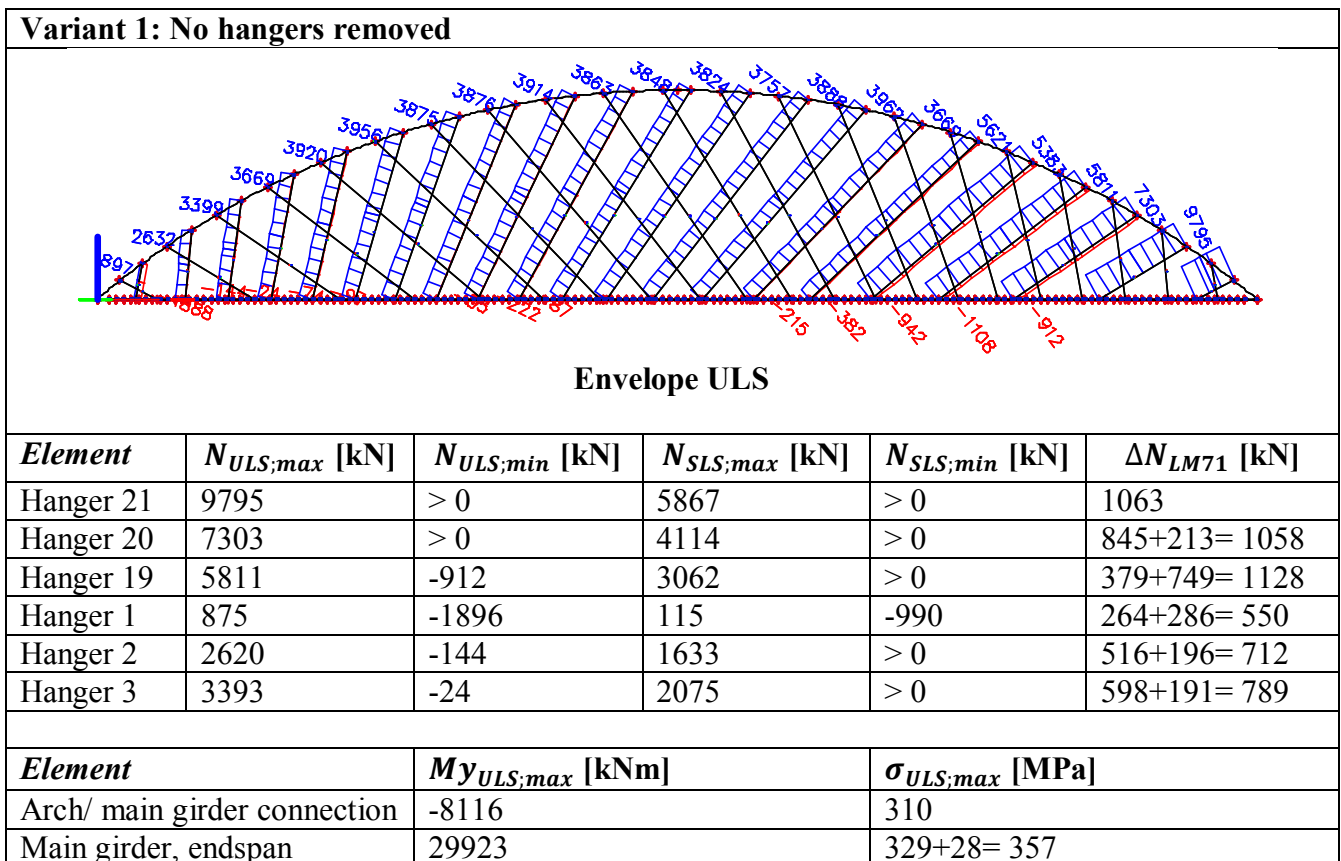
Mesh 80

# ANNEX H: VARIANT STUDY OUTER HANGERS

In this annex the effects of the outer hangers on the overall force distribution are investigated. 9 variants have been composed where different outer hangers have been removed.

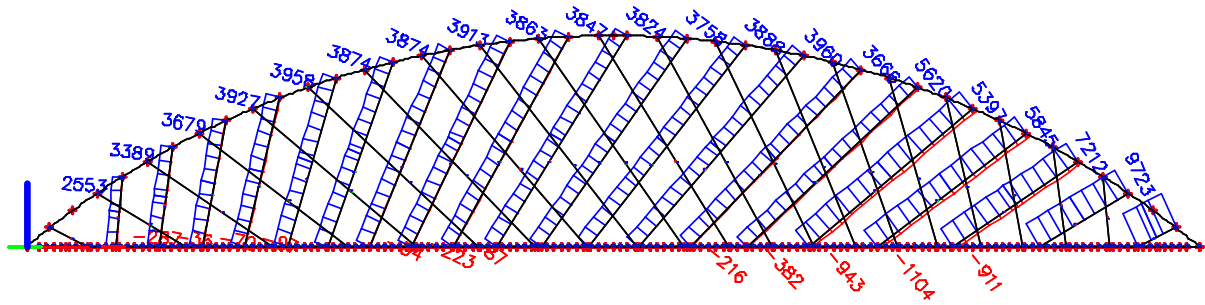
## Boundary conditions for the evaluation of the hanger forces:

Arch cross-section: 2300x3400x41x38  
 Main girder cross-section: 3500x1800x35x35  
 Hanger diameter: Ø150mm (hangers 1 to 16)  
 Ø200mm (hangers 17 to 21)  
 Load case: Maximal hanger forces → mobile load (LC7) ULS/SLS  
 Force amplitude ( $\Delta N_{LM71}$ ) → Mobile load case  
 Maximal stresses → Envelope ULS  
 Maximal bending moment → Envelope ULS



The additional stress due to the transverse bending moment at the endspan ( $\sigma_{Mdeck}$ ), can be approximated at  $\frac{140000 \cdot 10^6}{13.8 \cdot 0.3661 \cdot 10^9} = 28 \text{ MPa}$ . See paragraph 4.3.2 and 4.4.2 for more information.

**Variant 2: Hanger number 1 removed**

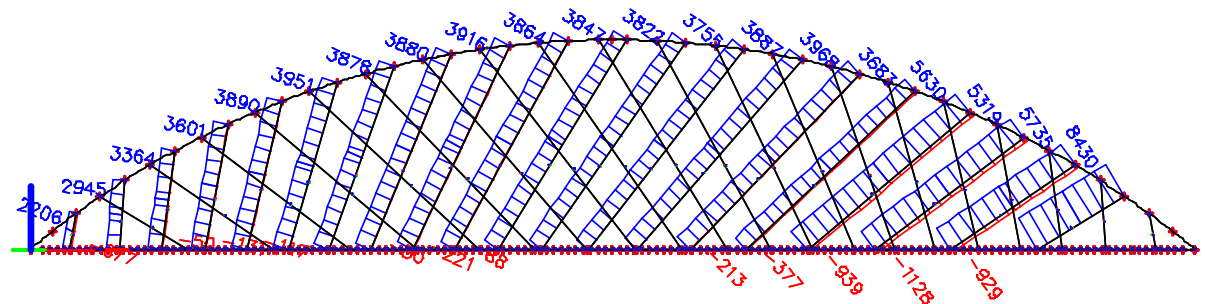


**Envelope ULS**

<i>Element</i>	$N_{ULS,max}$ [kN]	$N_{ULS,min}$ [kN]	$N_{SLS,max}$ [kN]	$N_{SLS,min}$ [kN]	$\Delta N_{LM71}$ [kN]
Hanger 21	9723	> 0	5717	> 0	1054
Hanger 20	7212	> 0	4019	> 0	816+186= 1002
Hanger 19	5845	-911	3110	> 0	756+383= 1139
Hanger 2	2537	-70	1630	> 0	557+246= 803
Hanger 3	3382	-36	2071	> 0	597+194= 791
Hanger 4	3675	-70	2214	> 0	628+199= 827

<i>Element</i>	$M_{y_{ULS,max}}$ [kNm]	$\sigma_{ULS,max}$ [MPa]
Arch/ main girder connection	-7714	319
Main girder, endspan	30198	329+28= 357

**Variant 3: Hanger number 21 removed**

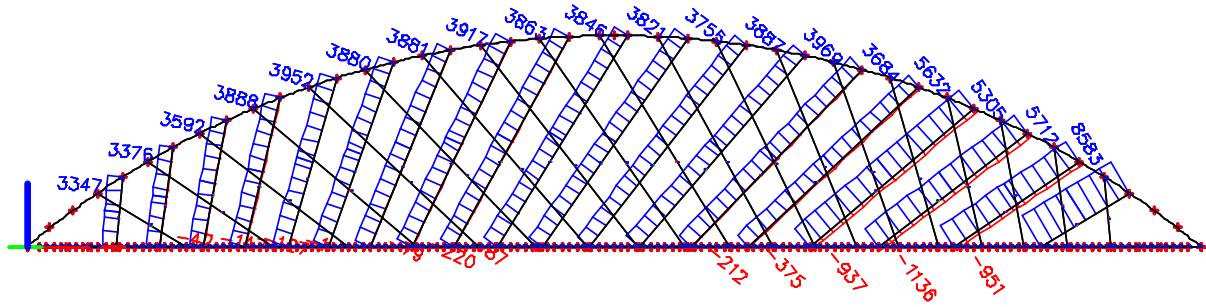


**Envelope ULS**

<i>Element</i>	$N_{ULS,max}$ [kN]	$N_{ULS,min}$ [kN]	$N_{SLS,max}$ [kN]	$N_{SLS,min}$ [kN]	$\Delta N_{LM71}$ [kN]
Hanger 20	8430	> 0	4790	> 0	950+189= 1139
Hanger 19	5735	-929	3041	> 0	742+382= 1124
Hanger 18	5319	-1128	2795	> 0	718+399= 1117
Hanger 1	2183	-677	1008	> 0	314+110= 424
Hanger 2	2932	> 0	1871	> 0	536+155= 691
Hanger 3	3358	-50	2051	> 0	596+194= 790

<i>Element</i>	$M_{y_{ULS,max}}$ [kNm]	$\sigma_{ULS,max}$ [MPa]
Arch/ main girder connection	-20355	351
Main girder, endspan	32781	333+28= 361

**Variant 4: Hanger number 1, 21 removed**

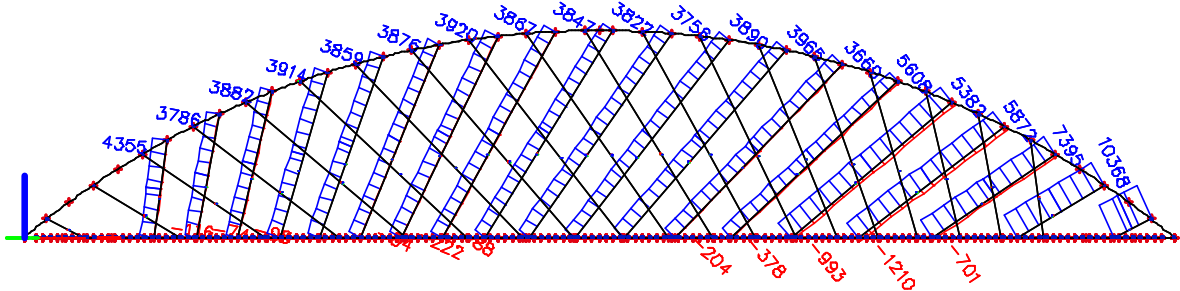


**Envelope ULS**

<i>Element</i>	$N_{ULS,max}$ [kN]	$N_{ULS,min}$ [kN]	$N_{SLS,max}$ [kN]	$N_{SLS,min}$ [kN]	$\Delta N_{LM71}$ [kN]
Hanger 20	8583	> 0	4820	> 0	936+143= 1079
Hanger 19	5712	-951	3037	> 0	745+390= 1135
Hanger 18	5305	-1136	2792	> 0	719+402= 1121
Hanger 2	3329	> 0	2092	> 0	600+175= 775
Hanger 3	3370	-42	2063	> 0	599+195= 794
Hanger 4	3588	-147	2149	> 0	621+207= 828

<i>Element</i>	$M_{y_{ULS,max}}$ [kNm]	$\sigma_{ULS,max}$ [MPa]
Arch/ main girder connection	-22004	353
Main girder, endspan	34297	336+28= 364

**Variant 5: Hanger number 1, 2 removed**

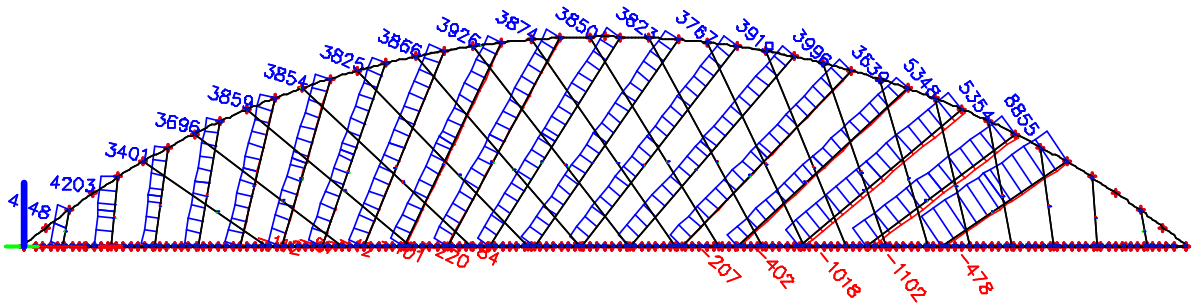


**Envelope ULS**

<i>Element</i>	$N_{ULS,max}$ [kN]	$N_{ULS,min}$ [kN]	$N_{SLS,max}$ [kN]	$N_{SLS,min}$ [kN]	$\Delta N_{LM71}$ [kN]
Hanger 21	10368	> 0	6134	> 0	1170
Hanger 20	7395	> 0	4132	> 0	798+84= 882
Hanger 19	5872	-701	3125	> 0	729+325= 1054
Hanger 3	4342	-116	2685	> 0	800+280= 1080
Hanger 4	3781	-74	2281	> 0	648+207= 855
Hanger 5	3579	-98	2245	> 0	629+179= 808

<i>Element</i>	$M_{y_{ULS,max}}$ [kNm]	$\sigma_{ULS,max}$ [MPa]
Arch/ main girder connection	-10598	313
Main girder, endspan	37917	342+28= 370

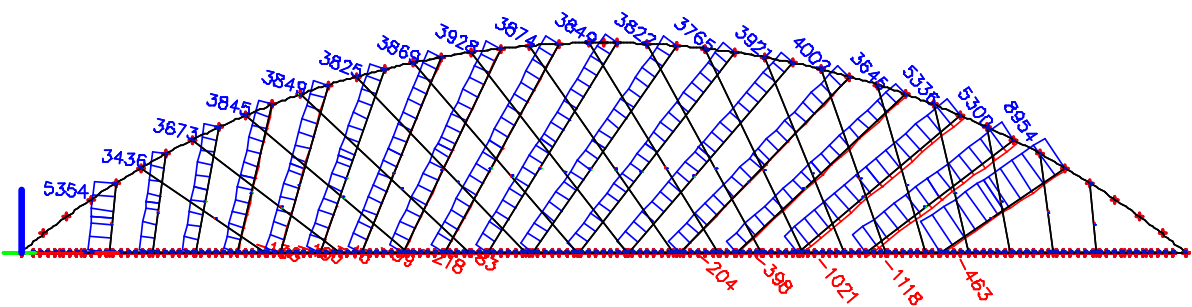
**Variant 6: Hanger number 20, 21 removed**



**Envelope ULS**

<i>Element</i>	$N_{ULS,max}$ [kN]	$N_{ULS,min}$ [kN]	$N_{SLS,max}$ [kN]	$N_{SLS,min}$ [kN]	$\Delta N_{LM71}$ [kN]
Hanger 19	8855	-478	4835	> 0	1058+409= 1467
Hanger 18	5354	-1102	2823	> 0	720+399= 1119
Hanger 17	5348	-1018	2939	> 0	770+407= 1177
Hanger 1	4130	> 0	2061	> 0	423
Hanger 2	4195	> 0	2588	> 0	581+37= 618
Hanger 3	3395	> 0	2100	> 0	599+179= 778
<b>Element</b>					
	$My_{ULS,max}$ [kNm]		$\sigma_{ULS,max}$ [MPa]		
Arch/ main girder connection	-27815		384		
Main girder, endspan	34341		351+28= 379		

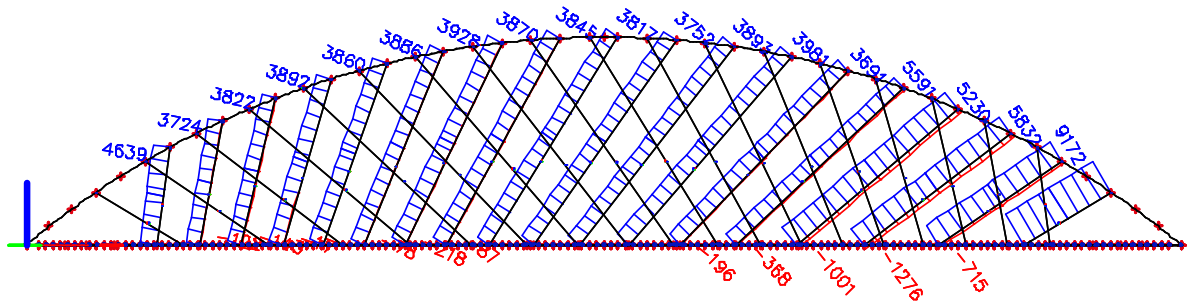
**Variant 7: Hanger number 1, 20, 21 removed**



**Envelope ULS**

<i>Element</i>	$N_{ULS,max}$ [kN]	$N_{ULS,min}$ [kN]	$N_{SLS,max}$ [kN]	$N_{SLS,min}$ [kN]	$\Delta N_{LM71}$ [kN]
Hanger 19	8954	-463	4877	> 0	1063+401= 1464
Hanger 18	5300	-1118	2797	> 0	718+403= 1121
Hanger 17	5336	-1021	2934	> 0	770+408= 1178
Hanger 2	5340	> 0	3153	> 0	639+31= 670
Hanger 3	3430	> 0	2134	> 0	604+176= 780
Hanger 4	3670	> 0	2231	> 0	629+189= 818
<b>Element</b>					
	$My_{ULS,max}$ [kNm]		$\sigma_{ULS,max}$ [MPa]		
Arch/ main girder connection	34348		391		
Main girder, endspan	33468		348+28= 376		

**Variant 8: Hanger number 1, 2, 21 removed**

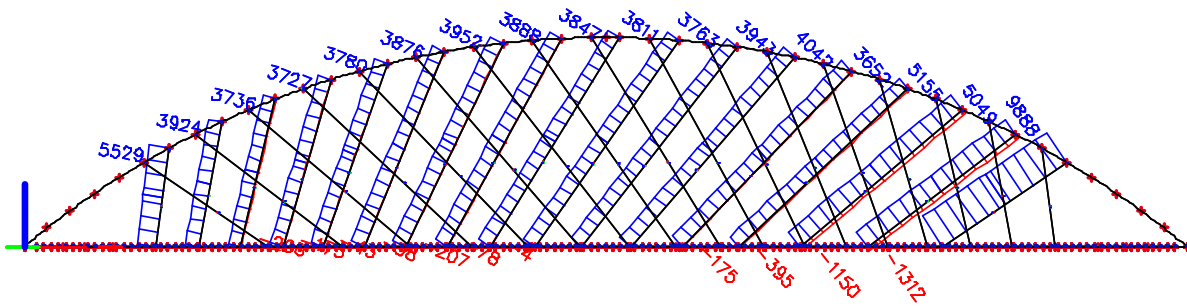


**Envelope ULS**

<i>Element</i>	$N_{ULS,max}$ [kN]	$N_{ULS,min}$ [kN]	$N_{SLS,max}$ [kN]	$N_{SLS,min}$ [kN]	$\Delta N_{LM71}$ [kN]
Hanger 20	9172	> 0	5172	> 0	962+31= 993
Hanger 19	5832	-715	3104	> 0	726+328= 1054
Hanger 18	5230	-1276	2750	> 0	728+435= 1163
Hanger 3	4626	> 0	2900	> 0	827+256= 1083
Hanger 4	3720	-123	2237	> 0	643+242= 885
Hanger 5	3820	-143	2201	> 0	624+174= 798

<i>Element</i>	$My_{ULS,max}$ [kNm]	$\sigma_{ULS,max}$ [MPa]
Arch/ main girder connection	-28547	362
Main girder, endspan	47306	369+28= 397

**Variant 9: Hanger number 1, 2, 20, 21 removed**



**Envelope ULS**

<i>Element</i>	$N_{ULS,max}$ [kN]	$N_{ULS,min}$ [kN]	$N_{SLS,max}$ [kN]	$N_{SLS,min}$ [kN]	$\Delta N_{LM71}$ [kN]
Hanger 19	9888	> 0	5392	> 0	1086+255= 1341
Hanger 18	5049	-1312	2656	> 0	713+443= 1156
Hanger 17	5155	-1150	2831	> 0	766+434= 1200
Hanger 3	5517	> 0	3528	> 0	879+148= 1027
Hanger 4	3920	> 0	2412	> 0	662+184= 846
Hanger 5	3724	-200	2145	> 0	620+175= 795

<i>Element</i>	$My_{ULS,max}$ [kNm]	$\sigma_{ULS,max}$ [MPa]
Arch/ main girder connection	-49391	420
Main girder, endspan	42319	366+28= 394

# ANNEX I: FATIGUE PROPERTIES

## I.1 Decisive hanger for fatigue verification

In this paragraph an attempt is made to determine the hanger which is affected most by fatigue, based on reasoning and by making assumptions. After the fatigue verification of the decisive hanger is performed, the assumptions are verified.

The following loads should be considered for the fatigue verification:

- Traffic loading
- Vortex induced vibrations
- Rain and wind induced vibrations

Common wind loading is not considered as problematic for the fatigue life of the hangers, because in the reviewed literature this effect was never mentioned as problematic.

### *Traffic loading*

Due to traffic loading, stresses are caused by two different phenomena:

- Stresses from axial forces
- Stresses from bending moments due to deflection of the main girder

### *Axial forces*

The stresses due to axial forces are obtained by making use of a mobile load case for both tracks. Because not all hangers have the same diameter, the stress amplitude should be calculated in order to compare the hangers.

### *Bending moments due to rotation of the main girder*

To evaluate the impact of the deflected main girder on the total stresses in the hangers a simplification is made. It is assumed that the largest rotations will also lead to the largest bending moments in the hangers. In reality the amount of cable- or beam action and bending stiffness of the hangers play an important role in the magnitude of these stresses. However for the quick determination of the decisive hanger this assumption is accurate enough.

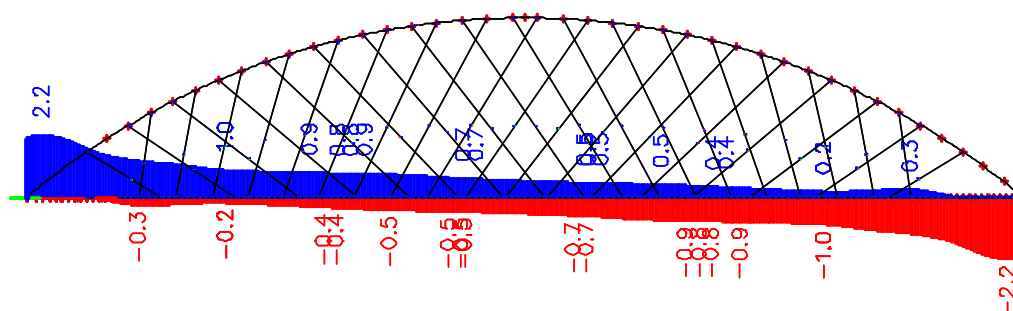


Figure 142: Maximal and minimal rotations of the main girder caused by mobile loading

### ***Vortex induced vibrations***

To evaluate the impact of vortex induced vibrations, the natural frequency plays an important role. In annex J, the natural frequencies of the hangers are determined and the in plane frequencies will be used.

It is assumed that long hangers with a low natural frequency are more susceptible for vortex induced vibrations. This is based on an article by Gauthier and Krontal [8] where they stated that because of the low natural frequency of long hangers, the fatigue performance is hard to validate.

### ***Rain and wind induced vibrations***

All hangers are susceptible for rain and wind induced vibrations (RWIV) according to the criteria given by DIN-FB103:

$$n_1 > 6,5 \text{ Hz}$$

$$D < 70 \text{ mm}$$

DIN-FB103 provides a factor through which the angle of the hanger is incorporated calculation. This angular factor (c-factor) can be determined with Figure 143. Because all hangers have to be verified for RWIV the angular factor is used to determine the decisive hanger.

High c-factors result in an unfavorable RWIV loading.

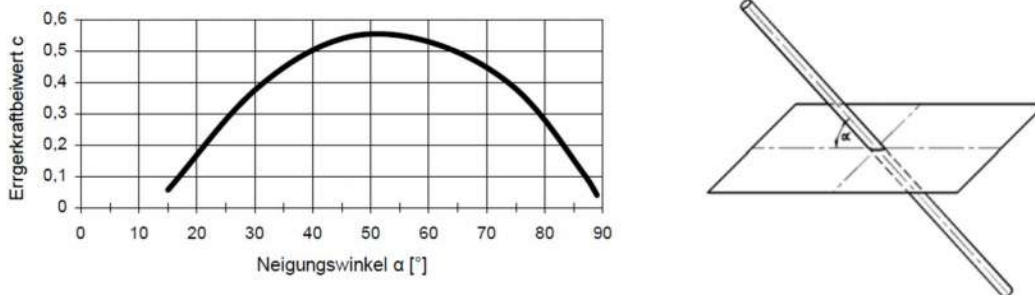


**Figure 143: Excitation force coefficient as a function of the angle**

### ***Conclusion***

In Table 55 an overview of the influential parameters is given, which were determined in previous paragraphs.

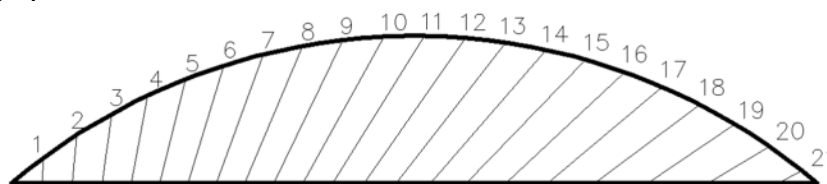


**Figure 144: Numbering of hangers**

Hanger nr.	Diameter Ø [mm]	Traffic			Vortex		Rain and wind	
		$\Delta N$ [kN]	$\Delta\sigma; N$ [MPa]	$\Delta\phi$ [mrad]	Lnet [m]	$n_1$ [Hz]	Angle [°]	c-factor
3	200	2088	66	1,6	18.879	2,38	82	0,2
4	150	1166	66	1,5	24.960	1,64	79	0,25
5	150	1189	67	1,2	30.476	1,46	76	0,3
6	150	1175	66	1,1	35.426	1,31	73	0,35
7	150	1209	68	1,2	39.810	1,17	70	0,45
8	150	1238	70	1,3	43.615	1,06	67	0,5
9	150	1257	71	1,2	46.819	0,97	64	0,5
10	150	1267	72	1,3	49.392	0,93	61	0,5
11	150	1296	73	1,2	51.291	0,90	58	0,55
12	150	1336	76	1,2	52.459	0,89	55	0,55
13	150	1387	78	1,2	52.822	0,89	52	0,55
14	150	1429	81	1,2	52.282	0,90	49	0,55
15	150	1437	81	1,2	50.714	0,91	46	0,55
16	150	1338	76	1,3	47.955	0,91	43	0,5
17	200	1976	63	1,3	43.790	0,92	40	0,5
18	200	1910	61	1,2	37.936	1,01	37	0,5
19	200	1715	55	1,1	30.017	1,37	34	0,4
20	220	1693	45	1,5	19.572	2,95	31	0,4

**Table 55: Overview of influence of different types of fatigue loading on all hangers**

It was concluded that hanger number 13 is most susceptible for fatigue because of the following arguments:

- Nearly maximum stress amplitudes due to traffic (49 MPa) and wind loading (166 MPa)
- Longest hanger (52,822m) and lowest natural frequency (0,89 Hz) therefore assumed to be most susceptible for the effects of vortex induced vibrations
- Highest c-factor (0,55), therefore high RWIV loading

If for all hangers a similar diameter was applied, the outer hangers would be more susceptible for fatigue damage caused by traffic loading. Because all hangers were dimensioned for a maximum design stress of 240 MPa the stress amplitudes in the outer hangers are relatively low.

Remark: this conclusion is based on the following assumptions:

- long hangers with a low natural frequency are damaged most by vortex induced vibrations
- The angle of the hanger has a large influence on the fatigue damage caused by rain and wind induced vibrations

## I.2 Fatigue resistance of hanger connection

The fatigue resistance of the hanger connection can be determined with the DIN-FB103, annex II-H. This annex describes the design and fatigue verification of steel rod hanger connections.

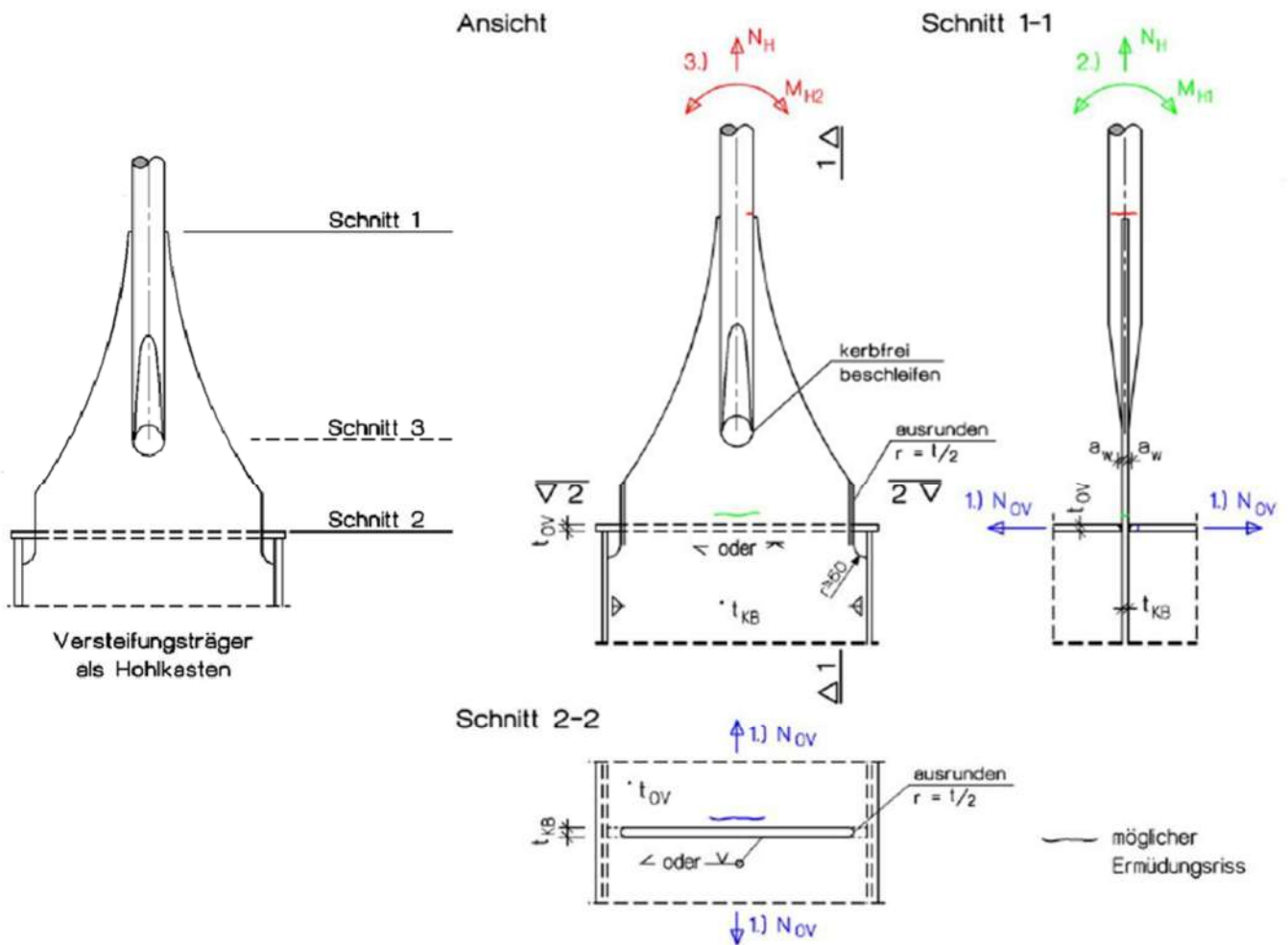


Figure 145: Hanger connection according to DIN-FB103, anhang II-H.

According to the designers guide to annex II-H [2] of the DIN-FB103 the following detail categories can be assigned to different sections (Schnitt 1 to 3) of the hanger connection. The designers guide refers to DIN-FB 103 for the determination of detail categories. These detail categories are linked to corresponding detail categories from NEN-EN 1993-1-9.

The geometry of the connection detail must be determined by the guidelines given in DIN-FB103. If the connection is fabricated according to Figure 145 and Figure 146, the detail categories are valid. Special attention must be paid to treatment of the welds and rounding of the edges.

**Section 1 (Schnitt 1)**

For bending around the strong axis of the hanger connection plate (Y-direction) and out of plane of the arch plane, section 1 is decisive. In Figure 146 a detailed drawing of the recommended hanger connection is given.

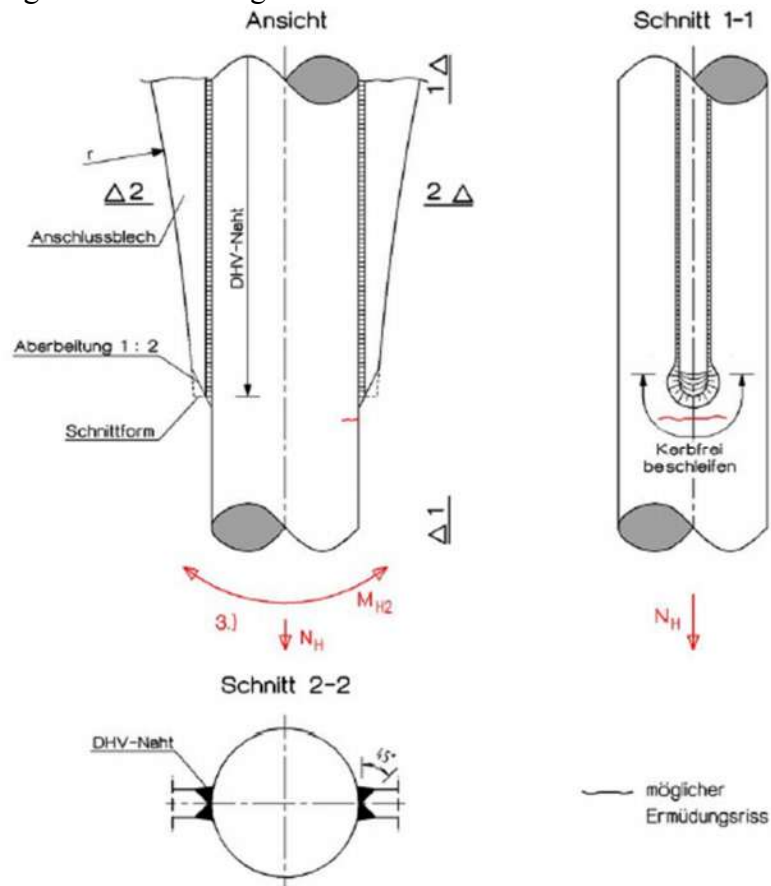


**Figure 146: Recommended connection detail between steel rod hanger and connection plate.**

According to DIN-FB103 the connection detail shown in Figure 146, corresponds to detail category 90. In figure 148 the detail category as defined in the DIN-FB103 is shown. According to [25], the detail category shown in figure 148 corresponds to the detail category shown in figure 149 which is obtained from the NEN-EN 1993-1-9. If the guidelines for the design of the hanger connections are applied correctly, the detail automatically fulfills the requirements for detail category 90.

Kerbfall	Konstruktionsdetail DIN-FB 103:2003, Tabelle II-L.3, Detail 2
90	$\frac{r}{w} \geq \frac{1}{3}$ oder $r > 150\text{mm}$
71	$\frac{1}{6} \leq \frac{r}{w} \leq \frac{1}{3}$
56	$\frac{r}{w} \leq \frac{1}{6}$

**Figure 147: Detail category for section 1 according to DIN-Fachbericht 103 (table II-L.3 detail 2)**

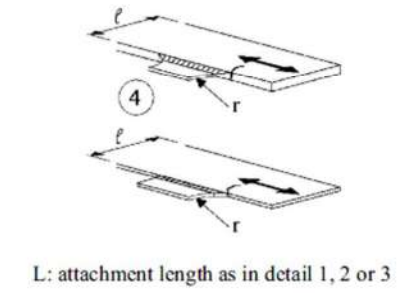
80	$r > 150\text{mm}$		3) Longitudinal fillet welded gusset with radius transition to plate or tube; end of fillet weld reinforced (full penetration); length of reinforced weld $> r$ .	<u>Details 3) and 4):</u> Smooth transition radius $r$ formed by initially machining or gas cutting the gusset plate before welding, then subsequently grinding the weld area parallel to the direction of the arrow so that the transverse weld toe is fully removed.
90	$\frac{r}{L} \geq \frac{1}{3}$ or $r > 150\text{mm}$	 L: attachment length as in detail 1, 2 or 3	4) Gusset plate, welded to the edge of a plate or beam flange.	
71	$\frac{1}{6} \leq \frac{r}{L} \leq \frac{1}{3}$			
50	$\frac{r}{L} < \frac{1}{6}$			

Figure 148: Detail category for section 1 according to NEN-EN 1993-1-9 (table 8.4 detail 4)

### Section 2 (Schnitt 2)

For bending around the weak axis of the hanger connection plate (Z-direction), and in plane of the arch, section 2 is decisive. The detail category corresponding to this specific section is determined by DIN-FB 103 as shown in figure 150. According to [25] the detail category determined by DIN-FB103 corresponds to the detail category shown in figure 151 which is obtained from the NEN-EN 1993-1-9. When a connection plate with a thickness larger than 25mm is applied, the size effect must be incorporated.

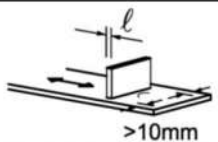
80	$t \leq 50$	
----	-------------	--

Figure 149: Detail category for section 2 according to DIN-FB 103 (table II-L.4 detail 3)

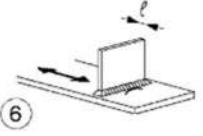
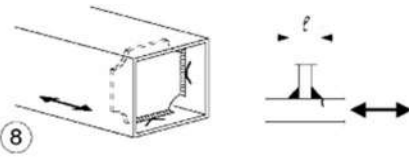
80	$t \leq 50\text{mm}$		<u>Transverse attachments:</u> 6) Welded to plate. 7) Vertical stiffeners welded to a beam or plate girder. 8) Diaphragm of box girders welded to the flange or the web. May not be possible for small hollow sections. The values are also valid for ring stiffeners.	<u>Details 6) and 7):</u> Ends of welds to be carefully ground to remove any undercut that may be present. 7) $\Delta\sigma$ to be calculated using principal stresses if the stiffener terminates in the web, see left side.
71	$50 < t \leq 80\text{mm}$			

Figure 150: Detail category for section 2 according to NEN-EN 1993-1-9 (table 8.4 detail 6)

**Section 3 (Schnitt 3)**

When the guidelines for the geometry of the hanger connection are not followed, section 3 could become decisive. In Figure 151 the detail category from DIN-FB 103 is shown that corresponds to section 3 according to [2]. According to [25] this detail category corresponds to the same detail category in the Eurocode, shown in Figure 152.

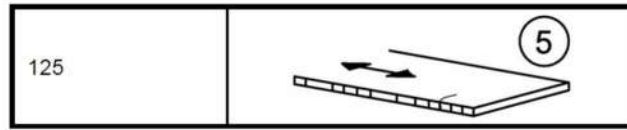


Figure 151: Detail category for section 3 according to DIN-FB 103 (table II-L.1 detail 5)

140		<p><u>Sheared or gas cut plates:</u></p> <p>4) Machine gas cut or sheared material with subsequent dressing.</p> <p>5) Material with machine gas cut edges having shallow and regular drag lines or manual gas cut material, subsequently dressed to remove all edge discontinuities.</p>	<p>4) All visible signs of edge discontinuities to be removed. The cut areas are to be machined or ground and all burrs to be removed.</p> <p>Any machinery scratches for example from grinding operations, can only be parallel to the stresses.</p>
125		<p>Machine gas cut with cut quality according to EN 1090.</p>	<p><u>Details 4) and 5):</u></p> <ul style="list-style-type: none"> <li>- Re-entrant corners to be improved by grinding (slope <math>\leq \frac{1}{4}</math>) or evaluated using the appropriate stress concentration factors.</li> <li>- No repair by weld refill.</li> </ul>

Figure 152: Detail category for section 3 according to NEN-EN 1993-1-9 (table 8.1 detail 5)

**Hanger-arch and hanger-main girder connection**

In Figure 145 the decisive section for axial force and bending moment in the main girder is shown. This detail is also used for the hanger-arch connection. The detail category that corresponds to the axial force ( $N_{OV}$ ) is shown in figure Figure 153. According to [25] this detail category corresponds to the same detail category in the Eurocode, shown in Figure 154. For a safe estimation, a detail category 45 is used.

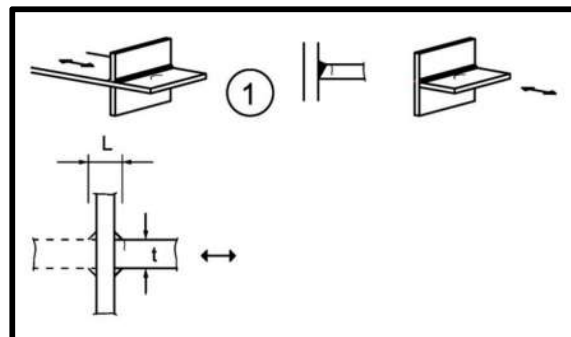


Figure 153: Detail category for arch/ main girder connection according to DIN-FB 103 (table II-L.5 detail 1)

Detail category	Constructional detail		Description	Requirements
80	$l < 50$ mm	all t [mm]	<p><u>Cruciform and Tee joints:</u></p> <p>1) Toe failure in full penetration butt welds and all partial penetration joints.</p>	<p>1) Inspected and found free from discontinuities and misalignments outside the tolerances of EN 1090.</p> <p>2) For computing <math>\Delta\sigma</math>, use modified nominal stress.</p> <p>3) In partial penetration joints two fatigue assessments are required. Firstly, root cracking evaluated according to stresses defined in section 5, using category 36* for <math>\Delta\sigma_w</math> and category 80 for <math>\Delta\tau_w</math>. Secondly, toe cracking is evaluated by determining <math>\Delta\sigma</math> in the load-carrying plate.</p>
71	$50 < l \leq 80$	all t		
63	$80 < l \leq 100$	all t		
56	$100 < l \leq 120$	all t		
56	$l > 120$	$t \leq 20$		
50	$120 < l \leq 200$	$t > 20$		
45	$200 < l \leq 300$	$t > 30$		
40	$l > 300$	$t > 50$		
As detail 1 in Table 8.5	flexible panel		2) Toe failure from edge of attachment to plate, with stress peaks at weld ends due to local plate deformations.	<p><u>Details 1) to 3):</u></p> <p>The misalignment of the load-carrying plates should not exceed 15 % of the thickness of the intermediate plate.</p>
36*			3) Root failure in partial penetration Tee-butt joints or fillet welded joint and effective full penetration in Tee-butt joint.	

Figure 154: Detail category for arch/ main girder connection according to NEN-EN 1993-1-9 (table 8.5 detail 1)

### I.3 Hanger connection according to guidelines DIN-Fachbericht 103

The steel rod hangers are welded through a connection plate to the main girder and arch. DIN-FB103 [2] provides a geometric description. Based on predefined stress levels corresponding to a specified steel grade, the diameter as well as the other dimensions of the hanger connection can be determined. In Figure 155 the geometrical description is given.

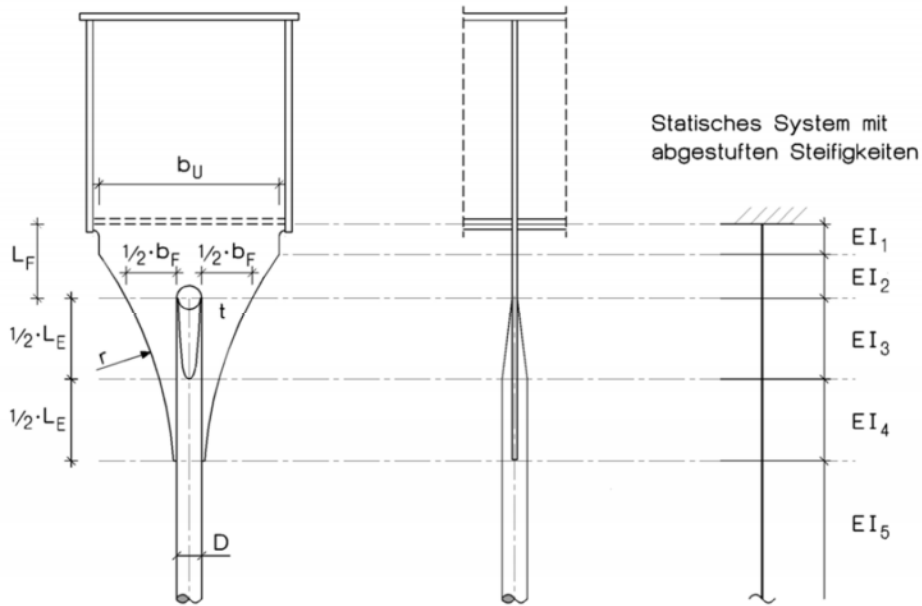


Figure 155: Recommended geometry and modeling of a welded hanger connection [2]

Where:

Hanger diameter ( $D$ ): 
$$D = 2 \cdot \sqrt{\frac{N_{max}}{\pi \cdot \sigma}}$$

Connection plate thickness ( $t$ ): 
$$t = 0,2 \cdot D$$

Width at location of hole ( $b_f$ ): 
$$b_f = \frac{N_{max}}{\sigma_{netto} \cdot t}$$

Embedment length ( $L_E$ ): 
$$L_E = \frac{N_{max}}{2 \cdot \tau \cdot t}$$

Connection plate width ( $b_u$ ): 
$$b_u = 1,5 \cdot (b_f + D)$$

Outer radius ( $r$ ): 
$$r = 1,9 \cdot \left( \frac{L_E^2}{b_f} + 0,25 \cdot b_f \right)$$

Free connection plate height ( $L_f$ ): 
$$L_f = 0,45 \cdot L_E$$

For steel grade S460 the following values for  $\sigma$ ,  $\sigma_{netto}$  and  $\tau$  are given:

$$\sigma = 240 \text{ N/mm}^2$$

$$\sigma_{netto} = 225 \text{ N/mm}^2$$

$$\tau = 80 \text{ N/mm}^2$$

For the modeling of the hanger connection, all hangers with a similar hanger diameter will be assigned with similar connection plates. In figure 157 a hanger connection is shown for a hanger of diameter 150mm, the following values were calculated.



Stiffness I-1 to I-3 can simply be modeled by a rectangular cross-section with similar dimensions.

$$I.4_y = \frac{1}{12} \cdot 0,03 \cdot \left( \frac{0,376+0,15}{2} - 0,15 \right)^3 + \frac{\pi \cdot 0,15^4}{64} = 6,19 \cdot 10^{-5} m^4$$

$$I.4_z = \frac{\pi \cdot 0,15^4}{64} = 2,49 \cdot 10^{-5} m^4 \quad (\text{Standard EI of hanger } \varnothing 150)$$

$$A.4 = 0,03 * \left( \frac{0,376+0,15}{2} - 0,15 \right) + \frac{\pi \cdot 0,15^2}{4} = 2,11 \cdot 10^{-2} m^2$$

Section I-4 is modeled as a cross type section, as shown in Figure 157. The stiffness in y- and z-direction is approached as exact as possible. Also the cross-sectional area is kept similar. This is done by iteration.

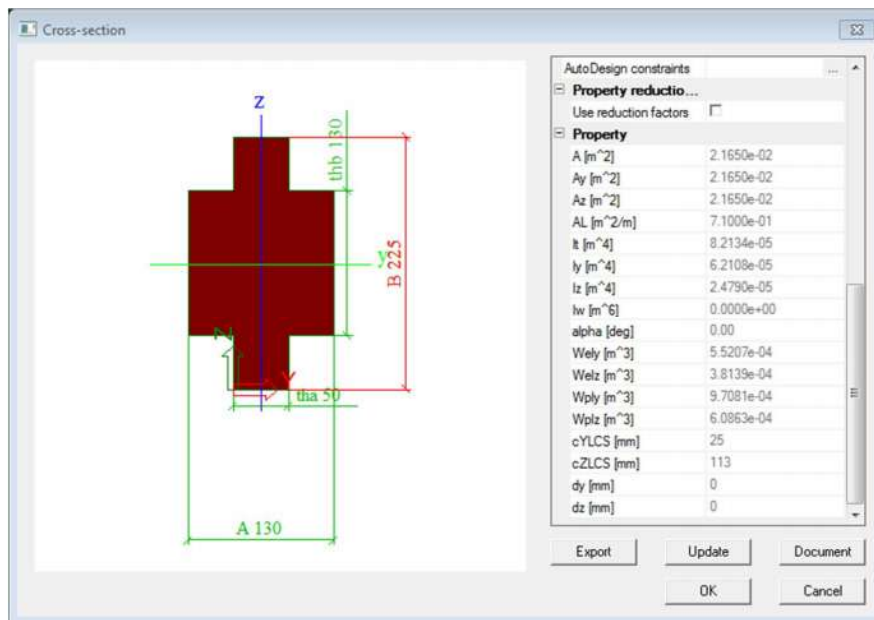


Figure 157: Cross section for the modeling of section 4

$$I.5_{y;z} = \frac{\pi \cdot 0,15^4}{64} = 2,49 \cdot 10^{-5} m^4$$

### ***Steel weight hanger connection and diaphragm***

The hanger connection plate is connected to the diaphragm. For the final comparison the steel weights are calculated. For each hanger an additional steel weight of two connections and the diaphragm for the arch and main girder must be taken into account.

### ***Steel weight connection***

The steel volume of the hanger connection is estimated as follows:

$$\text{Volume connection plate} = \left( \frac{1170}{2} \cdot (105 + 295 + 2 \cdot 445) \cdot 30 \right) = 0,022 \text{ m}^3$$

$$\text{Hanger connection } \varnothing 150: \quad 0,022 \text{ m}^3 \cdot 7850 \frac{\text{kg}}{\text{m}^3} \approx 180 \text{ kg}$$

By scaling the weight of the hanger connection by the quadratic ratio of the diameters a good estimation is obtained.

$$\text{Hanger connection } \varnothing 200: \quad \frac{200^2}{150^2} \cdot 180 \text{ kg} \approx 320 \text{ kg}$$

$$\text{Hanger connection } \varnothing 220: \quad \frac{220^2}{150^2} \cdot 180 \text{ kg} \approx 387 \text{ kg}$$

### ***Steel weight diaphragm***

The thickness of the connection plate/ diaphragm is determined as  $t = 0,2 \cdot D$

$$\text{Diaphragm arch } \quad \varnothing 150: \quad 2,3 \cdot 3,4 \cdot 0,03 \cdot 7,85 = 1,84 \text{ ton}$$

$$\text{Diaphragm main girder } \quad \varnothing 150: \quad 3,5 \cdot 1,8 \cdot 0,03 \cdot 7,85 = 1,48 \text{ ton}$$

$$\text{Diaphragm arch } \quad \varnothing 200: \quad 2,3 \cdot 3,4 \cdot 0,04 \cdot 7,85 = 2,46 \text{ ton}$$

$$\text{Diaphragm main girder } \quad \varnothing 200: \quad 3,5 \cdot 1,8 \cdot 0,04 \cdot 7,85 = 1,98 \text{ ton}$$

$$\text{Diaphragm arch } \quad \varnothing 220: \quad 2,3 \cdot 3,4 \cdot 0,044 \cdot 7,85 = 2,7 \text{ ton}$$

$$\text{Diaphragm main girder } \quad \varnothing 220: \quad 3,5 \cdot 1,8 \cdot 0,044 \cdot 7,85 = 2,18 \text{ ton}$$

### ***Conservation surface hanger connection***

To determine the total amount of conservation area, the paint surface of the connections must be taken into account.

$$\text{Surface connection plate } \varnothing 150 = 2 \cdot \left( \frac{1170}{2} \cdot (105 + 295 + 2 \cdot 445) \right) = 1,51 \text{ m}^2$$

$$\text{Surface connection plate } \varnothing 200 = \frac{200^2}{150^2} \cdot 1,51 = 2,68 \text{ m}^2$$

$$\text{Surface connection plate } \varnothing 220 = \frac{220^2}{150^2} \cdot 1,51 = 3,24 \text{ m}^2$$

# ANNEX J: NATURAL HANGER FREQUENCIES

In this annex the natural frequencies are calculated. The procedure to determine the natural frequencies of the hangers is obtained from ‘vibrations of continuous systems’ by Leissa and Qatu [26]. They give the general solution of the differential equation for an axially tensioned Euler-Bernoulli beam.

Differential equation:

$$EI \frac{\partial^4 w}{\partial x^4} + \rho A \frac{\partial^2 w}{\partial t^2} = T \frac{\partial^2 w}{\partial x^2}$$

General solution:

$$w(x) = C_1 \sin\left(\frac{\beta_1 \cdot x}{l}\right) + C_2 \cos\left(\frac{\beta_1 \cdot x}{l}\right) + C_3 \sinh\left(\frac{\beta_2 \cdot x}{l}\right) + C_4 \cosh\left(\frac{\beta_2 \cdot x}{l}\right)$$

$$\beta_{1,2} = \sqrt{\pm \frac{Tl^2}{2EI} + \sqrt{\left(\frac{Tl^2}{2EI}\right)^2 + \frac{\rho A \omega^2 l^4}{EI}}}$$

Boundary conditions for a hanger with hinged connections are:

$$w(x = 0 = l) = 0$$

$$\frac{d^2 w}{dx^2}(x = 0 = l) = 0$$

For fixed connections the boundary conditions are specified as:

$$w(x = 0 = l) = 0$$

$$\frac{dw}{dx}(x = 0 = l) = 0$$

The natural frequencies can be determined by solving the frequency equation. The frequency equation can be obtained by equating the determinant of the coefficient matrix to zero. The solutions of the frequency equation can be obtained more easily by plotting the graph and determining the solutions. In this annex the natural frequencies for the out of plane bending modes are determined by using MAPLE for hanger 3 and 13. The in plane bending frequencies are determined in table 58.

The length which is used to determine the natural frequencies is the internal length between the bottom flange of the arch and the upper flange of the main girder. This length is approximated by the following formula:

$$L_{net} = L_{system} - \frac{1}{2}h_{arch} - \frac{1}{2}h_{main\ girder}$$

In table 56 the natural frequencies are determined for the longest and shortest hanger for the in- and out of plane bending modes.

Modeling	$n_1$ [Hz]	$n_2$ [Hz]	$n_3$ [Hz]	$n_4$ [Hz]	$n_5$ [Hz]	$n_6$ [Hz]	$n_7$ [Hz]	$n_8$ [Hz]
Hanger nr. 3 fixed connections	3,46	8,42	15,44	24,66	36,13	-	-	-
Hanger nr. 3 hinged connections	2,38	6,18	12,02	20,05	30,34	-	-	-
Hanger nr. 13 fixed connections	0,96	1,97	3,06	4,26	5,61	7,11	8,80	10,67
Hanger nr. 13 hinged connections	0,89	1,81	2,81	3,93	5,17	6,58	8,15	9,91

Table 56: Natural frequencies of hanger number 3 and 13

***Simplified method for natural frequencies in plane of the arch (hinged connections)***

To determine the natural bending frequency in plane of the arch (hinged connections), the following formula can be used. This formula is derived from the differential equation mentioned above. For beams with hinged connections a correlation between buckling load and natural frequency exists. The bending frequency due to beam action ( $n_{i,EI}$ ) is increased with an amplification factor to incorporate the cable action in the total frequency.

$$f_i = f_{i,EI+T} = f_{i,EI} \cdot \sqrt{1 + \frac{T}{N_{crit,i}}}$$

The boundary conditions are implemented in the  $n_{i,EI}$  and  $N_{crit,i}$ . For a hanger with hinged connections, the following formulas are used to determine  $n_{i,EI}$  and  $N_{crit,i}$ .

$$n_{i,EI} = \frac{1}{2\pi} \left( \frac{i \cdot \pi}{l} \right)^2 \sqrt{\frac{EI}{\rho A}}$$

$$N_{crit,i} = \left( \frac{i \cdot \pi}{l} \right)^2 EI$$

In table 58 the natural frequencies of the in plane bending mode are determined for all hangers by using the formulas shown above.

***Natural frequencies of a cable***

To evaluate the effect of the amount of beam and cable action in the natural frequency of a hanger, also the natural frequencies of a cable are calculated. This is done with the following formula:

$$n_{i,T} = \frac{1}{2\pi} \left( \frac{i \cdot \pi}{l} \right) \sqrt{\frac{T}{\rho A}}$$

In table 57 the natural frequencies of the hangers, modeled as cables are determined.

Hanger nr.	Lsystem [m]	Lnet [m]	Diameter [mm]	$\mu$ [kg/m]	N;PERM [kN]	Natural cable frequencies				
						Mode 1	Mode 2	Mode 3	Mode 4	Mode 5
						n1 (EI) [Hz]	n2 (EI) [Hz]	n3 (EI) [Hz]	n4 (EI) [Hz]	n5 (EI) [Hz]
3	21,779	18,879	200	247	1530	2,09	4,17	6,26	8,34	10,43
4	27,860	24,960	150	139	852	1,57	3,14	4,71	6,28	7,85
5	33,376	30,476	150	139	1047	1,43	2,85	4,28	5,70	7,13
6	38,326	35,426	150	139	1158	1,29	2,58	3,87	5,16	6,45
7	42,710	39,810	150	139	1177	1,16	2,31	3,47	4,63	5,78
8	46,515	43,615	150	139	1151	1,04	2,09	3,13	4,18	5,22
9	49,719	46,819	150	139	1130	0,96	1,93	2,89	3,86	4,82
10	52,292	49,392	150	139	1154	0,92	1,85	2,77	3,69	4,62
11	54,191	51,291	150	139	1176	0,90	1,80	2,69	3,59	4,49
12	55,359	52,459	150	139	1184	0,88	1,76	2,64	3,52	4,40
13	55,722	52,822	150	139	1196	0,88	1,76	2,64	3,52	4,39
14	55,182	52,282	150	139	1200	0,89	1,78	2,67	3,56	4,45
15	53,614	50,714	150	139	1154	0,90	1,80	2,70	3,60	4,50
16	50,855	47,955	150	139	1030	0,90	1,80	2,70	3,59	4,49
17	46,690	43,790	200	247	1529	0,90	1,80	2,70	3,60	4,50
18	40,836	37,936	200	247	1346	0,97	1,95	2,92	3,89	4,87
19	32,917	30,017	200	247	1478	1,29	2,58	3,87	5,16	6,45
20	22,472	19,572	220	298	3364	2,71	5,42	8,14	10,85	13,56

Table 57: Natural of the hangers, modeled as cables

### Hanger number 3 with fixed connections

#### Determining out of plane natural frequencies of hanger number 3 (fixed-fixed)

restart :

$$w1 := C1 \cdot \sin\left(\frac{\beta1 \cdot x}{l}\right) + C2 \cdot \cos\left(\frac{\beta1 \cdot x}{l}\right) + C3 \cdot \sinh\left(\frac{\beta2 \cdot x}{l}\right) + C4 \cdot \cosh\left(\frac{\beta2 \cdot x}{l}\right) :$$

Boundary conditions

$$BC1 := \text{simplify}(\text{subs}(x=0, w1)) = 0 :$$

$$BC2 := \text{simplify}(\text{subs}(x=0, \text{diff}(w1, x))) = 0 :$$

$$BC7 := \text{simplify}(\text{subs}(x=l, w1)) = 0 :$$

$$BC8 := \text{simplify}(\text{subs}(x=l, \text{diff}(w1, x))) = 0 :$$

Obtaining frequency equation

with(LinearAlgebra) :

$$M1, F := \text{GenerateMatrix}(\{BC1, BC2, BC7, BC8\}, \{C1, C2, C3, C4\}) :$$

$$\text{Frequencyequation} := \text{simplify}(\text{Determinant}(M1)) :$$

$$\frac{-2 \beta1 \beta2 + 2 \beta1 \cos(\beta1) \cosh(\beta2) \beta2 + \sin(\beta1) \beta1^2 \sinh(\beta2) - \sin(\beta1) \beta2^2 \sinh(\beta2)}{l^2} \quad (1)$$

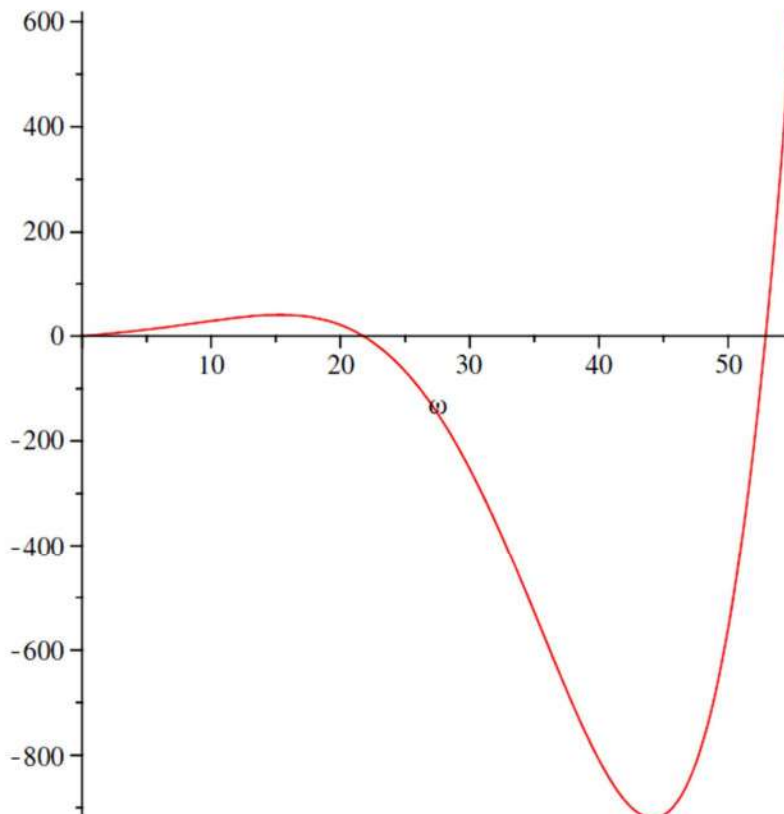
$$\beta1 := \left( -\frac{T \cdot l^2}{2 \cdot EI} + \left( \left( \frac{T \cdot l^2}{2 \cdot EI} \right)^2 + \frac{\rho A \cdot \omega^2 \cdot l^4}{EI} \right)^{0.5} \right)^{0.5} :$$

$$\beta2 := \left( \frac{T \cdot l^2}{2 \cdot EI} + \left( \left( \frac{T \cdot l^2}{2 \cdot EI} \right)^2 + \frac{\rho A \cdot \omega^2 \cdot l^4}{EI} \right)^{0.5} \right)^{0.5} :$$

Parameters hanger number 3

$$T := 1530000 : EI := \frac{2.1 \cdot 10^{11} \cdot \pi \cdot 0.200^4}{64} : \rho A := 0.25 \cdot \pi \cdot 0.200^2 \cdot 7850 : l := 18.879 :$$

with(plots) : plot(Frequencyequation, \omega = 0..55) :



Natural frequencies of hanger nr. 3 bending mode 1 to 5 (fixed-fixed connections)

$$\omega_1 := \text{fsolve}(\text{abs}(\text{Frequencyequation}), \omega = 0..25) : f_1 := \text{evalf}\left(\frac{\omega_1}{2 \cdot \pi}\right);$$

3.464934489

$$\omega_2 := \text{fsolve}(\text{abs}(\text{Frequencyequation}), \omega = 40..60) : \text{evalf}\left(\frac{\omega_2}{2 \cdot \pi}\right);$$

8.419778905

(3)

$$\omega_3 := \text{fsolve}(\text{abs}(\text{Frequencyequation}), \omega = 80..100) : \text{evalf}\left(\frac{\omega_3}{2 \cdot \pi}\right);$$

15.44275678

(4)

$$\omega_4 := \text{fsolve}(\text{abs}(\text{Frequencyequation}), \omega = 100..200) : \text{evalf}\left(\frac{\omega_4}{2 \cdot \pi}\right);$$

24.66351856

(5)

$$\omega_5 := \text{fsolve}(\text{abs}(\text{Frequencyequation}), \omega = 200..300) : \text{evalf}\left(\frac{\omega_5}{2 \cdot \pi}\right);$$

36.12548172

(6)

### Hanger number 13 with fixed connections

**Determining out of plane natural frequencies of hanger number 13 (fixed-fixed)**

restart :

$$w1 := C1 \cdot \sin\left(\frac{\beta1 \cdot x}{l}\right) + C2 \cdot \cos\left(\frac{\beta1 \cdot x}{l}\right) + C3 \cdot \sinh\left(\frac{\beta2 \cdot x}{l}\right) + C4 \cdot \cosh\left(\frac{\beta2 \cdot x}{l}\right) :$$

**Boundary conditions**

$$BC1 := \text{simplify}(\text{subs}(x=0, w1)) = 0 :$$

$$BC2 := \text{simplify}(\text{subs}(x=0, \text{diff}(w1, x))) = 0 :$$

$$BC7 := \text{simplify}(\text{subs}(x=l, w1)) = 0 :$$

$$BC8 := \text{simplify}(\text{subs}(x=l, \text{diff}(w1, x))) = 0 :$$

**Obtaining frequency equation**

with(LinearAlgebra) :

$$M1, F := \text{GenerateMatrix}(\{BC1, BC2, BC7, BC8\}, \{C1, C2, C3, C4\}) :$$

$$\text{Frequencyequation} := \text{simplify}(\text{Determinant}(M1)) :$$

$$\frac{-2 \beta1 \beta2 + 2 \beta1 \cos(\beta1) \cosh(\beta2) \beta2 + \sin(\beta1) \beta1^2 \sinh(\beta2) - \sin(\beta1) \beta2^2 \sinh(\beta2)}{l^2} \quad (1)$$

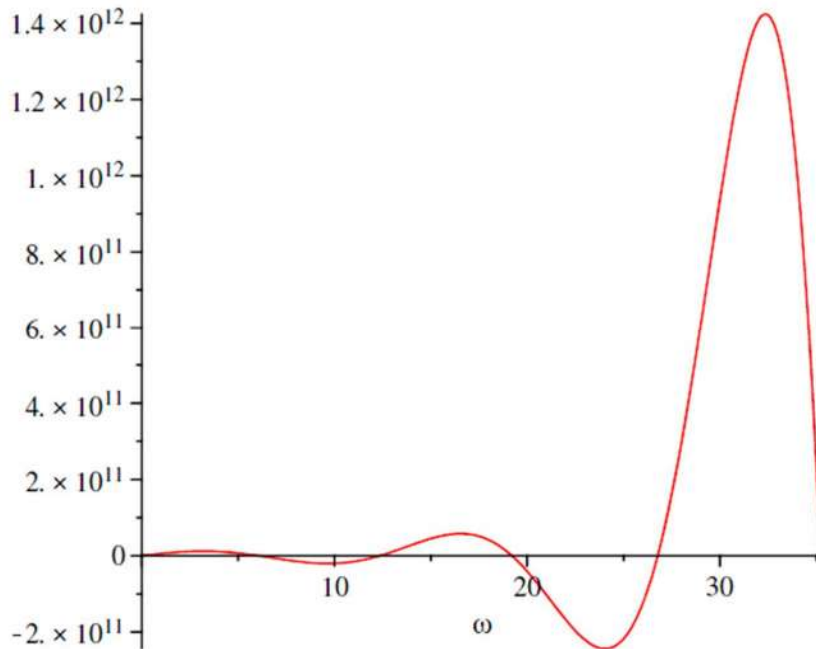
$$\beta1 := \left( -\frac{T \cdot l^2}{2 \cdot EI} + \left( \left( \frac{T \cdot l^2}{2 \cdot EI} \right)^2 + \frac{\rho A \cdot \omega^2 \cdot l^4}{EI} \right)^{0.5} \right)^{0.5} :$$

$$\beta2 := \left( \frac{T \cdot l^2}{2 \cdot EI} + \left( \left( \frac{T \cdot l^2}{2 \cdot EI} \right)^2 + \frac{\rho A \cdot \omega^2 \cdot l^4}{EI} \right)^{0.5} \right)^{0.5} :$$

**Parameters hanger number 13**

$$T := 1196000 : EI := \frac{2.1 \cdot 10^{11} \cdot \pi \cdot 0.150^4}{64} : \rho A := 0.25 \cdot \pi \cdot 0.150^2 \cdot 7850 : l := 52.822 :$$

with(plots) : plot( Frequencyequation,  $\omega = 0 \dots 35.3$ );



Natural frequencies of hanger nr. 13 bending mode 1 to 8 (fixed-fixed connections)

$$\omega_1 := \text{fsolve}(\text{abs}(\text{Frequencyequation}), \omega = 0..7) : f1 := \text{evalf}\left(\frac{\omega_1}{2 \cdot \pi}\right);$$

0.9618083674 (2)

$$\omega_2 := \text{fsolve}(\text{abs}(\text{Frequencyequation}), \omega = 7..15) : \text{evalf}\left(\frac{\omega_2}{2 \cdot \pi}\right);$$

1.967141482 (3)

$$\omega_3 := \text{fsolve}(\text{abs}(\text{Frequencyequation}), \omega = 15..20) : \text{evalf}\left(\frac{\omega_3}{2 \cdot \pi}\right);$$

3.055482930 (4)

$$\omega_4 := \text{fsolve}(\text{abs}(\text{Frequencyequation}), \omega = 20..30) : \text{evalf}\left(\frac{\omega_4}{2 \cdot \pi}\right);$$

4.259799300 (5)

$$\omega_5 := \text{fsolve}(\text{abs}(\text{Frequencyequation}), \omega = 30..40) : \text{evalf}\left(\frac{\omega_5}{2 \cdot \pi}\right);$$

5.605992615 (6)

$$\omega_6 := \text{fsolve}(\text{abs}(\text{Frequencyequation}), \omega = 40..50) : \text{evalf}\left(\frac{\omega_6}{2 \cdot \pi}\right);$$

7.113635668 (7)

$$\omega_7 := \text{fsolve}(\text{abs}(\text{Frequencyequation}), \omega = 50..60) : \text{evalf}\left(\frac{\omega_7}{2 \cdot \pi}\right);$$

8.797198144 (8)

$$\omega_8 := \text{fsolve}(\text{abs}(\text{Frequencyequation}), \omega = 60..70) : \text{evalf}\left(\frac{\omega_8}{2 \cdot \pi}\right);$$

10.66727156 (9)

Natural bending frequencies hangers with hinged connections																					
							Mode 1			Mode 2			Mode 3			Mode 4			Mode 5		
Hanger nr.	Lsystem [m]	Lnet [m]	Ø [mm]	EI [Nm <sup>2</sup> ]	μ [kg/m]	N;PERM [kN]	n1 (EI) [Hz]	Ncrit;1 [kN]	n1 [Hz]	n2 (EI) [Hz]	Ncrit;2 [kN]	n2 [Hz]	n3 (EI) [Hz]	Ncrit;3 [kN]	n3 [Hz]	n4 (EI) [Hz]	Ncrit;4 [kN]	n4 [Hz]	n5 (EI) [Hz]	Ncrit;5 [kN]	n5 [Hz]
3	21,779	18,879	200	16493361	247	1530	1,14	457	2,38	4,56	1827	6,18	10,26	4110	12,02	18,24	7308	20,05	28,49	11418	30,34
4	27,860	24,960	150	5218603	139	852	0,49	83	1,64	1,96	331	3,70	4,40	744	6,45	7,82	1323	10,03	12,23	2067	14,53
5	33,376	30,476	150	5218603	139	1047	0,33	55	1,46	1,31	222	3,14	2,95	499	5,20	5,25	887	7,75	8,20	1386	10,86
6	38,326	35,426	150	5218603	139	1158	0,24	41	1,31	0,97	164	2,76	2,18	369	4,44	3,88	657	6,46	6,07	1026	8,85
7	42,710	39,810	150	5218603	139	1177	0,19	32	1,17	0,77	130	2,44	1,73	292	3,88	3,08	520	5,56	4,81	812	7,52
8	46,515	43,615	150	5218603	139	1151	0,16	27	1,06	0,64	108	2,18	1,44	244	3,45	2,56	433	4,90	4,00	677	6,58
9	49,719	46,819	150	5218603	139	1130	0,14	23	0,97	0,56	94	2,01	1,25	211	3,15	2,22	376	4,45	3,47	587	5,94
10	52,292	49,392	150	5218603	139	1154	0,12	21	0,93	0,50	84	1,91	1,12	190	2,99	2,00	338	4,20	3,12	528	5,57
11	54,191	51,291	150	5218603	139	1176	0,12	20	0,90	0,46	78	1,85	1,04	176	2,89	1,85	313	4,04	2,90	489	5,34
12	55,359	52,459	150	5218603	139	1184	0,11	19	0,89	0,44	75	1,82	1,00	168	2,82	1,77	299	3,94	2,77	468	5,20
13	55,722	52,822	150	5218603	139	1196	0,11	18	0,89	0,44	74	1,81	0,98	166	2,81	1,75	295	3,93	2,73	461	5,17
14	55,182	52,282	150	5218603	139	1200	0,11	19	0,90	0,45	75	1,83	1,00	170	2,85	1,78	301	3,98	2,79	471	5,25
15	53,614	50,714	150	5218603	139	1154	0,12	20	0,91	0,47	80	1,86	1,07	180	2,90	1,90	320	4,07	2,96	501	5,38
16	50,855	47,955	150	5218603	139	1030	0,13	22	0,91	0,53	90	1,87	1,19	202	2,95	2,12	358	4,17	3,31	560	5,58
17	46,690	43,790	200	16493361	247	1529	0,21	85	0,92	0,85	340	1,99	1,91	764	3,30	3,39	1358	4,94	5,30	2122	6,95
18	40,836	37,936	200	16493361	247	1346	0,28	113	1,01	1,13	452	2,25	2,54	1018	3,87	4,52	1810	5,96	7,06	2828	8,57
19	32,917	30,017	200	16493361	247	1478	0,45	181	1,37	1,80	723	3,15	4,06	1626	5,61	7,21	2891	8,87	11,27	4517	12,99
20	22,472	19,572	220	24147930	298	3364	1,17	622	2,95	4,67	2489	7,16	10,50	5600	13,28	18,66	9955	21,59	29,16	15554	32,16

Table 58: In plane bending frequencies of the hangers

\*Lnet = distance between upper flange of the main girder, and bottom flange of the arch. It is estimated with the following formula:

$$Lnet = Lsystem - \frac{1}{2}h_{arch} - \frac{1}{2}h_{main\ girder} = Lsystem - 0,5 \cdot 2,3m - 0,5 \cdot 3,5m = Lsystem - 2,9m$$

